

I. SYNTHESIS, CHARACTERIZATION,  
AND BASE CATALYSIS OF ORGANIC-  
FUNCTIONALIZED MOLECULAR SIEVES

II. SELECTIVE OXIDATION OF ETHANE  
VIA HETEROPOLYANION-CONTAINING  
SOLID CATALYSTS

Thesis by

Andrea P. Wight

In Partial Fulfillment of the Requirements for the  
degree of

Doctor of Philosophy

CALIFORNIA INSTITUTE OF TECHNOLOGY

Pasadena, California

2004

(Defended May 14, 2004)

© 2004

Andrea P. Wight

All Rights Reserved

*To Rob, for always believing in me*

*And Robbie, to show him what is possible*

## ACKNOWLEDGEMENTS

I would like to first thank Professor Mark Davis for giving me the opportunity to work in his group for these past five years. His guidance has allowed me to grow and mature as a scientist. He has provided many opportunities for me to increase my abilities as a researcher and responsibilities as a team member. I would also express my gratitude for the other members of my thesis committee: Dr. Jay Labinger, Professor George Gavalas, and Dr. Stacey Zones. Their time, advice, and support have been invaluable to me as I have worked to complete my thesis.

I am grateful for the financial support of this work from Chevron Research and Technology Co. (Part One) and BP (Part Two). Our collaborators at Chevron (Stacey Zones) and BP (George Salem and Muin Haddad) provided thoughtful guidance and suggestions for each of projects. I would also like to acknowledge the support of a National Science Foundation Graduate Fellowship and a Philanthropic Educational Organization Scholar Award.

My colleagues in the Davis group have been a source of knowledge, empathy, and humor over the years. The training and guidance provided by Chris Jones, Joe Holles, and Chris Dillon helped me to begin my thesis research, and they have always taken the time to field my many questions even after departing our group. Jon Galownia has allowed me the benefit of his mechanical skills and has suffered with me in equipment maintenance and repair. John Murphy, my unfortunate office mate, has had the patience and sense of humor to listen to my ramblings about research, life, and my son's escapades on a daily basis.

Ileana Carpen has been my constant coffee companion and friend, from first year classes, through qualifiers, candidacy, research, and finally job hunting (the best part). Her support and friendship has helped me through all of the ups and downs of graduate school.

I would like to thank my parents for their unwavering encouragement and support throughout my life, inspiring me to set my goals as high as my imagination could take me. They have always helped me to believe that I could do anything I wanted to do and that my life is made by my own choices. They have shown me how to have faith in myself and in God to find the best path in life and take advantage of each and every opportunity that presents itself.

Finally, this thesis is dedicated my husband, Rob, who was willing to move 1800 miles unemployed to let me follow my dreams, and to my son, Robbie, to show him that one can do anything one wants to do, if one puts their mind to it.

## ABSTRACT

This thesis is composed of two separate and unrelated projects. The first project examines the preparation of functional groups that can serve as immobilized bases in molecular sieves. Many heterogeneous, base catalysts are not able to promote diverse reaction types that require strong bases as catalysts. Additionally, some of the stronger solid base catalysts are sensitive to carbon dioxide and moisture in air and therefore are not easily suitable for recycling. Organic-functionalized molecular sieves possess an organic moiety within the pore space of a molecular sieve by incorporation of an organosilane directly into the synthesis gel of the molecular sieve. Previous work reported by Davis and co-workers demonstrated the incorporation of an acid site in zeolite Beta (\*BEA type) and its use in shape-selective acid catalysis.

Here, a phosphonium functionality is prepared from halogen-containing alkyl groups in \*BEA to allow the incorporation of a strong base (OH<sup>-</sup>) within the molecular sieve for base catalysis. Characterization of the phosphonium-containing material prepared is accomplished. Shape-selective chemical reactions and ion-exchanges are presented, and the results of these experiments suggest that the functional groups are located within the molecular sieve pore space, although the exact structure of these moieties is not conclusively obtained.

The second part of this thesis examines the use of niobium- and pyridine-exchanged heteropolyanions as catalyst precursors for the selective oxidation of light alkanes with dioxygen. The versatility of many oxidation catalysts is limited, thereby restricting potential usefulness. Alkenes, typically used as feedstock, are becoming costly as their demand for use in many other industrial processes increases. The use of light alkanes as

reactants for selective oxidation would allow one to take advantage of an under-utilized and relatively inexpensive feedstock for selective oxidation.

Niobium- and pyridine-exchanged heteropolyanions (HPAs) have been shown to produce highly active and selective catalysts for the oxidation of propane and *n*-butane to acrylic acid and maleic acid, respectively, by Davis and co-workers. Specifically, molybdophosphoric acid and molybdovanadophosphoric acid were exchanged with niobium oxalate and pyridine to produce the exchanged HPAs (denoted NbPMo<sub>12</sub>pyr and NbPMo<sub>11</sub>Vpyr, respectively). Preliminary work in these studies indicates that the exchanged HPAs may also be effective for the oxidation of ethane to acetic acid. The application of this catalyst system to the selective oxidation of ethane to acetic acid and ethylene is explored here.

The exchanged heteropolyanions give higher ethane conversion at elevated pressures (230 psig and 280°C) but better yields at atmospheric pressure and 380°C. Variations of steam flow rates or reaction temperatures are not observed to improve acetic acid space-time-yield (STY). Lower gas-hourly-space-velocity (GHSV) causes the ethylene and acetic acid to over-oxidize to CO<sub>x</sub>. The maximum STY of acetic acid using NbPMo<sub>12</sub>pyr is 0.021 mmol/min/g catalyst at 380°C, 0 psig, and flows of 16: 8: 16: 20 mL/min of ethane: oxygen: helium: steam.

At elevated pressure (230 psig) the addition of vanadium into the Keggin ion precursor is shown to decrease conversion (from 6.0% to 2.2%) but improve selectivity to ethylene (from 23.2% to 46.8%). The formation of acetic acid is not affected (0.002 mmol/min/g catalyst). At atmospheric pressure the addition of vanadium into the Keggin precursor does have a favorable affect on the acetic acid formation. NbPMo<sub>11</sub>Vpyr is

shown to have a maximum acetic acid production of 0.062 mmol/min/g catalyst at 380°C, 0 psig, and flows of 16: 8: 16: 20 mL/min of ethane: oxygen: helium: steam.

The addition of both Nb and pyridine to the HPA is crucial for active catalyst formation, for reactions both at atmospheric pressure and 230 psig. Substitution of other metals for Nb does not yield materials that give significant ethane conversion.

Higher ethane/oxygen ratios increase the selectivity to acetic acid over NbPMo<sub>12</sub>pyr at atmospheric pressure. The oxidation of ethylene over NbPMo<sub>12</sub>pyr is accomplished, and the results indicate that acetic acid is formed from ethylene during the oxidation of ethane. D<sub>2</sub>O is substituted as the source of steam, and the observation that acetic acid contains deuterium shows that the steam in the feed is involved in its formation.

The data obtained from NbPMo<sub>11</sub>Vpyr suggest that this precursor can give a catalyst that is active and selective for producing ethylene and acetic acid from ethane and dioxygen. Further experimentation is necessary to optimize performance.

## TABLE OF CONTENTS

Acknowledgements .....	iv
Abstract .....	vi
Table of Contents .....	ix
List of Figures .....	xii
List of Schemes .....	xvi
List of Tables .....	xix
<b>Chapter 1: Preface</b> .....	1
<b>Part One: Synthesis, Characterization, and Base Catalysis of Organic-Functionalized Molecular Sieves</b> .....	5
<b>Chapter 2: Introduction and Objectives</b> .....	6
2.1 Heterogeneous Base Catalysis .....	7
2.2 Zeolites .....	8
2.3 Objectives .....	9
2.4 References .....	11
<b>Chapter 3: Design and Preparation of Organic-Inorganic Hybrid Catalysts</b> .....	20
3.1 Introduction .....	21
3.2 Organic-Inorganic Hybrid Materials .....	22
3.2.1 Grafting of Organic Moiety onto Solid Surfaces .....	22
3.2.2 Direct Incorporation of Organic Moiety: Ordered, Mesoporous Materials .....	42
3.2.3 Organic-Functionalized Molecular Sieves (OFMS) .....	58
3.2.4 Hybrid Materials with Organic Groups in the Network .....	61
3.2.5 Imprinted Silicas .....	67
3.3 Future Directions of Organic-Inorganic Hybrid Materials .....	69
3.4 Acknowledgements .....	70
3.5 References .....	71
<b>Chapter 4: Synthesis and Characterization of Base-Containing Organic-Functionalized Molecular Sieves</b> .....	117
4.1 Introduction .....	118
4.2 Experimental Section .....	118
4.2.1 Silica Zeolite Beta Preparation .....	118
4.2.2 Quaternary Ammonium OFMS Preparation .....	119
4.2.3 Halogenated Propyl-OFMS Preparation .....	120
4.2.4 Quaternary Phosphonium Organosilane Preparation .....	120
4.2.5 Quaternary Phosphonium OFMS Preparation .....	122
4.2.6 Extraction of *BEA Samples .....	122

4.2.7 Nucleophilic Displacement of X-*BEA Samples .....	123
4.2.8 Tethering of Organosilanes onto Controlled Pore Glass .....	123
4.2.9 Ion-Exchange of OFMS Samples .....	125
4.3 Results and Discussion.....	127
4.3.1 Quaternary Ammonium OFMS Preparation .....	127
4.3.2 Quaternary Phosphonium OFMS Preparation.....	131
4.3.3 Quaternary Phosphonium OFMS Ion-Exchange .....	134
4.4 References .....	136
<b>Chapter 5: Base Catalysis of Organic-Functionalized Molecular Sieves .....</b>	<b>175</b>
5.1 Introduction .....	176
5.2 Experimental Section .....	176
5.2.1 Knoevenagel Condensation .....	176
5.2.2 Michael Addition.....	177
5.3 Results and Discussion.....	178
<b>Chapter 6: Summary and Conclusions for Part One.....</b>	<b>191</b>
<b>Part Two: Selective Oxidation of Ethane via Heteropolyanion-Containing Solid</b>	
Catalysts.....	196
<b>Chapter 7: Selective Oxidation of Light Alkanes .....</b>	<b>197</b>
7.1 Introduction .....	198
7.2 Ethane Selective Oxidation Catalysts.....	200
7.3 Heteropolyanions.....	201
7.4 Objectives .....	203
7.5 References .....	204
<b>Chapter 8: Reactivity of Niobium- and Pyridine-Exchanged Heteropolyanions</b>	
for the Conversion of Ethane .....	211
8.1 Introduction .....	212
8.2 Experimental Section .....	215
8.2.1 NbPMo <sub>12</sub> pyr Preparation.....	215
8.2.2 NbPMo <sub>11</sub> Vpyr Preparation.....	216
8.2.3 Reactivity Studies.....	217
8.3 Results and Discussion.....	218
8.3.1 Study of Nb <sub>0.4</sub> PMo <sub>12</sub> pyr in High Pressure Ethane Reactions .....	218
8.3.2 Study of Nb <sub>0.4</sub> PMo <sub>12</sub> pyr in Atmospheric Pressure Ethane Reactions .....	221
8.3.3 Study of Nb <sub>0.68</sub> PMo <sub>11</sub> Vpyr in Ethane Reactions .....	227
8.3.4 Study of Nb <sub>0.4</sub> PMo <sub>12</sub> pyr Reactivity at Other Flow Compositions.....	232
8.3.5 Ethane Reactivity with Metals Other Than Nb .....	232
8.3.6 Study of Ethylene Reactions with Nb <sub>0.4</sub> PMo <sub>12</sub> pyr .....	233
8.4 References .....	236

<b>Chapter 9: Summary and Conclusions of Part Two</b> .....	271
<b>Chapter 10: Conclusions</b> .....	280
<b>Appendices:</b> .....	286
<b>Appendix A: BTRS, Jr. Reactors</b> .....	287
<b>Appendix B: Flammability Calculations</b> .....	292
B.1 Flammability Limit Data .....	292
B.2 Temperature Corrections.....	292
B.3 Pressure Corrections .....	293
B.4 Quenching Distance.....	294
B.5 References.....	296
<b>Appendix C: Reactivity Data Tables</b> .....	298

## LIST OF FIGURES

<b>Chapter 2 Figures:</b> .....	13
Figure 2.1: Tetrahedral zeolite precursors. ....	13
Figure 2.2: Three-dimensional zeolite structure (Faujasite).....	14
<b>Chapter 4 Figures:</b> .....	137
Figure 4.1: N-trimethoxysilylpropyl-N,N,N-trimethylammonium chloride. ....	137
Figure 4.2: $^{13}\text{C}$ liquid NMR of 3-bromopropyltrimethoxysilane obtained from United Chemicals Technologies, Inc., in $\text{CD}_2\text{Cl}_2$ . ....	138
Figure 4.3: $^{13}\text{C}$ liquid NMR of 1 M trimethylphosphine solution in toluene obtained from Aldrich, in $\text{CD}_2\text{Cl}_2$ . Inset is $^{31}\text{P}$ liquid NMR. ....	139
Figure 4.4: $^{13}\text{C}$ liquid NMR of P-trimethoxysilylpropyl-P,P,P-trimethylammonium bromide, in $\text{CD}_2\text{Cl}_2$ . Inset is $^{31}\text{P}$ liquid NMR. ....	140
Figure 4.5: XRD of *BEA materials: (A) Si-*BEA as-made, (B) Si-*BEA after extraction with acetic acid twice, (C) Q-*BEA as-made, and (D) Q-*BEA after extraction with acidified pyridine twice. ....	141
Figure 4.6: TGA of as-made Si-*BEA, showing (A) TEAF weight loss and (B) derivative of weight loss. ....	142
Figure 4.7: TGA of Si-*BEA after two pyridine extractions, showing (A) weight loss and (B) derivative of weight loss. ....	143
Figure 4.8: TGA of calcined Si-*BEA after pyridine sorption, showing (A) weight loss and (B) derivative of weight loss. ....	144
Figure 4.9: TGA of Si-*BEA after two pyridine extractions and two water washings, showing (A) weight loss and (B) derivative of weight loss. ....	145
Figure 4.10: TGA of Q-*BEA after two pyridine extractions and two water washings, showing (A) weight loss and (B) derivative of weight loss. ....	146
Figure 4.11: $\text{N}_2$ adsorption Q-*BEA, after (A) extraction and (B) calcination. The dotted line is the $\text{N}_2$ adsorption of Si-*BEA after extraction. ....	147

Figure 4.12: $^{29}\text{Si}$ CP/MAS NMR of *BEA: (A) as made Q-*BEA, (B) extracted Q-*BEA and (B) extracted Q-*BEA after evacuation at 200°C overnight. ....	148
Figure 4.13: $^{29}\text{Si}$ CP/MAS NMR of *BEA: (A) as made Si-*BEA, (B) extracted Si-*BEA. ....	149
Figure 4.14: $^{13}\text{C}$ CP/MAS NMR of ammonium-containing CPG: (A) Q-CPG as-made, (B) after heating to 25°C under vacuum, (C) after heating to 100°C under vacuum, (D) after heating to 200°C under vacuum, and (E) after ion-exchange with nitric acid. ....	150
Figure 4.15: $^{29}\text{Si}$ CP/MAS NMR of Q-CPG (A) as-made, (B) after heating under vacuum at 25°C, (C) after heating under vacuum to 100°C, (D) after heating under vacuum to 200°C. ....	151
Figure 4.16: $^{13}\text{C}$ CP/MAS NMR of (A) Br-CPG, (B) $\text{P}^+\text{Br}^-$ -CPG, and (C) $\text{P}^+\text{Br}^-$ -CPG after heat treatment to 300°C. ....	152
Figure 4.17: XRD of *BEA materials: (A) as-made Si-*BEA, (B) as-made Br-*BEA, (C) extracted Br-*BEA, (D) $\text{P}^+\text{Br}^-$ -*BEA, and (E) $\text{P}^+\text{Ph}_3\text{Br}^-$ -*BEA. ....	153
Figure 4.18: DSC of extracted *BEA materials: (A) Br-*BEA, (B) Cl-*BEA, and (C) Si-*BEA. ....	154
Figure 4.19: $^{29}\text{Si}$ CP/MAS NMR of (A) $\text{P}^+\text{Br}^-$ -*BEA, and (B) $\text{P}^+\text{Ph}_3\text{Br}^-$ -*BEA. ....	155
Figure 4.20: $^{31}\text{P}$ MAS NMR of (A) $\text{P}^+\text{Br}^-$ -*BEA, (B) $\text{P}^+\text{Br}^-$ -CPG, and (C) $\text{P}^+\text{Br}^-$ -CPG heated to 300°C under vacuum. ....	156
Figure 4.21: $^{31}\text{P}$ MAS NMR of (A) $\text{P}^+\text{Ph}_3\text{Br}^-$ -*BEA, (B) $\text{P}^+\text{Ph}_3\text{Cl}^-$ -*BEA, and (C) $\text{P}^+\text{Ph}_3\text{Cl}^-$ -CPG. ....	157
Figure 4.22: XRD of as-made $\text{P}_{\text{quat}}$ -*BEA. ....	158
Figure 4.23: $^{31}\text{P}$ MAS NMR of as-made $\text{P}_{\text{quat}}$ -CPG. ....	159
Figure 4.24: XRD of *BEA materials: (A) $\text{P}^+\text{NO}_3^-$ -*BEA and (B) $\text{P}^+\text{BPh}_4^-$ -*BEA. ....	160
Figure 4.25: $^{29}\text{Si}$ CP/MAS NMR of ion-exchanged $\text{P}^+\text{NO}_3^-$ -*BEA. ....	161
Figure 4.26: FTIR Spectra of (A) $\text{P}^+\text{NO}_3^-$ -CPG, (B) $\text{P}^+\text{NO}_3^-$ -*BEA (from Cl), and (C) $\text{P}^+\text{NO}_3^-$ -*BEA (from Br). ....	162
Figure 4.27: $^{11}\text{B}$ MAS NMR of $\text{NaBPh}_4$ exchanged materials: (A) Si-*BEA after extraction, (B) $\text{P}^+\text{BPh}_4^-$ -*BEA (from Cl), and (C) $\text{P}^+\text{BPh}_4^-$ -*BEA (from Br), and (D) $\text{P}^+\text{BPh}_4^-$ -CPG (from Cl). ....	163

<b>Chapter 8 Figures:</b> .....	237
Figure 8.1: Nb <sub>x</sub> PMo <sub>12</sub> pyr, with varying Nb/Keggin ratios.....	237
Figure 8.2: Phosphomolybdic acid and its niobium- and pyridine-exchanged forms. ....	238
Figure 8.3: Phosphovanadomolybdic acid and its niobium- and pyridine-exchanged forms. ....	239
Figure 8.4: Nb <sub>x</sub> PMo <sub>11</sub> Vpyr, with varying Nb/Keggin ratios.....	240
Figure 8.5: Autoclave Engineers BTRS, Jr. reactor schematics: (A) high pressure reactor system and (B) low pressure reactor system.....	241
Figure 8.6: Ethane reactivity of NbPMo <sub>12</sub> pyr at 280°C, 230 psig, 8: 4: 27: x mL/hr (ethane: oxygen: helium: steam) on high pressure reactor. ....	243
Figure 8.7: Space time yield of products for NbPMo <sub>12</sub> pyr at 280°C, 230 psig, 8: 4: 27: x mL/hr (ethane: oxygen: helium: steam) on high pressure reactor. ....	244
Figure 8.8: Selectivity vs. conversion for NbPMo <sub>12</sub> pyr at 280°C, 230 psig, 8: 4: 27: x mL/hr (ethane: oxygen: helium: steam) on high pressure reactor. ....	245
Figure 8.9: Ethane reactivity of NbPMo <sub>12</sub> pyr at 280°C, 230 psig, 8: 4: 27: 10 mL/hr (ethane: oxygen: helium: steam) on high pressure reactor. Catalyst volume was varied.....	246
Figure 8.10: Space time yield of products for NbPMo <sub>12</sub> pyr at 280°C, 230 psig, 8: 4: 27: 10 mL/hr (ethane: oxygen: helium: steam) on high pressure reactor. Catalyst volume was varied.....	247
Figure 8.11: Ethane reactivity of NbPMo <sub>12</sub> pyr at 380°C, 0 psig, 16: 8: 16: x mL/hr (ethane: oxygen: helium: steam) on high pressure reactor. ....	248
Figure 8.12: Space time yield of products for NbPMo <sub>12</sub> pyr at 380°C, 0 psig, 16: 8: 16: x mL/hr (ethane: oxygen: helium: steam) on high pressure reactor. ....	249
Figure 8.13: Selectivity vs. conversion for NbPMo <sub>12</sub> pyr at 380°C, 0 psig, 16: 8: 16: x mL/hr (ethane: oxygen: helium: steam) on high pressure reactor. ....	250
Figure 8.14: Ethane reactivity with temperature of NbPMo <sub>12</sub> pyr at 0 psig, 16: 8: 16: 20 mL/hr (ethane: oxygen: helium: steam) on high pressure reactor, except 280°C run on low pressure reactor.....	251

Figure 8.15: Ethane reactivity with Nb loading of NbPMo <sub>12</sub> pyr at 380°C, 0 psig, 16: 8: 16: 20 mL/hr (ethane: oxygen: helium: steam) on low pressure reactor. ....	252
Figure 8.16: Space time yield of products for Nb loading of NbPMo <sub>12</sub> pyr at 380°C, 0 psig, 16: 8: 16: 20 mL/hr (ethane: oxygen: helium: steam) on low pressure reactor. ....	253
Figure 8.17: Selectivity vs. conversion for Nb loading of NbPMo <sub>12</sub> pyr at 380°C, 0 psig, 16: 8: 16: 20 mL/hr (ethane: oxygen: helium: steam) on low pressure reactor. ....	254
Figure 8.18: Ethane reactivity with Nb loading of NbPMo <sub>11</sub> Vpyr at 380°C, 0 psig, 8: 4: 8: 10 mL/hr (ethane: oxygen: helium: steam) on low pressure reactor, V <sub>catalyst</sub> = 0.3 mL. ....	255
Figure 8.19: Space time yield of products for Nb loading of NbPMo <sub>11</sub> Vpyr at 380°C, 0 psig, 8: 4: 8: 10 mL/hr (ethane: oxygen: helium: steam) on low pressure reactor, V <sub>catalyst</sub> = 0.3 mL. ....	256
Figure 8.20: Selectivity vs. conversion for Nb loading of NbPMo <sub>11</sub> Vpyr at 380°C, 0 psig, 8: 4: 8: 10 mL/hr (ethane: oxygen: helium: steam) on low pressure reactor, V <sub>catalyst</sub> = 0.3 mL. ....	257
<b>Appendix Figures:</b> .....	287
Figure A.1: Autoclave Engineers BTRS, Jr. reactor (high pressure reactor).....	287
Figure A.2: Autoclave Engineers BTRS, Jr. reactor (low pressure reactor).....	288
Figure A.3: Configuration of reactor tube in the reactor furnace on high pressure reactor.....	289
Figure A.4: Configuration of reactor tube in the reactor furnace on low pressure reactor.....	290
Figure A.5: Temperature profile in reactor tube filled with glass wool on low pressure reactor. ....	291
Figure B.1: Ethane flammability data for various pressures. ....	297

## LIST OF SCHEMES

<b>Chapter 2 Schemes:</b> .....	15
Scheme 2.1: Knoevenagel condensation.....	15
Scheme 2.2: Aldol condensation.....	16
Scheme 2.3: Michael addition.....	17
Scheme 2.4: Mesoporous grafting of a quaternary ammonium-containing organosilane.....	18
<b>Chapter 3 Schemes:</b> .....	79
Scheme 3.1: Chlorination and subsequent reaction with a Grignard reagent to functionalize silica.....	79
Scheme 3.2: Example of grafting organosilanes onto silanol-containing surface.....	80
Scheme 3.3: A synthetic route to organosilanes.....	81
Scheme 3.4: Knoevenagel condensation of benzaldehyde and ethyl cyanoacetate.....	82
Scheme 3.5: Example of a nitroaldol condensation.....	83
Scheme 3.6: Example of a Michael addition reaction.....	84
Scheme 3.7: Proposed mechanism of nitroaldol condensation.....	85
Scheme 3.8: Imine silica preparation from aminopropyl silica.....	86
Scheme 3.9: Synthesis of guanidine organosilanes.....	87
Scheme 3.10: Linstead-Knoevenagel condensation.....	88
Scheme 3.11: Synthesis of perfluorosulfonyl fluoride silane and subsequent hydrolysis to the perfluorosulfonic acid silane.....	89
Scheme 3.12: Esterification and Grignard modification of the ordered, mesoporous materials.....	90
Scheme 3.13: Monoglyceride synthesis from glycidol and fatty acids.....	91

Scheme 3.14: Preparation of amine-containing MCM-41 hybrids for monoglyceride synthesis. ....	92
Scheme 3.15: Synthesis of guanidine hybrid materials. ....	93
Scheme 3.16: Immobilization of imidazole on ordered, mesoporous materials. ....	94
Scheme 3.17: Aldol condensation and intramolecular Michael addition of benzaldehyde and 2'-hydroxyacetophenone to flavanone. ....	95
Scheme 3.18: Synthesis of coumarins and chromenes via base catalyzed condensations. ...	96
Scheme 3.19: Proposed mechanism of coumarin and chromene formation. ....	97
Scheme 3.20: Preparation of silica-supported phase transfer catalysts. ....	98
Scheme 3.21: Oxidation of mercaptopropyl-functionalized silicas to give sulfonic acid sites. ....	99
Scheme 3.22: Acid catalyzed addition of 2-methylfuran and acetone. ....	100
Scheme 3.23: <b>(A)</b> Synthesis of TEMPO-ether-silane. <b>(B)</b> Synthesis of TEMPO-amide-MCM-41. ....	101
Scheme 3.24: Products of nucleophilic substitution of chloropropylsilane and (-)-ephedrine. ....	102
Scheme 3.25: Synthesis of (R)-1-phenyl-propan-1-ol from benzaldehyde and diethylzinc. ....	103
Scheme 3.26: Co-condensation of organosilanes and tetraalkoxysilanes for the assembly of ordered, mesoporous, organic-inorganic hybrid solids. ....	104
Scheme 3.27: Synthesis of cyclodextrin-containing organosilane. ....	105
Scheme 3.28: Phosphorous-containing organosilane and mesoporous material syntheses. ....	106
Scheme 3.29: Synthesis of phosphonic acid sites in SBA-15. ....	107
Scheme 3.30: Shape-selective behavior of OFMS catalysts. ....	108
Scheme 3.31: Shape-selective imine reactions with OFMS materials. <b>(A)</b> Reaction of 4-(dimethylamino)benzaldehyde. <b>(B)</b> Reaction of 4-dimethylamino-1-naphthaldehyde. ....	109

Scheme 3.32: Interaction modes of phenylphosphonic acid with guanidine-functionalized, imprinted xerogels. <sup>31</sup> P MAS NMR chemical shifts are listed for each configuration. ....	110
Scheme 3.33: Imprinting of amorphous silica. The example illustrated is for organizing three aminopropyl groups. ....	111
Scheme 3.34: One (A) and two (B) point interactions of aminopropyl-imprinted silicas. ....	112
Scheme 3.35: Acid and base catalyzed reactions in one-pot reactions. ....	113
<b>Chapter 4 Schemes:</b> .....	164
Scheme 4.1: Preparation of P-trimethoxysilylpropyl-P,P,P-trimethylammonium bromide by nucleophilic displacement. ....	164
Scheme 4.2: Preparation of phosphonium-functionalized *BEA from Br-*BEA by nucleophilic displacement. ....	165
Scheme 4.3: Tethering of organosilanes onto CPG and preparation of phosphonium-functionalized CPG. ....	166
Scheme 4.4: Hofmann degradation of quaternary ammonium compounds. ....	167
Scheme 4.5: Substitution degradation of quaternary phosphonium compounds. ....	168
Scheme 4.6: Shape-selective nucleophilic displacement within extracted Br-*BEA. ....	169
Scheme 4.7: Shape-selective ion-exchange within P <sup>+</sup> Br <sup>-</sup> *BEA. ....	170
<b>Chapter 5 Schemes:</b> .....	183
Scheme 5.1: Knoevenagel condensation of benzaldehyde (1) and malononitrile (2). ....	183
Scheme 5.2: Knoevenagel condensation of 1-pyrenecarboxaldehyde (4) and malononitrile (2). ....	184
Scheme 5.3: Michael addition of 2-cyclohexen-1-one (6) and nitromethane (7). ....	185
Scheme 5.4: Michael addition of methylvinylketone (9) and ethylcyanoacetate (10). ....	186

## LIST OF TABLES

<b>Chapter 2 Tables:</b> .....	19
Table 2.1: Catalytic uses for zeolites. ....	19
<b>Chapter 3 Tables:</b> .....	114
Table 3.1: Knoevenagel condensation of various aldehydes and ketones with ethyl cyanoacetate in cyclohexane using aminopropyl silica. ....	114
Table 3.2: Knoevenagel condensation of ethyl cyanoacetate and pentan-3-one using imine-based silica hybrids. ....	115
Table 3.3: Nitrogen sorption data for organosilanes grafted onto zeolite Y. ....	116
<b>Chapter 4 Tables:</b> .....	171
Table 4.1: Organic-functional group loadings per gram of silica during nucleophilic displacement reaction. ....	171
Table 4.2: Organic-functional group loadings per gram of silica after nitrate ion-exchange. ....	172
Table 4.3: Organic-functional group loadings per gram of silica after 0.001 N NaOH ion-exchange. ....	173
Table 4.4: Organic-functional group loadings per gram of silica after bromide ion-exchange. ....	174
<b>Chapter 5 Tables:</b> .....	187
Table 5.1: Knoevenagel condensation of <b>1</b> and <b>2</b> (see Scheme 5.1). ....	187
Table 5.2: Knoevenagel condensation of <b>4</b> and <b>2</b> (see Scheme 5.2). ....	188
Table 5.3: Michael addition of <b>4</b> and <b>5</b> (see Scheme 5.3). ....	189
Table 5.4: Michael addition of <b>9</b> and <b>10</b> (see Scheme 5.4). ....	190

<b>Chapter 7 Tables:</b> .....	206
Table 7.1: Current commercial production of chemical intermediates.....	206
Table 7.2: Alkane oxidations of development interest.....	207
Table 7.3: Selective ethane oxidation catalysts.....	208
Table 7.4: Gas-phase oxidations with heteropolyanion catalysts.....	209
Table 7.5: Selective oxidation of light alkanes with HPAs.....	210
<b>Chapter 8 Tables:</b> .....	258
Table 8.1: <i>n</i> -Butane reactivity at 380°C.....	258
Table 8.2: Propane reactivity at 380°C.....	259
Table 8.3: Temperature effects for NbPMo <sub>12</sub> pyr at 230 psig, 8: 4: 27: 10 mL/hr (ethane: oxygen: helium: steam) on high pressure reactor.....	260
Table 8.4: Ethane reactivity of NbPMo <sub>12</sub> pyr at 280°C, 230 psig, (8: 4: 27: 0) mL/hr (ethane: oxygen: helium: steam) on high pressure reactor. Catalyst volume was varied.....	261
Table 8.5: Ethane reactivity of PMo <sub>12</sub> , NbPMo <sub>12</sub> , PMo <sub>12</sub> pyr, and NbPMo <sub>12</sub> pyr at 280°C, 230 psig, 8: 4: 27: 10 mL/hr (ethane: oxygen: helium: steam) on high pressure reactor.....	262
Table 8.6: Ethane reactivity with temperature of NbPMo <sub>12</sub> pyr at 0 psig, 16: 8: 16: 20 mL/hr (ethane: oxygen: helium: steam) on high pressure reactor.....	263
Table 8.7: Comparison of ethane reactivity of NbPMo <sub>12</sub> pyr between reactors and pressures. Reactor and flows used noted in table.....	264
Table 8.8: Ethane reactivity of PMo <sub>12</sub> , NbPMo <sub>12</sub> , PMo <sub>12</sub> pyr, and NbPMo <sub>12</sub> pyr at 380°C, 0 psig, 16: 8: 16: 20 mL/hr (ethane: oxygen: helium: steam) on low pressure reactor.....	265
Table 8.9: Comparison of ethane reactivity of NbPMo <sub>11</sub> Vpyr between reactors and pressures. Reactor and flows used noted in table.....	266
Table 8.10: Comparison of ethane reactivity of (A) NbPMo <sub>11</sub> Vpyr prepared with NbCl <sub>5</sub> and synthetic Keggin and (B) NbPMo <sub>11</sub> Vpyr prepared with purchased Keggin and ammonium niobium oxalate, all on the low pressure reactor at a Nb/Keggin ratio of 0.68.....	267

Table 8.11: Comparison of ethane reactivity of NbPMo <sub>12</sub> pyr for different flow compositions at 380°C, 0 psig, on low pressure reactor, using 0.6 mL of catalyst. ....	268
Table 8.12: Comparison of ethane reactivity of various metal-exchanged MPMo <sub>12</sub> pyr at 380°C, 0 psig, 16: 8: 16: 20 mL/hr (ethane: oxygen: helium: steam) on low pressure reactor. ....	269
Table 8.13: Ethylene reactivity of NbPMo <sub>12</sub> pyr at 0 psig, 16: 8: 16: 20 mL/hr (ethylene: oxygen: helium: steam) on low pressure reactor. ....	270
<b>Appendix Tables:</b> .....	298
Table C.1: Ethane reactivity of NbPMo <sub>12</sub> pyr at 280°C, 230 psig, 8: 4: 27: x mL/hr (ethane: oxygen: helium: steam) on high pressure reactor. ....	298
Table C.2: Ethane reactivity of NbPMo <sub>12</sub> pyr at 280°C, 230 psig, (8: 4: 27: 10) mL/hr (ethane: oxygen: helium: steam) on high pressure reactor. Volume of catalyst varied.....	299
Table C.3: Ethane reactivity of NbPMo <sub>12</sub> pyr at 380°C, 0 psig, 16: 8: 16: x mL/hr (ethane: oxygen: helium: steam) on high pressure reactor. ....	300
Table C.4: Ethane reactivity with temperature of NbPMo <sub>12</sub> pyr at 0 psig, 16: 8: 16: 20 mL/hr (ethane: oxygen: helium: steam) on high pressure reactor, except 280°C run on low pressure reactor. ....	301
Table C.5: Ethane reactivity with Nb loading of NbPMo <sub>12</sub> pyr at 380°C, 0 psig, 16: 8: 16: 20 mL/hr (ethane: oxygen: helium: steam) on low pressure reactor. ....	302
Table C.6: Ethane reactivity with Nb loading of NbPMo <sub>11</sub> Vpyr at 380°C, 0 psig, 8: 4: 8: 10 mL/hr (ethane: oxygen: helium: steam) on low pressure reactor, V <sub>catalyst</sub> = 0.3 mL. ....	303

CHAPTER ONE

PREFACE

This thesis is composed of two separate and unrelated projects. The first project examines the preparation of functional groups that can serve as immobilized bases in molecular sieves. Organic-functionalized molecular sieves (OFMSs) have been previously reported by Davis and co-workers. These molecular sieves possess an organic moiety within the pore space of a zeolite, specifically Beta (\*BEA type). The OFMSs are prepared by incorporation of an organosilane directly into the synthesis gel of zeolite \*BEA. Previous work demonstrated the incorporation of an acid site in the OFMS and the use of the material for shape-selective acid catalysis. The objective of this project was to incorporate a strong base,  $\text{OH}^-$ , into the OFMS by attaching a positively charged organic moiety, e.g., an ammonium-containing functionality, within the molecular sieve pore space. Part One of this thesis describes this work and is arranged as follows:

Chapter 2 provides an introduction to heterogeneous base catalysis. The challenges associated with other attempts to incorporate strong bases within a porous material are discussed. An introduction to zeolites is also presented, including common catalytic applications of zeolites. Finally, the prior work of Davis and co-workers on OFMS and their use as acid catalysts is presented.

Chapter 3 provides an overview of the state of the art of organic-inorganic hybrid catalysts. Several different techniques for the preparation of organic-inorganic hybrid materials are discussed, including grafting of organic moieties, direct incorporation of a tethered organic during material preparation, and inclusion of organic moieties within the structural network of the material. The characterization of these hybrid materials by a range of analytical techniques is described. The application of these materials to a

variety of catalytic reactions is discussed. Finally, comments on the potential directions of development for organic-inorganic hybrid catalysts are presented.

Chapter 4 presents results on the incorporation of a positively charged organic moiety into an OFMS. Methods for the preparation of molecular sieves containing ammonium, halide, and phosphonium functionalities are described. Characterization of the prepared materials is discussed. Analytical techniques presented include powder X-ray diffraction, thermogravimetric analysis with simultaneous differential scanning calorimetry, nitrogen sorption, Fourier transform infrared spectroscopy, and multinuclear solution and solid state MAS nuclear magnetic resonance spectroscopy. The exchange of the halide-containing phosphonium-functionalized materials to the hydroxide form is discussed.

Chapter 5 describes the use of the hydroxide-exchanged phosphonium-functionalized materials in base catalysis. The methods for base reactions are presented. Catalytic results for the Knoevenagel condensation and Michael addition reactions using the prepared materials are discussed. Chapter 6 presents a summary of the characterization and catalytic results for the base-containing OFMSs.

The second part of this thesis examines the use of niobium- and pyridine-exchanged heteropolyanions as catalyst precursors for the selective oxidation of light alkanes with dioxygen. The use of the exchanged heteropolyanions for the selective oxidation of light alkanes has previously been reported by Davis and co-workers. These heteropolyanions were shown to produce highly active and selective catalysts for the oxidation of propane and *n*-butane to acrylic acid and maleic acid, respectively. The

objective of this project is to explore whether this catalyst system could be used for the selective oxidation of ethane to acetic acid and ethylene.

Chapter 7 provides background for selective oxidation catalyst systems. The advantages of the use of light alkanes as feedstock are discussed. An overview of alkane oxidation catalysts is presented, and general results for ethane oxidation are discussed. Finally, an introduction to heteropolyanions and their use as oxidation catalysts is presented.

Chapter 8 presents work reported by Davis and co-workers using niobium- and pyridine-exchanged phosphomolybdates as catalyst precursors in selective oxidation. The prior results obtained for the oxidation of *n*-butane and propane to maleic acid and acrylic acid, respectively, are discussed. The preparation of the exchanged HPA catalysts is described. The equipment and methods used to examine ethane reactivity are discussed. Reactivity results for ethane oxidation to acetic acid and ethylene are presented for the exchanged HPAs, at both elevated pressure (230 psig) and atmospheric pressure. The effect of reaction parameters, such as feed flow composition, reaction temperature, and space velocity are studied. The composition of HPA precursor is varied, including Nb/Keggin loadings, incorporation of other exchanged metals, and the substitution of one vanadium in the Keggin unit. The source of the acetic acid is probed by the examining the oxidation of ethylene and D<sub>2</sub>O at low conversions. Chapter 9 presents a summary of the catalytic results for the selective oxidation of ethane to acetic acid and ethylene using niobium- and pyridine-exchanged HPAs.

PART ONE

SYNTHESIS, CHARACTERIZATION, AND  
BASE CATALYSIS OF ORGANIC-  
FUNCTIONALIZED MOLECULAR SIEVES

## CHAPTER TWO

### INTRODUCTION AND OBJECTIVES

## 2.1 Heterogeneous Base Catalysis

Because of the value of crude oil refining, acidic heterogeneous catalysts have been very extensively researched over the past 50 years. The field of solid base catalysis has received relatively little attention.<sup>1</sup> The first base catalysts studied were alkali metals or metal oxides dispersed or ion-exchanged on ceramic supports, such as zeolites.

Alkali-exchanged zeolites have been shown to be useful as base catalysts for the Knoevenagel condensation (see Scheme 2.1) of aldehydes to create carbon-carbon double bonds.<sup>2</sup> Many other solid base catalysts have also been studied, including ion-exchange resins, modified silicas such as xonotlite<sup>3</sup> and hydrotalcite<sup>4</sup> and sepiolites,<sup>5</sup> and supports with surface oxynitrides.<sup>6,7</sup> Amine and ammonium groups are also effective homogeneous catalysts for the Knoevenagel condensation reaction.<sup>8</sup>

Of particular interest is catalysis requiring a strong base. Even weak bases can be used to catalyze the Knoevenagel reaction, and many of these solid base catalysts are not sufficient for more diverse reactions requiring stronger bases as catalysts.<sup>1,9</sup> Several carbon-carbon bond formation reactions are catalyzed by strong bases, such as alkali-metal alkoxides or hydroxides.<sup>1,10</sup> Reactions such as the aldol condensation (see Scheme 2.2) and Michael addition (see Scheme 2.3) can offer a method to create carbon-carbon bonds on the industrial scale, useful in the preparation of fine chemicals, if a suitable strong base heterogeneous catalyst is found.

Metal or metal oxide particles in zeolites are strong bases and have been shown to run Michael additions, whereas the weaker alkali-exchanged zeolites (NaX, CsX) cannot. However, the base sites from metal or metal oxide particles in zeolites are sensitive to carbon dioxide and moisture in air and therefore are not easily suitable for recycling.<sup>11</sup>

Leaching of the active sites over extended time is also a concern and can limit the catalyst's industrial utility.<sup>12</sup>

Rodriguez *et al.* have shown that a quaternary ammonium moiety can be grafted onto the surface of mesoporous materials, specifically MCM-41.<sup>12,13</sup> Ion-exchange of the chloride was accomplished by contact with a tetramethylammonium hydroxide solution in methanol. They demonstrated that the material was able to catalyze the Knoevenagel and aldol condensations, and the Michael addition under mild reaction conditions. The catalyst was also recyclable and stable over multiple reactions.

## 2.2 Zeolites

Zeolites are inorganic polymeric frameworks of tetrahedral alumina ( $\text{AlO}_4^{-1}$ ) and silica ( $\text{SiO}_4$ ) units (see Figure 2.1). The  $\text{SiO}_4$  unit has no net charge while the  $\text{Al}^{+3}$  substitution creates an overall negative charge on the  $\text{AlO}_4^{-1}$  unit. The negative charge from aluminum substitution causes the zeolite surface to have an overall negative charge. To balance this charge, a cation,  $\text{M}^+$ , resides within the zeolite. The cation can be either inorganic (e.g.,  $\text{Na}^+$ ,  $\text{K}^+$ ) or organic (e.g., quaternary ammonium compounds). Other heteroatoms besides Al, such as B, P, V, Ti, Zn, Mo, can also be incorporated into the zeolite matrix.<sup>14-17</sup>

The tetrahedral units are created by hydrolyzing the precursors (e.g., inorganic oxides, inorganic salts or organic sources) to make a sol-gel.<sup>18</sup> If the cation is an organic molecule (e.g., tetraethylammonium, TEA), it may also serve to direct the synthesis to a particular structure, thus that organic is called a "structure-directing agent" (SDA). The gel condenses into crystalline units. Depending on synthesis conditions (composition, temperature, time, and structure-directing agents), the crystallite units assemble into well-

defined structures (see Figure 2.2). How the crystallites assemble into long range structural order defines the framework's dimensionality (1D, 2D, or 3D pore network), pore size (3 to 18 Å) and shape, cage size (created by interconnecting multidimensional pores), and crystal size. To date, over 100 different zeolite structures have been synthesized. Each structure is assigned a three-letter identification code. Subsets within each structure code identify specific composition of heteroatoms (e.g., Al) that share the same structure.

The catalytic activity of zeolites for reactions can be tailored by properly selecting structure, cations, and framework composition (see Table 2.1). Post-synthetic treatment of the zeolite can also be done (ion-exchange with inorganic cations, calcining, and addition of guest molecules) to modify the zeolite for catalytic application. Preparation of robust, versatile and easily prepared zeolite materials for a broader range of applications has been of considerable interest.

### **2.3 Objectives**

Previous work by Jones and co-workers reported the integration of organic-functional moieties covalently tethered within zeolite \*BEA via a direct synthesis method.<sup>19-22</sup> These materials, organic-functionalized molecular sieves (OFMSs), were prepared using tetraethylammonium fluoride (TEAF) as the SDA, with a typical gel composition of 1 SiO<sub>2</sub>/ 0.03 R-Si/ 0.54 TEAF/ 7.25 H<sub>2</sub>O. A variety of functional groups, including phenethyl, cyanoethyl, iodopropyl, bromopropyl, allyl, dimethylaminopropyl, and mercaptopropyl moieties were incorporated into the \*BEA framework by adding the corresponding organosilane into the zeolite synthesis gel.<sup>20</sup> The OFMSs were characterized by TGA, <sup>29</sup>Si CP/MAS NMR, XRD, and Raman and UV-visible

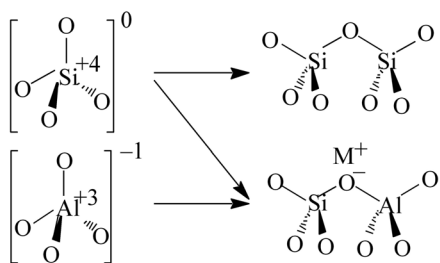
spectroscopy. The SDA, TEAF, was removed from the pores by a variety of solutions while maintaining the integrity of the zeolite structure and the organic moiety. After SDA removal, OFMSs containing acidic sites were formed by either sulphonation of phenethyl-containing OFMS or oxidation of mercaptopropyl functionality with hydrogen peroxide. The acid-containing OFMSs were shown to be useful as acid catalysts in the reaction of cyclohexanone and ethylene glycol and also demonstrated shape-selectivity in the reaction of 1-pyrenecarboxaldehyde with ethylene glycol. A more detailed discussion of the OFMS materials may be found in Chapter 2.2.3. However, no strong base (i.e., hydroxide) site has been covalently attached within a zeolite structure. The goal of this project was to incorporate a strong base site within the zeolite pore space for base catalysis.

## 2.4 References

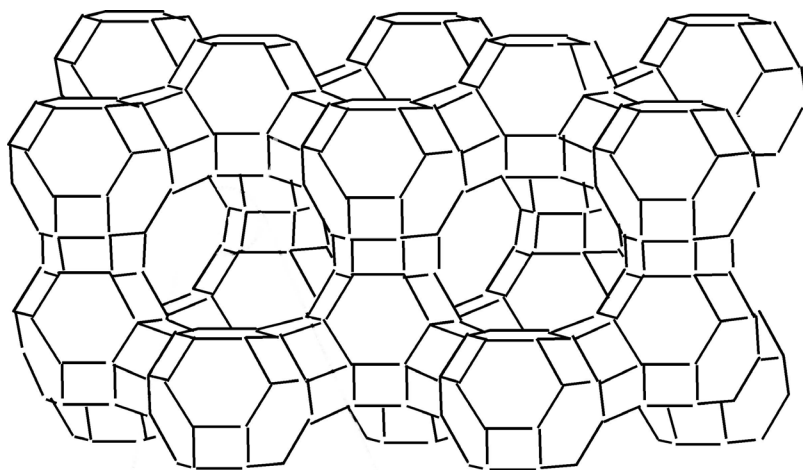
- (1) Hattori, H. *Chem. Rev.* **1995**, *95*, 537.
- (2) Corma, A. *et al.*, *Appl. Catal.* **1990**, *59*, 237.
- (3) Laszlo, P. *Acc. Chem. Res.* **1986**, *19*, 121.
- (4) Corma, A. *et al.*, *Appl. Catal., A* **1994**, *114*, 215.
- (5) Corma, A.; Martin-Aranda, R. M. *J. Catal.* **1991**, *130*, 130.
- (6) Ernst, H. *et al.*, *Appl. Catal., A* **2000**, *200*, 117.
- (7) Doskocil, E. J. *et al.*, *Catalysis* **2000**, *15*, 40.
- (8) Jones, G. In *Organic Reactions*; Cope, A. C., Adams, A., Blatt, A. H., Boekelheide, V., Cairns, T. L., Cram, D. J., Eds.; John Wiley & Sons, Inc.: New York, 1967; Vol. 15.
- (9) Kloetstra, K. R.; van Bekkum, H. *J. Chem. Soc., Chem. Comm.* **1995**, 1005.
- (10) Choudary, B. M. *et al.*, *J. Mol. Catal. A: Chem.* **1999**, *146*, 279.
- (11) Meyer, U. *et al.*, *Catal. Lett.* **1999**, *59*, 201.
- (12) Rodriguez, I. *et al.*, *Appl. Catal., A* **2000**, *194-195*, 214.
- (13) Rodriguez, I. *et al.*, *Chem. Commun.* **1999**, 593.
- (14) Dyer, A. *An Introduction to Molecular Sieves*; John Wiley & Sons: New York, 1988.
- (15) Davis, M. E.; Lobo, R. F. *Chem. Mater.* **1992**, *4*, 756.
- (16) *Catalysis and Zeolites: Fundamentals and Applications*; Weitkamp, J.; Puppe, L., Eds.; Springer: Berlin, 1999.

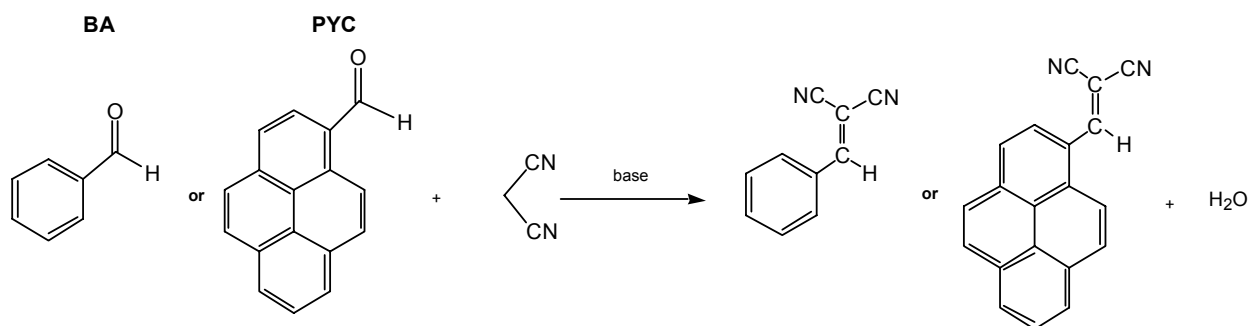
- (17) Davis, M. E.; Wagner, P. In *Photofunctional zeolites: synthesis, characterization, photo-catalytic reactions, light harvesting*; 1 ed.; Anpo, Masakazu, Eds.; Nova Science: Huntington, NY, 2000.
- (18) Brinker, C. J.; Scherer, G. W. *Sol-Gel Science: The Physics and Chemistry of Sol-Gel Processing*; Academic Press, Inc.: Boston, 1990.
- (19) Jones, C. W. *et al.*, *Nature* **1998**, 393, 52.
- (20) Tsuji, K. *et al.*, *Microporous Mesoporous Mater.* **1999**, 29, 339.
- (21) Jones, C. W. *et al.*, *Microporous Mesoporous Mater.* **1999**, 33, 223.
- (22) Jones, C. W. *et al.*, *Microporous Mesoporous Mater.* **2001**, 42, 21.
- (23) Hoffmann, T. *et al.*, *J. Am. Chem. Soc.* **1998**, 120, 2768.
- (24) Davis, M. E. *Microporous Mesoporous Mater.* **1998**, 21, 173.

**Figure 2.1** Tetrahedral zeolite precursors. Adapted from ref. 17.

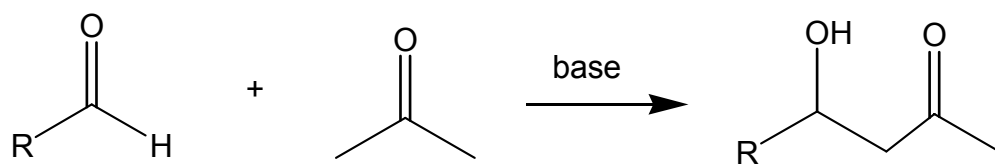


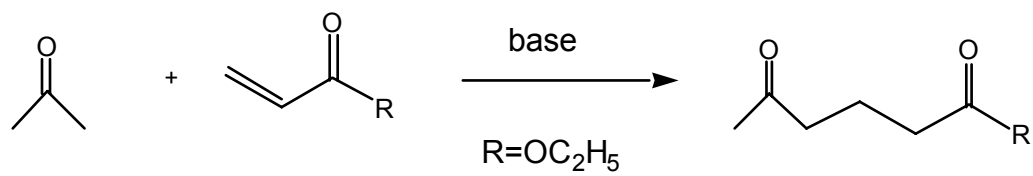
**Figure 2.2** Three-dimensional zeolite structure (Faujasite).



**Scheme 2.1** Knoevenagel condensation.

**Scheme 2.2** Aldol condensation. Adapted from ref. 23.



**Scheme 2.3** Michael addition. Adapted from ref. 11.

**Scheme 2.4** Mesoporous grafting of a quaternary ammonium-containing organosilane.

Adapted from ref. 12.

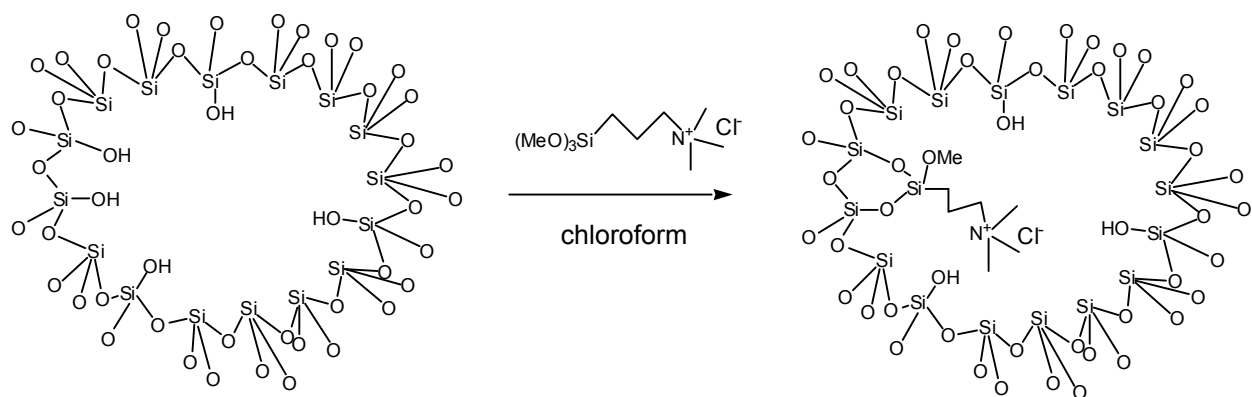


**Table 2.1** Catalytic uses for zeolites. Adapted from ref. 24.

Modification	Catalytic Site	Uses
Heteroatom Substitution	Ti (TS-1)	Epoxidations
Ion-Exchange of M <sup>+</sup>	Na <sup>+</sup> , K <sup>+</sup> , Ca <sup>2+</sup> , Sr <sup>2+</sup> , Ba <sup>2+</sup>	Weak acid/base catalysis
	Cs <sup>+</sup>	Base catalysis
	H <sup>+</sup> , Ce <sup>3+</sup> , La <sup>3+</sup>	Acid catalysis
Metal Particles	Pt, Ni, Pd	Hydrogenation

CHAPTER THREE

DESIGN AND PREPARATION OF  
ORGANIC-INORGANIC HYBRID  
CATALYSTS

Reprinted with permission from the article

[A. P. Wight, and M. E. Davis, *Chemical Reviews*, **2002**, *102*, 3589-3614]

© 2002 American Chemical Society

### 3.1 Introduction

Solid catalysts provide numerous opportunities for recovering and recycling catalysts from reaction environments. These features can lead to improved processing steps, better process economics and environmentally friendly industrial manufacturing. Thus, the motivating factors for creating recoverable catalysts are large.

Traditional heterogeneous catalysts are rather limited in the nature of their active sites and thus the scope of reactions that they can accomplish. Soluble organic catalysts can catalyze a much larger variety of reaction types than traditional solid catalysts but suffer from their inability (or high degree of difficulty) to be recycled. Since much is known about organic catalysts, the immobilization of these entities onto solids to create organic-inorganic hybrid catalysts can be accomplished with some aspects of design. The goal is to utilize the organic moiety as the active site and the solid to provide avenues to recovery and possibly recyclability of the organic active site.

These hybrids can be synthesized by a number of methods: (i) adsorption of the organic species into the pores of the support, (ii) construction of the organic molecule piece by piece within the confines of cavities of the support (the “ship-in-bottle” technique), (iii) attachment of the desired functionality to the support by covalent bond formation or (iv) direct synthesis into the final composite material. The types of solids used can be organic, e.g., polymers<sup>1,2</sup> or inorganic, e.g., silica and alumina. This review will focus on work reported since 1995 that involves the synthesis and catalytic applications of organic-inorganic hybrid materials (we will not discuss polymeric solids) where the organic functionality is covalently attached to porous inorganic solids. Organometallic complexes attached to the solids are discussed elsewhere in this issue.

Here, we specifically address the use of organic-inorganic hybrid materials for use as catalysts. A recent special issue of *Chemistry of Materials* has compiled selected topics concerning organic-inorganic composites and deals with both the materials science and catalytic applications of these materials.<sup>3</sup>

## 3.2 Organic-Inorganic Hybrid Materials

### 3.2.1 Grafting of Organic Moiety onto Solid Surfaces

There are numerous methods that have been utilized to attach organic groups to silica surfaces via the formation of covalent bonds. Chlorination of the silica surface followed by subsequent reaction with Grignard reagents can be used to form silicon-carbon bonds (Scheme 3.1).<sup>4</sup> The use of Grignard reagents limits the variety of functional groups that can be tethered to the surface. However, the formation of a silicon-carbon bond between the organic moiety and the surface is desirable because of the stability of the Si-C bond.<sup>5</sup>

Another well-studied technique of silica surface functionalization is the grafting of organic groups onto a silanol-containing surface using a trichloro- or trialkoxy-organosilane (Scheme 3.2). Numerous organosilanes are commercially available. Additionally, techniques for synthesizing organosilanes are documented in the literature (e.g., Scheme 3.3).<sup>6-8</sup> The availability of the silanol groups can determine whether the grafted silicon atom is tethered via one, two, or three silicon-oxygen bonds. These types of silicon atoms are denoted as  $T^1(\text{MeSi}(\text{OSi})(\text{OR}')_2)$ ,  $T^2(\text{MeSi}(\text{OSi})_2(\text{OR}'))$ , and  $T^3(\text{MeSi}(\text{OSi})_3)$  sites, respectively. The R' functionality can be either an alkyl or H (if water is present to cause the hydrolysis). In the absence of water, the chloro-

organosilanes require an amine, e.g., triethylamine, for the reaction with surface silanols to proceed. This is not the case with alkoxy-organosilanes.

Several reviews concerning grafting on silicas have been published.<sup>5,9</sup> Depending on the organosilane and available number of surface silanol groups, organic loadings of 0.3 to 2 mmol per g solid can be obtained.<sup>5</sup> The covalently attached organic groups can be sufficiently stable for recycling and reuse, and can easily be modified to create a variety of catalytic sites.

#### 3.2.1.1 Amorphous Solid Supports

For catalytic applications, aminopropyl-functionalized silicas have been the most widely studied organic-inorganic hybrid solids. Angeletti and co-workers showed that these hybrid organic-inorganic solids can be effective base catalysts for the Knoevenagel condensation reaction (Scheme 3.4) at room temperature in continuous flow reactors.<sup>10</sup> The aminopropyl-silica gave yields of 66 to 98% for condensations of a variety of aldehydes and cyclohexanone. The loading of the amino groups was 0.79 mmol per gram silica, and the catalyst could be recycled. The basicity of the primary amine was not sufficient to catalyze the Michael addition reaction as would be expected from soluble amine reactions. However, Angeletti *et al.* did find that in addition to the immobilization, the surface provided other effects. That is, the hydrophilic silanol groups on the surface improved reaction rates by strongly adsorbing the product water molecules.<sup>11</sup>

Macquarrie and co-workers later reported the use of aminopropyl silica as a base catalyst.<sup>12</sup> The catalyst gave yields of 8 to 99%, depending on the substrate, at levels of 10 mmol catalyst per mole substrate (Table 3.1). As expected, aldehydes showed greater reactivity than ketones, and 100% yields could be approached. The loading of amino

groups was around 1 mmol per gram silica. Yields in the ketone reactions improved as water was removed during the course of the reaction (compare entries 5 and 6 in Table 3.1). Although the catalyst could be reused by decanting of the product mixture and adding new reactants, it was deactivated after isolation from the solution and exposure to atmosphere. Infrared spectroscopy of the poisoned catalyst suggested the formation of amide groups from the reaction of the surface aminopropyl group with the ester of ethyl cyanoacetate. Additionally, the effect of solvent on the reaction rate was studied.

Increases in the polarizability of the solvent decreased the reaction rate (cyclohexane>hexane>toluene>1,2-dichloroethane>chlorobenzene). It was speculated that the low polarity solvents were favored because of the partitioning effect onto the silica surface. That is, the polarity of the surface encourages the reactants to leave the non-polar solvent phase and move to the surface to react with the amine groups.

The catalytic effects of grafted primary, secondary, and tertiary amines on silica have been investigated using base catalyzed reactions such as the nitroaldol condensation and Michael addition reactions (Schemes 2.5 and 2.6, respectively).<sup>13</sup> It was found that in the supported amine systems, the catalyst activity followed the order: primary>secondary>tertiary. A mechanism for the nitroaldol condensation on the supported catalyst was hypothesized based on previous reports of imine formation with this type of catalyst in solution (Scheme 3.7).<sup>14</sup> Experimental results from infrared spectroscopy of the working catalyst were consistent with the proposed mechanism.<sup>13</sup> Variations in the substitution of the aromatic ring of the aldehydes showed little effect on the yield and selectivity of the aminopropyl-functionalized silica catalyst.

Utting and Macquarrie have investigated the use of the imine-based active sites for catalyzing the Knoevenagel condensation and Michael addition reactions.<sup>15</sup> A variety of imine supported silicas were prepared by modifying grafted aminopropyl silicas (Scheme 3.8). IR spectroscopy confirmed the imine formation by the appearance of bands in the range of 1690 to 1640  $\text{cm}^{-1}$ . Yields in the Knoevenagel condensation of pentan-3-one and ethyl cyanoacetate ranged from 23% to 99% after 5 to 6 hours, depending on the substituent on the imine catalyst (Table 3.2). Substituent effects were shown to be significant in the activity of the catalyst. The Michael addition reaction of nitromethane and 2-cyclohexen-1-one gave yields of 45 to 58% for some of the imine catalysts tested. The stability of a phenolate-based catalyst showed that the imine bond was intact in alcohol solutions, but was cleaved in acidic or basic solutions. Most of the bond cleavage (40 to 60% of phenolate groups lost) occurred within the first 5 hours of contact with the solution media.

More recently, Macquarrie and co-workers examined guanidines tethered to silica as base catalysts for epoxidation reactions.<sup>16,17</sup> The guanidine functional groups were attached either by modification of a grafted chloropropyl group or by synthesis of the guanidine silane with subsequent grafting (Scheme 3.9). Conversions of cyclohexenone to epoxide ranged from 40 to 85%, depending on the support and method of tethering. The grafted guanidine silane-based amorphous silica had a loading of 1.1 mmol per g solid. These catalysts gave 55% conversion and the lowest selectivity to epoxide (42%). A guanidine-based catalyst prepared by grafting onto MCM-41 (which is referred to as “Micelle Templated Silica,” MTS), had both improved conversion and selectivity (85 and 65%, respectively) compared to the amorphous silica. It was observed that passivation of

the surface hydroxyl groups by *N,O*-bis-trimethylsilylacetamide was required in order to prevent significant decomposition of the hydrogen peroxide that was used as the oxidant. Passivation of the unreacted silanol groups was performed after grafting of the chloropropyl group. All of the guanidine-based catalysts produced a number of side products. One of the major side products, 3-methoxycyclohexanone, was formed by the Michael addition of the solvent, methanol, to cyclohexenone. A change of solvent to isopropanol resulted in higher selectivity of 93% to the epoxide, but the overall conversion decreased to 34%.

Using guanidine grafted hybrid silicas, Macquarrie *et al.* reported the ability to catalyze the Linstead variation of the Knoevenagel condensation to react malonic acid with aldehydes (Scheme 3.10).<sup>17</sup> The guanidine catalysts were used to promote this reaction instead of triethylamine that typically functions as both catalyst and solvent. High temperatures are usually required for the homogeneous reaction. The elevated temperatures normally cause the malonic acid to degrade by decarboxylation, and excess quantities of the acid must be used to achieve desirable amounts of product. The supported guanidine catalyst gave conversions of 78 to 95%, with selectivities of 50% using only stoichiometric amounts of malonic acid.

Acid functional groups have also been used as organic modifiers to silica surfaces. Harmer and co-workers have attached a perfluorosulfonic moiety onto silica for use in acid catalysis applications.<sup>18</sup> The perfluorosulfonic group is a strong acid and has excellent chemical and thermal stability. The perfluorosulfonyl fluoride silane (Scheme 3.11) was synthesized in a manner similar to the hydrosilylation procedure previously described (Scheme 3.3), using the corresponding olefin. The acid sites were generated by

hydrolysis of the perfluorosulfonyl fluoride functionality. Harmer also reported the use of the perfluorosulfonic acid silane in the co-condensation of silica, using traditional sol-gel techniques. Activities of both the grafted and co-condensed silica hybrids were reported as similar. The grafted acid catalyst was tested in several acid-catalyzed reactions, such as aromatic alkylation, alkene isomerization, and Friedel-Crafts acylation, and the respective conversions were 99, 95, and 89%. In the alkylation and isomerization reactions, the hybrid catalyst significantly outperformed some of the alternative solid resin catalysts currently used, e.g., Nafion resin NR 50 and Amberlyst-15. The hybrid catalyst achieved a conversion of 43% for the alkylation of benzene with dodec-1-ene at 80°C for one hour, conditions where the traditional acid resins gave 3 to 5%. It is interesting to note that the acid loadings of the solid catalysts are 0.2, 0.9 and 4.6 mequiv H<sup>+</sup> per gram catalyst for the hybrid silica, Nafion NR 50, and Amberlyst-15 resins, respectively. In spite of lower number density of acid sites, the hybrid silica catalyst still outperformed the resins in the reactions reported.

### 3.2.1.2 Ordered, Mesoporous Solids

The amorphous solids discussed above have large distributions in pore diameters and void volumes. The ordered mesoporous materials, e.g., the M41S family of solids,<sup>19,20</sup> have relatively uniform pore sizes and void volumes. The pore sizes of these materials can be tailored based on the synthesis method used and can range from about 15 to 100 Å. Larger pore sizes of 50 to 300 Å can also be obtained in the SBA family of solids, e.g., SBA-15.<sup>21,22</sup> The ordered, mesoporous materials can serve as more well defined supports than amorphous solids onto which organic groups can be grafted.

The grafting of organic functional groups onto ordered, mesoporous materials has been accomplished and these hybrid solids have been used as catalysts.<sup>5,20,23,24</sup> Numerous functionalized propyltrialkoxo silanes have been employed to tether organic moieties onto the mesoporous silicas, and <sup>13</sup>C MAS NMR was used to verify the integrity of the grafted groups. Additionally, nitrogen sorption isotherms reveal decreased amounts of pore volume as the grafted organic moiety size increased.<sup>25</sup>

Grignard reagents can be used in functionalizing mesoporous materials.<sup>26</sup> In addition to the chlorinating procedures mentioned above for amorphous silicas (Scheme 3.1), esterification of the surface can be accomplished with alcohols (Scheme 3.12). The etherification prevents surface silanol groups from reacting with the Grignard reagent to form Si-O-MgX bonds. The Grignard reagent cleaves Si-OR' functionalities to form a carbon moiety attached directly to surface Si. However, this procedure gave surface silicon atoms with multiple organic groups attached (Me<sub>2</sub>Si(OSi)<sub>2</sub> and Me<sub>3</sub>Si(OSi)). The formation of these sites was attributed to the breaking of the framework Si-O bonds. It was speculated that the harshness of the refluxing alcohol temperatures for the esterification caused the cleavage and hydrolysis of the Si-O-Si framework bonds. Replacement of butanol with methanol to lower the refluxing temperature eliminated Me<sub>3</sub>Si(OSi) sites, but not Me<sub>2</sub>Si(OSi)<sub>2</sub> sites, indicating that some framework hydrolysis still occurred. Bulkier substituents on the Grignard reagents gave lower organic incorporation in the final organic-inorganic hybrid material.

Traditional catalysts for  $\alpha$ -monoglyceride synthesis (Scheme 3.13) are tertiary amines and ammonium salts, but they are difficult to isolate from the product. Brunel and co-workers introduced amine species into MCM-41 silicas by the grafting method

and used the solids as base catalysts (Scheme 3.14).<sup>27</sup> The materials were analyzed by IR and MAS-NMR spectroscopy, elemental analysis and thermogravimetry. Pore sizes of around 31 Å and high pore volumes were obtained. Pure-silica MCM-41 and chloropropyl-grafted MCM-41 did not provide catalytic activity as expected. However, it was shown that the surface silanol groups caused the glycidol to polymerize. For the amine-containing catalysts, the polymerization competed with monoglyceride synthesis to give yields of 16 to 70% monoglyceride. The piperidine-functionalized MCM-41 was more active than the primary amine-containing solid. The steric hindrance around the piperidine was speculated to prevent the glycidol from reaching the surface, and thus limited the side polymerization to give improved yields. Unreacted silanol groups were passivated by the addition of hexamethyldisilazane vapor. Poisoning of the surface silanol sites increased the yields from 62 to 90%.

Amine-containing-MCM-41 mesoporous materials were studied by Brunel and co-workers as catalysts for the Knoevenagel condensation of benzaldehyde and ethyl cyanoacetate.<sup>14</sup> Nucleophilic displacement of chloro- and iodopropyl-MTS materials by piperidine were used as catalysts and compared to piperidine alone as a homogeneous base catalyst. The solids were investigated by IR and <sup>13</sup>C MAS NMR spectroscopy, X-ray diffraction, and nitrogen sorption. Organic loadings of 0.7 to 1.7 mmol per gram were obtained and the available pore volume decreased with increased functional group size. The primary amine was more active than piperidine, nearing 100% yield after 2 hours. A mechanism was proposed that involved imine formation of the primary amine with the aldehyde (similar to the nitroaldol condensation shown in Scheme 3.7). This

mechanism was supported by the observed activity of the primary vs. tertiary amine.

Both catalysts (aminopropyl and piperidinopropyl) were recyclable.

Sartori and co-workers used aminopropyl-functionalized MCM-41 as a catalyst for the nitroaldol condensation of aldehydes and nitroalkanes.<sup>28</sup> The activities of the amine sites were found to follow the order primary>secondary>tertiary (98, 34, 5% yields, respectively, under identical reaction conditions). The mechanism for the reaction was speculated to be through the formation of an imine, as described above. Recycling of the primary, aminopropyl catalyst was reported, and consecutive yields of 98, 95, 95, 90, and 84% in 5 sequential reactions were obtained.

Jacobs and co-workers introduced a guanidine moiety into MCM-41 via grafting methods.<sup>29</sup> MCM-41 (or amorphous silicas) were grafted with trimethoxysilylpropoxymethyloxirane, then reacted with 1,5,7-triazabicyclo[4.4.0]dec-5-ene (TBD) to create guanidine base catalysts (Scheme 3.15). The investigators used an oxirane ring opening reaction to attach the TBD in order to take advantage of mild synthesis conditions (298 K for 10 hours) and to prevent the formation of acids (HCl and HBr) that could poison the base sites. Successful synthesis of the hybrid material was verified by NMR and IR spectroscopies and nitrogen sorption. The catalyst was active for the Michael addition of ethylcyanoacetate or diethyl malonate to various ketones and enones, and gave yields of 34 to 100%. Reaction conditions were mild (313 to 353 K), and the rates were fast (reaction completed in 0.5 to 5 hours). The most difficult reaction was the addition of diethyl malonate to cyclohexenone, which required 60 hours to achieve only 2.7% yield at 353 K. Additionally, the reaction of ethylcyanoacetate with methyl vinyl ketone gave 34% yield using the TBD-containing

MCM-41 solid, but only 7% for the TBD-containing amorphous silica-hybrid under identical reaction conditions. It was speculated that, in general, the MCM-41 hybrids are more active as catalysts than the amorphous silica counterparts due to higher organic loadings. The utility of the MCM-41 hybrid was further demonstrated by use in the Knoevenagel condensation of ethylcyanoacetate or malononitrile with various aldehydes at extremely mild conditions (293 to 343 K). Yields ranged from 9 to 98%, depending on the reactants.

Kantam and Sreekanth have recently used the TBD-containing MCM-41 hybrid materials as base catalysts to perform transesterifications of  $\beta$ -keto esters.<sup>30</sup> The hybrid materials were prepared by grafting of trimethoxysilylpropoxymethyloxirane onto MCM-41 and subsequent modification with TBD, as described above (Scheme 3.15). The TBD-containing materials were active as catalysts for transesterifications by a wide variety of alcohols, giving yields of 45 to 100%, depending on the ester and alcohol. The catalyst was active with primary, secondary, tertiary, allyl, and alkynic alcohols, where they were aliphatic (saturated and unsaturated) or aromatic. The catalyst was recyclable for several reaction cycles, showing only slight loss in yield.

Recently, imidazole groups were grafted onto mesoporous materials for use as base catalysis in the Knoevenagel condensation between ethylcyanoacetate and benzaldehyde.<sup>31</sup> The immobilization was performed through an alkoxy silane linking, (3-glycidyoxypropyl)trimethoxysilane, similar to the guanidine work by Jacobs *et al.* (Scheme 3.16). The mesoporous materials MCM-41, MCM-48, KIT-1, SBA-1, and SBA-15 were used as the supports. Functional group attachments were verified by IR spectroscopy. Loadings on KIT-1 of 0.65 to 1.80 mmol per gram of support were

obtained. About 50% of the glycidyoxypropyl functionalities reacted with imidazole to form a supported base moiety. Conversion with the imidazole-KIT-1 catalyst was 64%, which is less than the homogeneous imidazole-catalyzed reaction (96%) at similar reaction conditions. Repeated use of the solid catalyst showed a decrease in conversion. It was speculated that the active sites were poisoned due to benzoic acid contamination in the benzaldehyde. Treatment of the recycled catalyst with 2% KOH/ethanol improved its reactivity.

Corma and co-workers grafted a quaternary ammonium-containing organosilane onto MCM-41 silicas<sup>32,33</sup> for use as a Brønsted base catalyst. A commercially available quaternary ammonium chloride organosilane was grafted onto MCM-41, followed by ion-exchange to the hydroxide form. Ion-exchange of the chloride to hydroxide was accomplished with a 0.21 M solution of tetramethylammonium hydroxide (TMAOH) in methanol (MeOH). Ion-exchange was allowed to occur for 10 minutes, after which the solids were isolated and washed thoroughly with MeOH. The structure of MCM-41 remained intact after the ion-exchange, and <sup>29</sup>Si MAS NMR and elemental analyses indicated no leaching of organic groups occurred. Most of the quaternary sites were exchanged to hydroxyl anions.<sup>33</sup> The organic loadings were 0.88 to 1.22 mmol per gram, and the catalysts were active for the Knoevenagel condensation of benzaldehyde and ethyl cyanoacetate, giving conversions of 77 to 88% after 2 hours at 60°C in CHCl<sub>3</sub> as solvent.<sup>32</sup> Rodriguez *et al.* showed that good yields were obtained with high polarity solvents (EtOH>CH<sub>3</sub>CN>HCCl<sub>3</sub>>Cl<sub>4</sub>C).<sup>33</sup> However, conversions improved to 90 to 95% in 30 minutes under solvent-free conditions. Recycling of the catalyst showed no deactivation or leaching. The initial rates of reaction were proportional to the number of

organic moieties, indicating full accessibility of the organic groups within the support. Michael addition reactions of various ketones with ethyl cyanoacetate were also accomplished with these grafted solids. The catalysts were very selective for the Michael addition product. Conversions of 35 to 72% were obtained within a few hours, at temperatures ranging from 20 to 80°C. These reaction conditions were more mild than those used with other solid base catalysts such as Cs-MCM-41.<sup>34</sup> The hybrid solid was also able to catalyze the aldol condensation and subsequent intramolecular Michael addition of benzaldehyde and 2'-hydroxyacetophenone to yield flavanone at 130°C in a solvent-free reaction (Scheme 3.17).<sup>33</sup> Conversion of 65% with a 78% selectivity was obtained in 8 hours.

Rodriguez *et al.* reported the use of their Brønsted base catalyst in the synthesis of chromenes and coumarins (useful as pharmaceutical intermediates, dyes, and fragrances).<sup>33</sup> These compounds can be synthesized by the base-catalyzed condensation of salicylaldehydes with diethyl 2-pentenedicarboxylate (Scheme 3.18). Use of the hybrid solids as catalysts produced the chromene with selectivities as high as 90%. Conventional liquid bases, such as piperidine, have greater selectivity to coumarins. Rodriguez *et al.* speculated that a mechanism such as described in Scheme 3.19 could explain the observed behavior. The intermediate phenoxide anion was formed in both pathways, but the subsequent cyclization to chromene was faster than to coumarin. The formation of coumarin involved the elimination of an ethoxy group. In order for the coumarin to preferentially be formed, the ethoxy leaving group must be stabilized; a strong base catalyst can effect this stabilization. Rodriguez and co-workers used dimethyl amine naphthalene (DMAN) as a base catalyst to probe the reaction mechanism

in an attempt to explain the observed selectivity. The basicity of the DMAN could be controlled by choice of solvent. Results showed that the chromene pathway is preferred for base catalysts of lower strength, while coumarins are formed with stronger bases, as expected from the proposed mechanism. TMAOH in solution is a stronger base than the hybrid solid, and it showed greater selectivity to the coumarin formation.

Catalysts for use in triphasic reactions have also been prepared by immobilizing phase transfer catalysts (PTC) onto silica.<sup>35</sup> The immobilization of  $P^+R_4X^-$  or  $N^+R_4X^-$  onto a solid allows the quaternary site to act at the phase boundary between an organic and aqueous phase.<sup>36</sup> The heterogenization of the organic catalyst allows for easy recovery, which is not often possible with the homogeneous equivalent.<sup>36</sup> Traditional triphasic, heterogeneous catalysts are phase transfer catalysts immobilized onto polymer resins, and chemical and thermal stability are often major issues with the resin catalysts. The inorganic solids are normally more stable to harsh chemical environments and higher temperatures. Phase transfer silica-based catalysts were synthesized by first being chlorinated with carbon tetrachloride at elevated temperature (Scheme 3.20).<sup>35</sup> Functionalization via brominated Grignard reagents was then performed. Finally, after washing and drying, the functionalized silica was reacted with triphenylphosphine under reflux. The quaternization reactions were catalyzed by either nickel (II) bromide trihydrate ( $NiBr_2$ ) or palladium diacetate ( $Pd(OAc)_2$ ). The hybrid solids were characterized by  $^{13}C$  MAS NMR, elemental analyses, and IR spectroscopy. Organic loadings were approximately 0.4 mmol brominated functional group per gram at the intermediate step and 0.3 mmol quaternarized phosphonium in the final catalyst (based on elemental analyses). Clark and co-workers showed that the catalysts were thermally

stable, recyclable, and active for nucleophilic substitution and oxidative bromination reactions. Decomposition of the phosphonium group was observed only at temperatures over 300°C. The unsupported phase transfer catalysts catalyzed the oxidative bromination of benzene in the presence of hydrogen peroxide with yields of 24 to 44% in one hour. Silica-supported PTCs also catalyzed this reaction and were recyclable, although they had lower activity (5% yields). The yields could be improved to 16% by pretreating the catalyst with ultrasound to remove trapped gas pockets. The hybrid solids also overcame poor solubility issues with traditional PTCs and worked in a greater variety of solvents.<sup>5</sup>

Acid sites have also been incorporated into ordered, mesoporous materials. Jacobs and co-workers prepared acid-containing hybrid solids by both grafting and co-condensation (see below) methods.<sup>37,38</sup> When preparing the hybrid materials by grafting, MCM-41 silicas were first grafted with 3-mercaptopropyltrimethoxysilane (MPTS).<sup>38</sup> The materials were characterized by IR (to show the S-H vibration at 2575 cm<sup>-1</sup>) and <sup>13</sup>C MAS NMR. It is noteworthy to mention that dimerization of the thiol groups can occur at the relatively high functional loadings obtainable in mesoporous materials. The resulting disulfide groups were detected in small amounts by <sup>13</sup>C MAS NMR. The thiol functionalities were then oxidized into sulfonic acid groups by hydrogen peroxide (Scheme 3.21). Functional group loadings were 1.0 to 1.5 mmol sulfonic acid sites per gram silica, as determined by TGA and titration. The percentage of mercaptopropyl groups that were oxidized to acid sites was not reported. The acid catalysts were tested in the reaction of 2-methylfuran with acetone to produce 2,2-bis(5-methylfuryl)propane (DMP) (Scheme 3.22). Acidic zeolites (H-USY, H-\*BEA) were used for comparison to

the hybrid solid and quickly deactivated due to oligomerization of the furan. The sulfonic acid-functionalized mesoporous materials showed conversions of about 57% with selectivities of 92%. The recyclability of the catalysts was not reported.

Brunel and co-workers tethered a 2,2,6,6-tetramethyl-1-piperidinyloxy (TEMPO) moiety onto MCM-41 silica by various grafting methods.<sup>39</sup> TEMPO is a useful homogeneous catalyst for oxidation of alcohols to aldehydes and carboxylates under mild reaction conditions. Previous work in heterogenizing TEMPO involved the immobilization of TEMPO onto supports such as polymers and amorphous silicas. The mesoporous support has a greater surface area, a highly ordered pore structure, and large number of available silanol sites for grafting compared to the previously utilized solids. The synthesis of the TEMPO hybrids is schematically outlined in Scheme 3.23. Loadings of 1 to 2 mmol aminopropyl groups per gram solid were obtained, as determined by elemental analysis and TGA. Of these groups, about 0.4 to 0.8 mmol TEMPO per gram solid were obtained after modification. The direct grafting of the TEMPO organosilane yielded about 0.6 mmol TEMPO per gram, as determined by TGA.

The oxidation of  $\alpha$ -methyl glucoside, benzyl alcohol, and 1,4-pentanediol were catalyzed by the TEMPO hybrids in aqueous solution.<sup>39</sup> The  $\alpha$ -methyl glucoside was oxidized to 1-*O*-methyl glucuronate at 0°C with NaOCl, giving almost 100% conversion within 30 minutes for both the ether- and amide-TEMPO-MCM-41 catalysts. The selectivity was over 95% to the carboxylic acid product. No leaching of the TEMPO groups was observed. The catalysts were also useful in the reaction of benzyl alcohol with oxygen and copper (I) chloride in DMF. Conversion over the ether-TEMPO-MCM-41 was 35%, and selectivity to benzaldehyde was 99%. Under similar conditions, the

homogeneous TEMPO gave 94% conversion and 99% selectivity. The small amount of water present in the reaction media prevented the over oxidation to benzoic acid. The lower activity of the supported TEMPO is reasonable because the proposed mechanism of the reaction requires two adjacent TEMPO molecules to be involved in a disproportionation step. The organic loading in the MCM-41 material was not sufficient to have a significant number of TEMPO moieties in close proximity to each other. Oxidation of the 1,4-pentanediol to  $\gamma$ -valerolactone was also catalyzed by the TEMPO-containing hybrid solids, giving 50% conversion with over 95% selectivity. The amide-TEMPO-MCM-41 was treated with hydrogen bromide prior to reaction to transform unreacted aminopropyl groups into ammonium bromides. Prior work has shown that the presence of these ammonium species can improve catalytic activity in the diol oxidation. As expected, the HBr treated amide-TEMPO-MCM-41 was more active than the untreated material and gave 99% conversion with over 95% selectivity under similar conditions to the ether linked TEMPO.

Chiral functionalities can also be grafted into silicas through similar techniques as described above. Brunel and co-workers have introduced chirality into mesoporous silicas via the grafting method.<sup>40-45</sup> The chiral hybrid catalysts were then used to perform enantioselective reactions. Bellocq *et al.* described the immobilization of the chiral amino-alcohol (-)-ephedrine on MCM-41-type silicas via nucleophilic modification of the halopropyl groups.<sup>40</sup> Reaction of a chloropropylsilane with ephedrine yielded the desired ephedrine organosilane, but cyclization of the silane also occurred by replacement of the alkoxy groups on silicon with the hydroxyl group of the ephedrine (Scheme 3.24). A cleaner reaction was possible when the substitution occurred after grafting of the

chloropropylsilane onto the MCM-41 solids. Although chloropropyl group loadings on the mesoporous materials was 1.2 to 1.4 mmol per gram, only 58 to 76% of these were displaced by ephedrine. The ephedrine loadings ranged from 0.83 to 0.88 mmol per gram. Similar grafting of amorphous silica had lower overall functional group loadings (due to lower density of surface silanol groups) of 0.5 to 0.9 mmol per gram chloropropyl moieties. However, a higher percentage of 60 to 84% of the chloropropyl moieties tethered on amorphous silica were displaced by ephedrine during modification, giving 0.44 to 0.53 mmol per gram ephedrine. Bellocq *et al.* concluded that the greater steric hindrance in the mesopores of MCM-41, compared to amorphous silica, hindered the nucleophilic attack by ephedrine. The ephedrine hybrids were then used in enantioselective addition reactions (Scheme 3.25). Amorphous silica hybrids produced high selectivities to the 1-phenyl-propan-1-ol of 80 to 85%, but had low enantiomeric excess (ee) of 11 to 22%. The MCM-41 hybrids also gave 84 to 87% selectivity but had 37% ee. Bellocq *et al.* noted that residual alkoxy groups on the functionalized MCM-41 surface for the organosilane grafting needed to be hydrolyzed by NaHCO<sub>3</sub> in methanol prior to addition of the ephedrine to prevent the cyclization products (as described above). Removal of the residual alkoxy groups improved the selectivity to 91% with an ee of 40%.

Further work improved the surface coverage of organic groups by utilizing a sol-gel method of functionalizing aluminosilicate mesoporous materials, Al-MTS.<sup>45</sup> The Al-MTS materials were exposed to chloropropylsilane in toluene in the presence of water and NH<sub>4</sub>F-*p*TsOH. The chloropropyl moiety loadings were increased from 2.1 mmol per gram via traditional anhydrous conditions to 4.4 mmol per gram by the new tethering

procedure. Modification by (-)-ephedrine then resulted in increased loadings of 1.9 mmol per gram for chloropropyl-containing Al-MTS prepared by the new technique (as compared to 1.3 mmol per gram for chloropropyl-containing Al-MTS from anhydrous methods). The increased organic loadings greatly reduced the available void space within the materials; Al-MTS supports of larger initial pore diameters (8.3 nm instead of 3.6 nm) were then used. The catalysts were studied in enantioselective addition reactions (Scheme 3.25). The ephedrine-containing Al-MTS catalysts prepared by anhydrous techniques gave 93% selectivity and 47% ee, similar to the ephedrine-containing MTS silicates described above. However, the ephedrine-containing Al-MTS catalysts prepared by the sol-gel method gave 98% selectivity and 64% ee. These results were comparable to that of the homogeneous (-)-ephedrine catalyst, that gave 98% selectivity and 65% ee. The improved activities and enantioselectivity of the ephedrine-containing Al-MTS catalyst was attributed to the higher organic coverage of the surface (preventing racemic reaction on unfunctionalized surfaces) and the larger initial pore diameter, which allowed for increased accessibility to the active sites on the support.

Lasperas *et al.* compared the (+)-ephedrine-modified MCM-41 materials to (-)-ephedrine.<sup>42</sup> As previously discussed, the (-)-ephedrine MCM-41 hybrid gave 37% ee to the (R)-isomer at conversions of 89 to 99% with selectivities of 84 to 89% to the secondary alcohol. The (+)-ephedrine hybrid yielded the (S)-1-phenyl-propan-1-ol, in 26% ee, with similar conversions and selectivities. This suggests that the heterogeneous, chiral solids conform to the asymmetric induction observed in homogeneous chiral catalysts.

Recently, Kim *et al.* reported the anchoring of a proline derivative onto mesoporous silicas for use as catalysts in the preparation of chiral secondary alcohols.<sup>46</sup> The proline moiety was incorporated by modification of grafted chloropropyl species on amorphous silica, MCM-41 and SBA-15. The surface silanol groups were passivated by hexamethyldisiloxane (HMDS) after grafting of the chloropropyl silane to prevent sites for racemization to occur. The mesostructures of both MCM-41 and SBA-15 were stable throughout the modification procedure as observed by XRD. Nitrogen adsorption data showed that the MCM-41 samples had pore diameters of 23 to 24 Å; the SBA samples had diameters around 85 Å. <sup>13</sup>C CP/MAS NMR confirmed the integrity of the proline functional groups after grafting and modification. The catalytic properties of these hybrids were tested in the asymmetric addition of diethylzinc to benzaldehyde in the presence of *n*-BuLi. The analogous homogeneous reaction system resulted in 87% yield with 93% ee. Grafting of the proline onto amorphous silica gave 41% ee at only 69% yield. Passivation of the surface with HMDS after grafting slightly improved results (43% ee and 74% yield). The MCM-41 hybrids showed better results of 84 and 96% yield (not passivated and passivated, respectively) and ee's (26 and 64%). SBA hybrids were the best catalysts of all, with 52 and 75% ee and 97 and 98% yield for not passivated and passivated surfaces, respectively.

### 3.2.1.3 Microporous Molecular Sieves

The grafting of various organic moieties onto zeolites has been reported.<sup>47</sup> In general, modification of zeolites by organosilanes has been used to passivate the silanol groups on the external surface or to adjust the pore diameter. Brunel and co-workers functionalized zeolite Y (calcined and dealuminated) of various Si/Al ratios with

3-chloropropyltrimethoxysilane (CPS) and 3-aminopropyltriethoxysilane (APS) to study the influence of the Al sites and pore size on the grafting.<sup>47</sup> Modification of the amine-functionalized zeolites was then performed by the addition of 4-anisoyl chloride and 2,3-butanedione. The samples were characterized by elemental analyses, IR, <sup>13</sup>C MAS NMR, adsorption, XRD and TGA.

The micropore volume of the zeolite Y solid decreased substantially by one-third or more after functionalization (Table 3.3).<sup>47</sup> Subsequent modification of the amine groups further reduced the pore volume. Organic loadings were 0.97 to 1.48 mmol per gram, as determined by TGA. Modification of the amino-groups appeared to occur on about half of the amines (organic loadings of 0.46 to 0.61 mmol per gram; however, the elemental analyses were inconsistent with the TGA data). Comparisons of available external and internal surface areas of the solid, before and after treatments, suggest that most of the functionalization occurs on the external surface and at the pore mouths of the zeolite. Diffusion limitations of the organosilanes and the high reactivity of the silanes likely produces reaction at the silanol functional groups around the openings of the pores and prevents penetration within the crystal. Most of the micropores and inner cavities of the zeolite would then be blocked by the deposited organosilane. Brunel *et al.* pointed out that larger, sterically-hindered functional groups are much more easily grafted and are more accessible catalytic sites for mesoporous materials than in zeolites.<sup>48</sup> Functionalization on the external surface of the zeolite eliminates shape-selectivity and nullifies some of the motivation behind using zeolites in catalysis.

### 3.2.2 *Direct Incorporation of Organic Moiety: Ordered, Mesoporous Materials*

Although grafting of organosilanes onto surfaces through hydroxyl groups is a well-studied and an often used method of forming organic-inorganic hybrid materials, the tethering is done by covalently attaching the organosilane to a surface silicon atom through the silicon (surface)-oxygen-silicon (external)-carbon bond in the organosilane (Scheme 3.2). The silicon-oxygen bond is then external to the surface and can be cleaved at conditions encountered in some catalytic reactions.<sup>4</sup> Obviously, if this occurs the solids will not be able to function as recyclable catalysts. It would be desirable to have the carbon bound directly to a silicon atom on the surface. By incorporating the organosilane into the synthesis mixture during the formation of the solid, the functional group presents itself of the surface and the silicon in the silicon-carbon bond in the organosilane is on the surface of the material (Scheme 3.26). This forms a more uniform dispersion throughout the solid. In this “one-pot” method, the organosilanes are co-hydrolyzed and condensed with other silica reagents, e.g., tetraalkoxysilanes, water, and the appropriate organizing molecules (used for the synthesis of ordered, mesoporous materials and zeolites), to create the synthesis mixture. Issues of importance when selecting the preparation conditions include the solubility of the organosilane in the mixture, stability of the organic functional group under reaction conditions (pH, temperature), ease of organizing molecule (structure directing agent, SDA) extraction (for ordered, mesoporous materials and zeolites) and stability of the organic functional group during the extraction process. High loadings of functional groups (up to 3 mmol per gram catalyst) can be obtained by co-condensation.<sup>5</sup>

In order to have a useful catalyst after synthesis, one must be able to extract the organizing molecules (Scheme 3.26) from within the pores to create porosity; calcining the material would destroy the incorporated functional groups. Extraction techniques have been developed for both mesoporous and microporous materials.<sup>49-53</sup> Extraction of the SDA can be most effectively accomplished by acidic methanol solutions.<sup>37</sup> Ordered, mesoporous materials can be designed with specific pore sizes based on the SDA and organic functionality used, but there is a lower limit to the pore size (ca. 15-20 Å). Several reviews concerning advances in co-condensation of mesoporous hybrid materials have been published.<sup>5,9,54</sup>

Mann and co-workers reported the first incorporation of organic groups into mesoporous materials by co-condensation methods.<sup>55</sup> Phenyl- and *n*-octyl-functionalities were incorporated into MCM-41 silica by the “one-pot” method using TEOS as the silica source and hexadecyltrimethylammonium bromide (C<sub>16</sub>TMABr) as the SDA. The SDA was extracted in acidified ethanol at 75°C for 24 hours. The structure of the phenyl-MCM-41 material was preserved throughout the extraction as observed by XRD. Octyl-MCM-41 was less stable to the extraction process than the phenyl-MCM-41. The mole percent of organosilane was varied to determine its effect on the assembly of MCM-41. Phenyl-functionalized MCM-41 was prepared with concentrations as high as 20 mole %, while the *n*-octyl-functionalized material remained high quality for up to 10% organosilane. TEM images of the materials confirmed the hexagonal structure, and nitrogen sorption data showed a decrease in pore size from 30 Å for all-silica MCM-41 to 24 and 18 Å for the 10 and 20% phenyl-MCM-41 materials, respectively. This work showed the possibility of directly tethering an organic functionality to the walls of the

ordered mesoporous silicate (organic groups and presence of Si-C bond confirmed by IR and NMR studies). Slade and co-workers later showed that the addition of swelling agents, such as mesitylene, could be used in the phenyl-MCM-41 synthesis to increase the pore size of the material to around 30-40 Å.<sup>56</sup>

Mann *et al.* synthesized MCM-41 materials with other functional groups such as mercaptopropyl, amine, epoxide, imidazole, and allyl.<sup>49</sup> MCM-41 silicas were prepared by using various organosilanes and C<sub>16</sub>TMABr as the SDA at conditions of basic pH. The amine and imidazole organosilanes were also incorporated into a neutral synthesis gel using *n*-dodecylamine as the SDA. Hexagonal ordered phases were obtained and characterized by XRD. Structural order was lost at concentrations approaching and exceeding 20%. Also, the basic synthesis procedures produced more ordered materials than did neutral pH synthesis method. The SDAs were extracted by acidic alcohol solutions. The amine and mercaptopropyl functionalized MCM-41 silicas were stable to extraction; however, the epoxide, imidazole, and allyl silicas lost structural order. The amount of organic incorporation, as determined by <sup>29</sup>Si NMR, increased as the concentration of organosilanes increased, and <sup>13</sup>C CP/MAS NMR revealed that the most of the organic groups were still intact after synthesis and extraction. Because of the alkaline conditions of the synthesis gel, the epoxide ring opened to form a diol, and the acidic extraction then substituted the β hydroxyl with a chloride.

Hall *et al.* have reported the synthesis of a bifunctional mesoporous material via the co-condensation method.<sup>57</sup> Phenyltriethoxysilane and various other organosilanes (allyl, amino- and mercapto-propyl) were added to TEOS in the presence of C<sub>16</sub>TMABr (SDA) under basic synthesis conditions. Ordered MCM-41 phases were obtained for materials

with 20% total organosilane or less (by XRD).  $^{29}\text{Si}$  CP/MAS NMR established the presence of  $\text{T}^n$  sites. An increase in the  $\text{T}^n$  sites was observed as the amount of organosilanes in the gel increased. The SDA was removed by acidic ethanol extraction at refluxing conditions. After extraction, the bifunctional materials were less ordered.  $^{13}\text{C}$  CP/MAS NMR verified the functional groups were intact. The combination of phenyl and aminopropyl functionalities gave the most stable hybrids, while phenyl and allyl functionalities provided the highest structural disorder. Pore diameters were reported to be *ca.* 35 Å for the bifunctional materials. Work was also performed with co-condensation methods to produce functionalized MCM-48-type materials. Only phenyl was successfully incorporated into an ordered MCM-48 structure. Hall *et al.* suggested that further study into the functionalization of MCM-48 would be beneficial in order to develop an organic hybrid material with a 3-dimensional pore structure (MCM-41 has a 1-dimensional pore structure).

Stein and co-workers incorporated an organic substituent into MCM-41 that could subsequently be modified.<sup>51</sup> Vinyltriethoxysilane was added to TEOS and  $\text{C}_{16}\text{TMABr}$  (SDA) under basic synthesis conditions. Heating the reaction mixture to 87°C for 24 hours was found to provide solids with structural order. Extraction of the SDA was performed by refluxing in acidic methanol solutions. XRD and TEM data showed that the structure remained ordered during extraction. IR spectroscopy and elemental analyses were used to confirm the complete removal of the SDA.  $^{13}\text{C}$  CP/MAS NMR data verified the integrity of the vinyl groups, i.e., the vinyl functionality was unaltered during the synthesis and extraction steps. The material and functional groups were thermally stable up to 280 to 290°C under flowing nitrogen. Bromination of this material

was performed, and IR and  $^{13}\text{C}$  CP/MAS NMR spectroscopy were used to confirm complete bromination of the vinyl groups after 6 days of reaction. Nitrogen sorption experiments revealed a pore size reduction from 22 to 18 Å after the bromination of the vinyl groups. The incorporation of a reactive vinyl group provides the opportunity to tailor the solids by post-synthetic reactions to create a wide variety of useful organic functional groups.

More recent work has involved the co-condensation of methacrylate moieties into MCM-41 materials.<sup>58</sup> The organosilane 3-(trimethoxysilyl)propyl methacrylate was added to a reaction mixture with TEOS and cetyltrimethylammonium chloride ( $\text{C}_{16}\text{TMACl}$ ) under basic synthesis conditions to make a methacrylate hybrid MCM-41 material (MA-MCM). The presence of the methacrylate moiety was observed by IR spectroscopy in as-made samples. IR also showed the Si-C stretch at 1165 to 1170  $\text{cm}^{-1}$ , similar to that listed in previous work.<sup>59</sup> No  $^{29}\text{Si}$  CP/MAS NMR data were reported to confirm the presence of the Si-C bond. Extraction of the SDA by refluxing ethanol removed 30% of the  $\text{C}_{16}\text{TMACl}$ . Use of an ethanol/NaCl solution at room temperature improved the extraction to 95%, but a loss of structural order occurred. The most efficient extraction solvent was found to be acidic ethanol at reflux conditions to completely remove the SDA (verified by IR) with no structural loss. Increasing amounts of methacrylate silane decreased the order of the resulting material. Loadings of 0.23 to 0.28 g methacrylate per gram silica were obtained, as determined by TGA. (Hybrid materials prepared by grafting had loadings of 0.16 g methacrylate per gram silica.) The materials were thermally stable up to 200°C under vacuum. Nitrogen sorption measurements showed a reduction of pore size from *ca.* 23 Å for calcined MA-MCM to

18 Å for extracted materials. Reaction with bromine demonstrated the accessibility of the functional groups.

Cyclodextrin moieties have also been incorporated into mesoporous silicas by co-condensation.<sup>60</sup> Cyclodextrins have useful applications in the removal of organics from water and in chiral separations. Their immobilization onto silica allows them to be used in a recoverable fashion in aqueous systems. Mercaptopropyl- and amino-functionalized mesoporous solids were prepared according to the method of Richer and Mercier<sup>61</sup> (see below), using nonionic surfactants as SDAs to create the mesoporous structure denoted MSU.<sup>62</sup> The thiol- and amino-moieties were extracted by refluxing ethanol to remove the nonionic surfactant and then contacted with monochlorotriazinyl  $\beta$ -cyclodextrin. Nitrogen sorption and IR Spectroscopy showed no incorporation of the cyclodextrin. The MSU hybrids had pore diameters of 40 to 50 Å, which should have been sufficient to allow cyclodextrin (15.3 x 7.8 Å) to enter the pores. It was speculated that reaction of the cyclodextrins at pore openings prevented the remaining cyclodextrins from entering the mesopores. In order to incorporate the organic throughout the silica, the direct synthesis method was employed. Cyclodextrin-containing organosilanes were prepared by modification of aminopropylsilane (Scheme 3.27). The organosilane mixture was then co-condensed with TEOS in the presence of dodecylamine (SDA) to yield cyclodextrin-silica hybrid HMS materials. 1,3,5-trimethylbenzene (TMB) was added as a swelling agent. SDA removal was performed by ethanol extraction. Cyclodextrin loadings of 0.14 to 0.39 mmol per gram were obtained. TEM images, nitrogen sorption, and XRD patterns exhibited the expected wormhole morphology of HMS materials with approximately 40 Å pore diameters.

Contrary to usual trends with co-condensed hybrids, incorporation of cyclodextrins in the synthesis gel resulted in a pore size increase of the HMS materials (30 Å for silica-HMS). It was speculated that the cyclodextrin acted as a swelling agent during the synthesis, similar to other results observed with mesitylene<sup>56</sup> and 1,3,5-trimethylbenzene.<sup>63</sup> Pore volumes were reduced as more cyclodextrin was added to the reaction mixture. The hybrid solids were shown to be useful in the removal of *p*-nitrophenol from aqueous solutions.

### 3.2.2.1 Base Catalysis

The initial work on base catalysis using co-condensed, mesoporous hybrid solids was performed by Macquarrie in 1996.<sup>50</sup> Adapting a neutral surfactant route to HMS,<sup>64</sup> Macquarrie and co-workers incorporated aminopropyl functional groups. TEOS and trimethoxy(3-aminopropyl)silane were hydrolyzed in the presence of *n*-dodecylamine (SDA) and water in ethanol. Room temperature condensation occurred for 18 hours. The SDA was then removed by refluxing ethanol. Complete SDA removal was obtained after three extractions. In a similar manner, 2-cyanoethyl-(trimethoxy)silane was also incorporated into a hybrid material. Analysis of the filtrate, IR spectroscopy of the recovered solids, and TGA of the final material provided evidence to suggest complete SDA removal without damage to the functional groups. This synthesis method (with a neutral surfactant) resulted in a solid material that was easily extracted under relatively mild conditions, as compared to the ionic surfactant SDAs. The TGA analysis showed two high temperature losses from the amino-MCM-41 material: a small loss at 300°C and a larger loss at 575°C. Similar analysis of the cyano-MCM-41 material showed only one large loss at temperatures over 500°C. Based on these observations and IR analyses of

materials treated to 600°C, Macquarrie *et al.* claimed that both the 300 and 500°C weight losses were from the functional groups. IR spectra showed the presence of some intact functional groups after the thermal treatment to 600°C. <sup>13</sup>C MAS NMR was not reported to confirm the IR. Macquarrie *et al.* pointed out that this high thermal stability had not previously been observed in other aminopropyl-functionalized silicas. Nitrogen sorption data gave pore sizes that varied from 29 to 39 Å.

In work related to the study of the Knoevenagel condensation catalysis by aminopropyl silica formed by grafting, Macquarrie and co-workers also examined aminopropyl-functionalized mesoporous HMS materials prepared by co-condensation.<sup>65</sup> The HMS materials were more catalytically active than the functionalized silicas under optimized conditions (i.e., solvent). The HMS materials have higher organic loadings (2 to 3 mmol per gram instead of 1) and higher turnover numbers (4 to 5 times higher).<sup>5</sup> Previous work with the grafted aminopropyl silica (discussed in the previous section) suggested that deactivation occurred by amide formation and that there was a solvent dependency on the catalytic activity for the Knoevenagel condensation of aldehydes.<sup>12</sup> The HMS-based catalysts showed similar solvent effects as with the grafted aminopropyl-silica. However, the HMS-based catalysts were slightly less sensitive to the solvent effects, e.g., toluene has comparable performance to cyclohexane. It was speculated that the increased polarity of the HMS-based catalysts compared to amorphous silica improved the partitioning of reactants from the solvent phase to the active site, thus making the HMS-based material less sensitive to solvent. The amino-HMS catalysts did not reveal amide formation from the reaction of the ethyl cyanoacetate with the amine, as did the silica analogues. However, the presence of some

unknown adsorbed organic species was observed on the used HMS catalysts and likely was the cause of catalyst deactivation.

Macquarrie and co-workers placed *N,N*-dimethyl-aminopropyl groups onto amorphous silica and ordered, mesoporous materials.<sup>66</sup> Loadings of 0.85 to 1.0 mmol per gram silica were obtained by grafting of *N,N*-dimethyl-3-aminopropyltrimethoxysilane. IR spectroscopy indicated the presence of the N-(CH<sub>3</sub>) stretch at 2760 cm<sup>-1</sup>. Additionally hybrid mesoporous materials were made by co-condensing the organosilane with TEOS in the presence of *n*-dodecylamine (SDA) to make a HMS mesoporous material. The SDA was removed by refluxing ethanol. As observed with aminopropyl, the *N,N*-dimethylaminopropyl functionality was thermally stable to temperatures of 400 to 650°C by TGA. Functional group concentrations varied from 1.2 to 2.2 mmol per gram of solid and had a pore size of around 56 Å. The higher loadings of functional groups produced less ordered materials. Michael addition reactions of nitroalkanes and carbonyl compounds were investigated using these solids as catalysts. The dimethylamino-mesoporous solids were significantly more active than the dimethylamino- amorphous silica (conversions of *ca.* 85 and 60%, respectively). The selectivity to Michael addition products was high for all catalysts tested. The mesoporous hybrids showed no leaching of functional groups and were thus recyclable catalysts. Some deactivation of the mesoporous hybrids was observed, but the amorphous silica analogue had greater deactivation. The new solid base catalysts showed better performance than conventional resin catalysts such as Amberlyst A-27.<sup>67</sup>

Macquarrie and co-workers attempted to co-condense guanidine silanes into an ordered, mesoporous material for use as base catalysts in epoxidation reactions, similar to

work done with grafted materials above.<sup>17</sup> Only amorphous solids were obtained. Macquarrie attributed this to the positive charge of the guanidine moiety in synthesis mixture, citing previous examples of charged silanes not being observed to form ordered materials.<sup>68</sup> Material was then prepared by co-condensation of chloropropyl silane with TEOS into a functionalized-mesoporous silica. The chloro-mesoporous material was then passivated (see previous section) and modified (Scheme 3.9) to form a guanidine-containing hybrid material. These hybrid catalysts had high selectivity (89%) and reasonable conversion (65%).

### 3.2.2.2 Phase Transfer Catalysis

Quaternary phosphonium functional groups can also be incorporated via the co-condensation method into mesoporous materials. Corriu and co-workers used the neutral surfactant synthesis (*n*-hexadecylamine) to co-condense 3-(diphenylphosphino)propyltriethoxysilane, as well as its sulfide and quaternary derivatives, with TEOS (Scheme 3.28).<sup>68</sup> X-ray diffraction patterns showed the expected low angle peak characteristic of the HMS type material from the neutral synthesis method for both the diphenylphosphino-organosilane and its sulfide derivative. The phosphonium organosilane did not result in an ordered HMS material. SDA removal was accomplished by refluxing ethanol. A diphenylphosphino-HMS material could also be quantitatively modified after synthesis by sulfonation and quaternization procedures similar to those used to prepare the organosilanes after 2 hours in refluxing ethanol. No structural degradation was observed during these post-synthetic modifications. Pore size analyses showed that the HMS hybrid materials ranged from 30 to 36 Å. Quaternization of the phosphorous centers with benzyl bromide (1 equiv.) or  $\alpha,\alpha'$ -dibromoparaxylene

(0.5 equiv.) in dichloromethane at 20°C was performed.<sup>69</sup> The HMS materials had 83, 93, and 100% reaction after 72 hours, showing that the phosphorous groups within the pores of the HMS were accessible. No catalysis with these materials was reported. The phosphonium-containing hybrid materials may be useful as phase transfer catalysts, like other materials described above.

### 3.2.2.3 Acid Catalysis

The incorporation of mercaptopropyl functionalities by grafting techniques is discussed above.<sup>38</sup> The thiol groups incorporated by either method can be oxidized to sulfonic acid sites (also described above). In addition to studying the grafted analogues above, Jacobs and co-workers co-condensed 3-mercaptopropyltrimethoxysilane (MPTS) with TEOS in the presence of hexadecyltrimethylammonium bromide (C<sub>16</sub>TMABr) or *n*-dodecylamine as SDAs, to prepare thiol-containing MCM-41 or HMS, respectively. The SDAs were removed by extraction (acid solution or refluxing ethanol, for MCM-41 and HMS, respectively). Both thiol and disulfide moieties were detected by IR and <sup>13</sup>C NMR spectroscopies. The thiol functionalities were then oxidized into sulfonic acid groups by hydrogen peroxide (Scheme 3.21). The acid catalysts were tested in the reaction of 2-methylfuran with acetone to produce 2,2-bis(5-methylfuryl)propane (DMP) (Scheme 3.22). The sulfonic acid-functionalized mesoporous materials showed conversions of 52 to 85% with selectivities of 87 to 96%. The sulfonic acid-containing materials prepared by co-condensation methods behaved similarly to those prepared by grafting methods (see above). The recyclability of the catalysts was not reported.

Jacobs and co-workers also studied the use of these sulfonic acid-functionalized materials, prepared by both grafting and co-condensation methods, in the acid-catalyzed

synthesis of monoglycerides by direct esterification of glycerol with fatty acids.<sup>70</sup> The mesoporous hybrids were found to be more active than other solid acid catalysts, such as H-USY and Amberlyst-15. Sulfonic acid-functionalized amorphous silica gave 51% yield, where Amberlyst-15 and H-USY had about 44% and 36% yield, respectively. Sulfonic-acid functionalized HMS material, produced by co-condensation with TEOS in the presence of *n*-dodecylamine, as described above, gave approximately 52% yield, while the grafted MCM-41 sulfonic acid-containing material gave 47 to 53% yield. The hybrid mesoporous catalysts were stable to recycling.

Other work involving the use of sulfonic acid-containing materials as catalysts for monoglyceride preparation from glycerol was reported by Pérez-Pariente and co-workers.<sup>71-73</sup> The sulfonic acid-containing catalysts were prepared by the co-condensation of 3-mercaptopropyltrimethoxysilane and TMOS with methyltrimethoxysilane in varying ratios (0 to 60% by mole of the total organosilanes from methyl silanes).<sup>71</sup> A mixture of SDAs ( $C_{16}$ TMABr, dodecyltrimethylammonium bromide,  $C_{12}$ TMABr, and decyltrimethylammonium bromide,  $C_{10}$ TMABr) and the use of TMAOH instead of NaOH was used to improve the structural order of the hybrid mesoporous materials. The SDA was removed by acidified ethanol. Pore sizes ranged from <10 to 14 Å, depending on the relative organosilane ratios and SDAs used. The sulfonic acid sites were then generated by oxidation with  $H_2O_2$ . Increasing ratios of the alkyl-containing silanes to mercaptopropyl silane resulted in an increased C/Si ratio in the final material. The incorporation of Si-CH<sub>3</sub> moieties was confirmed by <sup>13</sup>C CP/MAS NMR.

The effect of the increased hydrophobicity from the alkyl functionality on the activity of the sulfonic acid sites in the monoglyceride synthesis was then examined.<sup>72</sup> The sulfonic acid-functionalized catalyst containing no alkyl moieties gave a TON of 2 moles fatty acid per site per time after 8 hours of reaction with lauric acid. Increasing amounts of alkyl (up to 1.8 mmol methyl group per gram silica, corresponding to 40% methyl silane) improved the TON to 6 moles fatty acid per site per time during the same time. No further improvement was seen by increasing the methyl content to about 4.5 mmol methyl group per gram silica (60% methyl silane). The selectivity of the catalysts towards the monoglyceride product was improved with increasing methyl content. Similar effects were observed with the reaction of glycerol with oleic acid, with higher conversions observed with increasing methyl content.

Stein and colleagues have studied co-condensed mercaptopropyl silanes with tetra-alkoxy silanes to create mercaptopropyl-functionalized MCM-41 hybrids.<sup>37</sup> High organic loadings of 4.7 mmol per gram were obtained using (3-mercaptopropyl)triethoxysilane condensed with tetramethoxysilane (TMOS) in the presence of C<sub>16</sub>TMABr (SDA) under basic reaction conditions. Higher structural order, as determined by XRD and TEM, was obtained with TMOS as the silicon source rather than TEOS, due to its faster hydrolysis rate. Homogeneity of the reaction mixture and hydrolysis rate were controlled by using a 30% MeOH aqueous solution. Hydrolysis of the silanes was allowed to occur at room temperature for 12 hours and then the mixture was heated to 95°C for 36 hours in order to facilitate condensation into an ordered material. The heating of the reaction mixture was important to obtain ordered materials with high organic loadings. The SDA was extracted with an acidic MeOH solution, and

no structural or functional group degradation was observed (pore diameter of 14 Å). It was shown that the hybrid mercaptopropyl-MCM-41 could adsorb heavy metal ions (2.1 mmol of Hg<sup>2+</sup> per gram of dry mercaptopropyl-MCM-41). The adsorbed mercury could be removed by extraction in HCl. The thiol could also be oxidized by nitric acid to create a sulfonic acid site that was located within the mesopores. Some structural degradation was observed by XRD, and a loss of nitrogen sorption capacity was obtained after the oxidation. However, sulfur loadings remained at 4.7 mmol per gram. The treatment created some mesopores of 35 to 80 Å within the material due to pore collapse. However, 85% of the 14 Å pores remained intact. <sup>13</sup>C CP/MAS NMR showed the presence of sulfonic acid and the loss of thiol. Titration of the sulfonic acid MCM-41 with NaCl gave a proton exchange capacity of 1.76 mequiv. per gram. The acid sites were used as catalysts for the reaction of ethanol with 3,4-dihydro-2*H*-pyran to give 2-ethoxytetrahydropyran. Conversions of 96% were obtained in less than one-hour of reaction time at room temperature. The organic-inorganic hybrid was therefore useful as a substitute for sulfonated polymer catalysts.

Stucky and co-workers employed a triblock co-polymer SDA under acidic reaction conditions to create a mesoporous solid that incorporated a mercaptopropyl organosilane. Like other studies, oxidation of the thiol to sulfonic acid sites was accomplished.<sup>74</sup> These mercaptopropyl-SBA-15 hybrids were thermally stable up to 340°C. Organic loadings of 1.5 mmol per gram (10% organosilane: total silicon sources) to 2.9 (20% organosilane) were found by TGA. About 90% of the mercaptopropyl silanes were incorporated into the mesoporous material during the synthesis. Further modification steps with H<sub>2</sub>O<sub>2</sub> and acidification of the mercaptopropyl-hybrid was

required to form a sulfonic acid site (33 to 77% oxidation obtained with varying oxidation times) in the SBA-15 hybrids.<sup>74</sup> Proton exchange capacities of 0.5 to 1.16 mequiv. H<sup>+</sup> per gram silica were measured and the amount depended on the oxidation conditions. The post-synthesis modification step reduced the structural order in the solid and decreased pore size (pore sizes of 47 to 52 Å, as compared to 55 Å for the mercaptopropyl-SBA-15). Increased oxidation times during post-synthesis modifications enhanced the number of acid sites as determined by titration, but reduced structural order even further. The traditional sulfonic acid resin, Amberlyst-15, was stable to 260°C, while the SBA-15-based material revealed stability to 450°C. These solids thus give organic-inorganic hybrid materials with pore sizes of up to 67 to 73 Å, and proton exchange capacities of 1.26 to 2.24 mequiv. H<sup>+</sup> per gram silica. No disulfides were observed in contrast to the results obtained by Van Rhijn<sup>38</sup> and Lim<sup>37</sup> during post-synthesis oxidation. <sup>31</sup>P MAS NMR of adsorbed triethylphosphine oxide in the materials suggested the presence of strong Brønsted acid sites in the materials reacted with H<sub>2</sub>O<sub>2</sub>. The acidity of the sulfonic acid-SBA materials was compared to other heterogeneous acid catalysts by using the triethylphosphine oxide adsorption technique. The order of increasing acidity, as determined by the shift in <sup>31</sup>P NMR resonance of the adsorbed oxide, was Al-MCM-41 < USY < sulfonic acid-SBA-15 < Amberlyst-15.

In order to alter the hydrophobicity of the cavity surrounding the sulfonic acid sites, Stucky *et al.* incorporated a second functional group, either benzyl- or methyl- (via a triethoxysilane), in addition to the thiol functionalities during synthesis.<sup>74</sup> Additionally, the oxidant, H<sub>2</sub>O<sub>2</sub>, was included in the reaction mixture to oxidize the thiol functionalities during the bi-functional material synthesis. The sulfonic acid loadings in the

bi-functional materials were similar to those of the mono-functionalized sulfonic acid-hybrids (1.3 mequiv. per gram). XRD and nitrogen sorption analyses showed that the mesoporous materials had hexagonal order and pore sizes greater than 60 Å.  $^{13}\text{C}$  CP/MAS NMR of the bi-functional materials suggested the presence of both the sulfonic acid groups and either the benzyl or methyl moieties. No thiols or disulfides were observed in the  $^{13}\text{C}$  NMR. Although the incorporation of other functionalities was intended to influence the surface hydrophobicity and the acidity of the sulfonic acid sites, no clear conclusions were obtained. The mono- or bi-functional sulfonic-acid-containing SBA-15 hybrids were not tested as catalysts. However, these solids would likely be useful in acid-catalyzed reactions.

Richer and Mercier recently investigated the possibility of mercaptopropyl functional group incorporation by direct co-condensation in non-ionic surfactant templated MSU-X mesoporous materials.<sup>61</sup> TEOS and 3-mercaptopropyltrimethoxysilane (0 to 0.05 organosilane: TEOS) were co-condensed by a NaF catalyzed condensation process in the presence of various SDAs (Tergitol 15-S-12 ( $\text{C}_{15}\text{H}_{31}(\text{OCH}_2\text{CH}_2)_{10}\text{OH}$ ), Triton-X100 ( $\text{C}_8\text{H}_{17}\text{C}_6\text{H}_5(\text{OCH}_2\text{CH}_2)_8\text{OH}$ ), Igepal CA-720 ( $\text{C}_8\text{H}_{17}\text{C}_6\text{H}_5(\text{OCH}_2\text{CH}_2)_{10}\text{OH}$ ), Brij-76 ( $\text{C}_{18}\text{H}_{37}(\text{OCH}_2\text{CH}_2)_{10}\text{OH}$ )) at temperatures ranging from 15 to 60°C. The SDAs were removed by extraction with refluxing ethanol. Increasing organosilane content diminished the order for all surfactants studied. Ordered materials were obtained with organic loadings of less than 5 to 6% thiol. Pore diameters of 20 to 60 Å were determined by nitrogen sorption and depended on SDA, synthesis temperature, and organosilane content. Decreasing pore diameter was observed for increasing thiol content for all SDA systems. Elevated synthesis temperatures increased

the amount of mercaptopropyl incorporated into the silica. No oxidation of the thiol functionalities or catalysis studies were presented. However, it is likely that these materials also have the potential to be useful as sulfonic-acid-containing hybrid solids.

Corriu and co-workers co-condensed TEOS and trimethoxysilylpropyl-diethylphosphonate in the presence of the triblock copolymer EO<sub>20</sub>PO<sub>70</sub>EO<sub>20</sub> SDA under acidic reaction conditions with NaF as a catalyst to make SBA-15 mesoporous materials.<sup>75</sup> The SDA was removed by refluxing ethanol to yield the phosphonic acid diethyl ester-functionalized SBA-15 materials. <sup>31</sup>P and <sup>13</sup>C CP/MAS NMR established the presence of the diethylphosphonate moiety in the solids. Elemental analyses gave an organic loading of 1.33 mmol per gram (theoretical loading of 1.29). Nitrogen sorption showed the expected mesoporosity giving a type IV isotherm with pore size of 75 Å. The diethylphosphonate-containing SBA-15 materials were subsequently treated with trimethylchlorosilane (Me<sub>3</sub>SiCl) in refluxing toluene to passivate the surface silanol groups prior to the formation of the phosphonic acid sites. The acid sites were created by two methods (Scheme 3.29). After treatment to give the phosphoric acid sites, <sup>31</sup>P and <sup>13</sup>C CP/MAS NMR confirmed the presence of these acid sites. Structural integrity remained after the treatments. A titration measurement of the acid sites showed 1.08 mmol of acid sites per gram of solid in the materials. Although no catalysis was reported with these materials, acid catalysis should be possible with these phosphonic acid-containing materials.

### 3.2.3 *Organic-Functionalized Molecular Sieves (OFMS)*

As previously mentioned, co-condensation of organosilanes with TEOS during formation of the inorganic structure should provide a more even distribution of functional

groups than the use of grafting methods for ordered, mesoporous materials. Grafting onto zeolites has the additional complication of pore mouth clogging and is therefore unlikely to place functional groups within most of the microporous space. The ability to incorporate organic groups directly in the zeolite syntheses would be desirable to provide for uniform distribution within the void space. When introducing an organic functional group into a zeolite during the synthesis via co-condensation, the SDA for the particular zeolite structure must be removed by some means other than calcination, in order to preserve the integrity of the functional group. SDA extraction, as typically used in a co-condensed, ordered, mesoporous, hybrid material as described above, requires that the SDA be smaller than the pore size of the zeolite (not always the case). The SDA must also not have strong electrostatic interactions with the zeolite framework as well. These stipulations limit the range of molecules that can be used as SDAs. Cambor *et al.* published a fluoride-mediated synthesis procedure for the zeolite structure \*BEA that used tetraethylammonium fluoride (TEAF) as the SDA.<sup>76</sup> The molecular diameter of the TEAF is smaller ( $\sim 6$  Å) than the pores of \*BEA ( $7.6 \times 6.4$  Å). The fluoride-mediated synthesis also creates an essentially “defect-free” framework that has very little residual internal silanol groups. This eliminates the usual electrostatic interactions between positively charged SDAs and the negative framework.<sup>77</sup> The SDA is the fluoride salt that can readily be removed by extraction.

Jones *et al.* correlated the temperature at which SDAs burn out of a microporous zeolite in thermal gravimetric analysis (TGA) with the ease of SDA extraction.<sup>78</sup> It was observed that SDA's that are removed from microporous materials under  $400^{\circ}\text{C}$  tended to have less interaction with the surface and can be extracted.

Using the TEAF synthesis of \*BEA, Jones *et al.* demonstrated that a phenethyl moiety could be introduced as an organosilane and the organic group be incorporated during the synthesis.<sup>52,79</sup> The new organic-inorganic hybrids were denoted Organic Functionalized Molecular Sieves (OFMSs). The TEAF was extracted from the OFMS pores without damaging or leaching the phenethyl groups (verified by <sup>29</sup>Si CP/MAS NMR and Raman spectroscopy). Any small amount of organic groups on the external surface of the zeolite could be removed by washing with concentrated NaOH solutions. Post-synthesis and SDA extracted materials were sulfonated to create sulfonic acid sites, and shape-selective acidic catalysis was accomplished (Scheme 3.30). Poisoning experiments demonstrated that the catalytic functional groups were within the zeolite pores. This type of shape-selective catalysis is not possible with mesoporous materials and grafted zeolites.

Tsuji *et al.* synthesized \*BEA-type OFMSs with other polar groups, including basic functionalities.<sup>53</sup> These functional groups, such as aminopropyl, tolerated SDA extraction and were demonstrated to be located mainly within the zeolite pores. Extraction studies were conducted with various solutions such as water, methanol, acetonitrile, acetic acid, pyridine and pyridine/HCl solutions, to determine the extraction efficiency. The most efficient extraction solutions were aqueous acetic acid and aqueous HCl/pyridine. The addition of HCl increased the extraction efficiency of the pyridine and lowered the pH. The extracted OFMSs were exposed to aldehydes of differing molecular sizes, and shape-selective imine formation was observed by Raman spectroscopy (Scheme 3.31). The 4-(dimethylamino) benzaldehyde (DMBA) reacted with the OFMS to form an imine, while the larger aldehyde, 4-dimethylamino-1-naphthaldehyde

(DMNA), was excluded from the pores and did not form imines. The aminopropyl OFMS was also able to perform shape-selective Knoevenagel condensation reactions.

A synthetic method for converting an extracted organic-functionalized MCM-41 hybrid material to an OFMS with the \*BEA structure has been reported.<sup>79</sup> It was noted that the structural integrity of the MCM-41 sample used as the starting material was important to the purity of the OFMS obtained. Jones *et al.* also reported the synthesis of OFMS materials using various silica sources, synthesis temperatures, and heteroatoms in the framework. Other functional groups, such as alkenes and mercaptopropyl moieties, were incorporated into \*BEA to show that a wide variety of OFMSs could be prepared and, after appropriate post-synthesis modification, used to create a large number of different catalysts.

Later work incorporated mercaptopropyl functional moieties into the \*BEA structure to create thiol-containing OFMSs.<sup>80</sup> The thiol functionalities were then oxidized by H<sub>2</sub>O<sub>2</sub> to create sulfonic acid sites. Shape-selective acid catalysis was performed to compare these hybrid materials to the sulfonic acid sites created in OFMS by sulfonation of phenethyl moieties.

### 3.2.4 *Hybrid Materials with Organic Groups in the Network*

Co-condensation techniques may also be used to create organic-inorganic hybrid materials that lack long-range order and contain the organic moiety as part of the solid network. The organic functionality may be a part of the solid network if the organosilane contains more than one silicon center (necessary but not sufficient condition for incorporation into the network). Examples of these types of materials are provided below.

Incorporation of organic groups within the network of glasses to create organic-inorganic hybrid composite materials has been reported since the 1980s. These organic-inorganic hybrids have been denoted as “ORMOSILs” (organically modified silicas) by Schmidt<sup>81</sup> and “ceramers” by Wilkes and co-workers,<sup>82</sup> and they possess altered mechanical and physical properties from traditional ceramics and glasses. Much research has been dedicated over the past two decades towards studying the effects of organosilane addition on the sol-gel synthesis conditions and the applications of the resulting composites.<sup>83-91</sup> Physical parameters such as morphology, porosity, transparency, thermal and mechanical stability, as well as chemical properties such as solvent stability and hydrophobicity, can be affected by the addition of various organic substituents into the sol-gel processing of the ceramic materials. Polymerization of organic-functionalized trialkoxysilanes result in silsesquioxanes and this area has been reviewed by Baney *et al.*<sup>92</sup> The addition of a tetraalkoxysilane, such as TEOS or TMOS, as a cross-linking agent enables the formation of more fully condensed gels and ceramics, polysilsesquioxanes. The formation of organic-hybrid polysilsesquioxanes has been reviewed by Loy and Shea<sup>93</sup> and Sanchez and Ribot.<sup>94</sup> A review on the applications of these organically modified silicas lists novel composite materials, chromatography and separations, chemical sensors, dyes for optical applications, and catalytic active sites for catalysis.<sup>87</sup> However, little catalysis has yet to be reported for these materials.

Recent work by Corriu and co-workers examined the accessibility of the functional groups imbedded within the lattice of silica xerogels.<sup>95</sup> Bis- and tris(trialkoxysilyl)phosphine organosilanes and their derivatives were used to prepare xerogels.<sup>96</sup> The xerogels were then investigated to determine whether the organic

phosphorous centers were accessible to different reagents.  $^{31}\text{P}$  MAS NMR was used to quantify the interaction.  $\text{H}_2\text{O}_2$  and  $\text{S}_8$  were able to completely react with the phosphorous centers of all of the xerogels. Quaternization with methyl iodide resulted in 95 to 100% yield. Reaction with benzyl bromide was 85 to 100%, showing the effect of more steric hindrance for the bulkier reactant.

Inagaki and co-workers reported the synthesis of the first ordered mesoporous silica with organic groups evenly incorporated in the walls (periodic mesoporous organosilicas, "PMOs").<sup>97</sup> 1,2-bis(trimethoxysilyl)ethane (BTME) was hydrolyzed and condensed in the presence of the SDA, octadecyltrimethylammonium chloride ( $\text{C}_{18}\text{TMACl}$ ), under basic reaction conditions. Two highly ordered mesoporous structures were obtained (depending on the synthesis conditions): a two-dimensional hexagonal mesophase (hexagonal rod morphology, denoted HMM-1) and a three-dimensional hexagonal mesophase (spherical morphology, denoted HMM-2). Unlike the co-condensed mesoporous hybrids discussed above where concentrations greater than 10 to 20% of organosilane resulted in disordered materials, the PMOs had 100% organosilane utilization in the condensation reaction. Inagaki *et al.* attributed this difference to the flexibility in the framework given by the ethane moieties. The ammonium SDA was removed by acidic ethanol extraction. The HMM-1 and HMM-2 hexagonal structures were mesoporous, having pore sizes of 31 and 27 Å, respectively.  $^{29}\text{Si}$  and  $^{13}\text{C}$  CP/MAS NMR spectroscopy was used to verify the presence of Si-C bonds and of the ethane bridge. None of the Si-C bonds of the BTME were cleaved during the condensation process. The organic groups were stable up to 400°C by TGA. Inagaki *et*

*al.* proposed that modification of the functional groups could produce useful catalytic materials where both inorganic and organic active sites are present.

Inagaki later reported the synthesis of a third PMO phase, HMM-3.<sup>98</sup> The BTME organosilane was condensed in the presence of C<sub>16</sub>TACl (SDA) under basic reaction conditions. The SDA was removed by extraction with acidic ethanol. SEM and TEM images of the particles showed well-ordered decaoctahedral particles with cubic symmetry. Nitrogen sorption indicated mesoporosity with a pore diameter of 29 Å. <sup>29</sup>Si MAS NMR was used to verify that no degradation of the Si-C bonds occurred during synthesis, and <sup>13</sup>C CP/MAS NMR showed no destruction of the organic group.

About the same time, Stein and co-workers reported the use of 1,2-bis(triethoxysilyl)ethane (BTSE) or 1,2-bis(triethoxysilyl)ethylene (BTSEY) in the condensation of mesoporous silica using C<sub>16</sub>TABr (SDA) under basic reaction conditions.<sup>99</sup> The mesoporous materials, designated “unified organically functionalized mesoporous networks” (UOFMNs), have MCM-41 structures, although they appeared less structurally ordered than the organic-inorganic PMOs studied by Inagaki. Stein *et al.* suggested that the samples appear to have a morphology more similar to the MSU-X wormhole channel materials of Pinnavaia<sup>62</sup> than MCM-41. The SDA was removed by acidic methanol (as observed by IR spectroscopy). <sup>29</sup>Si MAS NMR data showed no cleavage of the Si-C bond occurred during material synthesis. <sup>13</sup>C CP/MAS NMR was used to verify the presence of the ethane and ethylene functional groups. Nitrogen sorption measurements confirmed the mesoporosity of the materials, with pore sizes of 21 to 24 Å. The UOFMN samples had greater hydrothermal stability than all-silica MCM-41 analogues.

Recently, Burleigh *et al.* reported the incorporation of BTSE into another PMO system using the triblock copolymer, Pluronic P123, as the SDA.<sup>63</sup> The SDA was extracted by refluxing acidic ethanol. In order to create even larger pores, 1,3,5-trimethylbenzene (TMB) was added as a swelling agent. The addition of TMB not only increased the pore size, but also altered the structural morphology. TEM images of material prepared with no TMB exhibited the expected wormhole structure with pore sizes of about 60 Å. The presence of TMB increased the pore size to 120 Å and changed the shape to cylindrical pores. Even greater amounts of TMB resulted in spherical pores of 200 Å diameter.

Ozin and co-workers also studied the co-condensation of 1,2-bis(triethoxysilyl)ethylene with TEOS using C<sub>16</sub>TABr (SDA) under basic reaction conditions.<sup>100</sup> Materials with lower amounts of BTSEY had hexagonal structural order. Loss of order was observed in the materials that had higher concentrations of the organosilane. FT-Raman, <sup>13</sup>C and <sup>29</sup>Si CP/MAS NMR spectroscopies were used to confirm the presence of the ethylene moieties and the Si-C bonds. Nitrogen sorption results indicated mesoporosity, with pore sizes of about 40 Å. Additionally, Ozin and co-workers co-condensed organosilane bis(triethoxysilyl)methane (BTM) with TEOS in the presence of a C<sub>16</sub>TABr (SDA) to create ordered hexagonal mesoporous materials.<sup>101</sup> As increasing ratios of BTM to TEOS were used, the order in the materials decreased. The SDA was removed by acidic methanol extraction, with no degradation of the structure. Nitrogen sorption indicated mesoporosity with a pore diameter of 31 Å. The integrity of the methylene groups within the walls and presence of the Si-C bonds was verified by the use of Raman, <sup>13</sup>C and <sup>29</sup>Si NMR spectroscopies.

Ozin and co-workers also investigated other functional groups as spacers in the PMO framework.<sup>102</sup> Various bis(trialkoxysilyl) organosilanes were condensed in the presence of C<sub>16</sub>TABr (SDA) under basic reaction conditions, creating ordered, hexagonal materials. The SDA was removed by acidic methanol extraction without structural damage. <sup>29</sup>Si CP/MAS NMR showed that benzene- and thiophene-containing PMOs had almost total cleavage of the Si-C bonds of the organic functional groups under the basic conditions of the reaction mixture. Condensation of the thiophene-containing PMO under acidic reaction conditions revealed only partial cleavage of the Si-C bonds. <sup>13</sup>C CP/MAS NMR data from these samples showed that the benzene and thiophene moieties were intact. Materials made with ferrocene, acetylene, and bi-thiophene spacers exhibited lower structural order and more Si-C bond cleavage.

Yamamoto *et al.* recently claimed the synthesis of zeolites with an organic moiety within the silica lattice.<sup>103</sup> The “zeolite with organic lattice” (ZOL) contained an organic group that is incorporated during the zeolite assembly. Bis(triethoxysilyl)methane (BTM) was condensed in the presence of tetrapropylammonium hydroxide (TPAOH) as the SDA. The resulting reaction mixture was heated under autogenous conditions at 170°C in a Teflon-lined autoclave, either static or rotating. The organic-inorganic hybrid solid (named ZOL-1) has MFI structure, with no contaminating amorphous phase observed by XRD. <sup>13</sup>C and <sup>29</sup>Si CP/MAS NMR data from the solids verified the presence of the organic moieties and Si-C bonds, but also indicated some cleavage of the Si-C bonds. The SDA could not be extracted. The zeolite synthesis was then attempted with no SDA, using an aluminosilicate version of the MFI synthesis. The MFI phase, ZOL-5, was obtained after crystallization of the gel at 190°C. <sup>13</sup>C and <sup>29</sup>Si CP/MAS NMR data

again showed the presence of the organic moieties and Si-C bonds, as well as some cleavage of the Si-C bonds. IR spectroscopy of the ZOL-5 sample showed both methyl and methylene vibrations. The organic groups appeared to not affect the hydrophobicity of the zeolite, as ZOL-5 was shown to have a water sorption similar to ZSM-5 with comparable Si/Al ratios. Yamamoto proposed the use of the bis(trialkoxysilyl) organosilanes with other SDAs to explore the possibility of synthesizing other zeolite phases with an organic lattice. If this early report can be verified, it will open a new area of microporous materials for catalysis.

### 3.2.5 *Imprinted Silicas*

Dickey and Pauling first demonstrated in 1949 that silica gels prepared with dye imprints specifically adsorbed dyes with similar structures.<sup>104</sup> Since that time there has been significant efforts to create “imprinted” solids. Davis *et al.* have reviewed these efforts up to around 1996.<sup>105</sup> The addition of organic groups (via organosilanes) to an assembly process that also contains molecules for organizing the organic groups into a three-dimensional configuration (imprint) can be used to create a porous hybrid material with ordered functional groups (after imprint removal). For example, Makote and Collinson report the sol-gel processing of phenyl- and methyl-trimethoxysilane with TEOS in the presence of dopamine as an imprint molecule.<sup>106</sup> The thin films produced from the gel, after removal of the imprint, preferentially adsorb dopamine compared to related compounds serotonin, epinephrine, and dihydroxynaphthalene.

In another type of assembly procedure, Sasaki and Alam created guanidine-containing imprinted silicas and studied the binding of phenylphosphonic acid.<sup>107</sup> Amorphous silica xerogels were prepared by condensation of TEOS. The

xerogels were then grafted with 1-trimethoxysilylpropyl-3-guanidinium chloride in the presence of varying amounts phenylphosphonic acid (PPA) as an imprint to direct the spatial orientation of guanidine-functional groups. PPA can interact with the protonated guanidine in either a one- or a two-point mode (Scheme 3.32).  $^{31}\text{P}$  NMR spectroscopy was used to distinguish the different binding modes. After the organic-inorganic hybrid xerogels were synthesized, the imprint PPA was removed by acidic solutions. The first extraction removed 93% of the total PPA imprint. Of the imprint remaining in the solids, 82% was bound by two guanidine moieties. Sasaki and Alam showed that the experimental binding constant for two-point adsorption was higher than for singly bound species.

Katz and Davis imprinted amorphous silica to create functionalized void spaces for shape-selective catalysis.<sup>108</sup> Imprints prepared to organize either one, two, or three aminopropyl functionalizations were incorporated into a sol-gel condensation of amorphous silica (Scheme 3.33). The surface silanols were passivated by trimethylchlorosilane and hexamethyldisilazane. Removal of the aromatic core of the imprint was performed by treatment with trimethylsilyliodide in acetonitrile using HCl as a catalyst.  $^{13}\text{C}$  CP/MAS NMR data were used to prove the integrity of the imprint in the as-made silica samples. The percent cleavages of the carbamates of the imprints were 73, 74, and 22% for the one-, two-, and three-aminopropyl functionalized imprints, respectively. Functional group loadings of 0.23, 0.23, and 0.07 mmol per gram, respectively, were estimated from the adsorption of benzoic acid onto the amine sites. As expected, removal of the three-aminopropyl functionalized carbamate was the most difficult. Argon sorption showed that the samples were microporous. The spatial

distribution of the functional groups was examined by various methods including the adsorption of probe molecules. The one-aminopropyl functionalized silica showed the expected amide ( $1710\text{ cm}^{-1}$ ) and carboxylic acid ( $1647\text{ cm}^{-1}$ ) peaks in IR spectroscopy after adsorption of azelaoyl chloride, while the two-aminopropyl functionalized silica had only a single, broad amide band in the IR, consistent with the two-point binding (Scheme 3.34). These materials were active as catalysts and able to perform shape-selective base catalysis (Knoevenagel condensation of malononitrile with isophthalaldehyde).

### 3.3 Future Directions of Organic-Inorganic Hybrid Materials

There are numerous organic-inorganic hybrid materials that have been prepared and characterized, but not yet tested as catalysts. Additionally, very few of the materials that have been exposed to reaction conditions have been rigorously tested for re-use. Thus, there are many opportunities for investigation with currently available materials. Since much is known about how organic moieties can serve as catalysts for homogeneous reactions, many elements of “design” can be used in future developments of organic-inorganic hybrid materials for use as recyclable catalysts.

Further work on exploring the incorporation of multiple functional group types, either randomly or in specific spatial arrangements is merited. Recently, the ability to have both acid and base functionalities on silica was reported.<sup>109</sup> Nafion acid resin was immobilized with silica using a previously reported technique.<sup>110</sup> Base functionalities, such as amines and guanidine, were also immobilized onto silica by co-condensation<sup>111</sup> or grafting.<sup>29</sup> Physical mixtures of the acid and base-immobilized catalysts were then used to perform sequential acid-base reactions in a one-pot reaction (Scheme 3.35). The

ability to have the tethered functional groups within the same silica matrix would be a desired extension of this work.

### **3.4 Acknowledgements**

APW acknowledges financial support from a National Science Foundation Graduate Fellowship and from Chevron Research and Technology Company.

### 3.5 References

- (1) Sellergren, B. *Chirality* **1989**, *1*, 63.
- (2) Wulff, G.; Schauhoff, S. *J. Org. Chem.* **1991**, *56*, 395.
- (3) *Chemistry of Materials*; Interrante, L. V.; Crivello, J.; Eckert, H.; Greedan, J.; Reichmanis, E.; Ward, M. D., Eds.; American Chemical Society: Columbus, 2001; Vol. 13.
- (4) Price, P. M.; Clark, J. H.; Macquarrie, D. J. *J. Chem. Soc., Dalton Trans.* **2000**, 101.
- (5) Clark, J. H.; Macquarrie, D. J. *Chem. Commun.* **1998**, 853.
- (6) Pirkle, W. H.; Pochapsky, T. C.; Mahler, G. S.; Corey, D. E.; Reno, D. S.; Alessi, D. M. *J. Org. Chem.* **1986**, *51*, 4991.
- (7) Deschler, U.; Kleinschmit, P.; Panster, P. *Angew. Chem. Int. Ed.* **1986**, *25*, 236.
- (8) Bols, M.; Skrydstrup, T. *Chem. Rev.* **1995**, *95*, 1253.
- (9) Moller, K.; Bein, T. *Chem. Mater.* **1998**, *10*, 2950.
- (10) Angeletti, E.; Canepa, C.; Martinetti, G.; Venturello, P. *Tetrahedron Lett.* **1988**, *29*, 2261.
- (11) Angeletti, E.; Canepa, C.; Martinetti, G.; Venturello, P. *J. Chem. Soc., Perkin Trans. 1* **1989**, 105.
- (12) Macquarrie, D. J.; Clark, J. H.; Lambert, A.; Mdoe, J. E. G.; Priest, A. *React. Funct. Polym.* **1997**, *35*, 153.
- (13) Bigi, F.; Carloni, S.; Maggi, R.; Mazzacani, A.; Sartori, G. *Stud. Surf. Sci. Catal.* **2000**, *130*, 3501.

- (14) Lasperas, M.; Llorett, T.; Chaves, L.; Rodriguez, I.; Cauvel, A.; Brunel, D. *Stud. Surf. Sci. Catal.* **1997**, *108*, 75.
- (15) Utting, K. A.; Macquarrie, D. J. *New J. Chem.* **2000**, *24*, 591.
- (16) Blanc, A. C.; Macquarrie, D. J.; Valle, S.; Renard, G.; Quinn, C. R.; Brunel, D. *Green Chem.* **2000**, *2*, 283.
- (17) Macquarrie, D. J.; Brunel, D.; Renard, G.; Blanc, A. C. Guanidine Catalysts Supported on Silica and Micelle Templated Silicas. New Basic Catalysts for Organic Chemistry. *13th International Zeolite Conference* [CD-ROM]; Elsevier Science: Amsterdam, 2001; *Stud. Surf. Sci. Catal.*, *135*, Paper 29.
- (18) Harmer, M. A.; Sun, Q.; Michalczyk, M. J.; Yang, Z. *Chem. Commun.* **1997**, 1803.
- (19) Kresge, C. T.; Leonowicz, M. E.; Roth, W. J.; Vartuli, J. C.; Beck, J. S. *Nature* **1992**, *359*, 710.
- (20) Beck, J. S.; Vartuli, J. C.; Roth, W. J.; Leonowicz, M. E.; Kresge, C. T.; Schmitt, K. D.; Chu, C. T.-W.; Olson, D. H.; Sheppard, E. W.; McCullen, S. B.; Higgins, J. B.; Schlenker, J. L. *J. Am. Chem. Soc.* **1992**, *114*, 10834.
- (21) Zhao, D.; Feng, J.; Huo, Q.; Melosh, N.; Fredrickson, G. H.; Chmelka, B. F.; Stucky, G. D. *Science* **1998**, *279*, 548.
- (22) Zhao, D.; Huo, Q.; Feng, J.; Chmelka, B. F.; Stucky, G. D. *J. Am. Chem. Soc.* **1998**, *120*, 6024.
- (23) Mukherjee, P.; Laha, S.; Mandal, D.; Kumar, R. *Stud. Surf. Sci. Catal.* **2000**, *129*, 283.
- (24) Brunel, D. *Microporous Mesoporous Mater.* **1999**, *27*, 329.

- (25) Kruk, M.; Jaroniec, M. In *Surfaces of Nanoparticles and Porous Materials*; Schwarz, J., Contescu, C., Eds.; Marcel Dekker: New York, 1998, 443.
- (26) Yamamoto, K.; Tatsumi, T. *Microporous Mesoporous Mater.* **2001**, 44-45, 459.
- (27) Cauvel, A.; Renard, G.; Brunel, D. *J. Org. Chem.* **1997**, 62, 749.
- (28) Demicheli, G.; Maggi, R.; Mazzacani, A.; Righi, P.; Sartori, G.; Bigi, F. *Tetrahedron Lett.* **2001**, 42, 2401.
- (29) Subba Rao, Y. V.; De Vos, D.; Jacobs, P. A. *Angew. Chem. Int. Ed.* **1997**, 36, 2661.
- (30) Kantam, M. L.; Sreekanth, P. *Catal. Lett.* **2001**, 77, 241.
- (31) Choi, Y.; Kim, K.-S.; Kim, J.-H.; Seo, G. Knoevenagel condensation between ethylcyanoacetate and benzaldehyde over base catalysts immobilized on mesoporous materials. *13th International Zeolite Conference* [CD-ROM]; Elsevier Science: Amsterdam, 2001; *Stud. Surf. Sci. Catal.*, 135, Paper 23.
- (32) Rodriguez, I.; Iborra, S.; Corma, A.; Rey, F.; Jorda, J. *Chem. Commun.* **1999**, 593.
- (33) Rodriguez, I.; Iborra, S.; Rey, F.; Corma, A. *Appl. Catal., A* **2000**, 194-195, 214.
- (34) Kloetstra, K. R.; van Bekkum, H. *J. Chem. Soc., Chem. Comm.* **1995**, 1005.
- (35) Clark, J. H.; Butterworth, A. J.; Tavener, S. J.; Teasdale, A. J. *J. Chem. Tech. Biotechnol.* **1997**, 68, 367.
- (36) Clark, J. H.; Macquarrie, D. J. *Chem. Soc. Rev.* **1996**, 25, 303.
- (37) Lim, M. H.; Blanford, C. F.; Stein, A. *Chem. Mater.* **1998**, 10, 467.
- (38) Van Rhijn, W. M.; De Vos, D.; Sels, B. F.; Bossaert, W. D.; Jacobs, P. A. *Chem. Commun.* **1998**, 317.

- (39) Brunel, D.; Fajula, F.; Nagy, J. B.; Deroide, B.; Verhoef, M. J.; Veum, L.; Peters, J. A.; van Bekkum, H. *Appl. Catal., A* **2001**, *213*, 73.
- (40) Bellocq, N.; Brunel, D.; Lasperas, M.; Moreau, P. *Stud. Surf. Sci. Catal.* **1997**, *108*, 485.
- (41) Bellocq, N.; Brunel, D.; Lasperas, M.; Moreau, P. *Supported Reagents and Catalysts in Chemistry* **1998**, *216*, 162.
- (42) Lasperas, M.; Bellocq, N.; Brunel, D.; Moreau, P. *Tetrahedron: Asymmetry* **1998**, *9*, 3053.
- (43) Bellocq, N.; Abramson, S.; Lasperas, M.; Brunel, D.; Moreau, P. *Tetrahedron: Asymmetry* **1999**, *10*, 3229.
- (44) Abramson, S.; Bellocq, N.; Lasperas, M. *Top. Catal.* **2000**, *13*, 339.
- (45) Abramson, S.; Lasperas, M.; Galarneau, A.; Desplantier-Giscard, D.; Brunel, D. *Chem. Commun.* **2000**, 1773.
- (46) Kim, S.-W.; Bae, S. J.; Hyeon, T.; Kim, B. M. *Microporous Mesoporous Mater.* **2001**, *44-45*, 523.
- (47) Cauvel, A.; Brunel, D.; DiRenzo, F.; Moreau, P.; Fajula, F. *Stud. Surf. Sci. Catal.* **1995**, *94*, 286.
- (48) Brunel, D.; Cauvel, A.; Fajula, F.; DiRenzo, F. In *Zeolites: A Refined Tool for Designing Catalytic Sites*; Bonneviot, L., Kaliaguine, S., Eds.; Elsevier Science: Amsterdam, 1995, 173.
- (49) Fowler, C. E.; Burkett, S. L.; Mann, S. *Chem. Commun.* **1997**, 1769.
- (50) Macquarrie, D. J. *Chem. Commun.* **1996**, 1961.
- (51) Lim, M. H.; Blanford, C. F.; Stein, A. *J. Am. Chem. Soc.* **1997**, *119*, 4090.

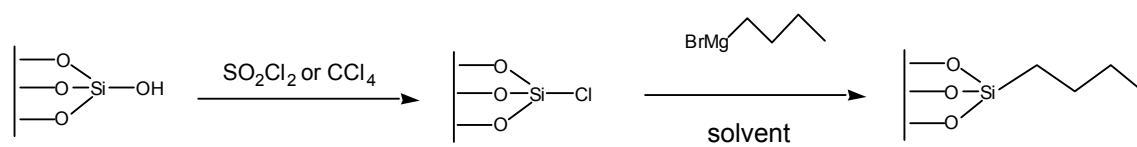
- (52) Jones, C. W.; Tsuji, K.; Davis, M. E. *Nature* **1998**, 393, 52.
- (53) Tsuji, K.; Jones, C. W.; Davis, M. E. *Microporous Mesoporous Mater.* **1998**, 29, 339.
- (54) Stein, A.; Melde, B. J.; Schrodin, R. C. *Adv. Mater.* **2000**, 12, 1403.
- (55) Burkett, S. L.; Sims, S. D.; Mann, S. *Chem. Commun.* **1996**, 1367.
- (56) Bambrough, C. M.; Slade, R. C. T.; Williams, R. T. *J. Mater. Chem.* **1998**, 8, 569.
- (57) Hall, S. R.; Fowler, C. E.; LeBeau, B.; Mann, S. *Chem. Commun.* **1999**, 201.
- (58) Moller, K.; Bein, T.; Fischer, R. X. *Chem. Mater.* **1999**, 11, 665.
- (59) Fowler, C. E.; LeBeau, B.; Mann, S. *Chem. Commun.* **1998**, 1825.
- (60) Huq, R.; Mercier, L.; Kooyman, P. J. *Chem. Mater.* **2001**, 13, 4512 .
- (61) Richer, R.; Mercier, L. *Chem. Mater.* **2001**, 13, 2999.
- (62) Bagshaw, S. A.; Prouzet, E.; Pinnavaia, T. J. *Science* **1995**, 269, 1242.
- (63) Burleigh, M. C.; Markowitz, M. A.; Wong, E. M.; Lin, J.-S.; Gaber, B. P. *Chem. Mater.* **2001**, 13, 4411.
- (64) Tanev, P. T.; Pinnavaia, T. J. *Chem. Mater.* **1996**, 8, 2068.
- (65) Macquarrie, D. J.; Jackson, D. B. *Chem. Commun.* **1997**, 1781.
- (66) Mdoe, J. E. G.; Clark, J. H.; Macquarrie, D. J. *Synlett* **1998**, 625.
- (67) Ballini, R.; Marziali, P.; Mozzicafreddo, A. *J. Org. Chem.* **1996**, 61, 3209.
- (68) Corriu, R. J. P.; Mehdi, A.; Reye, C. *Comptes Rendus de l' Academie des Sciences Serie IIc:Chimie* **1999**, 2, 35.
- (69) Corriu, R. J. P.; Hoarau, C.; Mehdi, A.; Reye, C. *Chem. Commun.* **2000**, 71.
- (70) Bossaert, W. D.; De Vos, D.; Van Rhijn, W. M.; Bullen, J.; Grobet, P. J.; Jacobs, P. A. *J. Catal.* **1999**, 182, 156.

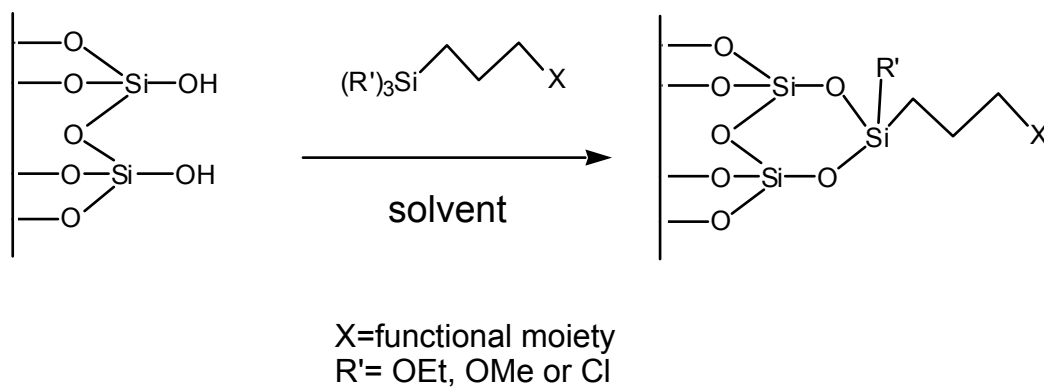
- (71) Diaz, I.; Marquez-Alvarez, C.; Mohino, F.; Perez-Pariente, J.; Sastre, E. *J. Catal.* **2000**, *193*, 283.
- (72) Diaz, I.; Marquez-Alvarez, C.; Mohino, F.; Perez-Pariente, J.; Sastre, E. *J. Catal.* **2000**, *193*, 295.
- (73) Diaz, I.; Marquez-Alvarez, C.; Mohino, F.; Perez-Pariente, J.; Sastre, E. *Appl. Catal., A* **2001**, *205*, 19.
- (74) Margolese, D.; Melero, J. A.; Christiansen, S. C.; Chmelka, B. F.; Stucky, G. D. *Chem. Mater.* **2000**, *12*, 2448.
- (75) Corriu, R. J. P.; Datas, L.; Guari, Y.; Mehdi, A.; Reye, C.; Thieuleux, C. *Chem. Commun.* **2001**, 763.
- (76) Camblor, M. A.; Corma, A.; Valencia, S. *Chem. Commun.* **1996**, 2365.
- (77) Camblor, M. A.; Villaescusa, L. A.; Diaz-Cabanas, M. J. *Top. Catal.* **1999**, *9*, 59.
- (78) Jones, C. W.; Tsuji, K.; Takewaki, T.; Beck, L. W.; Davis, M. E. *Microporous Mesoporous Mater.* **2001**, *48*, 57.
- (79) Jones, C. W.; Tsuji, K.; Davis, M. E. *Microporous Mesoporous Mater.* **1999**, *33*, 223.
- (80) Jones, C. W.; Tsapatsis, M.; Okubo, T.; Davis, M. E. *Microporous Mesoporous Mater.* **2001**, *42*, 21.
- (81) Schmidt, H. *J. Non-Cryst. Solids* **1985**, *73*, 681.
- (82) Huang, H. H.; Orlor, B.; Wilkes, G. L. *Polym. Bull.* **1985**, *14*, 557.
- (83) Wilkes, G. L.; Huang, H.-H.; H., G. R. In *Silicon-based polymer science: a comprehensive resource*; Zeigler, J. M., Fearon, F. W. G., Eds.; American Chemical Society: Washington, DC, 1990, 207.

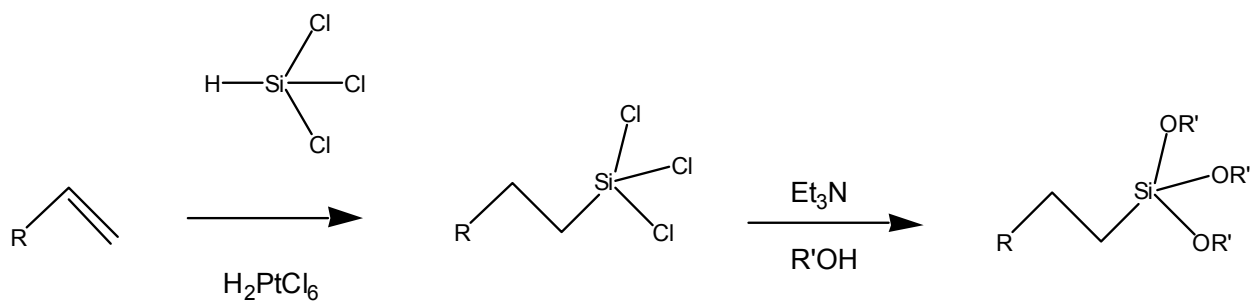
- (84) Loy, D. A.; Jamison, G. M.; Baugher, B. M.; Russick, E. M.; Assink, R. A.; Prabakar, S.; Shea, K. J. *J. Non-Cryst. Solids* **1995**, *186*, 44.
- (85) Wen, J.; Wilkes, G. L. *Chem. Mater.* **1996**, *8*, 1667.
- (86) Loy, D. A.; Jamison, G. M.; Baugher, B. M.; Myers, S. A.; Assink, R. A.; Shea, K. J. *Chem. Mater.* **1996**, *8*, 656.
- (87) Collinson, M. M. *Mikrochimica Acta* **1998**, *129*, 149.
- (88) Corriu, R. J. P. *European Journal of Inorganic Chemistry* **2001**, 1109.
- (89) Shea, K. J.; Loy, D. A. *Chem. Mater.* **2001**, *13*, 3306.
- (90) Cerveau, G.; Corriu, R. J. P.; Framery, E. *Chem. Mater.* **2001**, *13*, 3373.
- (91) Schottner, G. *Chem. Mater.* **2001**, *13*, 3422.
- (92) Baney, R. H.; Itoh, M.; Sakakibara, A.; Suzuki, T. *Chem. Rev.* **1995**, *95*, 1409.
- (93) Loy, D. A.; Shea, K. J. *Chem. Rev.* **1995**, *95*, 1431.
- (94) Sanchez, C.; Ribot, F. *New J. Chem.* **1994**, *18*, 1007.
- (95) Bezombes, J.-P.; Chuit, C.; Corriu, R. J. P.; Reye, C. *J. Mater. Chem.* **1999**, *9*, 1727.
- (96) Bezombes, J.-P.; Chuit, C.; Corriu, R. J. P.; Reye, C. *J. Mater. Chem.* **1998**, *8*, 1749.
- (97) Inagaki, S.; Guan, S.; Fukushima, Y.; Ohsuna, T.; Terasaki, O. *J. Am. Chem. Soc.* **1999**, *121*, 9611.
- (98) Guan, S.; Inagaki, S.; Ohsuna, T.; Terasaki, O. *J. Am. Chem. Soc.* **2000**, *122*, 5660.
- (99) Melde, B. J.; Holland, B. T.; Blanford, C. F.; Stein, A. *Chem. Mater.* **1999**, *11*, 3302.

- (100) Asefa, T.; MacLachlan, M. J.; Coombs, N.; Ozin, G. A. *Nature* **1999**, *402*, 867.
- (101) Asefa, T.; MacLachlan, M. J.; Grondey, H.; Coombs, N.; Ozin, G. A. *Angew. Chem. Int. Ed.* **2000**, *39*, 1808.
- (102) Yoshina-Ishii, C.; Asefa, T.; Coombs, N.; MacLachlan, M. J.; Ozin, G. A. *Chem. Commun.* **1999**, 2539.
- (103) Yamamoto, K.; Takahashi, Y.; Tatsumi, T. Synthesis of zeolites with organic lattice. *13th International Zeolite Conference* [CD-ROM]; Elsevier Science: Amsterdam, 2001; Stud. Surf. Sci. Catal., *135*, Paper 21.
- (104) Dickey, F. H. *Proc. Natl. Acad. Sci. USA* **1949**, *35*, 227.
- (105) Davis, M. E.; Katz, A.; Ahmad, W. R. *Chem. Mater.* **1996**, *8*, 1820.
- (106) Makote, R.; Collinson, M. M. *Chem. Mater.* **1998**, *10*, 2440.
- (107) Sasaki, D. Y.; Alam, T. M. *Chem. Mater.* **2000**, *12*, 1400.
- (108) Katz, A.; Davis, M. E. *Nature* **2000**, *403*, 286.
- (109) Gelman, F.; Blum, J.; Avnir, D. *Angew. Chem. Int. Ed.* **2001**, *40*, 3647.
- (110) Harmer, M. A.; Farneth, W. E.; Sun, Q. *J. Am. Chem. Soc.* **1996**, *118*, 7708.
- (111) Husing, N.; Schubert, U.; Mezei, R.; Fratzl, P.; Riegel, B.; Kiefer, W.; Kohler, D.; Mader, W. *Chem. Mater.* **1999**, *11*, 451.

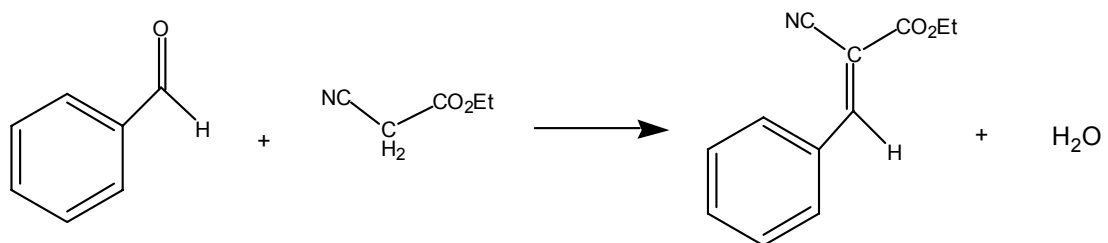
**Scheme 3.1** Chlorination and subsequent reaction with a Grignard reagent to functionalize silica.

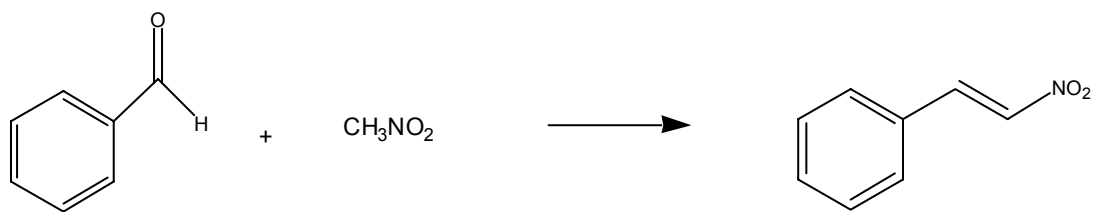


**Scheme 3.2** Example of grafting organosilanes onto silanol-containing surface.

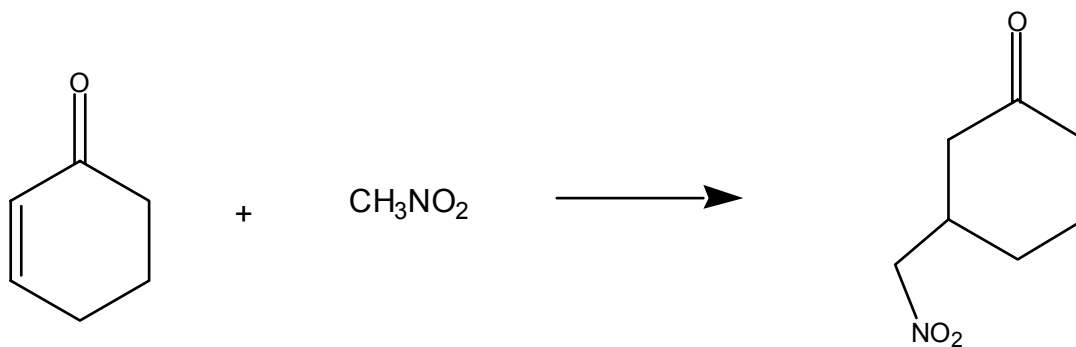
**Scheme 3.3** A synthetic route to organosilanes. Adapted from ref. 6.

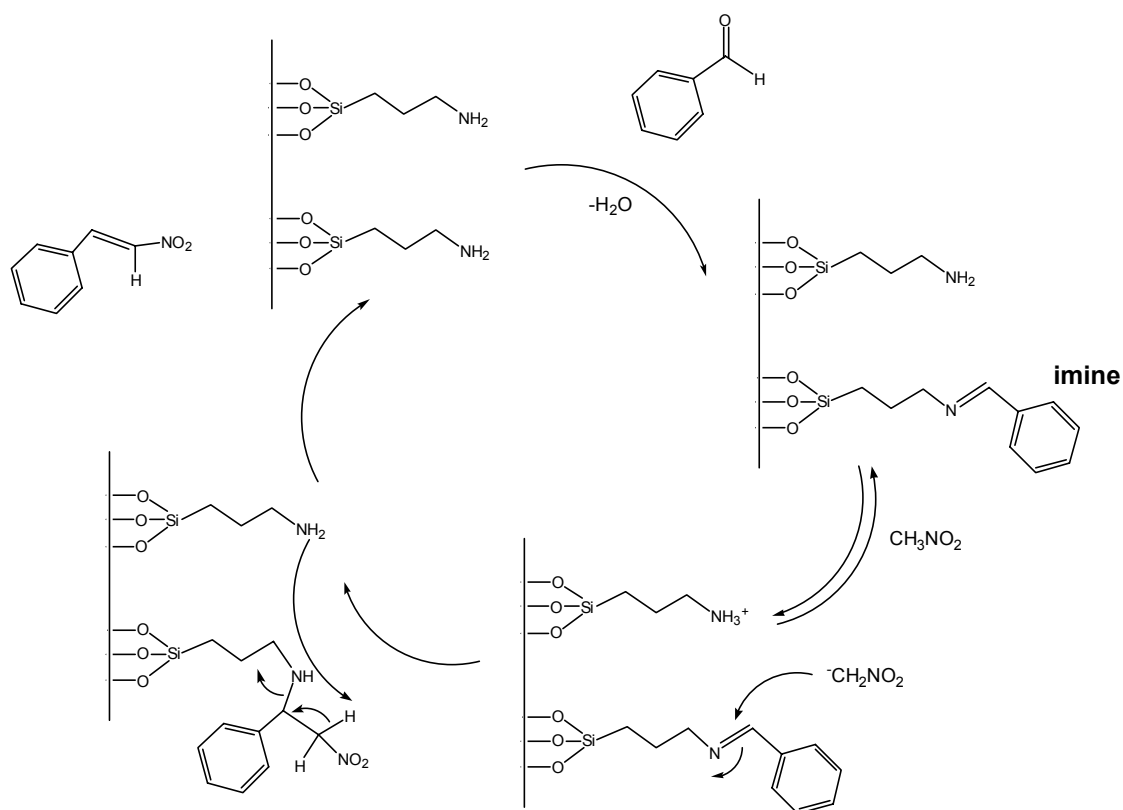
R = desired functional group

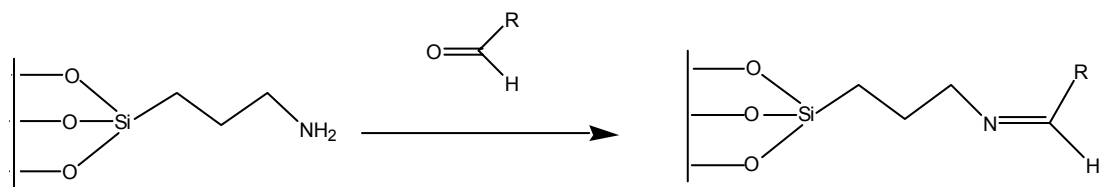
**Scheme 3.4** Knoevenagel condensation of benzaldehyde and ethyl cyanoacetate.

**Scheme 3.5** Example of a nitroaldol condensation.

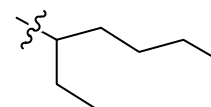
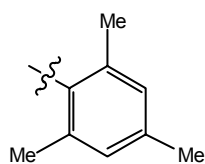
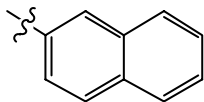
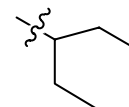
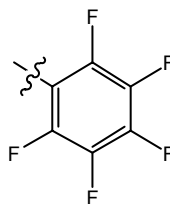
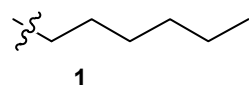
**Scheme 3.6** Example of a Michael addition reaction.

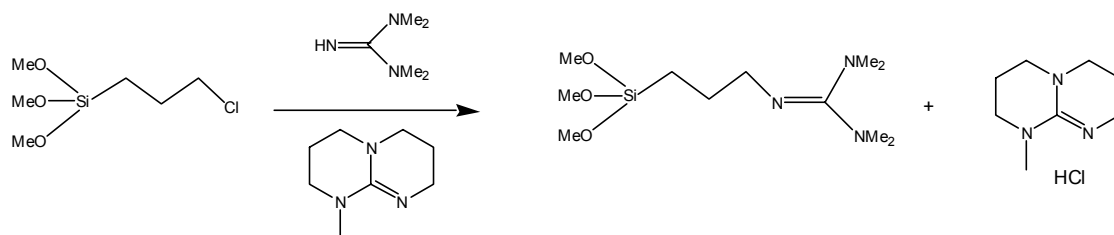


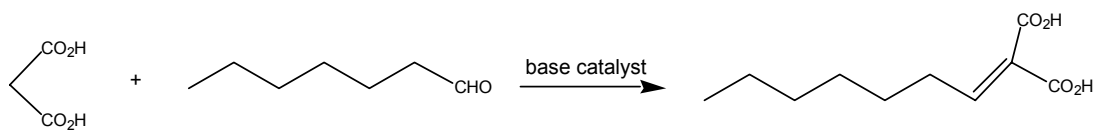
**Scheme 3.7** Proposed mechanism of nitroaldol condensation. Adapted from ref. 13.

**Scheme 3.8** Imine silica preparation from aminopropyl silica. Adapted from ref. 15.

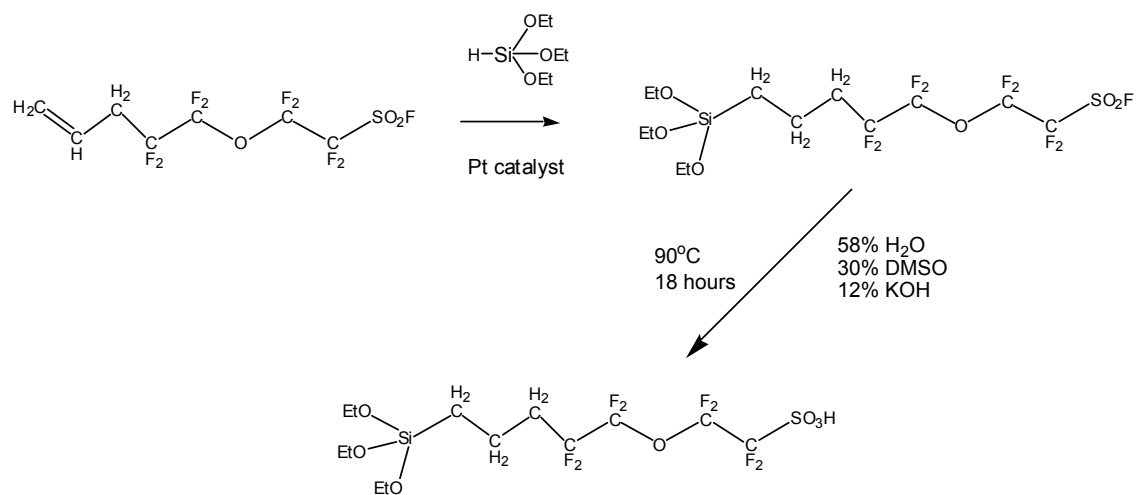
R =



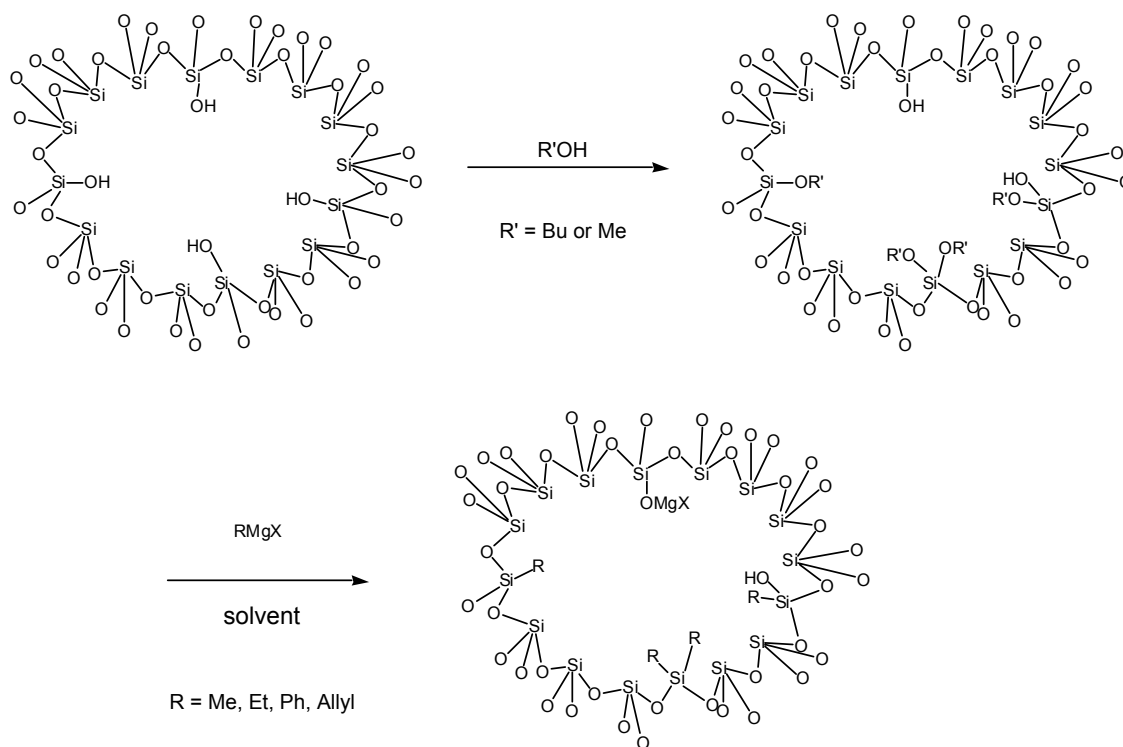
**Scheme 3.9** Synthesis of guanidine organosilanes. Adapted from ref. 17.

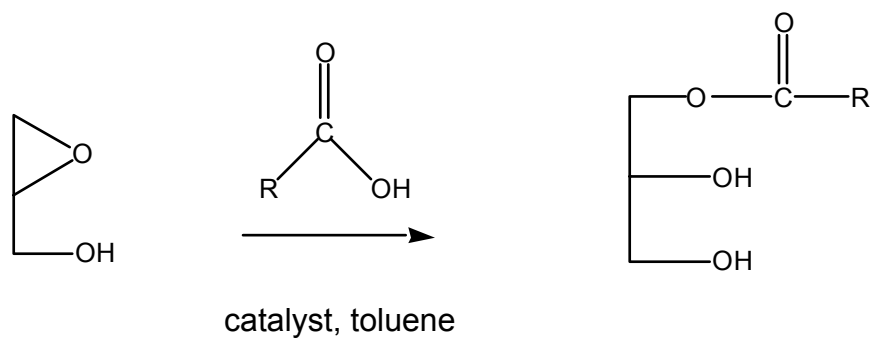
**Scheme 3.10** Linstead-Knoevenagel condensation. Adapted from ref. 17.

**Scheme 3.11** Synthesis of perfluorosulfonyl fluoride silane and subsequent hydrolysis to the perfluorosulfonic acid silane. Adapted from ref. 18.

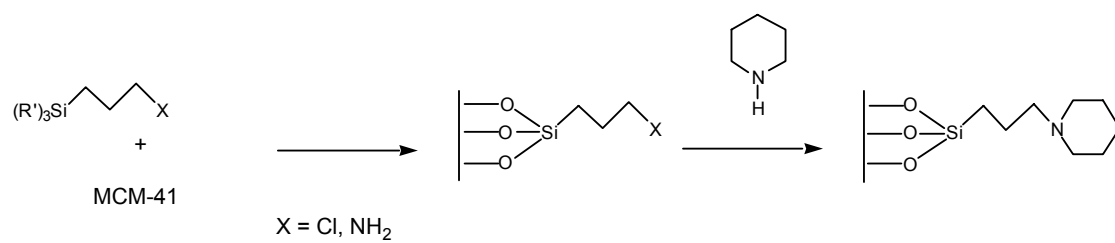


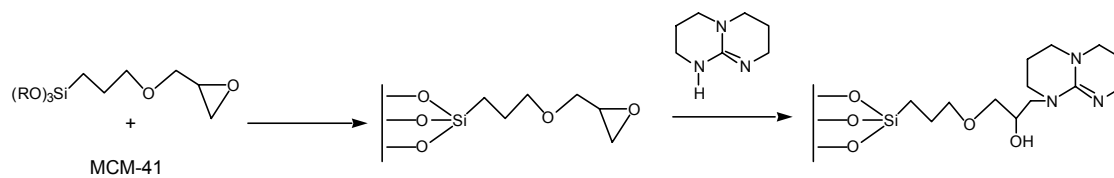
**Scheme 3.12** Esterification and Grignard modification of the ordered, mesoporous materials. Adapted from ref. 26.



**Scheme 3.13** Monoglyceride synthesis from glycidol and fatty acids.

**Scheme 3.14** Preparation of amine-containing MCM-41 hybrids for monoglyceride synthesis. Adapted from ref. 27.



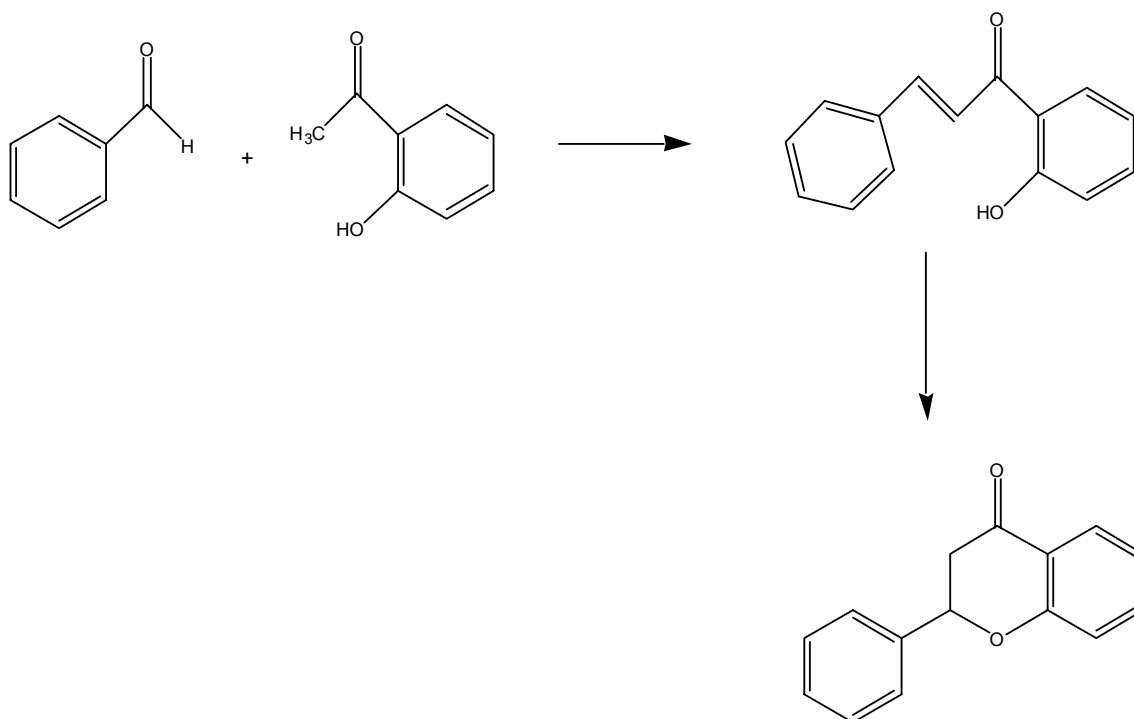
**Scheme 3.15** Synthesis of guanidine hybrid materials. Adapted from ref. 29.

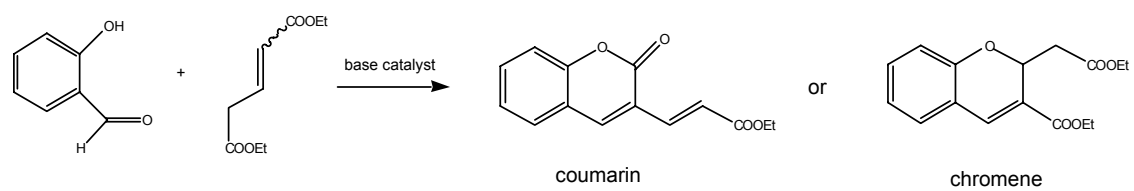
**Scheme 3.16** Immobilization of imidazole on ordered, mesoporous materials.

Adapted from ref. 31.

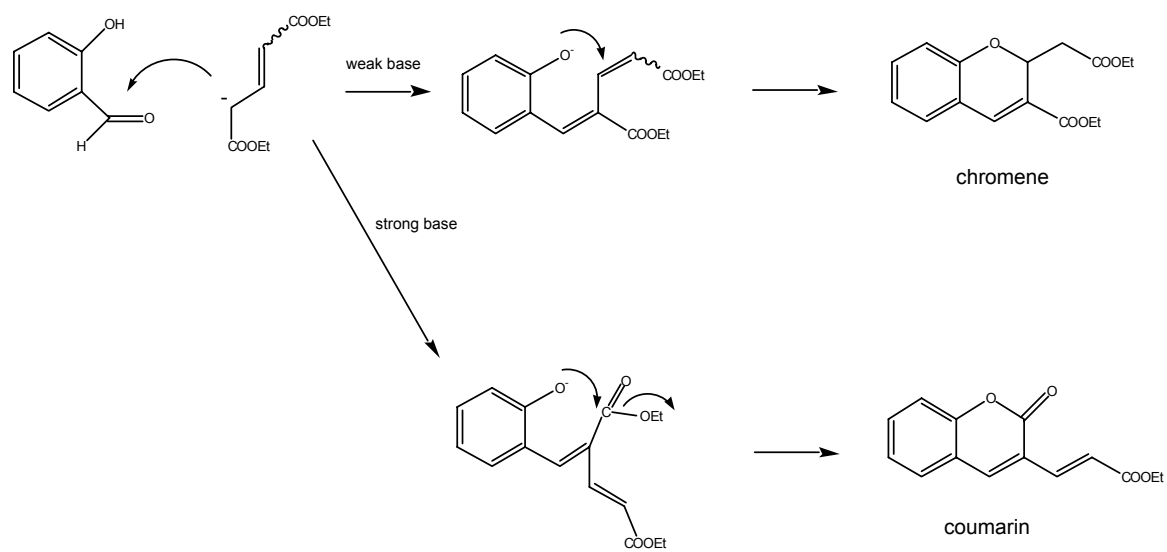


**Scheme 3.17** Aldol condensation and intramolecular Michael addition of benzaldehyde and 2'-hydroxyacetophenone to flavanone.



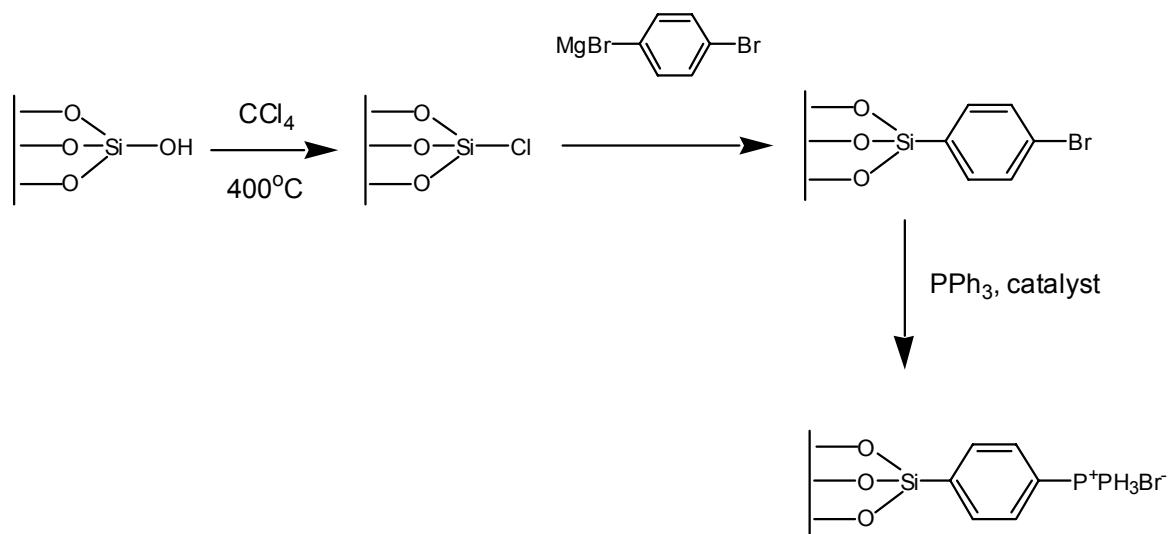
**Scheme 3.18** Synthesis of coumarins and chromenes via base catalyzed condensations.

**Scheme 3.19** Proposed mechanism of coumarin and chromene formation. Adapted from ref. 33.

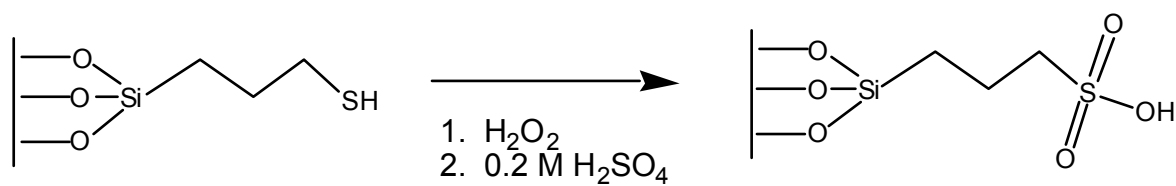


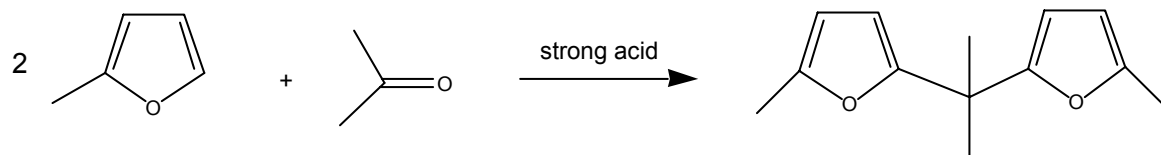
**Scheme 3.20** Preparation of silica-supported phase transfer catalysts. Adapted from ref.

35.

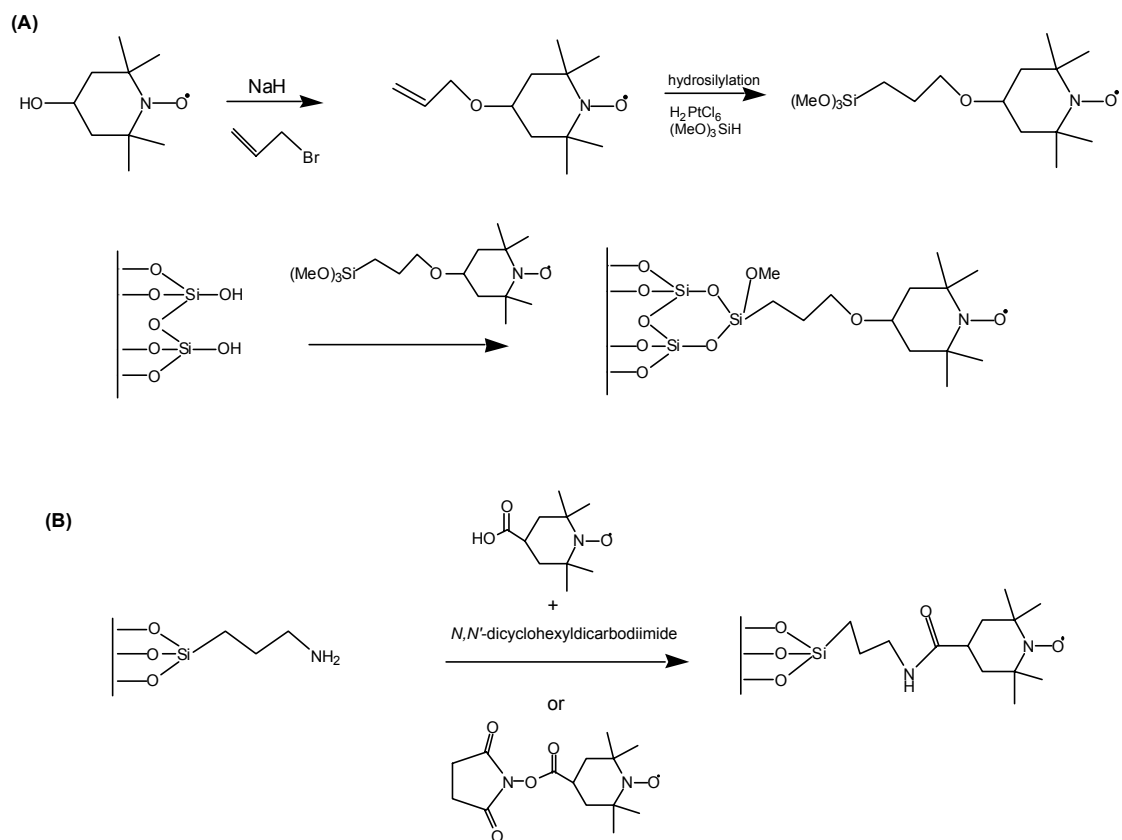


**Scheme 3.21** Oxidation of mercaptopropyl-functionalized silicas to give sulfonic acid sites. Adapted from ref. 38.

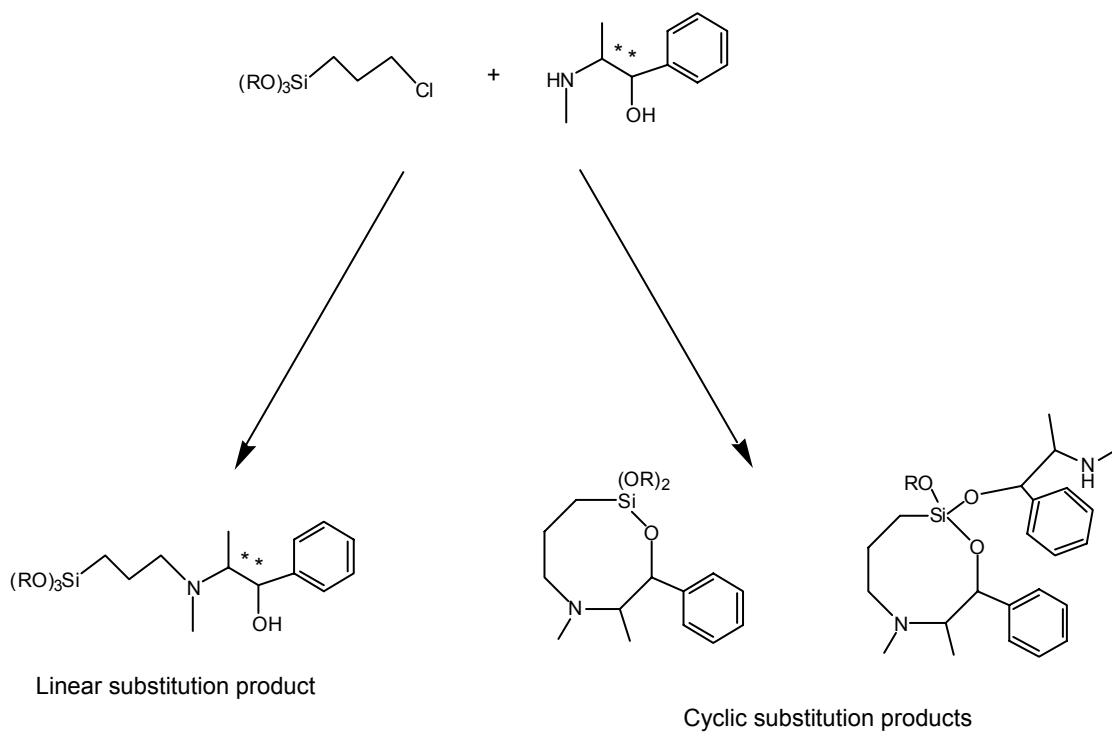


**Scheme 3.22** Acid catalyzed addition of 2-methylfuran and acetone.

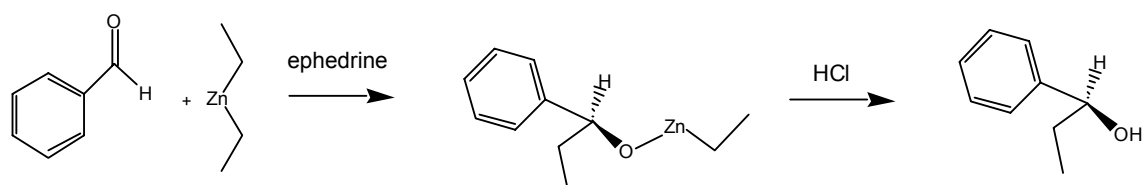
**Scheme 3.23** (A) Synthesis of TEMPO-ether-silane. (B) Synthesis of TEMPO-amide-MCM-41. Adapted from ref. 39.



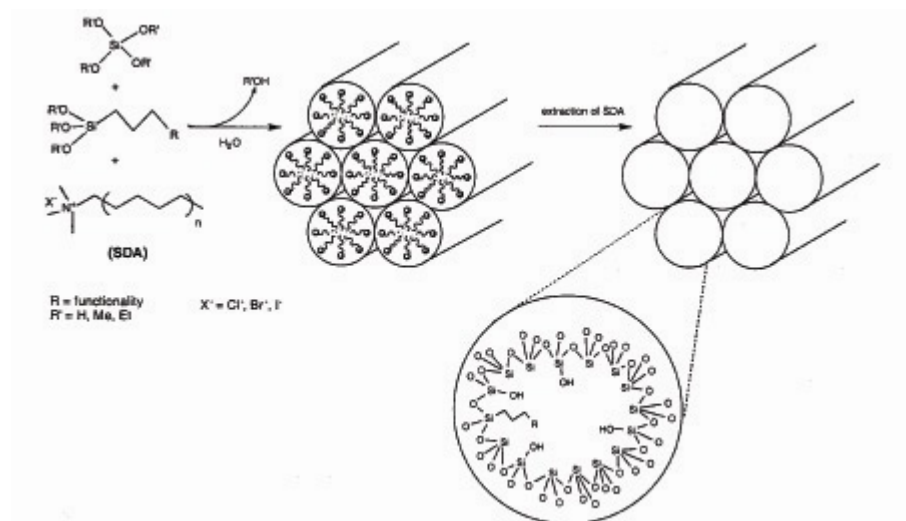
**Scheme 3.24** Products of nucleophilic substitution of chloropropylsilane and (-)-ephedrine. Adapted from ref. 40.

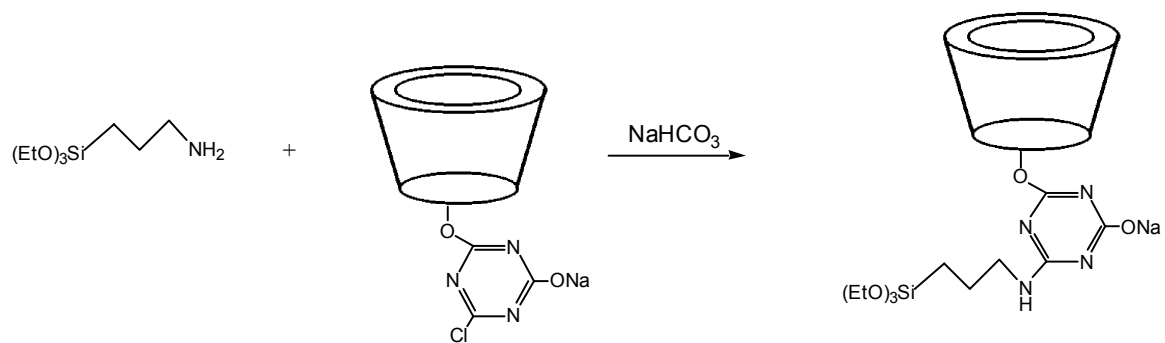


**Scheme 3.25** Synthesis of (R)-1-phenyl-propan-1-ol from benzaldehyde and diethylzinc.



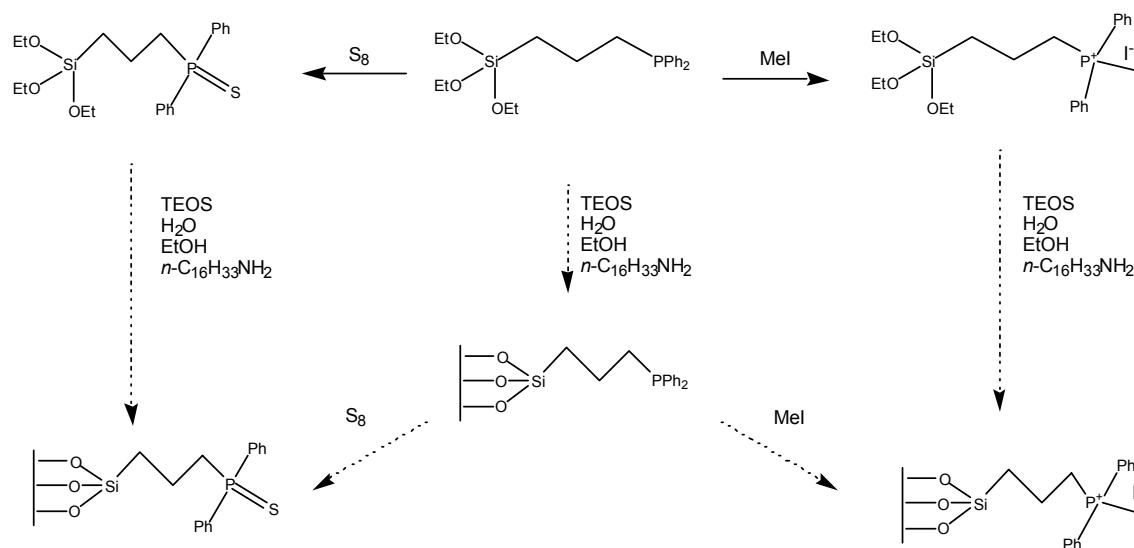
**Scheme 3.26** Co-condensation of organosilanes and tetraalkoxysilanes for the assembly of ordered, mesoporous, organic-inorganic hybrid solids.

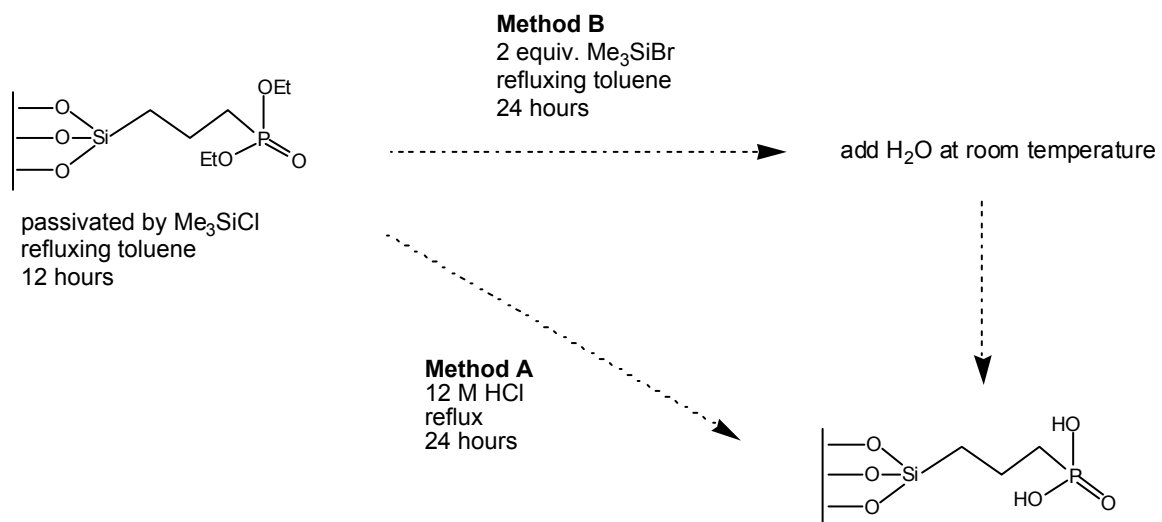


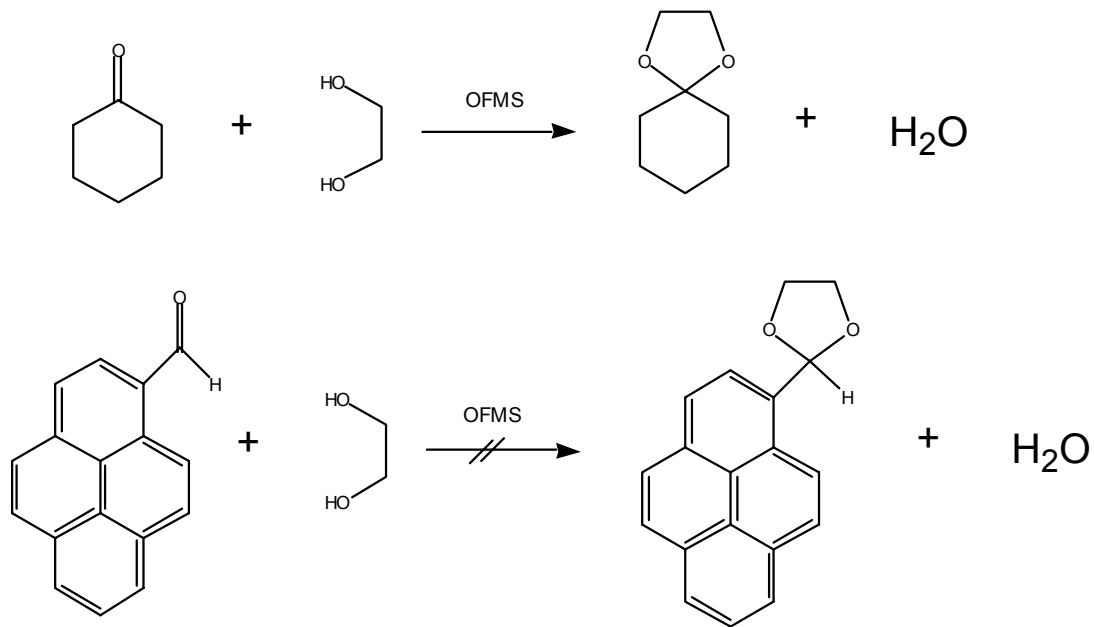
**Scheme 3.27** Synthesis of cyclodextrin-containing organosilane. Adapted from ref. 60.

**Scheme 3.28** Phosphorous-containing organosilane and mesoporous material syntheses.

Adapted from ref. 68.

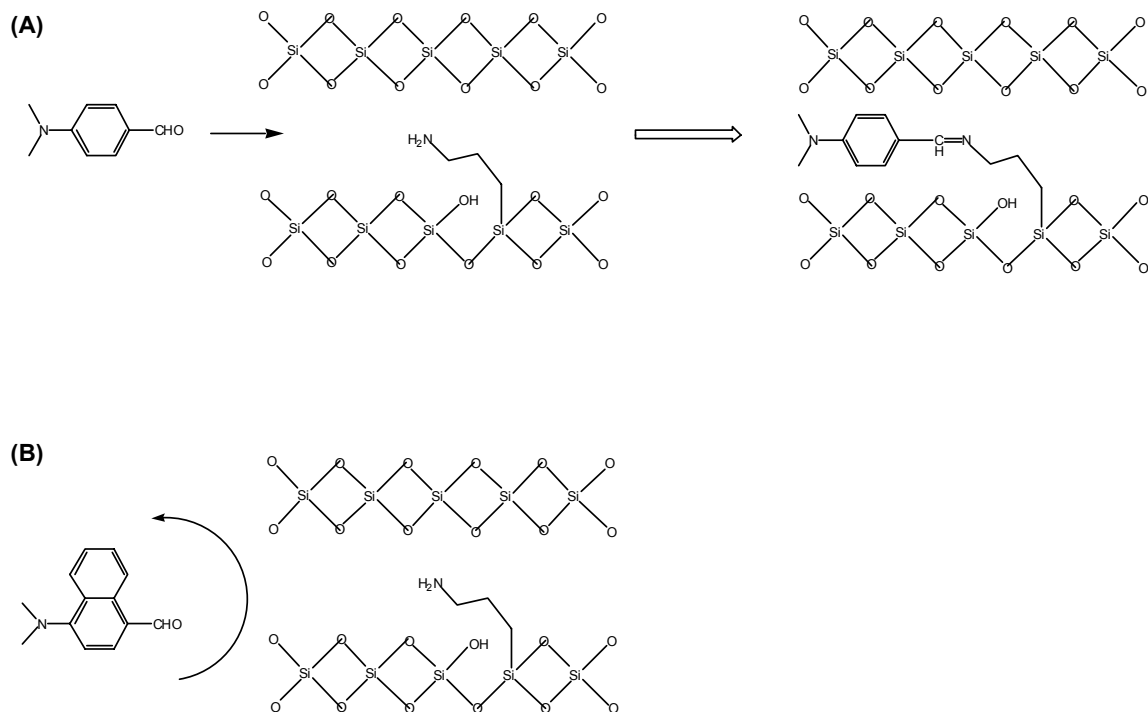


**Scheme 3.29** Synthesis of phosphonic acid sites in SBA-15. Adapted from ref. 75.

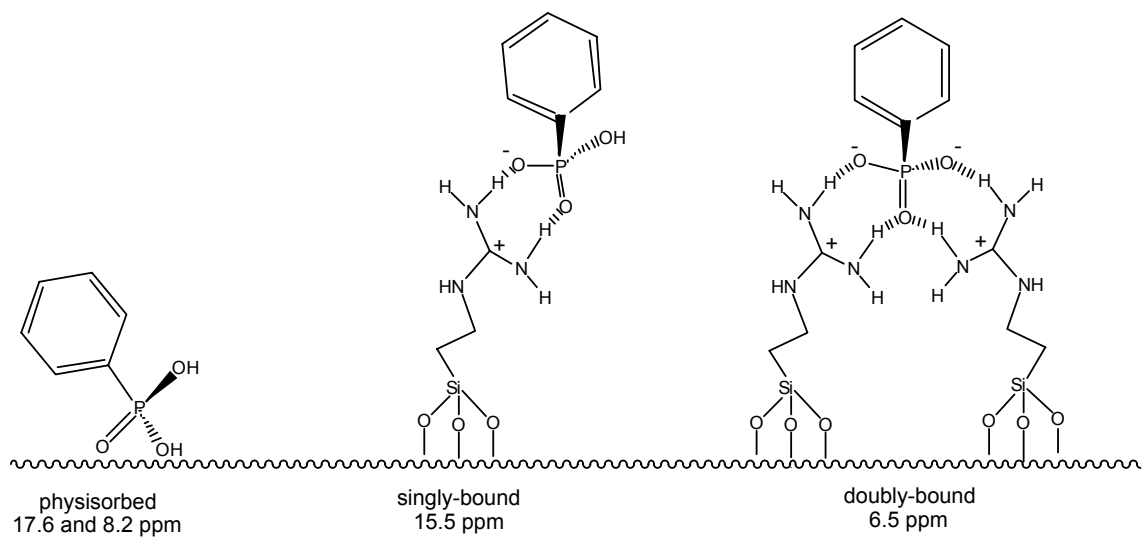
**Scheme 3.30** Shape-selective behavior of OFMS catalysts.

**Scheme 3.31** Shape-selective imine reactions with OFMS materials. **(A)** Reaction of 4-(dimethylamino)benzaldehyde. **(B)** Reaction of 4-dimethylamino-1-naphthaldehyde.

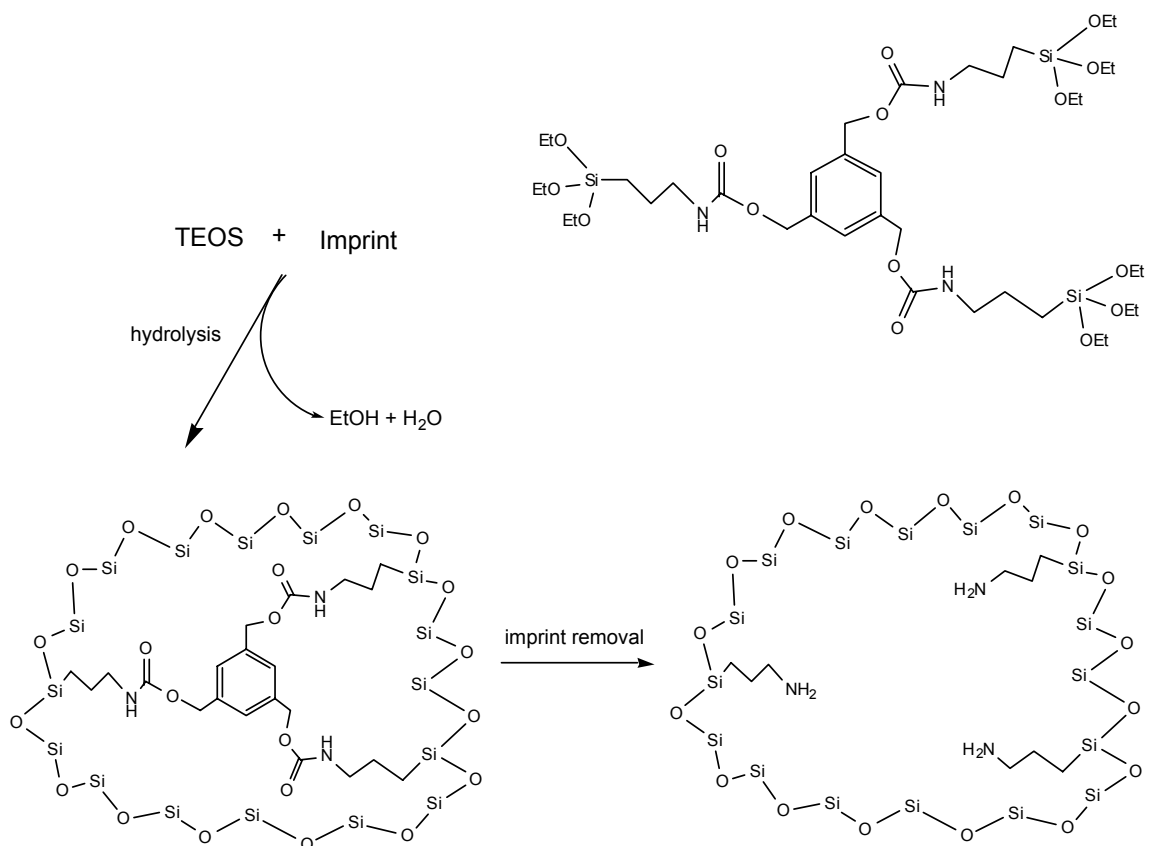
Adapted from ref. 53.



**Scheme 3.32** Interaction modes of phenylphosphonic acid with guanidine-functionalized, imprinted xerogels.  $^{31}\text{P}$  MAS NMR chemical shifts are listed for each configuration. Adapted from ref. 107.

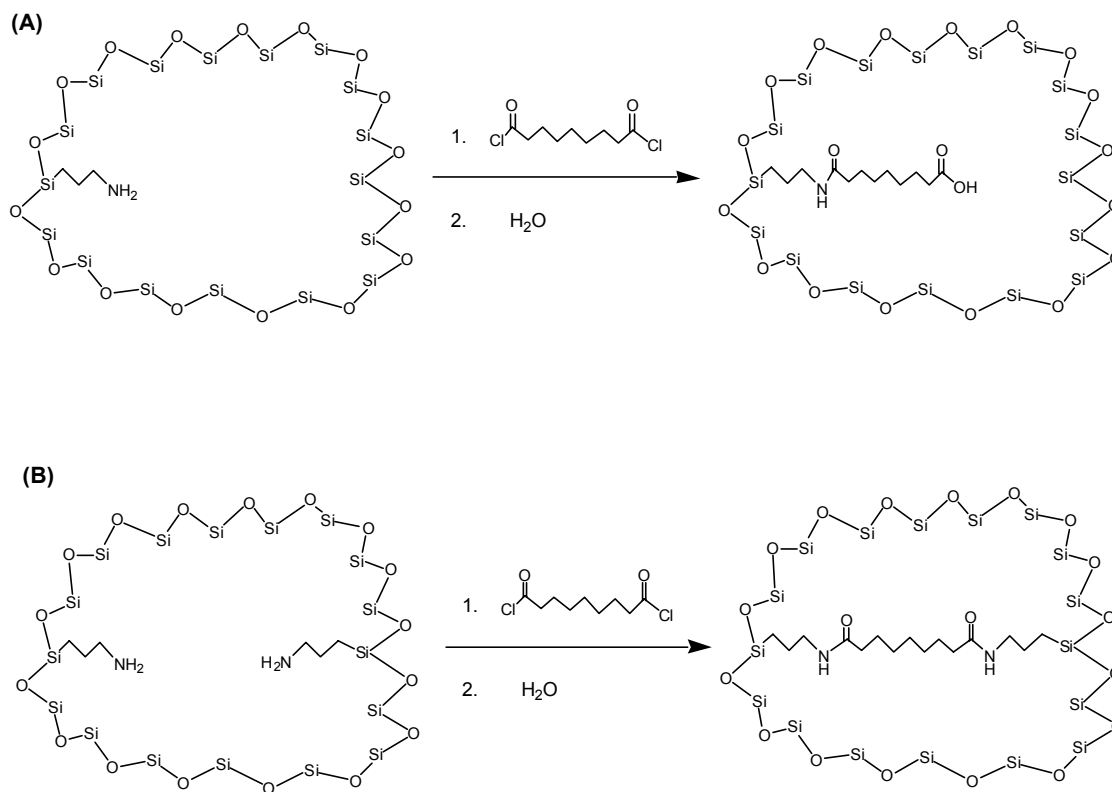


**Scheme 3.33** Imprinting of amorphous silica. The example illustrated is for organizing three aminopropyl groups. Adapted from ref. 105.



**Scheme 3.34** One (A) and two (B) point interactions of aminopropyl-imprinted silicas.

Adapted from ref. 108.



**Scheme 3.35** Acid and base catalyzed reactions in one-pot reactions. Adapted from ref.

109.

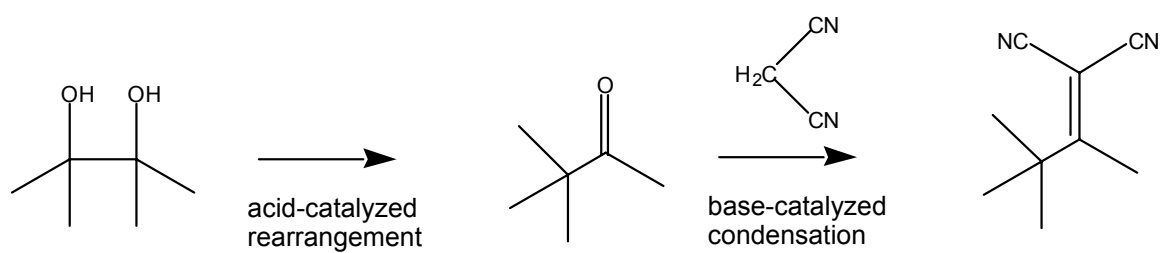
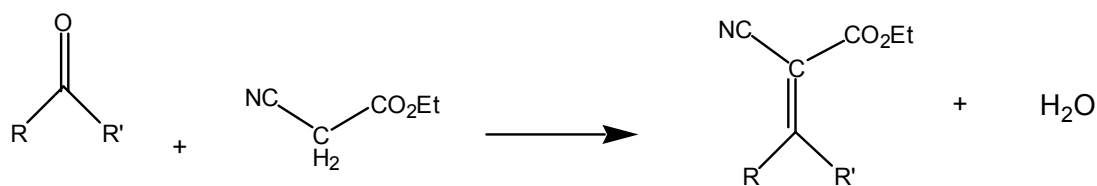


**Table 3.1** Knoevenagel condensation of various aldehydes and ketones with ethyl cyanoacetate in cyclohexane using aminopropyl silica. From ref. 12.



	R	R'	Temp (°C)	Time (hr)	Yield (%)
<b>1</b>	Ph	H	25	4	99
<b>2</b>	<i>n</i> -C <sub>5</sub> H <sub>11</sub>	H	25	7	97
<b>3</b>	<i>n</i> -C <sub>7</sub> H <sub>15</sub>	H	25	8	98
<b>4</b>	cyclo-C <sub>5</sub> H <sub>10</sub>	---	82	1	98 <sup>a</sup>
<b>5</b>	Et	Et	82	2	97 <sup>a</sup>
<b>6</b>	Et	Et	82	4	65
<b>7</b>	<i>n</i> -C <sub>4</sub> H <sub>10</sub>	Me	82	4	98 <sup>a</sup>
<b>8</b>	<i>t</i> -C <sub>4</sub> H <sub>10</sub>	Me	82	24	22 <sup>a</sup>
<b>9</b>	Me	Ph	82	24	68 <sup>a</sup>
<b>10</b>	Ph	Ph	82	72	8 <sup>a</sup>

<sup>a</sup> Water removed during reaction by a Dean and Stark trap.

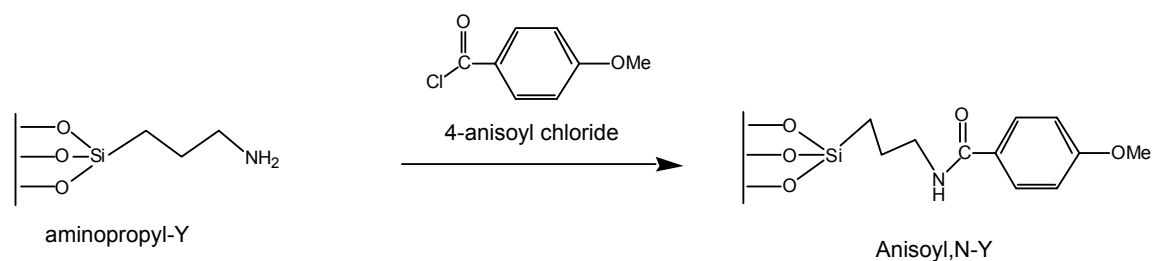
**Table 3.2** Knoevenagel condensation of ethyl cyanoacetate and pentan-3-one using imine-based silica hybrids. From ref. 15.

Imine <sup>a</sup>	% Yield with time						
	0.5 h	1 h	2 h	3 h	4 h	5 h	6 h
<b>1</b>	6.0	9.2	13.6	16.3	17.9	19.4	23.3
<b>2</b>	27.5	50.6	69.1	69.2	76.0	75.7	---
<b>3</b>	44.0	58.1	69.8	72.7	76.7	82.8	---
<b>4</b>	16.5	23.4	29.8	31.6	32.5	33.7	34.8
<b>5</b>	38.0	53.7	67.1	72.7	74.4	79.0	80.1
<b>6</b>	67.2	69.3	81.5	88.2	92.9	98.6	99.5
<b>7</b>	37.6	49.4	70.5	74.9	80.3	86.8	86.2

<sup>a</sup>Imine-based silica hybrid formation depicted in Scheme 8.

**Table 3.3** Nitrogen sorption data for organosilanes grafted onto zeolite Y. From ref.

47.



Support (Si/Al ratio)	Surface Area (m <sup>2</sup> /g)	External and Mesopore Surface Area (m <sup>2</sup> /g)	Micropore Volume (cm <sup>3</sup> /g)
unmodified HY (2.5)	751	48	0.31
chloropropyl-Y(2.5)	417	33	0.17
aminopropyl-Y (2.5)	479	37	0.19
unmodified HY (8)	720	126	0.26
chloropropyl -Y (8)	447	90	0.16
aminopropyl -Y (8)	422	92	0.15
Anisoyl,N-Y (8)	382	84	0.13
unmodified HY (17.5)	795	135	0.29
chloropropyl -Y (17.5)	537	91	0.20
aminopropyl -Y (17.5)	523	92	0.19
Anisoyl,N-Y (17.5)	431	83	0.15

## CHAPTER FOUR

SYNTHESIS AND CHARACTERIZATION  
OF BASE-CONTAINING ORGANIC-  
FUNCTIONALIZED MOLECULAR SIEVES

## 4.1 Introduction

Rodriguez and co-workers demonstrated the incorporation of a covalently tethered ammonium within a mesoporous material to enable the exchange of hydroxide within the pore space.<sup>1</sup> The work of Tsuji *et al.* demonstrated a method to incorporate organic functionality into a zeolite, \*BEA, via direct synthesis techniques using organosilanes, to make OFMSs.<sup>2</sup> These functionalities were shown to be useful as active sites for acidic catalysis. Modifications to the previously reported synthesis of OFMSs to adopt this strategy would allow one to place a strong Brønsted base within the pore space of a zeolite.

## 4.2 Experimental Section

### 4.2.1 Silica Zeolite Beta Preparation

Silica-containing Zeolite \*BEA (Si-\*BEA) was prepared according to known methods<sup>3</sup> to use as seed for OFMS synthesis (see below) and for control experiments. The gel was prepared by the dissolution of 13.14 g tetraethylammonium fluoride (TEAF, the structure-directing agent, purchased from Aldrich) in 13.83 g of water. Tetraethylorthosilicate (27.357 g, TEOS, purchased from Aldrich) was added dropwise to the aqueous solution with vigorous stirring. The silane was allowed to hydrolyze overnight at room temperature. Ethanol and excess water were completely removed from the resulting gel by rotovap. The composition of the final gel was 1 SiO<sub>2</sub>/ 0.54 TEAF/ 7.15 H<sub>2</sub>O. The gel was then divided into three Teflon-lined autoclaves. The autoclaves were heated under autogeneous pressure statically at 150°C for 7 days for crystallization to occur. The resulting zeolite \*BEA crystals were isolated by filtration and washed with water and acetone. The recovered crystals were dried overnight at 100°C. The

crystallinity of the material was verified by powder X-ray diffraction (XRD, Scintag XDS 2000 diffractometer with liquid nitrogen cooled GE detector using Cu K  $\alpha$  radiation).

#### 4.2.2 *Quaternary Ammonium OFMS Preparation*

The direct synthesis technique for OFMSs previously reported<sup>2</sup> was modified to allow the addition of an ammonium functionalized organosilane (N-trimethoxysilylpropyl-N,N,N-trimethylammonium chloride, purchased from Gelest, Inc as a 50% solution in methanol) to the gel precursor (see Figure 4.1). The gel was prepared by the dissolution of 7.109 g TEAF in 7.959 g of water. Because the ammonium-functionalized organosilane and TEOS are not miscible, ethanol (absolute, Aaper Alcohol) was used as a solvent to homogenize the silane mixture. A solution of 14.886 g of TEOS and 14.525 g of EtOH was prepared. The ammonium-functionalized organosilane (1.195 g) was then added to the ethanol solution. (It is important to note that without the use of ethanol, an inhomogeneous gel will form, which may result in a phase separation of the ammonium functionality within the resulting solids.) The silane/ethanol solution was added to the aqueous TEAF solution dropwise via pipet with vigorous stirring. The mixture was allowed to hydrolyze overnight at room temperature.

Ethanol, methanol, and excess water were completely removed from the resulting gel by rotovap. The composition of the final gel was 1 SiO<sub>2</sub>/ 0.03 R-silane/ 0.548 TEAF/ 7.63 H<sub>2</sub>O, similar to other OFMS gel compositions. The gel was then divided into two Teflon-lined autoclaves, with approximately 0.007 grams of Si-\*BEA seed crystal per gram of gel. The autoclaves were heated under autogeneous pressure and rotation at approximately 60 rpm at 140°C for no less than 14 days for crystallization to occur. The

crystals of ammonium-functionalized \*BEA (Q-\*BEA) were recovered by filtration and washing as above.

#### 4.2.3 Halogenated propyl- OFMS Preparation

Halogenated propyl-containing OFMSs (3-bromopropyl- and 3-iodopropyl-containing \*BEA) were prepared via the direct synthesis techniques as described by Tsuji and co-workers.<sup>2</sup> 3-chloropropyl-containing \*BEA was also synthesized using a similar procedure. A typical gel was prepared by the dissolution of 7.730 g TEAF in 7.959 g of water. A solution of 15.097 g of TEOS and 0.853 g of 3-bromopropyltrimethoxysilane (purchased from Gelest) was prepared. The silane mixture was added to the aqueous TEAF solution dropwise via pipet with vigorous stirring. The mixture was allowed to hydrolyze overnight at room temperature. Ethanol, and excess water were removed from the resulting gel by rotovap. The composition of the final gel was 1 SiO<sub>2</sub>/ 0.05 R-silane/ 0.58 TEAF/ 6.93 H<sub>2</sub>O. The gel was then divided into Teflon-lined autoclaves and seeded with Si-\*BEA as described above. The autoclaves were heated under autogeneous pressure and rotation at approximately 60 rpm at 140°C for 17 days for crystallization to occur. The crystals of bromopropyl-functionalized \*BEA (Br-\*BEA) were recovered by filtration and washing as above. The chloropropyl-functionalized \*BEA (Cl-\*BEA) and iodopropyl-functionalized \*BEA (I-\*BEA) were prepared similarly, using 3-chloropropyltrimethoxysilane and 3-iodopropyltrimethoxysilane, both obtained from Gelest. The synthesis times were 17 days for Cl-\*BEA and 15 to 17 days for I-\*BEA.

#### 4.2.4 Quaternary Phosphonium Organosilane Preparation

OFMSs were also made with a covalently tethered phosphonium moiety to compare the stability of the ammonium and phosphonium groups. The phosphonium

analogue, P-trimethoxysilylpropyl-P,P,P-trimethylammonium bromide, was prepared by nucleophilic displacement of 3-bromopropyltrimethoxysilane with trimethylphosphine (see Scheme 4.1). The 3-bromopropylorganosilane used in the organosilane preparation was purchased from United Chemicals Technologies, Inc. The material (see Figure 4.2) was dried over molecular sieves and degassed by freeze-pump-thaw cycling with liquid N<sub>2</sub>. Trimethylphosphine (see Figure 4.3) was obtained as a 1M solution in anhydrous toluene purchased from Aldrich. Toluene was purchased anhydrous from Alfa Aesar then stored over molecular sieves and degassed by freeze-pump-thaw cycling with liquid N<sub>2</sub>.

Toluene (17.59 g) was added to a round bottom Schlenk flask under argon. 3-bromopropyltrimethoxysilane (2.92 g) was to the toluene added via syringe purged with argon. The trimethylphosphine/toluene solution (23.02 g, stoichiometric excess) was added by measuring through a Schlenk graduated cylinder. The reaction mixture was allowed to stir at reflux under argon overnight. The product, P-trimethoxysilylpropyl-P,P,P-trimethylammonium bromide, was obtained as a white precipitate. The toluene mixture (with excess reagents) was removed by filtration through a glass wool-filled needle. The precipitate was washed with anhydrous petroleum ether. After washing, the solids were allowed to settle and excess ether was decanted via a syringe. The solids were dried under vacuum at room temperature for 3 hours, yielding a white powder (80% yield of phosphonium organosilane). The preparation of the compound was confirmed by <sup>13</sup>C and <sup>31</sup>P liquid NMR (see Figure 4.4). The phosphonium organosilane was stored under argon as the solid material until use in material preparation.

#### 4.2.5 Quaternary Phosphonium OFMS Preparation

The phosphonium-functionalized organosilane was used to prepare \*BEA materials as in the OFMS synthesis procedure described for Q-\*BEA. The phosphonium functionalized organosilane was mixed with anhydrous ethanol to prepare a 30% by weight solution and stored under inert. The gel was prepared by the dissolution of 8.946 g TEAF in 8.614 g of water. The aqueous mixture was purged with argon for 10 minutes. A solution of 17.85 g of TEOS (dried over molecular sieves) and 4.72 g of EtOH (anhydrous) was prepared. The phosphonium-functionalized organosilane/EtOH solution (2.83 g) was added to the TEOS/EtOH solution. The silane/ethanol solution was added to the aqueous TEAF solution dropwise via syringe with vigorous stirring. The mixture was allowed to hydrolyze overnight at room temperature. The gel was rotovaped and placed into autoclaves with seed Si-\*BEA at 140°C with rotation for 24 days. The composition of the final gel was 1 SiO<sub>2</sub>/ 0.03 R-silane/ 0.571 TEAF/ 9.50 H<sub>2</sub>O. The crystals of phosphonium-functionalized \*BEA (P<sub>quat</sub>-\*BEA) were recovered by filtration and washing.

#### 4.2.6 Extraction of \*BEA Samples

The removal of the SDA from zeolites is usually accomplished by calcination at elevated temperatures under air. However, since such a treatment would remove the organic functionalities in the OFMS materials as well, extraction was used to remove the TEAF from the pore space of the zeolite.<sup>2</sup> The as-made OFMS crystals isolated from the autoclave were stirred overnight in an acidified, aqueous pyridine solution (1 part aqueous 1M HCl to 1 part water) at 80°C to extract the SDA. The extracted crystals were isolated by filtration and washing with water. The pyridine extraction was repeated to

remove any residual TEAF. Alternatively, one may use an acetic acid solution (2 parts acetic acid: 5 parts water) at 80°C.<sup>2</sup>

#### 4.2.7 Nucleophilic Displacement of X- \*BEA Samples

Phosphonium-functionalized OFMSs may also be prepared by nucleophilic displacement of a halogenated moiety *after* preparation and extraction of the zeolite. Halogenated propyl-functionalized \*BEA (e.g., Br-\*BEA) was prepared and extracted as described above. The extracted Br-\*BEA (0.36 g) was added to toluene (18 mL, dried by distillation and stored over molecular sieves) using Schlenk techniques. Trimethylphosphine (3 mL of 1M solution) was added by graduated cylinder. An additional 30 mL of toluene was added by syringe through the graduated cylinder to rinse all of the trimethylphosphine into the flask. The mixture was refluxed under an inert atmosphere for four days (see Scheme 4.2). The solids were isolated by filtration and washing with toluene and acetone, yielding P<sup>+</sup>X<sup>-</sup>\*BEA (e.g., P<sup>+</sup>Br<sup>-</sup>\*BEA). The procedure was repeated to make P<sup>+</sup>Cl<sup>-</sup>\*BEA and P<sup>+</sup>I<sup>-</sup>\*BEA. Br-\*BEA was also reacted with triphenylphosphine in a similar manner to probe whether the organic moieties were located within the zeolite pore space or accessible from the surface.

#### 4.2.8 Tethering of Organosilanes onto Controlled Pore Glass

For purposes of control experiments, the organosilanes studied were tethered onto amorphous, mesoporous silica. The loading of organic functionalities are significantly higher after tethering onto mesoporous silica than what may be accomplished via direct synthesis techniques in OFMSs. This technique allows one to study the behavior of the organic moieties during various treatment methods, such as extraction, by <sup>13</sup>C CP/MAS

NMR. Because of the low number density of organic moieties in OFMS materials,  $^{13}\text{C}$  CP/MAS NMR can not detect the tethered organic moieties in the material.

The N-trimethoxysilylpropyl-N,N,N-trimethylammonium chloride was tethered onto amorphous silica, <sup>4</sup> (Controlled Pore Glass, CPG-240, 240 Å in pore diameter, purchased from Controlled Pore Glass, Inc.). The ammonium-containing organosilane (5.0 g) was added to a slurry of CPG (3.3 g) and toluene (200 mL). The mixture was allowed to stir at reflux at 110°C for 3-4 days. The solids were then recovered by filtration and washed with fresh toluene, water, and acetone. The solids were dried at 100°C overnight, to yield ammonium-containing CPG, Q-CPG.

The halogenated propyl-functionalized silanes (3-bromopropyltrimethoxysilane, 3-chloropropyltrimethoxysilane, and 3-iodopropyltrimethoxysilane) and the synthetically prepared phosphonium-functionalized organosilane were also each individually tethered onto CPG in a similar manner for characterization and control experiments. These materials were denoted Br-CPG, Cl-CPG, I-CPG, and P<sub>quat</sub>-CPG. To further examine the nucleophilic displacement reaction to prepare phosphonium-containing materials, the halogenated propyl-functionalized CPG materials were exposed to trimethylphosphine or triphenylphosphine to add the phosphonium moiety as described above with extracted zeolite \*BEA (see Scheme 4.3). The trimethylphosphonium-containing materials were denoted P<sup>+</sup>Br<sup>-</sup>-CPG, P<sup>+</sup>Cl<sup>-</sup>-CPG, and P<sup>+</sup>I<sup>-</sup>-CPG. The triphenylphosphonium-containing materials were denoted P<sup>+</sup>Ph<sub>3</sub>Br<sup>-</sup>-CPG and P<sup>+</sup>Ph<sub>3</sub>Cl<sup>-</sup>-CPG (I-CPG was not treated with triphenylphosphine).

The materials were analyzed by  $^{13}\text{C}$  and  $^{29}\text{Si}$  CP/MAS NMR and  $^{31}\text{P}$  MAS NMR to determine the success of the reaction.  $^{13}\text{C}$  CP/MAS spectra were taken on a Bruker

Advance 200 MHz spectrometer with a cross polarization accessory. Samples were packed in 7 mm zirconia rotors and spun at 4 kHz in air. Experiments were done using  $^{13}\text{C}$  contact time of 2 milliseconds. The recycle time was optimized in each sample and ranged from 1.5 to 3 seconds. Experiments were referenced externally to adamantane.  $^{29}\text{Si}$  CP/MAS spectra were also taken on the Bruker Advance 200 MHz spectrometer. Experiments were done using  $^{29}\text{Si}$  contact time of 2.5 milliseconds. Experiments were referenced externally using tetrakis(trimethylsilyl)silane, TKTMS.  $^{31}\text{P}$  MAS NMR spectra were taken on a Bruker Advance 500 MHz spectrometer. Samples were packed in a 2 mm zirconia rotor and spun at 10 kHz in air. Experiments were done using a 2 microsecond  $^{31}\text{P}$  pulse [ $^{31}\text{P}$  90°]. The recycle time was optimized in each sample. Experiments were referenced externally to 80% phosphorous acid. Quantitative phosphorous calculations were obtained from  $^{31}\text{P}$  MAS NMR using an external standard of sodium phosphate,  $\text{NaH}_2\text{PO}_4$ .

#### 4.2.9 Ion-exchange of OFMS Samples

After extraction and quaternization, phosphonium-containing \*BEA samples were ion-exchanged to probe the presence of the phosphonium moiety and to exchange the hydroxide into the materials for base catalysis testing. Ion-exchange was done by contacting the phosphonium halide (e.g.,  $\text{P}^+\text{Br}^-$ \*BEA, 0.19 g) with 80 mL of 1 N solution of nitric acid ( $\text{HNO}_3$ ) in water. The slurry was allowed to stir, covered, overnight at room temperature. The exchanged material,  $\text{P}^+\text{NO}_3^-$ \*BEA, was isolated by filtration and analyzed by Fourier transform infrared spectroscopy to determine if  $\text{NO}_3^-$  was present in the exchanged material. IR spectroscopy was done on samples as pressed KBr pellets, using a Nicolet Nexus 470 FT-IR equipped with a DTGS detector and KBr

beamsplitter, having a 1mW He-Ne laser (633 nm) and Happ-Genzel Apodization with a resolution of  $1.928 \text{ cm}^{-1}$ . Quantification of halide removal (and nitrate incorporation) by ion-exchange was done by titration of the filtrate with silver nitrate. A known amount (in excess) of aqueous silver nitrate (0.01 N) was added to the filtrate to precipitate halide anions from the solution. Aqueous potassium thiocyanate (0.01 N) was used to quantify the  $\text{Ag}^+$  remaining in solution, using iron (III) nitrate as an indicator.

After nitrate exchange, phosphonium-containing materials were also exchanged with sodium tetraphenylborate ( $\text{NaBPh}_4$ ) to determine if the functional groups were accessible; i.e., if the phosphonium moieties were within the pore space of the zeolite. The  $\text{NO}_3^-$ -exchanged material (e.g.,  $\text{P}^+\text{NO}_3^-$ -\*BEA, 0.2 g) was slurried in a 2.4% solution of  $\text{NaBPh}_4$  and water, covered, overnight at room temperature. The borate-exchanged materials (e.g.,  $\text{P}^+ \text{Ph}_4^-$ -\*BEA) were isolated by filtration and then examined by  $^{11}\text{B}$  MAS NMR to look for the presence of  $\text{BPh}_4$ .

To prepare the materials for catalytic applications, the  $\text{NO}_3^-$ -exchanged materials (e.g.,  $\text{P}^+\text{NO}_3^-$ -\*BEA, 0.3 g) were slurried with 15 mL of a 0.12 M solution of tetramethylammonium hydroxide (TMAOH) in methanol at room temperature for *10 minutes*, following the procedure of Rodriguez *et al.*<sup>1</sup> However, even after extensive washing with methanol after filtration, residual TMAOH remained in the zeolite and interfered with further catalytic testing. This hydroxide-exchange method was discarded.

Alternatively, the  $\text{NO}_3^-$ -exchanged materials (e.g.,  $\text{P}^+\text{NO}_3^-$ -\*BEA, 0.25 g) were stirred with 75 mL of a dilute solution of aqueous sodium hydroxide (0.001 N, pH ~9) at room temperature *for 20 minutes*. Note that longer stir times (~24 hours) in basic solutions would lead to dissolution of the silica. The exchanged material, e.g.,

$P^+OH^-$ -\*BEA, was isolated by filtration. The filtrate was collected and analyzed quantitatively for  $NO_3^-$  content (using colorimetric titration for  $NO_3^-$  by VWR CHEMETS kit #K-6902) to determine the amount of nitrate removal (and hydroxide incorporation) by ion-exchange. The solid materials were examined by IR to observe the disappearance of  $NO_3^-$ . Similar exchange procedures were performed on the equivalent functionalized-CPG materials to act as controls ( $P^+OH^-$ -CPG).

Finally, to test the hydroxide exchange, some of the  $P^+OH^-$ -\*BEA and  $P^+OH^-$ -CPG materials were stirred in a 0.0126 N aqueous solution of sodium bromide (NaBr, pH = 7.16). The hydroxide-exchanged solids (0.20 g) were mixed with 20 mL of NaBr solution at room temperature for five minutes, and the pH was measured. The slurry was allowed to stir, covered, overnight. The change in  $Br^-$  concentration, from  $AgNO_3$  titration, was measured to quantify the extent of hydroxide incorporation.

### 4.3 Results and Discussion

#### 4.3.1 Quaternary Ammonium OFMS Preparation

Quaternary ammonium-functionalized OFMSs were prepared using the direct synthesis method as described above. A white crystalline material was obtained after filtration. The material was of the zeolite \*BEA structure, as observed by XRD (see Figure 4.5). The extraction procedure, either by acetic acid or acidified pyridine, did not affect the \*BEA structure of Si-\*BEA or Q-\*BEA.

TEAF was removed from as-made Si-\*BEA by heat treatment from 137 to 400°C, as seen by thermogravimetric analysis (TGA, see Figure 4.6). TGA was performed on a DuPont 951 Thermogravimetric Analyzer, heated under nitrogen at 10°/min to 800°C. Si-\*BEA, extracted twice by the acidic pyridine solution, still has residual organic from

100-300°C, as seen by TGA (see Figure 4.7). There was no observed weight loss from 300-400°C, suggesting that the TEAF was almost completely removed (99% removal). Jones *et al.* correlated the temperature at which weight loss occurred with the affinity of the SDA for the zeolite framework.<sup>5</sup> Because the TEAF from the higher temperature region was removed, it is unlikely that the remaining organic after extraction is SDA. Calcined Si-\*BEA was contacted with the pyridine extraction solution. As seen in Figure 4.8, a weight loss from 100-300°C was again observed. The remaining organic in the extracted OFMSs was pyridine from the extraction.

In an attempt to remove the pyridine from the material after SDA extraction, two water washing steps at 80°C overnight were performed. Si-\*BEA extracted with acidic pyridine twice and then washed with water twice showed 99% removal of TEAF from the extraction and 96% removal of residual pyridine from water washing by TGA (see Figure 4.9). However, when a similar procedure was conducted on an ammonium-functionalized \*BEA sample, only 71% of the pyridine was removed (98% of TEAF was removed by extraction, see Figure 4.10). Subsequent washing steps with water could not remove the remaining pyridine remaining after extraction. The Si-\*BEA synthesis using TEAF as a SDA is known to result in a “defect-free” material.<sup>3</sup> In a material containing few defect sites, there is little framework charge. Defect sites arise from incompletely condensed Si-O bonds in the framework, specifically Si-O<sup>-</sup> or Si-OH sites. The addition of an organosilane into the framework creates such a defect site. The defects in the OFMS framework likely contributed to increased affinity for pyridine in the structure. Because residual pyridine would interfere with further study in base catalysis, only acetic acid solution was used for extraction to prepare materials for catalytic study.

After SDA extraction with acidified pyridine, Si-\*BEA material has a pore volume of 0.197 cc/g of liquid N<sub>2</sub>, as detected by nitrogen adsorption (see Figure 4.11, dotted line). Nitrogen adsorption measurements were done at 77K on an Omnisorp 100 sorption apparatus in static mode with fixed dosing. Samples were pretreated to 200°C under vacuum for 12 hours. Nitrogen adsorption capacities are reported at P/P<sub>0</sub> = 0.2. Calcined Si-\*BEA had a pore volume of 0.230 cc/g (data not shown). This indicated some residual organic (pyridine) remains in the pores after extraction. After extraction, Q-\*BEA had only 0.186 cc/g of pore volume (see Figure 4.8), less than that of extracted Si-\*BEA. This could be attributed to the presence of ammonium-containing moieties or to an increased amount of residual pyridine remaining in extracted OFMS materials than in Si-\*BEA materials. Calcination of the extracted Q-\*BEA showed an increase in porosity to 0.206 cc/g as the organic residue was removed.

The carbon-silicon bond of the ammonium-functionalized organosilane remained intact during the synthesis of the zeolite. <sup>29</sup>Si CP/MAS NMR of as-made Q-\*BEA materials exhibited the presence of a Si-C bond, a T<sup>3</sup> site, at -68 ppm (see Figure 4.12). This bond was not observed in Si-\*BEA, either as-made or extracted (see Figure 4.13). The presence of a Si-C bond remained during the extraction of Q-\*BEA. This suggests that at least some organic remains tethered in the material after extraction.

Due to inconsistencies from sample to sample in nitrogen sorption results, which require heating under vacuum to prepare samples for analysis, the thermal stability of the quaternary ammonium moieties was examined. N-trimethoxysilylpropyl-N,N,N-trimethylammonium chloride was tethered onto CPG-240 (see Figure 4.14). The Q-CPG was then heated to 100 and 200°C under vacuum for 12 hours. After heat treatment to

100°C,  $^{13}\text{C}$  CP/MAS NMR showed the beginning of degradation of the ammonium moiety (see Figure 4.14C). By 200°C, there is severe decomposition of the ammonium functionality (see Figure 4.14D). Ion-exchange in nitric acid did not affect the integrity of the functional group. Despite the observation of degradation of the organic moiety by  $^{13}\text{C}$  CP/MAS NMR, the T<sup>3</sup> peak in  $^{29}\text{Si}$  CP/MAS NMR remains, indicating that the Si-C bond remains intact (see Figure 4.15).

It is well known that quaternary ammonium compounds undergo Hofmann decomposition. The ammonium cations degrade irreversibly by an elimination mechanism, resulting in a tertiary amine and the corresponding olefin (see Scheme 4.4).<sup>6</sup> Phosphonium cations, however, do not degrade by the elimination pathway. Phosphonium hydroxide compounds degrade through a substitution mechanism to form a phosphine oxide (see Scheme 4.5).<sup>7</sup> They have been shown to be stable to temperature as high as 300°C, depending on the balancing anion.<sup>8,9</sup> Because of the limited stability of quaternary ammonium, work was discontinued on Q-\*BEA OFMSs. Efforts focused on examining the temperature stability of phosphonium-containing silicas.

Phosphonium-containing materials with differing anions were prepared by the nucleophilic displacement of the halogenated propyl-organosilane and trimethylphosphine as described previously.  $^{13}\text{C}$  CP/MAS NMR showed that the halogenated propyl-organosilane was tethered to the CPG surface without degradation (see Figure 4.16 for Br-CPG spectra; Cl- and I-CPG data not shown). After nucleophilic displacement ( $\text{P}^+\text{Br}^-$ -CPG), the  $^{13}\text{C}$  CP/MAS NMR indicated the presence of the expected shifts from the phosphonium moiety,<sup>7</sup> although some of the original material remained unreacted. Phosphine oxide was also detected in the samples. Heat treatment

experiments (data not shown) of phosphonium-functionalized CPG-240 exhibit increased thermal stability, depending on anion (I<Cl<Br). The P<sup>+</sup>Br<sup>-</sup>-CPG was stable under vacuum to 300°C. Because of the improved stability of the phosphonium moiety on CPG-240, attempts were made to prepare phosphonium-containing OFMSs using Br-\*BEA and Cl-\*BEA. I-\*BEA was not studied because of the limited stability (~100°C) of the phosphonium iodide tethered onto CPG.

#### 4.3.2 Quaternary Phosphonium OFMS Preparation

Phosphonium-containing OFMS material were prepared by nucleophilic displacement with extracted halogenated propyl-containing \*BEA (X-\*BEA). The OFMS syntheses of Br-\*BEA, Cl-\*BEA, and I-\*BEA all exhibited the \*BEA structure, as seen by XRD (see Figure 4.17 for Br-\*BEA; Cl- and I-\*BEA data not shown). Extraction in acetic acid did not affect the crystal structure. After extraction, an exothermic loss of the halogenated propyl-functional group at approximately 300°C was observed by DSC of the both Br-\*BEA and Cl-\*BEA materials that was not present in Si-\*BEA (Netzsch Jupiter 409 Thermogravimetric Analyzer with simultaneous Differential Scanning Calorimetry, heating at 1°/min in air, see Figure 4.18). In extracted Si-\*BEA, with no covalently tethered moieties, no such exotherm was observed.

The extracted Br-\*BEA material was reacted with trimethylphosphine to create the phosphonium functionality (see Scheme 4.2). The \*BEA structure was retained during the extraction procedure and nucleophilic substitution with trimethylphosphine (see Figure 4.17). <sup>29</sup>Si CP/MAS NMR indicated the Si-C bond was stable to the nucleophilic displacement reaction (see Figure 4.19). <sup>31</sup>P MAS NMR indicated the presence of a quaternary phosphonium moiety in P<sup>+</sup>Br<sup>-</sup>-\*BEA (see Figure 4.20). The

signal in  $P^+Br^-*$ BEA was low in the spectrum due to low number density.  $P^+Br^-$ -CPG formed from the Br-CPG control samples, which has higher number density of organic groups, also had a similar peak for the quaternary phosphonium moiety by  $^{31}P$  MAS NMR. The phosphonium moiety was stable to heat treatment up to 300°C under vacuum.

Extracted Br-\*BEA and Br-CPG were also reacted with triphenylphosphine to probe whether the bromopropyl-functionality was located within the pore space of the zeolite or on the surface (see Scheme 4.6). Triphenylphosphine was too bulky to access the intracrystalline pore space of the zeolite, but can access the pores of CPG.  $^{31}P$  MAS NMR showed no strong indication of a quaternary phosphonium moiety in  $P^+Ph_3Br^-*$ BEA or  $P^+Ph_3Cl^-*$ BEA, suggesting the organic moieties were located within the pore space of the zeolite (see Figure 4.21).  $P^+Ph_3Cl^-$ -CPG did show the quaternization reaction took place; however, the signal strength even in CPG was low.

Because  $^{31}P$  is 100% abundant,  $^{31}P$  MAS NMR can be performed quantitatively, using an external standard. The loading of halogen-containing moieties in the OFMS can be calculated from TGA weight loss at 300°C, allowing the yields on the displacement reactions within \*BEA and CPG to be calculated (see Table 4.1). Bromo-propyl loadings on Br-CPG were 0.42 mmol/g, whereas Br-\*BEA had only 0.041 mmol/g of bromo-propyl groups. After nucleophilic displacement,  $P^+Br^-$ -CPG had 0.36 mmol/g of phosphonium, according to  $^{31}P$  MAS NMR. The yield of the displacement reaction with trimethylphosphine in CPG was 86%.  $P^+Br^-*$ BEA showed only 0.0084 mmol/g of phosphonium by NMR, having a 21% yield on the displacement reaction. The lower reaction yield in \*BEA was likely due to diffusion limitations in the zeolite compared with the mesoporous CPG. The nucleophilic displacement reaction of

triphenylphosphine in CPG only had 3% yield. Because the trimethylphosphine displacement reaction was so low for \*BEA materials, an attempt was made to increase the phosphonium loadings in a  $P^+Br^-$ -\*BEA sample by directly incorporating a phosphonium-containing organosilane in an OFMS synthesis.

The phosphonium-containing OFMSs may be prepared by the direct synthesis method using the synthetically prepared P-trimethoxysilylpropyl-P,P,P-trimethylammonium bromide ( $P_{quat}$ -\*BEA). The \*BEA structure was formed (see Figure 4.22). A phosphonium loading of 0.42 mmol/g was observed by  $^{31}P$  MAS NMR on as-made material. After extraction with acetic acid, only 0.16 mmol/g remained in  $P_{quat}$ -\*BEA (removing 61% of the phosphonium species). Tethering of the phosphonium organosilane onto CPG ( $P_{quat}$ -CPG) resulted in an increase of phosphonium loading of 0.83 mmol/g (see Figure 4.23). A decrease in phosphonium was also observed when  $P_{quat}$ -CPG was exposed to extraction conditions (93% removal). The decrease in phosphonium content was likely due to extraction of organosilane not tethered to the silica, because it is unlikely that the extraction procedures could break the Si-C bond.

Other extraction methods showed some improvement. Soxhlet extraction in EtOH resulted in 80% removal of the phosphonium species. Soxhlet extraction in acetonitrile removed 34% of the phosphonium. Soxhlet extraction in DMF caused degradation. Similar treatments with as-made  $P_{quat}$ -\*BEA did not remove the SDA in any significant quantity. Soxhlet extraction in acetonitrile 4 times for 24-48 hrs per batch only removed 3% of TEAF. Because the SDA in  $P_{quat}$ -\*BEA could not be removed

without risking the integrity of the phosphonium group, all further work was done with  $P^+Br^-$ -\*BEA and  $P^+Br^-$ -CPG obtained from nucleophilic displacement.

#### 4.3.3 *Quaternary Phosphonium OFMS Ion-Exchange*

In order to probe the location of the phosphonium group,  $P^+Br^-$ -\*BEA materials were ion-exchanged with  $NO_3^-$  and  $BPh_4^-$  (see Scheme 4.7). The \*BEA structure was stable to ion-exchange modifications (see Figure 4.24).  $^{29}Si$  CP/MAS NMR showed the Si-C bond was stable to the ion-exchanges as well (see Figure 4.25).  $P^+Br^-$ -\*BEA and  $P^+Cl^-$ -\*BEA samples exchanged with  $HNO_3$  ( $P^+NO_3^-$ -\*BEA) exhibited absorbance in the IR spectrum at  $1384\text{ cm}^{-1}$ , characteristic of nitrate (see Figure 4.26).  $P^+Br^-$ -CPG also showed evidence of ion-exchange. Quantitative titration of the filtrate for  $Br^-$  indicated that the ion-exchange to nitrate in  $P^+Br^-$ -CPG was only 56% exchanged (see Table 4.2). No bromides could be detected with the  $AgNO_3$  test in the  $P^+Br^-$ -\*BEA exchange, in spite of the appearance of the nitrate in the IR. It was possible that the nitrate observed in the IR was merely physisorbed on the surface, not ion-exchanged.

$P^+Br^-$ -CPG and  $P^+Cl^-$ -CPG samples exchanged with  $NaBPh_4$  ( $P^+BPh_4^-$ -CPG) showed the presence of  $BPh_4^-$  at a chemical shift of -8 ppm in  $^{11}B$  MAS NMR (see Figure 4.27). (Note that trigonal boron was observed from the CPG itself.)  $P^+Br^-$ -\*BEA and  $P^+Cl^-$ -\*BEA samples exchanged with  $NaBPh_4$  ( $P^+BPh_4^-$ -\*BEA) did not indicate the presence of  $BPh_4^-$ . A small signal at -4.5 ppm was observed in the \*BEA samples. Extracted Si-\*BEA, which was never exposed to  $NaBPh_4$ , also contained the same signal, which was likely due to boron impurities in the raw materials used in OFMS synthesis. The  $BPh_4^-$  was too bulky to enter zeolite pores and thus would not exchange the  $NO_3^-$  from  $P^+NO_3^-$ -exchanged \*BEA materials.

In order to prepare the materials for catalytic studies, the nitrate-exchanged materials were contacted with 0.001 N aqueous NaOH. Note that an attempt was made to directly exchange the halide-containing materials (e.g.,  $P^+Br^-$ -CPG) with the NaOH solution, but no halide exchange was observed. Hydroxide-exchanged  $P^+NO_3^-$ -CPG resulted in 0.21 mmol/g of nitrate in the filtrate, with an exchange efficiency of 72% from nitrate to hydroxide (see Table 4.3). The total exchange efficiency, from bromide to hydroxide, was 40% for the phosphonium-containing CPG. Similarly exchanged  $P^+NO_3^-$ -BEA material gave 0.008 mmol/g of nitrate. This nitrate recovered could simply be due to physisorbed nitrate removal, since no  $Br^-$  was observed in the filtrate of the nitrate-exchange.

After hydroxide-exchange, some of the  $P^+OH^-$ -BEA and  $P^+OH^-$ -CPG was added to a 0.0126 N NaBr solution. The change in pH and  $Br^-$  concentration was observed to determine the presence of  $OH^-$  (see Table 4.4).  $P^+OH^-$ -CPG removed 0.29 mmol/g of  $Br^-$  from the solution and increased the pH of the solution to 9.10. Although the amount of  $Br^-$  removed by the  $P^+OH^-$ -CPG was consistent with expectations (0.21 mmol/g of  $OH^-$  expected in the sample), the removal of  $Br^-$  cannot be used as a probe for the presence of exchanged  $OH^-$ . A similar amount of  $Br^-$  was removed from solution with the  $P^+OH^-$ -BEA (0.36 mmol/g of  $Br^-$ ). This exceeded the expected loading of the original phosphonium-functional groups in  $P^+Br^-$ -BEA, and certainly cannot be the amount of hydroxide exchanged into the sample. The  $P^+OH^-$ -BEA sample did increase the pH of the solution to 7.55, but the pH change was most likely due to residual physisorbed hydroxide.

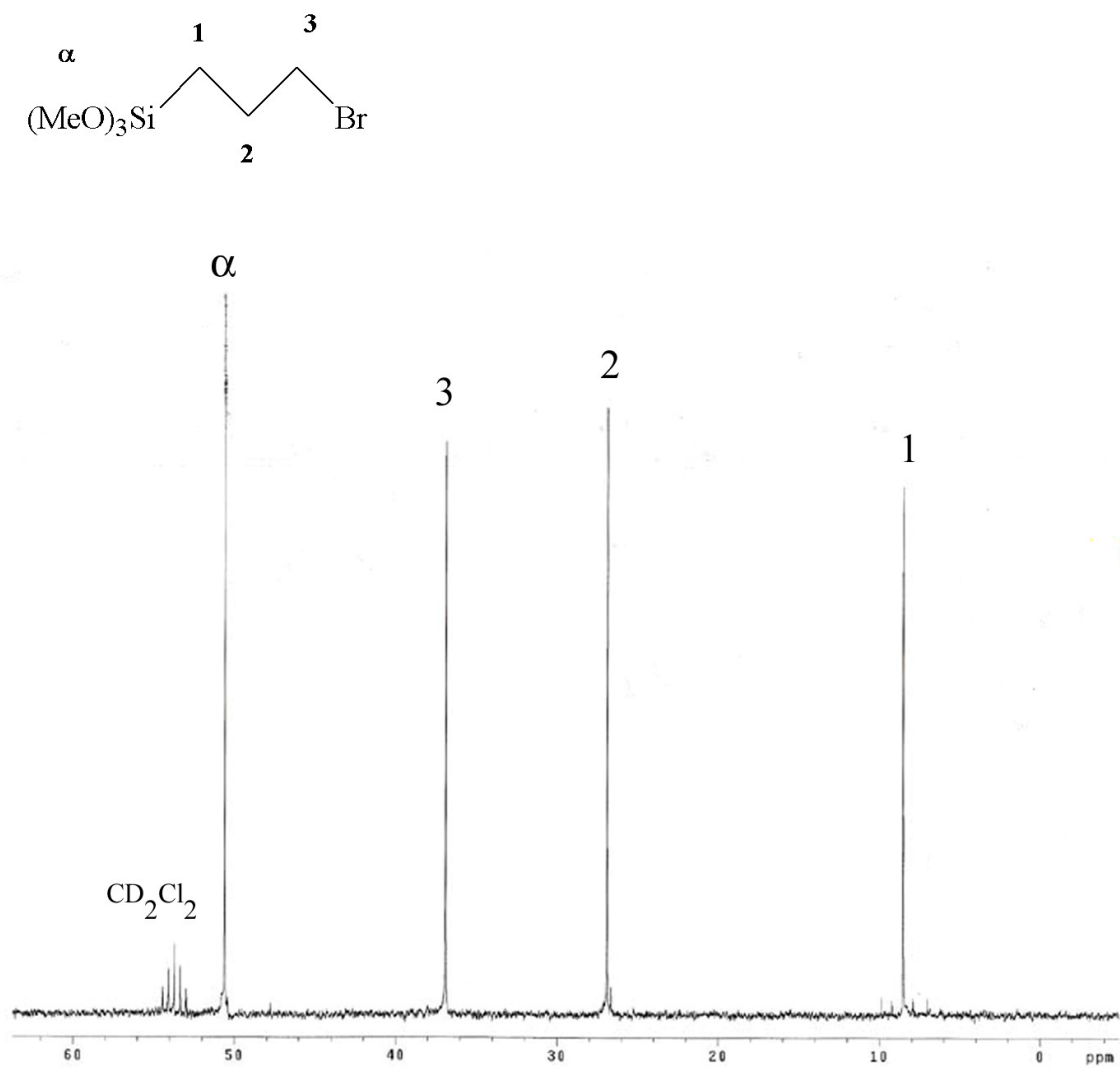
#### 4.4 References

- (1) Rodriguez, I. *et al.*, *Appl. Catal., A* **2000**, 194-195, 214.
- (2) Tsuji, K. *et al.*, *Microporous Mesoporous Mater.* **1999**, 29, 339.
- (3) Cambor, M. A. *et al.*, *Chem. Commun.* **1996**, 2365.
- (4) Macquarrie, D. J. *et al.*, *React. Funct. Polym.* **1997**, 35, 153.
- (5) Jones, C. W. *et al.*, *Microporous Mesoporous Mater.* **2001**, 48, 57.
- (6) de la Zerda, J. *et al.*, *J. Chem. Soc., Perkin Trans. 2* **1986**, 823.
- (7) Cristau, H.-J.; Plenat, F. In *The Chemistry of organophosphorous compounds*; Hartley, F. R., Ed.; John Wiley & Sons: Chichester, 1994; Vol. 3.
- (8) Dehmlow, E. V. *et al.*, *Tetrahedron Lett.* **1977**, 27, 2361.
- (9) Clark, J. H. *et al.*, *J. Chem. Technol. Biotechnol.* **1997**, 68, 367.

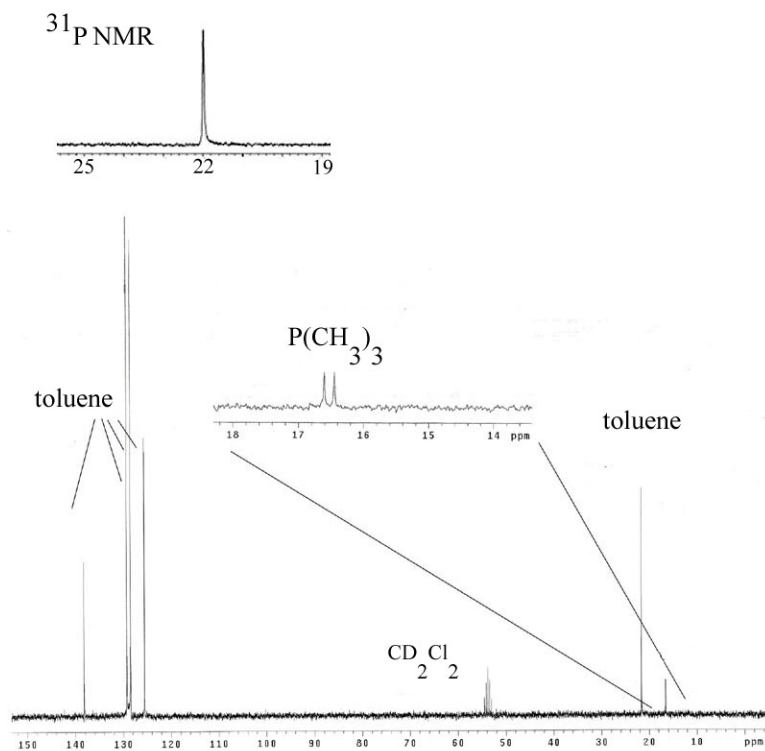
**Figure 4.1** N-trimethoxysilylpropyl-N,N,N-trimethylammonium chloride.



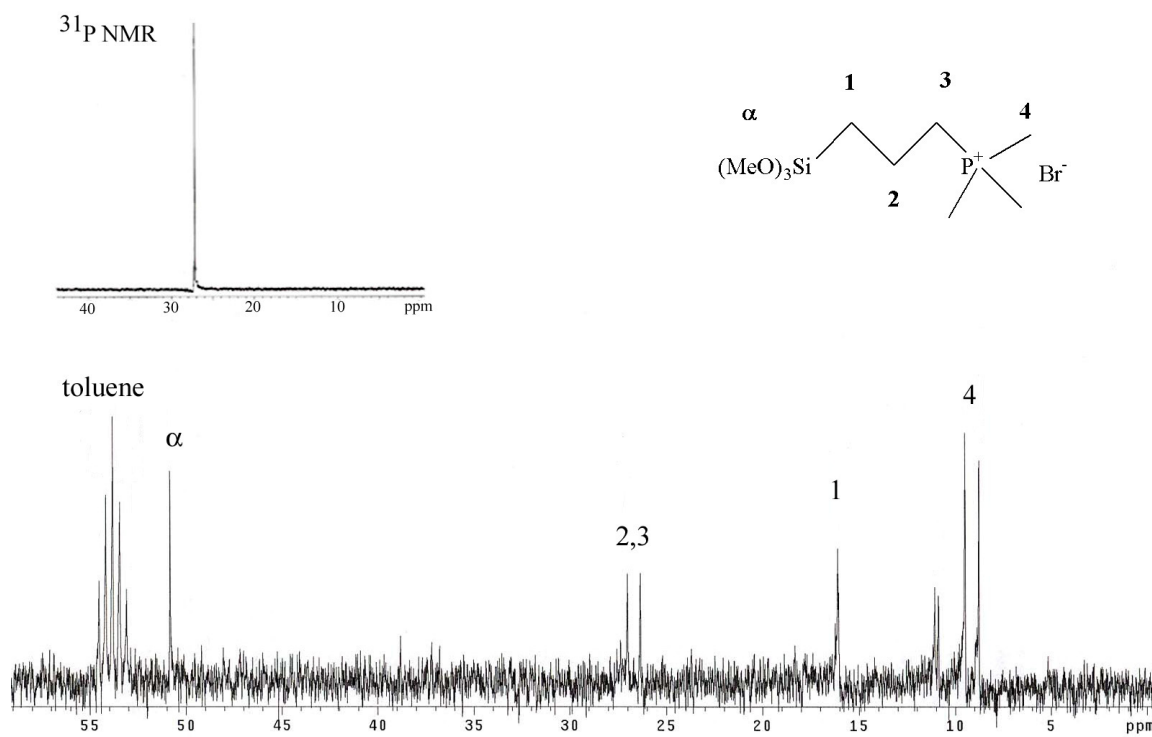
**Figure 4.2**  $^{13}\text{C}$  liquid NMR of 3-bromopropyltrimethoxysilane obtained from United Chemicals Technologies, Inc., in  $\text{CD}_2\text{Cl}_2$ .



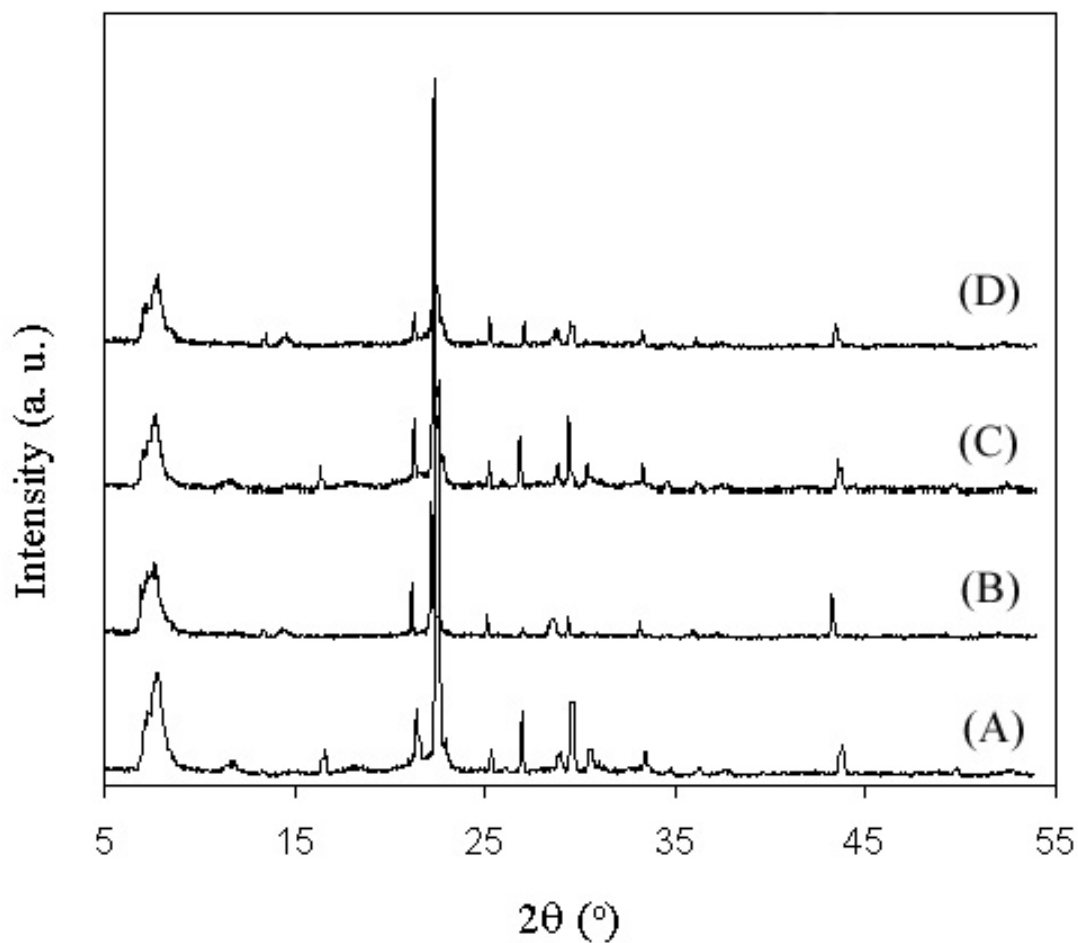
**Figure 4.3**  $^{13}\text{C}$  liquid NMR of 1 M trimethylphosphine solution in toluene obtained from Aldrich, in  $\text{CD}_2\text{Cl}_2$ . Inset is  $^{31}\text{P}$  liquid NMR.



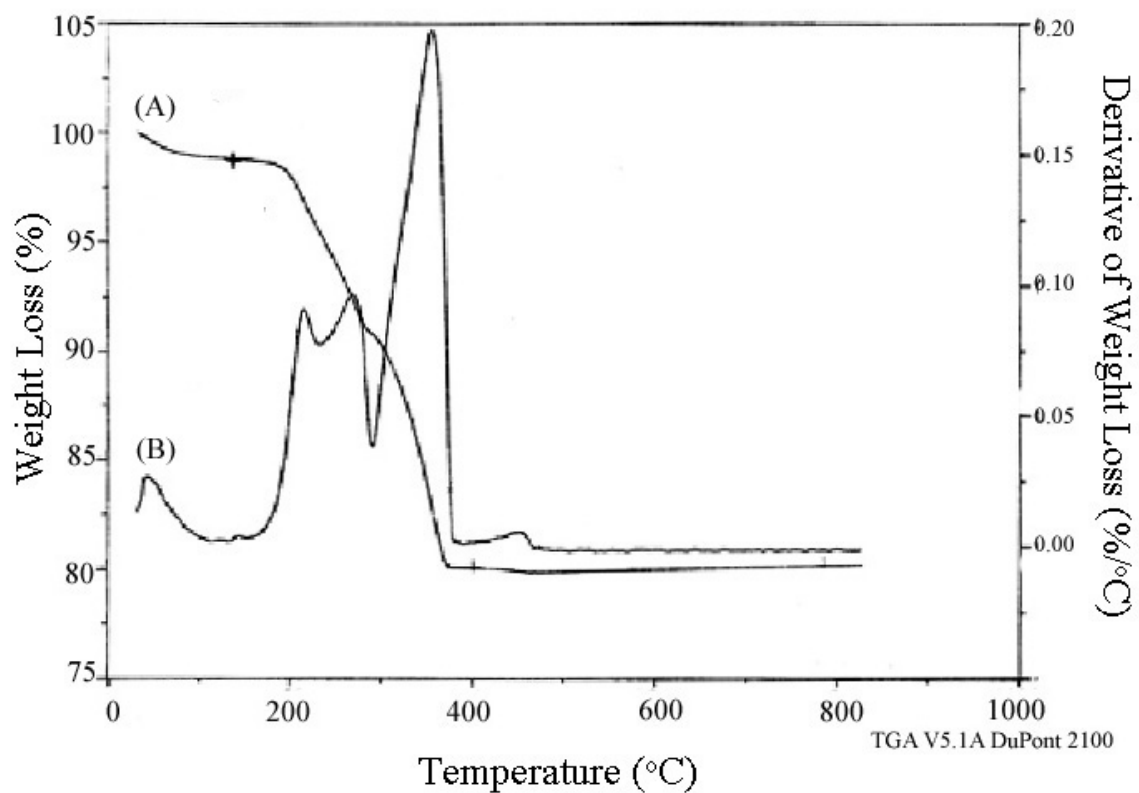
**Figure 4.4**  $^{13}\text{C}$  liquid NMR of P-trimethoxysilylpropyl-P,P,P-trimethylammonium bromide, in  $\text{CD}_2\text{Cl}_2$ . Inset is  $^{31}\text{P}$  liquid NMR.



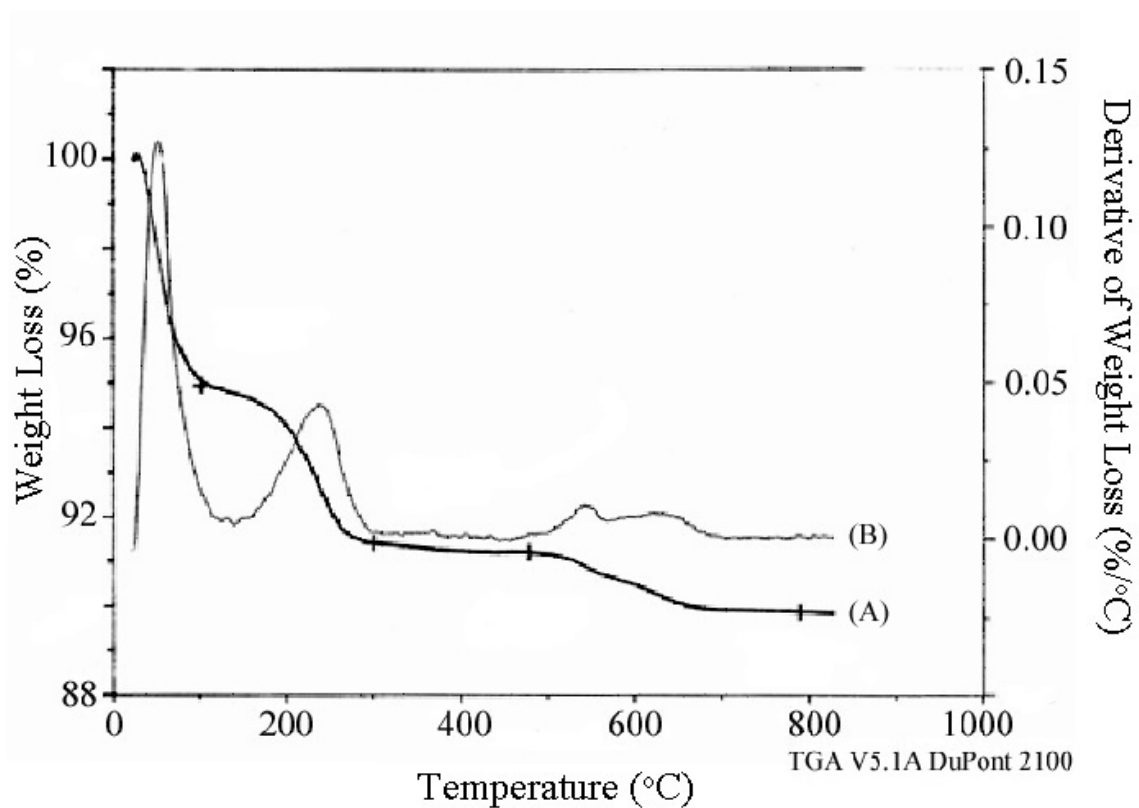
**Figure 4.5** XRD of \*BEA materials: (A) Si-\*BEA as-made, (B) Si-\*BEA after extraction with acetic acid twice, (C) Q-\*BEA as-made, and (D) Q-\*BEA after extraction with acidified pyridine twice.



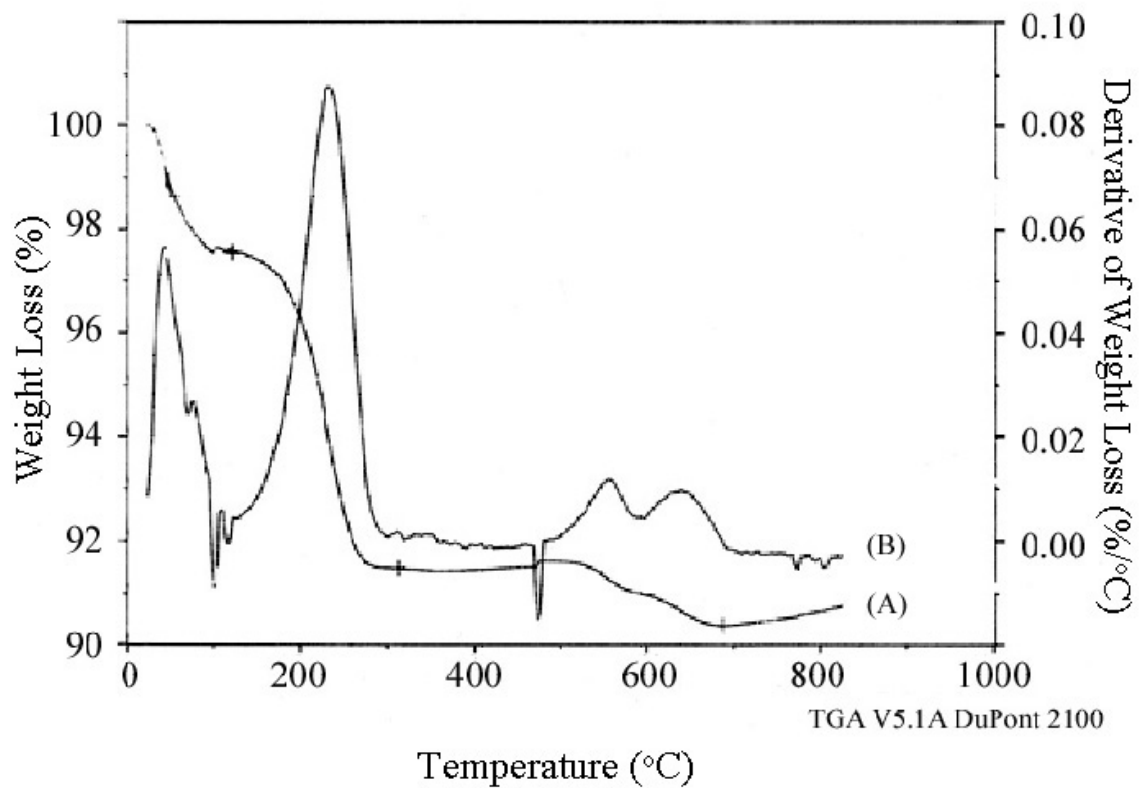
**Figure 4.6** TGA of as-made Si-\*BEA, showing (A) TEAF weight loss and (B) derivative of weight loss.



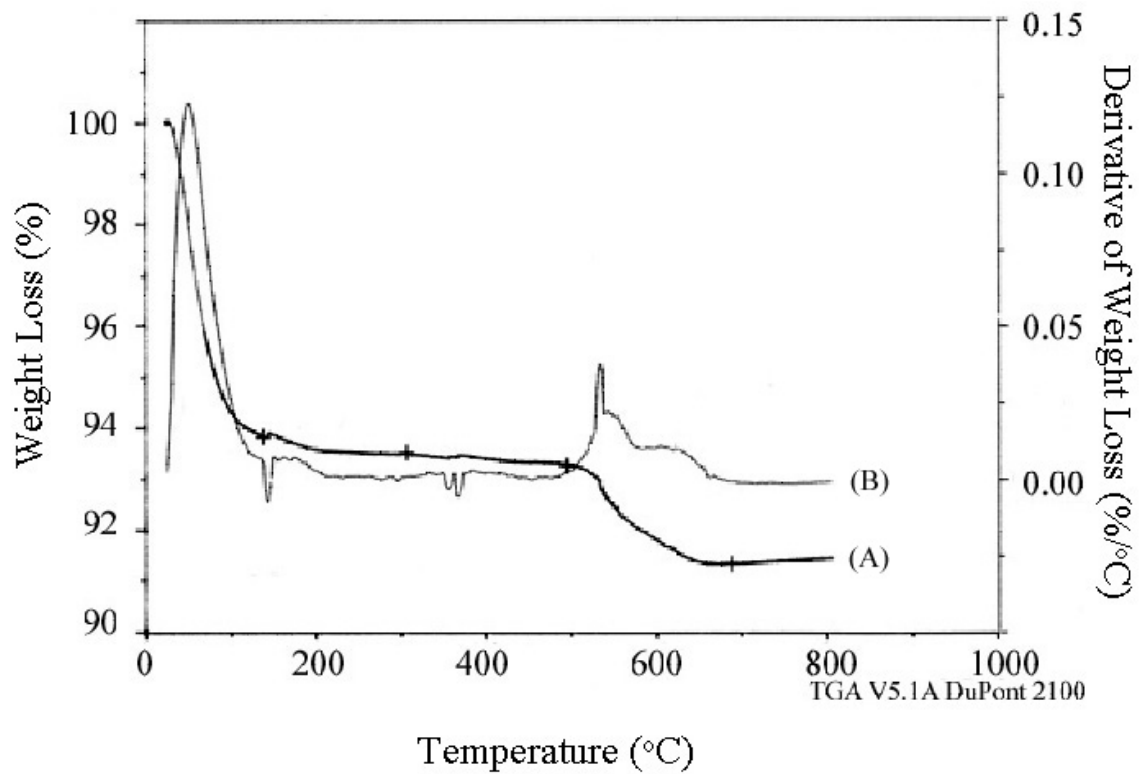
**Figure 4.7** TGA of Si-\*BEA after two pyridine extractions, showing (A) weight loss and (B) derivative of weight loss.



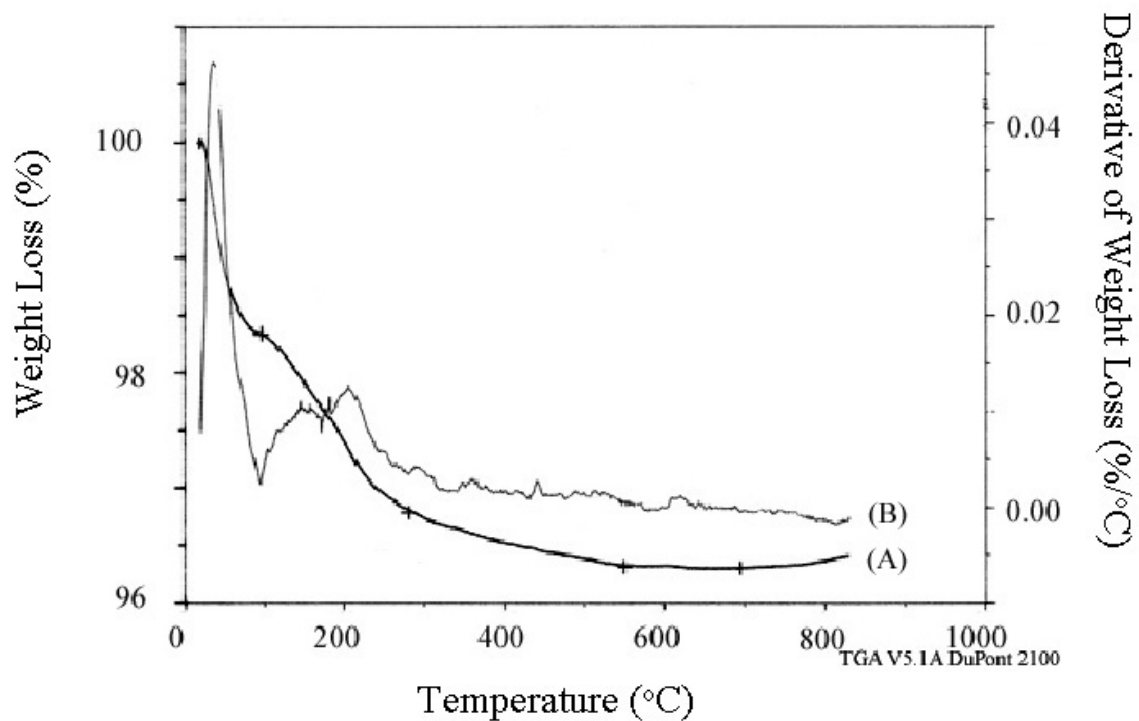
**Figure 4.8** TGA of calcined Si-\*BEA after pyridine sorption, showing (A) weight loss and (B) derivative of weight loss.



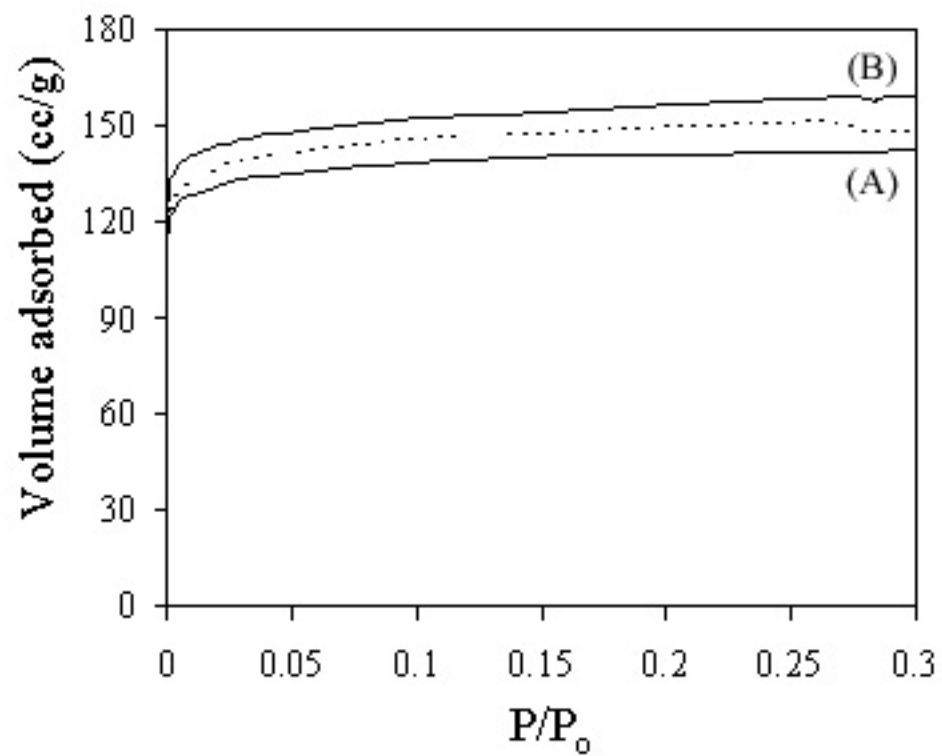
**Figure 4.9** TGA of Si-\*BEA after two pyridine extractions and two water washings, showing (A) weight loss and (B) derivative of weight loss.



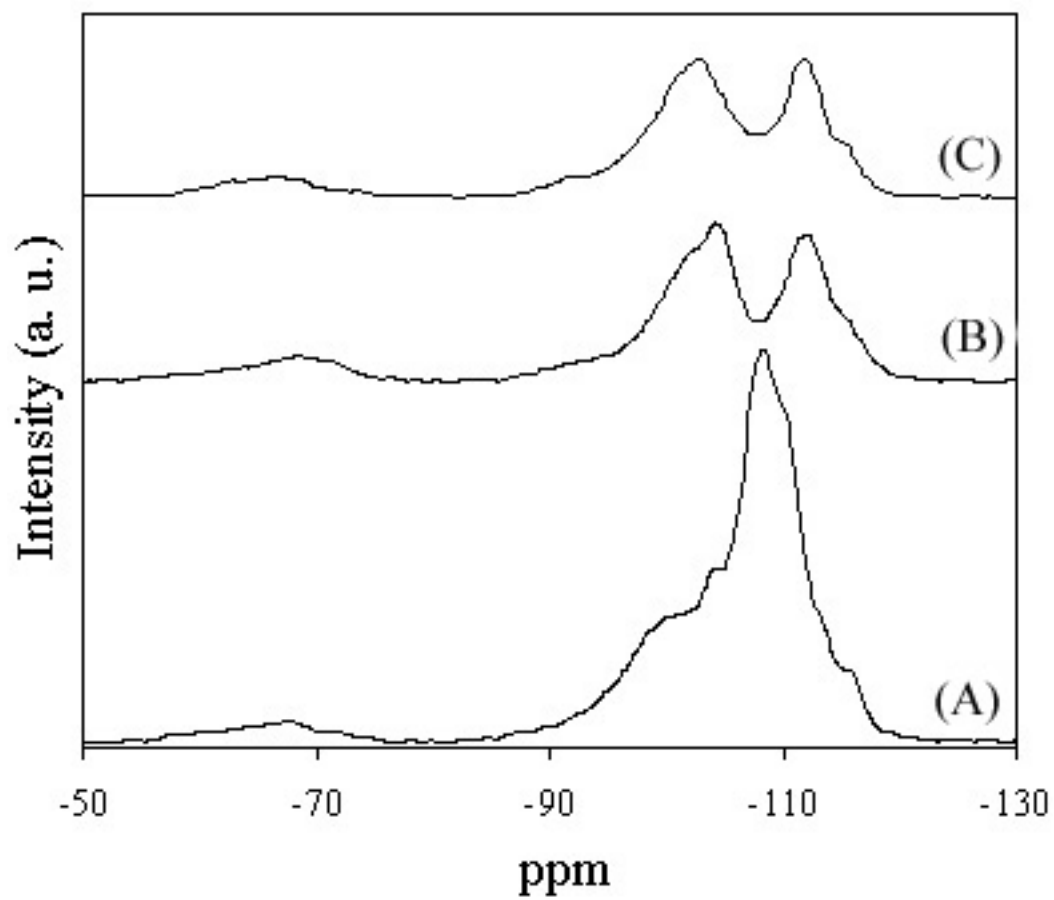
**Figure 4.10** TGA of Q-\*BEA after two pyridine extractions and two water washings, showing (A) weight loss and (B) derivative of weight loss.



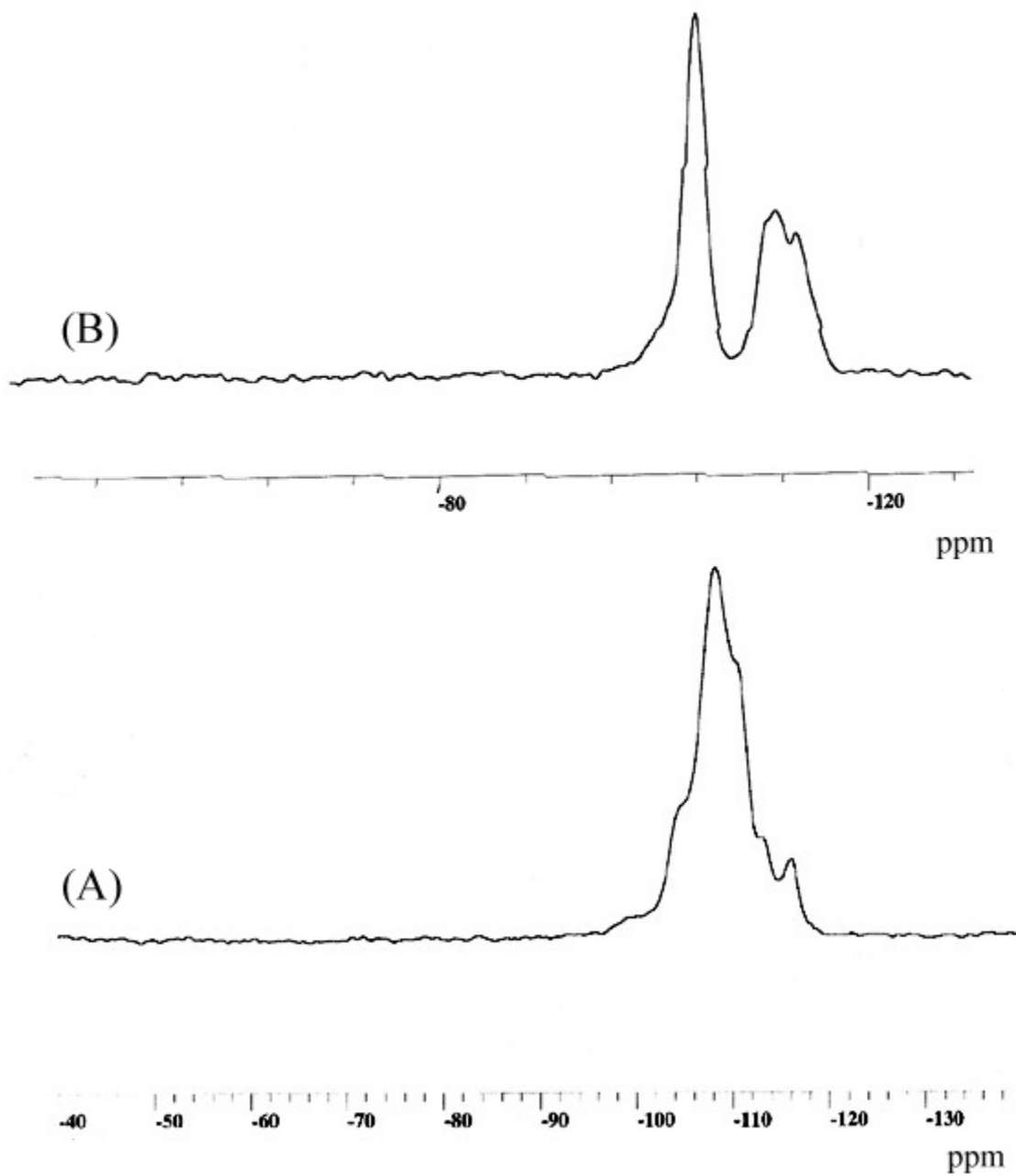
**Figure 4.11** N<sub>2</sub> adsorption Q-\*BEA, after (A) extraction and (B) calcination. The dotted line is the N<sub>2</sub> adsorption of Si-\*BEA after extraction.



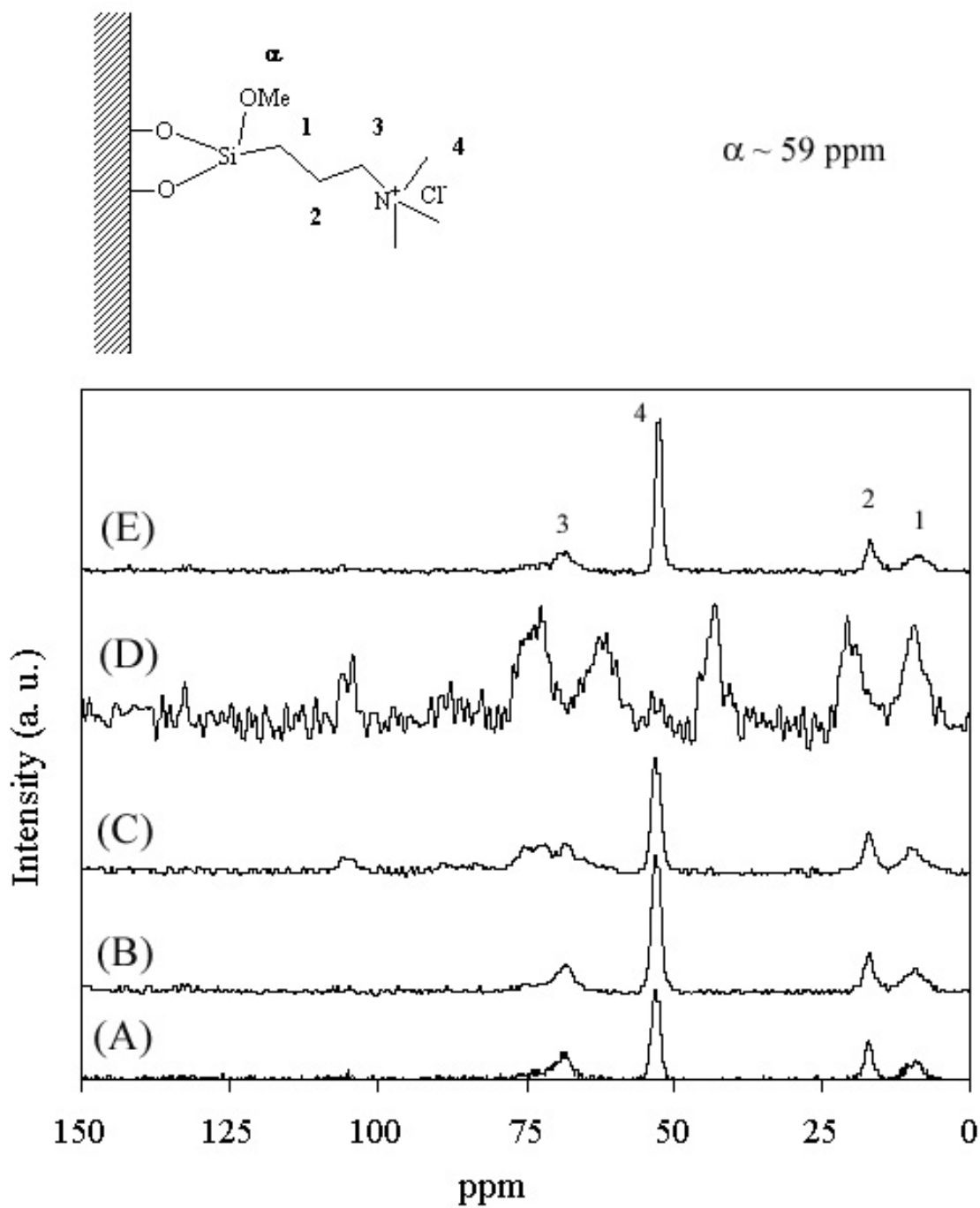
**Figure 4.12**  $^{29}\text{Si}$  CP/MAS NMR of \*BEA:(A) as made Q-\*BEA, (B) extracted Q-\*BEA and (B) extracted Q-\*BEA after evacuation at 200°C overnight.



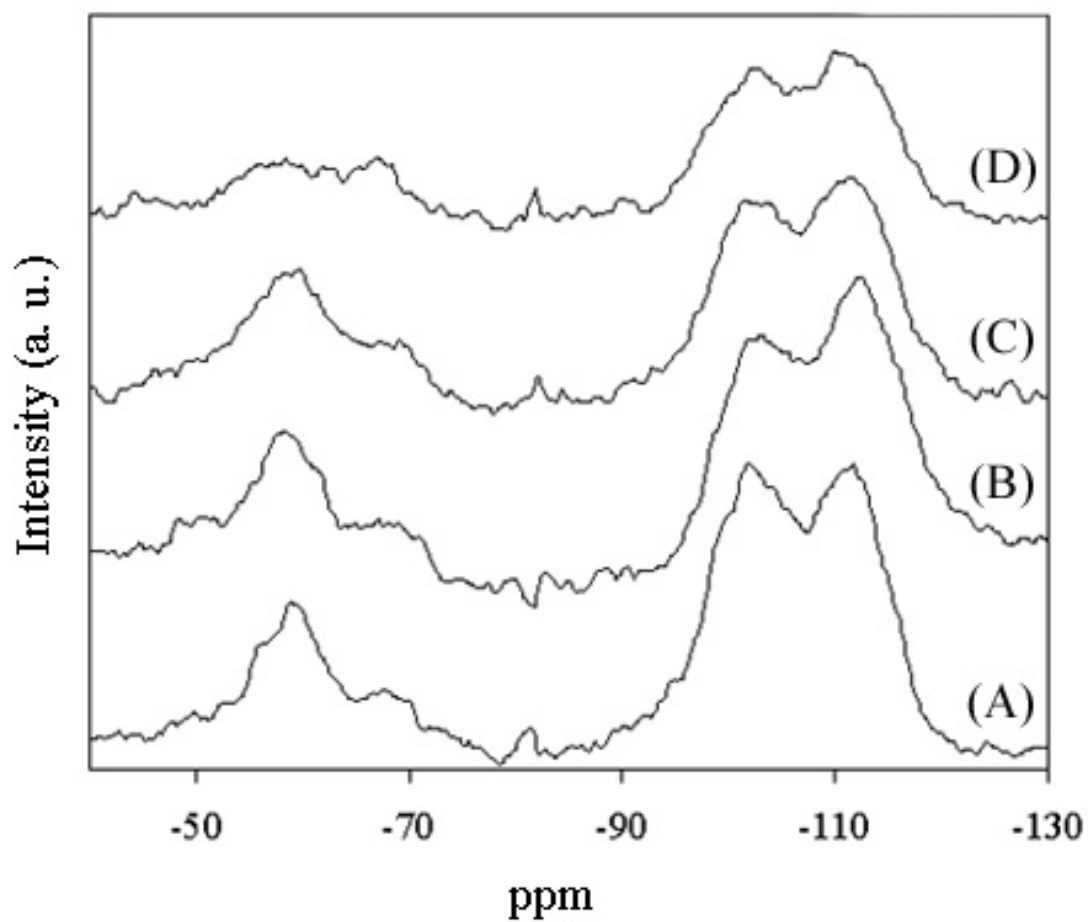
**Figure 4.13**  $^{29}\text{Si}$  CP/MAS NMR of \*BEA: (A) as made Si-\*BEA, (B) extracted Si-\*BEA.



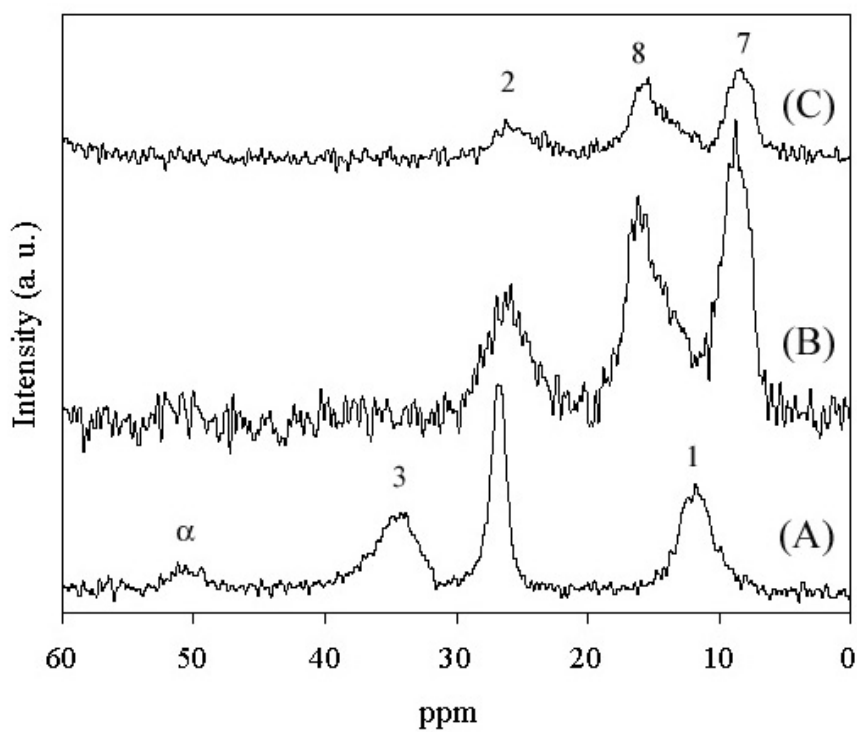
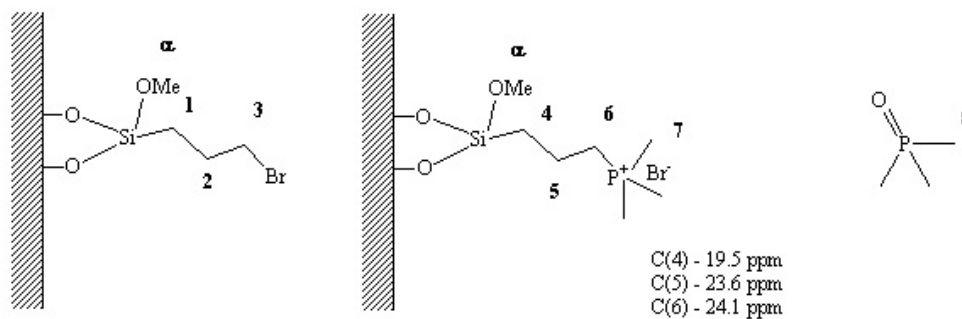
**Figure 4.14**  $^{13}\text{C}$  CP/MAS NMR of ammonium-containing CPG: (A) Q-CPG as-made, (B) after heating to 25°C under vacuum, (C) after heating to 100°C under vacuum, (D) after heating to 200°C under vacuum, and (E) after ion-exchange with nitric acid.



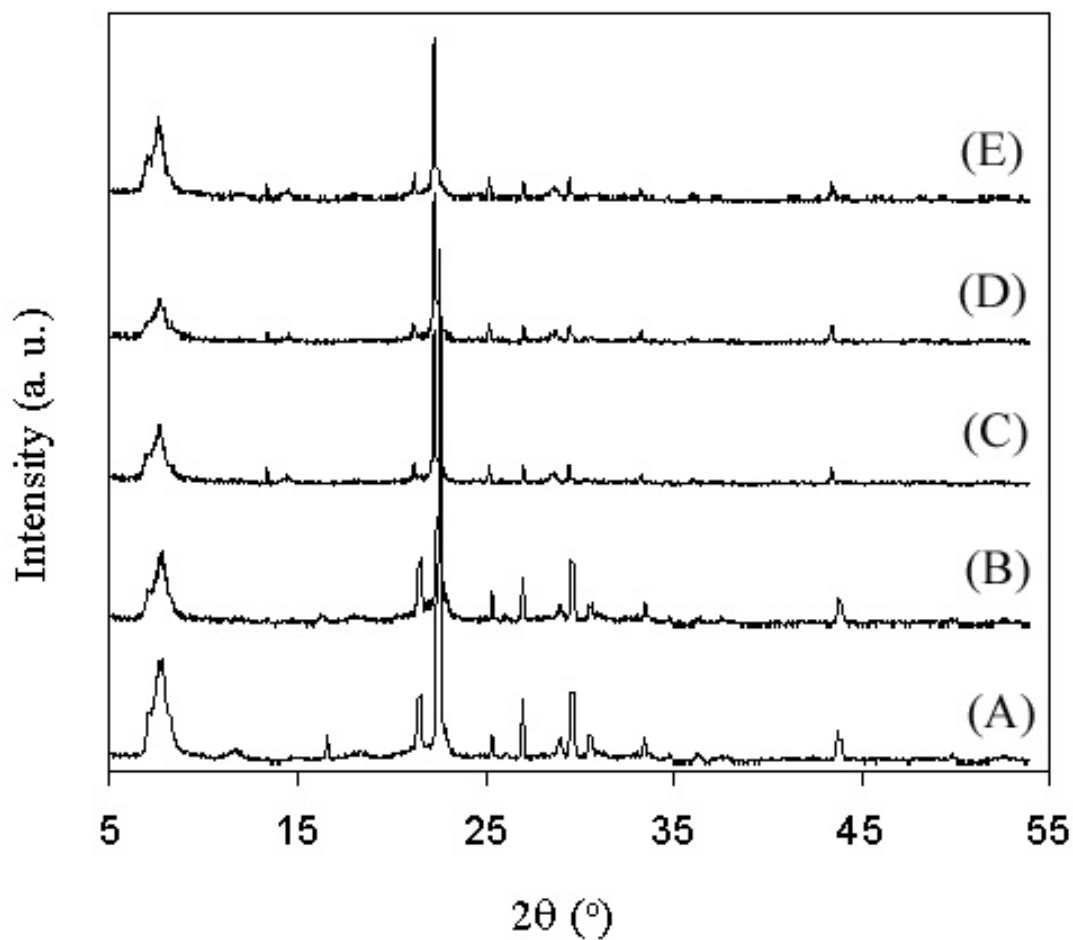
**Figure 4.15**  $^{29}\text{Si}$  CP/MAS NMR of Q-CPG (A) as-made, (B) after heating under vacuum at 25°C, (C) after heating under vacuum to 100°C, (D) after heating under vacuum to 200°C.



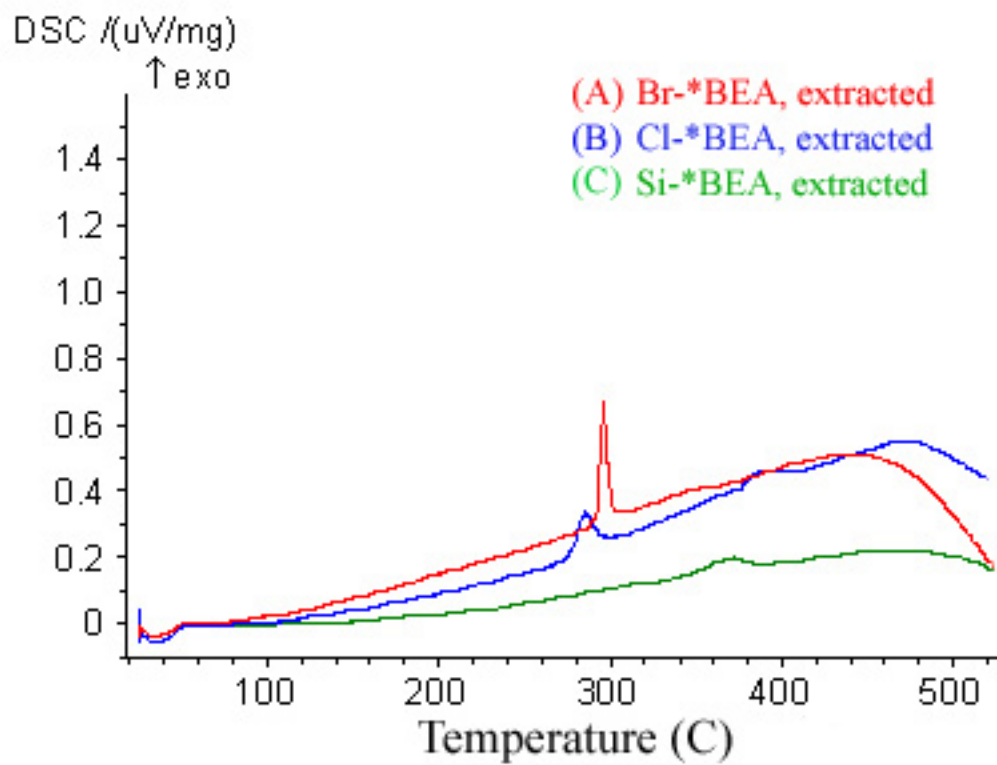
**Figure 4.16**  $^{13}\text{C}$  CP/MAS NMR of (A) Br-CPG, (B)  $\text{P}^+\text{Br}^-$ -CPG, and (C)  $\text{P}^+\text{Br}^-$ -CPG after heat treatment to  $300^\circ\text{C}$ .



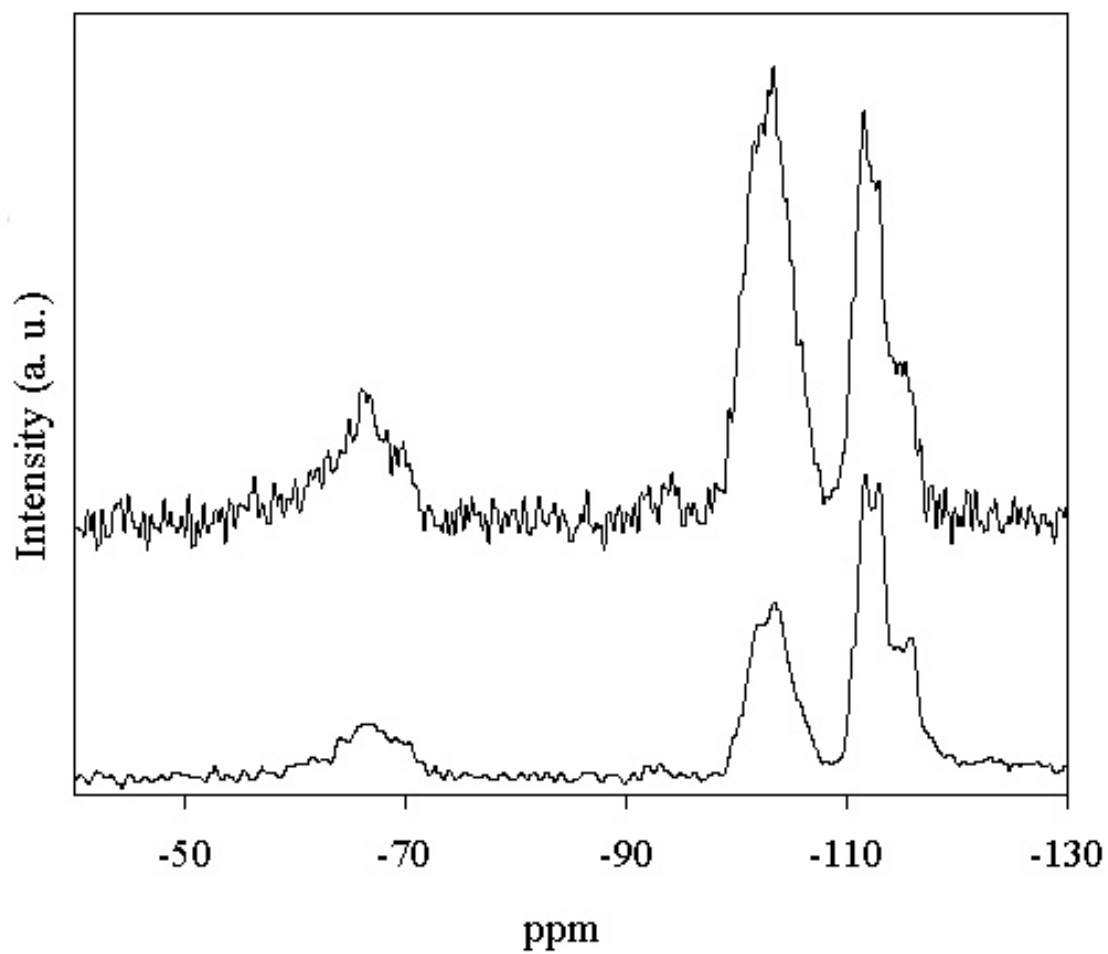
**Figure 4.17** XRD of \*BEA materials: (A) as-made Si-\*BEA, (B) as-made Br-\*BEA, (C) extracted Br-\*BEA, (D) P<sup>+</sup>Br<sup>-</sup>-\*BEA, and (E) P<sup>+</sup>Ph<sub>3</sub>Br<sup>-</sup>-\*BEA.



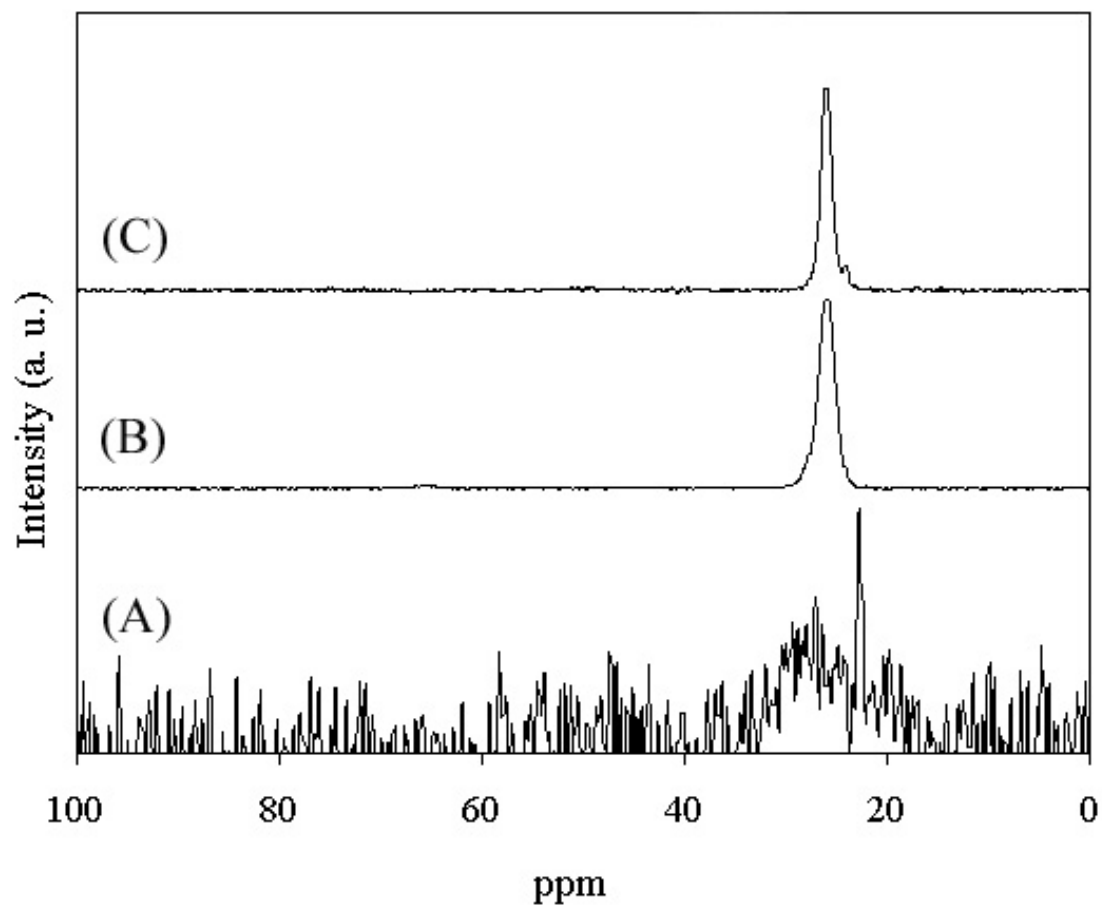
**Figure 4.18** DSC of extracted \*BEA materials: (A) Br-\*BEA, (B) Cl-\*BEA, and (C) Si-\*BEA.



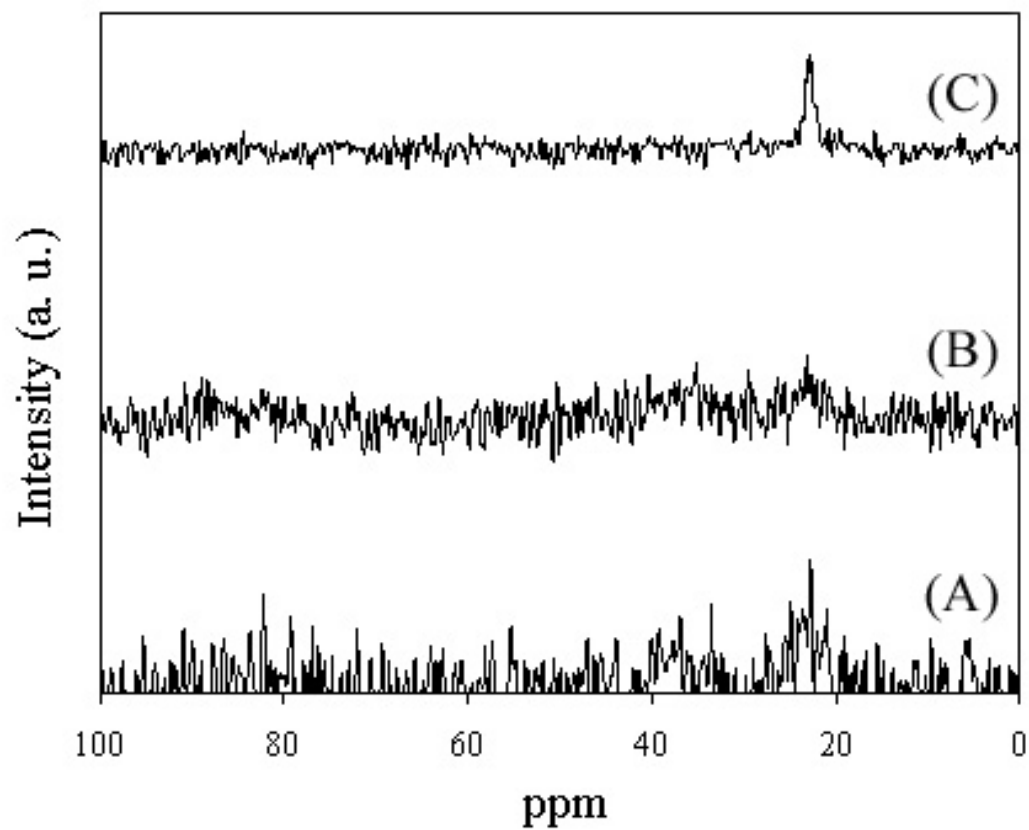
**Figure 4.19**  $^{29}\text{Si}$  CP/MAS NMR of (A)  $\text{P}^+\text{Br}^-$ -\*BEA, and (B)  $\text{P}^+\text{Ph}_3\text{Br}^-$ -\*BEA.

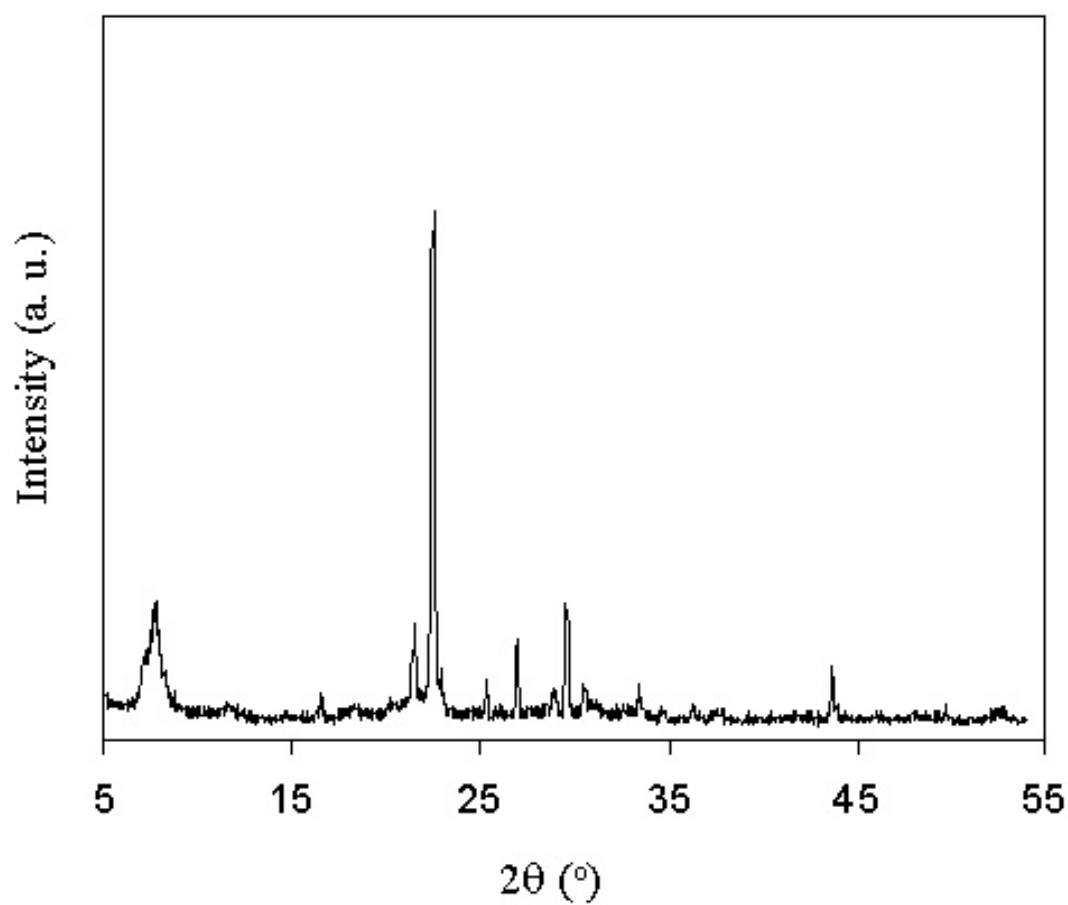


**Figure 4.20**  $^{31}\text{P}$  MAS NMR of (A)  $\text{P}^+\text{Br}^-$ -\*BEA, (B)  $\text{P}^+\text{Br}^-$ -CPG, and (C)  $\text{P}^+\text{Br}^-$ -CPG heated to  $300^\circ\text{C}$  under vacuum.

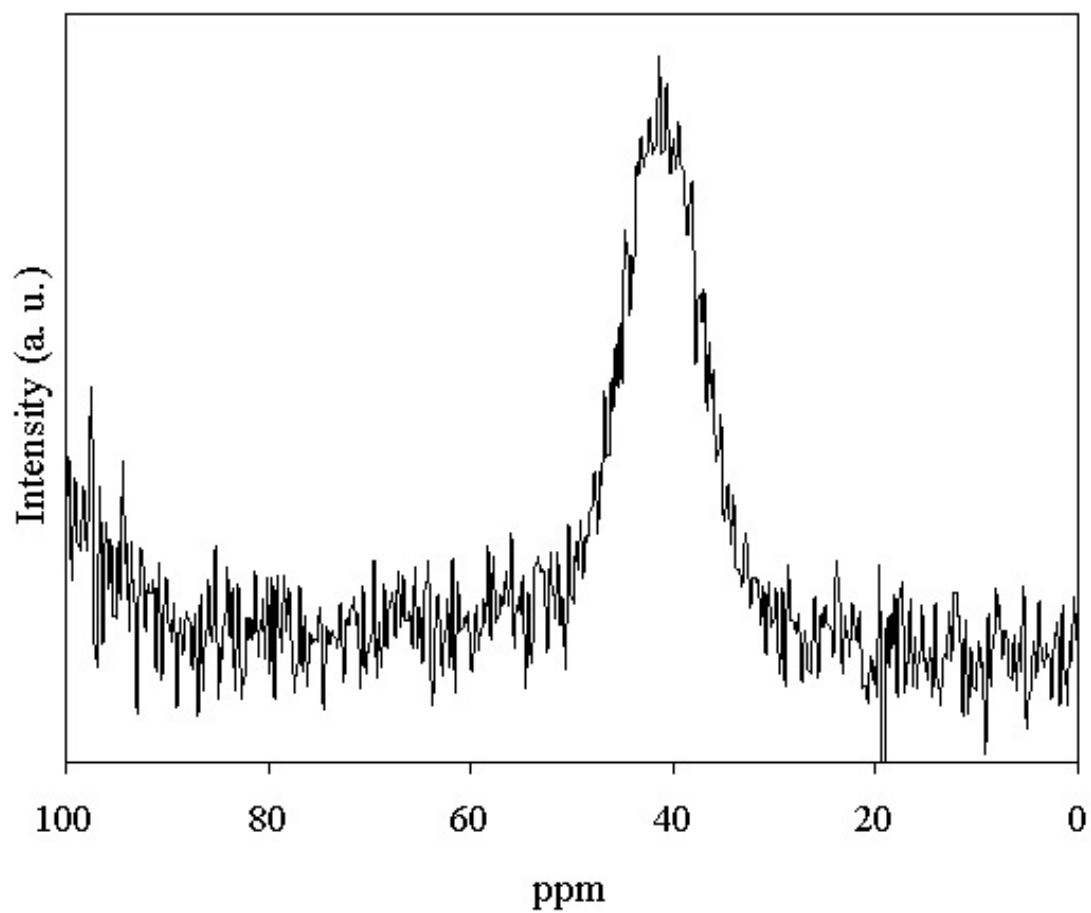


**Figure 4.21**  $^{31}\text{P}$  MAS NMR of (A)  $\text{P}^+\text{Ph}_3\text{Br}^- \cdot \text{BEA}$ , (B)  $\text{P}^+\text{Ph}_3\text{Cl}^- \cdot \text{BEA}$ , and (C)  $\text{P}^+\text{Ph}_3\text{Cl}^- \cdot \text{CPG}$ .

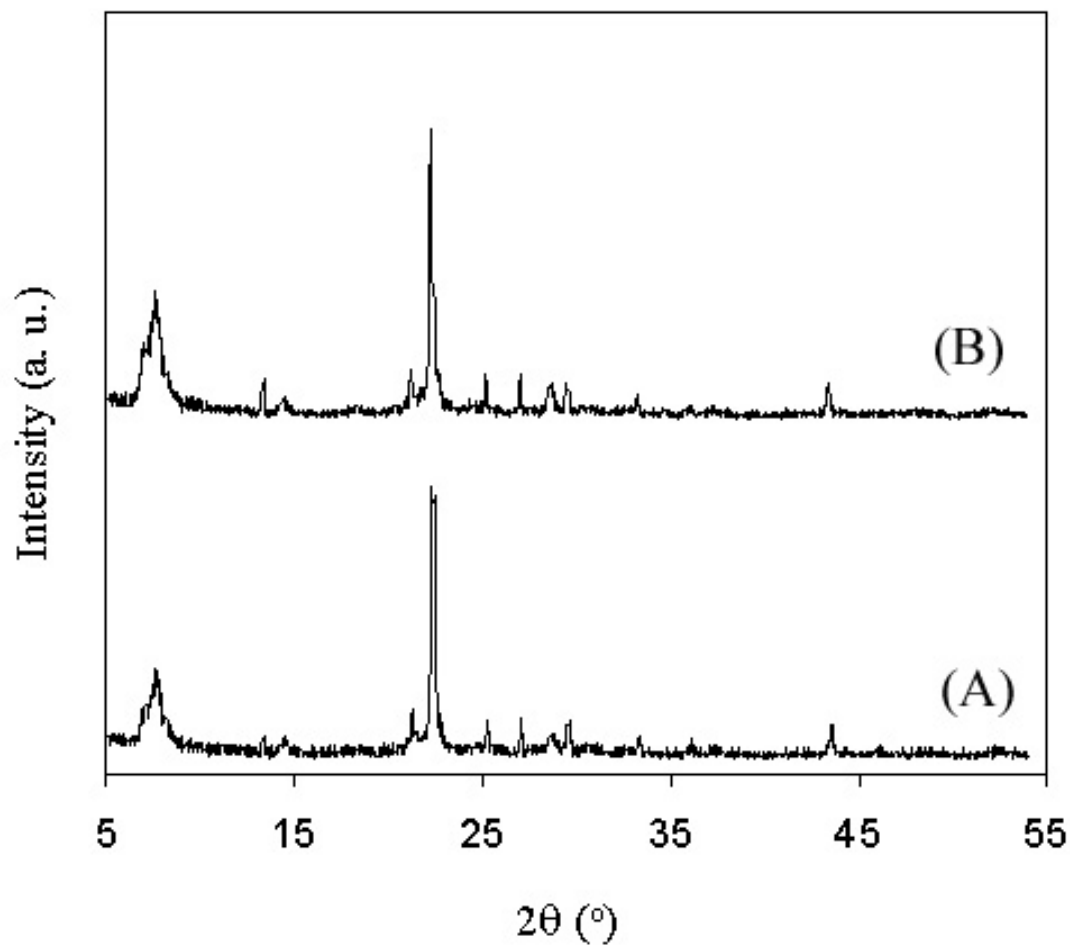


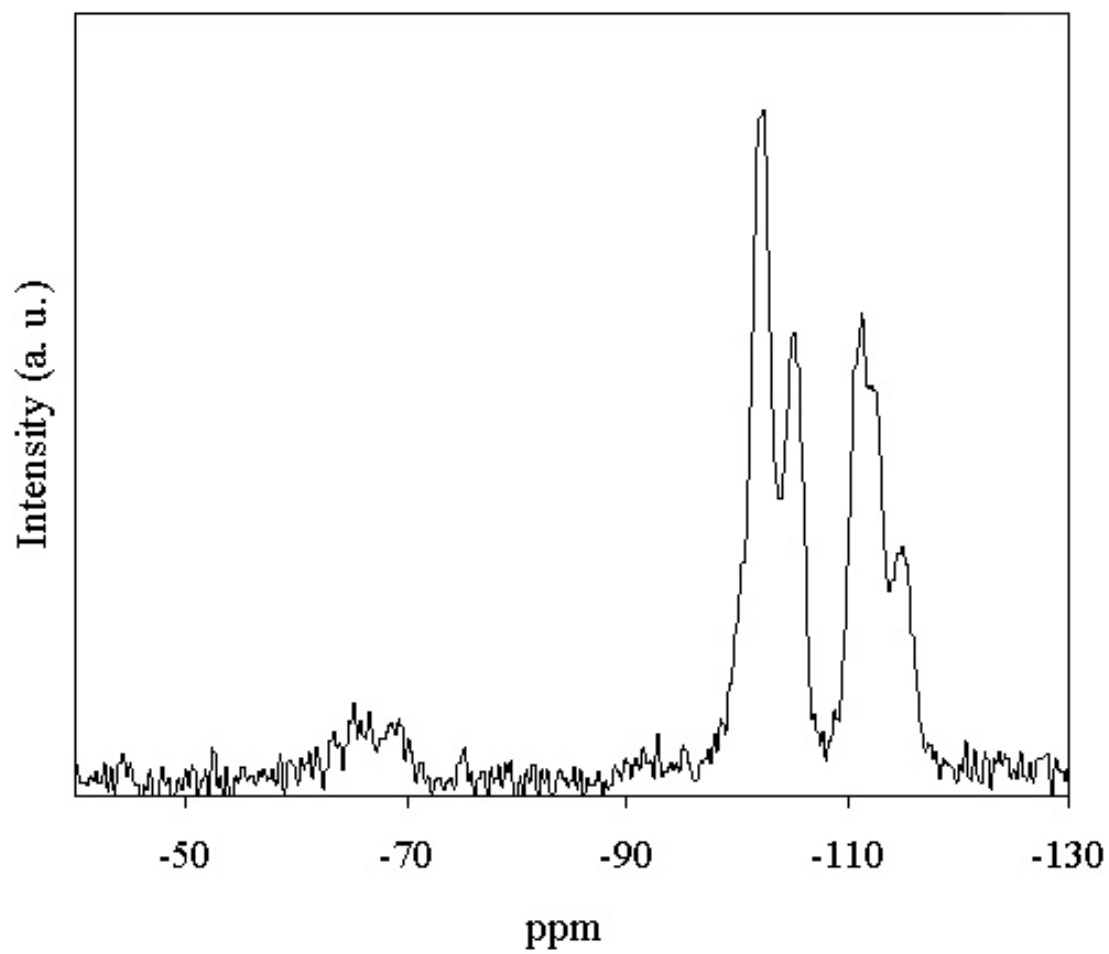
**Figure 4.22** XRD of as-made  $P_{\text{quat}}^* \text{BEA}$ .

**Figure 4.23**  $^{31}\text{P}$  MAS NMR of as-made  $\text{P}_{\text{quat}}\text{-CPG}$ .



**Figure 4.24** XRD of \*BEA materials: (A)  $P^+NO_3^-$ -\*BEA and (B)  $P^+BPh_4^-$ -\*BEA.



**Figure 4.25**  $^{29}\text{Si}$  CP/MAS NMR of ion-exchanged  $\text{P}^+\text{NO}_3^-$ -\*BEA.

**Figure 4.26** FTIR Spectra of (A)  $P^+NO_3^-$ -CPG, (B)  $P^+NO_3^-$ -\*BEA (from Cl), and (C)  $P^+NO_3^-$ -\*BEA (from Br).

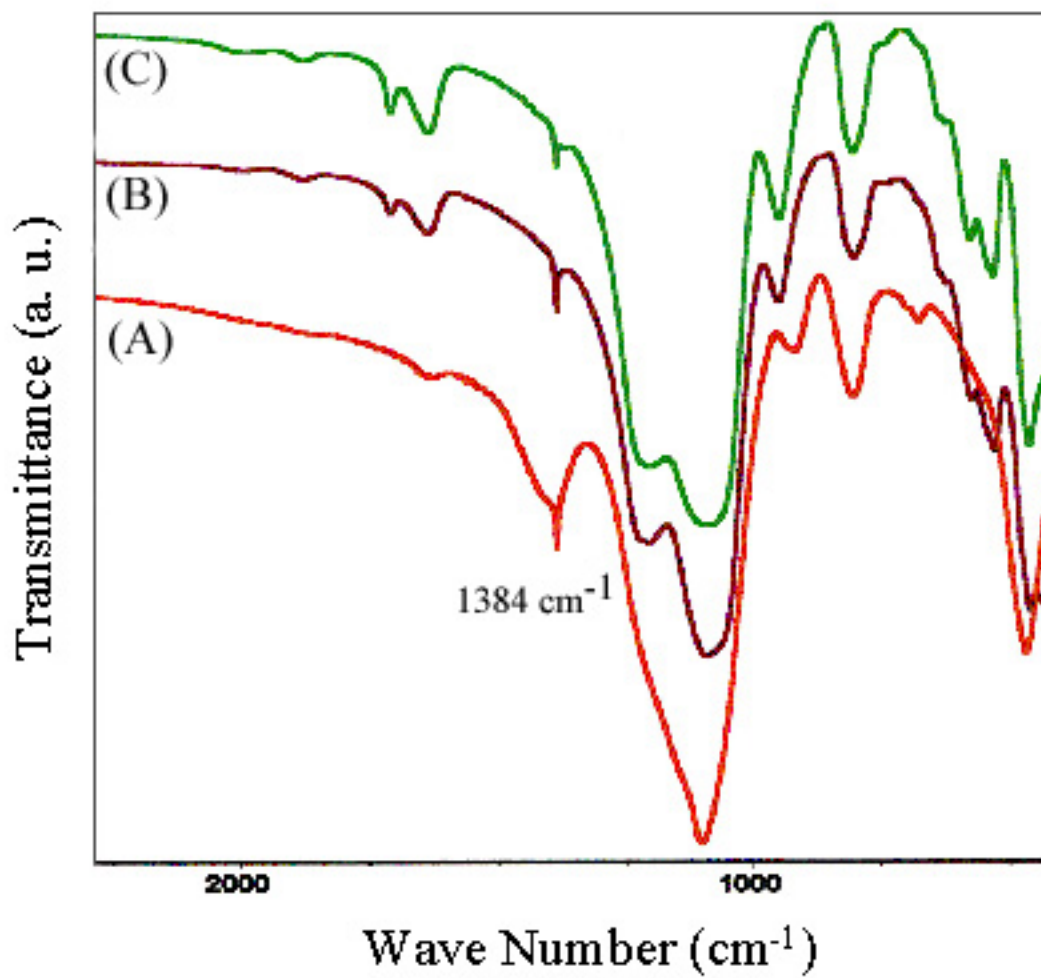
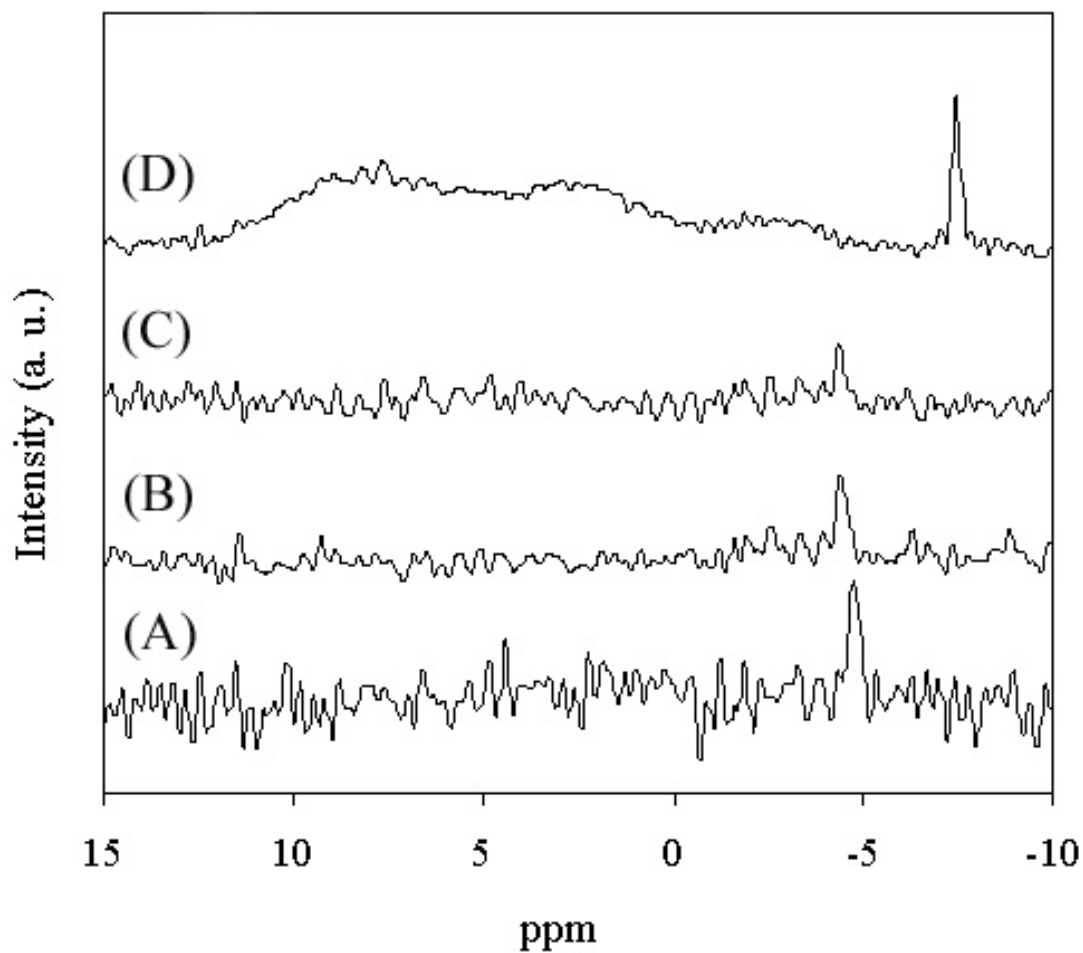
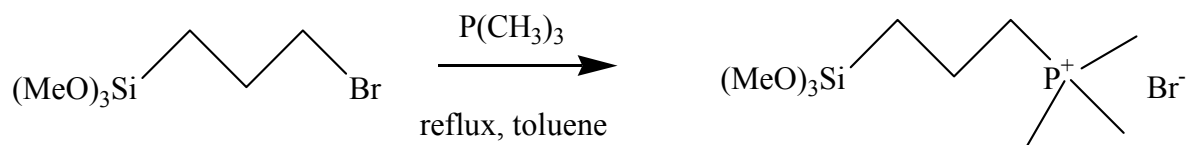


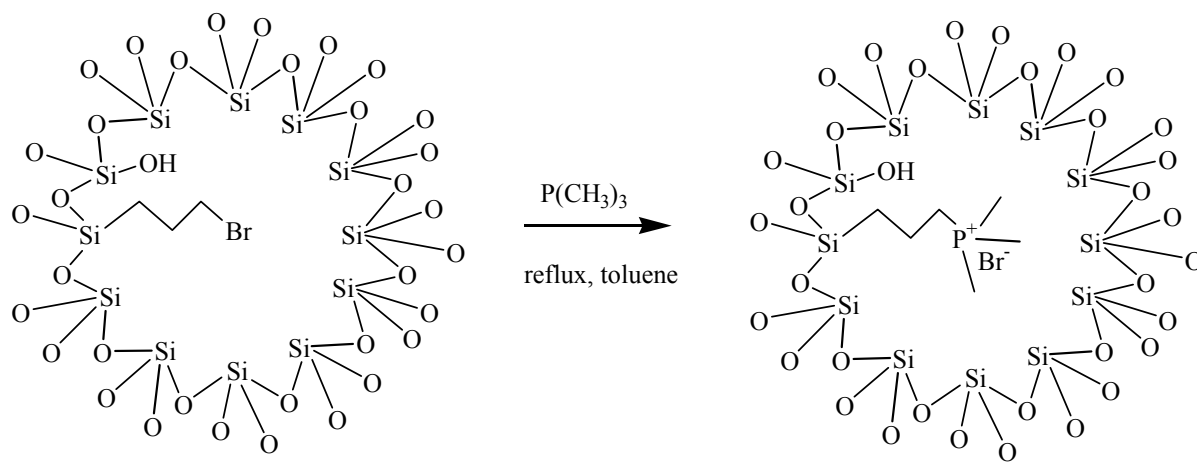
**Figure 4.27**  $^{11}\text{B}$  MAS NMR of  $\text{NaBPh}_4$  exchanged materials: (A)  $\text{Si-}^*\text{BEA}$  after extraction, (B)  $\text{P}^+\text{BPh}_4^-$ -\*BEA (from Cl), and (C)  $\text{P}^+\text{BPh}_4^-$ -\*BEA (from Br), and (D)  $\text{P}^+\text{BPh}_4^-$ -CPG (from Cl).



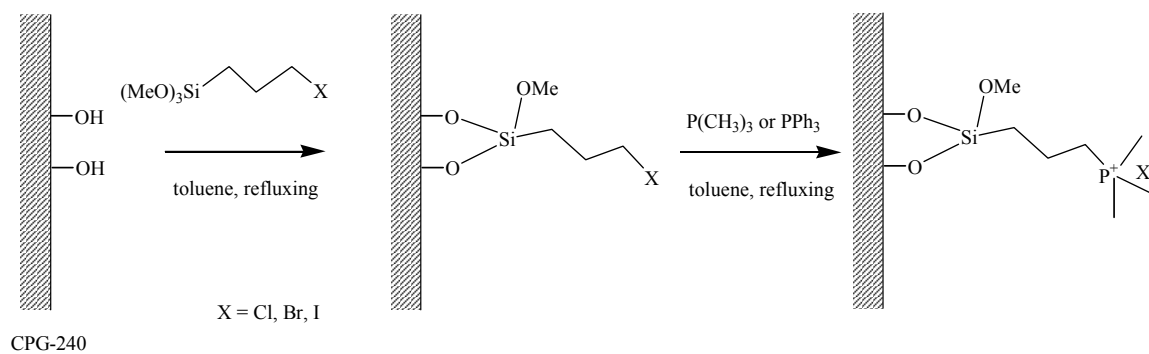
**Scheme 4.1** Preparation of P-trimethoxysilylpropyl-P,P,P-trimethylammonium bromide by nucleophilic displacement.

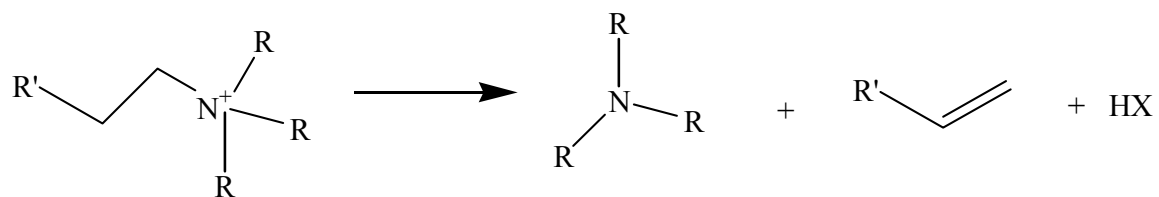


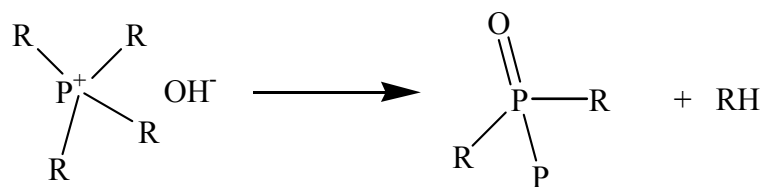
**Scheme 4.2** Preparation of phosphonium-functionalized \*BEA from Br-\*BEA by nucleophilic displacement.

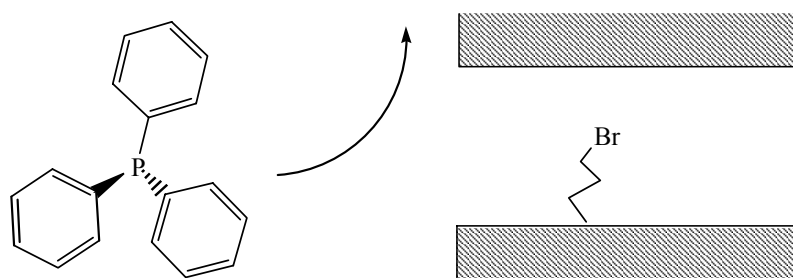
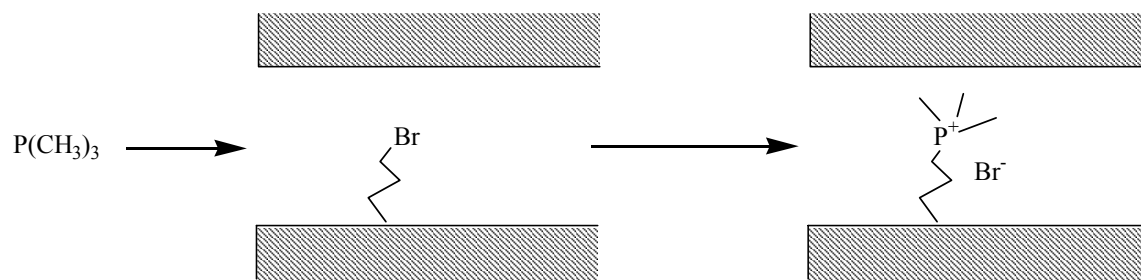


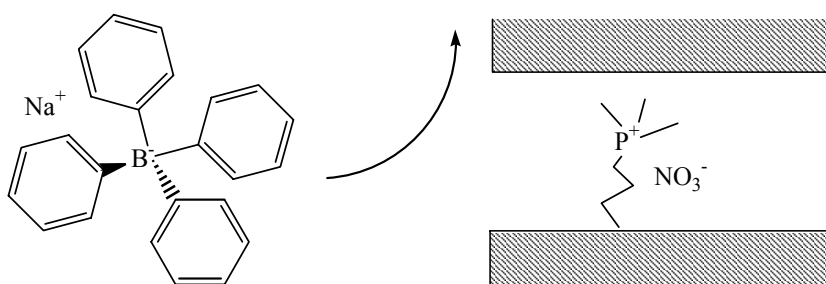
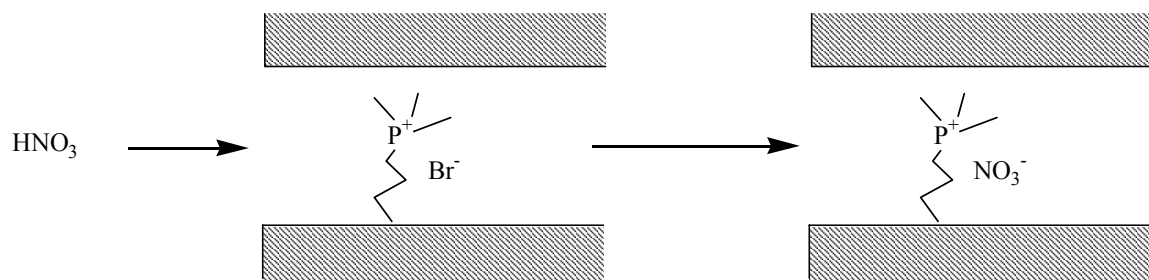
**Scheme 4.3** Tethering of organosilanes onto CPG and preparation of phosphonium-functionalized CPG.



**Scheme 4.4** Hofmann degradation of quaternary ammonium compounds.

**Scheme 4.5** Substitution degradation of quaternary phosphonium compounds.

**Scheme 4.6** Shape-selective nucleophilic displacement within extracted Br-\*BEA.

**Scheme 4.7** Shape-selective ion-exchange within  $P^+Br^-$ -\*BEA.

**Table 4.1** Organic-functional group loadings per gram of silica during nucleophilic displacement reaction.

Sample	Br-propyl <sup>a</sup> (mmol/g)	P <sup>+</sup> Br <sup>-</sup> <sup>b</sup> (mmol/g)	Reaction Yield (% reacted)
P <sup>+</sup> Br <sup>-</sup> -*BEA	0.041	0.0084	21
P <sup>+</sup> Br <sup>-</sup> -CPG	0.42	0.36	86
P <sup>+</sup> Ph <sub>3</sub> Br <sup>-</sup> -*BEA	0.040	0	0
P <sup>+</sup> Ph <sub>3</sub> Cl <sup>-</sup> -CPG	0.48	0.014	3
P <sub>quat</sub> -CPG <sup>c</sup>	-	0.83	-
P <sub>quat</sub> -*BEA <sup>c</sup>	-	0.42	-

<sup>a</sup>From TGA weight loss on bromopropyl-containing precursor

<sup>b</sup>From <sup>31</sup>P MAS NMR

<sup>c</sup>From the prepared phosphonium organosilane

**Table 4.2** Organic-functional group loadings per gram of silica after nitrate ion-exchange.

Sample	P <sup>+</sup> Br <sup>-</sup> <sup>a</sup> (mmol/g)	Br <sup>-</sup> removed <sup>b</sup> (mmol/g)	Exchange Efficiency (%)
P <sup>+</sup> Br <sup>-</sup> -*BEA	0.008	0 <sup>c</sup>	0
P <sup>+</sup> Br <sup>-</sup> -CPG	0.52	0.29	56

<sup>a</sup>From <sup>31</sup>P MAS NMR

<sup>b</sup>From AgNO<sub>3</sub> titration

<sup>c</sup>No Br<sup>-</sup> detected in filtrate by titration

**Table 4.3** Organic-functional group loadings per gram of silica after 0.001 N NaOH ion-exchange.

Sample	$P^+NO_3^-$ <sup>a</sup> (mmol/g)	$NO_3^-$ removed <sup>b</sup> (mmol/g)	Reaction Yield (% reacted)
$P^+NO_3^-$ -*BEA	0	0.008	-
$P^+NO_3^-$ -CPG	0.29	0.21	72

<sup>a</sup>From bromide removed

<sup>b</sup>From VWR titration kit

**Table 4.4** Organic-functional group loadings per gram of silica after bromide ion-exchange.

Sample	P <sup>+</sup> OH <sup>-</sup> <sup>a</sup> (mmol/g)	Br <sup>-</sup> exchanged <sup>b</sup> (mmol/g)	pH of filtrate (mmol OH/g)
P <sup>+</sup> OH <sup>-</sup> -*BEA	0.008	0.36	7.55
P <sup>+</sup> OH <sup>-</sup> -CPG	0.21	0.29	9.10

<sup>a</sup>From NO<sub>3</sub><sup>-</sup> removed

<sup>b</sup>From titration of NaBr filtrate and calculating the removal of Br<sup>-</sup> from solution

## CHAPTER FIVE

BASE CATALYSIS OF ORGANIC-  
FUNCTIONALIZED MOLECULAR SIEVES

## 5.1 Introduction

Development of efficient heterogeneous base catalysts remains of interest. Weak bases, such as amines and some alkali metal oxides, are appropriate for carbon-carbon bond formation reactions, such as the Knoevenagel condensation reaction (see Scheme 5.1). Other base-catalyzed reactions, such as the Michael addition, require stronger bases, e.g., alkali metals or hydroxides (see Scheme 5.2). Alkali metals are difficult to handle because of extreme sensitivity to moisture and air. The goal of developing hydroxide-containing OFMSs was to prepare a heterogeneous zeolite catalyst to be applied to strong base reactions, e.g., the Michael Addition. Confining the hydroxide moiety within the zeolite pore space would allow one to perform shape-selective base-catalyzed reactions. Hydroxide-containing materials ( $P^+OH^-$ -\*BEA and  $P^+OH^-$ -CPG) were prepared as described in Chapter 3 and used in base-catalyzed reactions as described below.

## 5.2 Experimental Section

### 5.2.1 *Knoevenagel Condensation*

$P^+OH^-$ -\*BEA and  $P^+OH^-$ -CPG (20-40 mg) were prepared for catalytic reaction by dehydration at 200°C under vacuum for two hours. Benzaldehyde, **1**, was purchased from Aldrich and malononitrile, **2**, was obtained from Avocado Research Chemicals. The reactants **1** and **2** (approximately 10 mmol each) were measured into a glass vial and sealed. The vial was purged with argon for 10 minutes. Acetonitrile (purchased from Alfa Aesar, dried over molecular sieves, and degassed by freeze-pump-thaw cycling with liquid  $N_2$ ) was added to the reactants via a syringe purged with argon (15 mL) to prepare the reaction solution. The solution was added to the reaction vessel containing the

dehydrated catalyst under argon via cannula. Reactions (see Scheme 5.1) were run at 60°C and observed for several hours to several days, depending on the catalyst. Reaction samples (~1 mL) were withdrawn from the reaction vessel via syringe. The solid catalyst was removed from the reaction mixture by syringe filter. A known amount of biphenyl (purchased from Aldrich) was added as a standard (solution in acetonitrile ~0.3 M). The sample was analyzed by GC/FID (HP 5890 Series II), using a HP-5MS capillary column, with a temperature ramp from 40°C to 200°C at a rate of 15°/min. As control experiments, TMAOH (homogeneous reaction), 3-aminoporoyl-functionalized silica (purchased from Aldrich), extracted Si-\*BEA, and CPG were also tested.

The ability of the P<sup>+</sup>OH<sup>-</sup>-\*BEA material to perform shape-selective base catalysis was tested by the Knoevenagel condensation reaction of 1-pyrenecarboxaldehyde, **4**, and malononitrile (see Scheme 5.2). Reactions were run similarly, except dichloroethane (purchased from Alfa Aesar, dried by refluxing with calcium hydride, distilled under vacuum, and degassed by freeze-pump-thaw cycling with liquid N<sub>2</sub>) was used as the solvent because **4** has limited solubility in acetonitrile. The GC/FID analysis for these reactions used a temperature program of 40°C to 280°C at a rate of 15°/min to allow the pyrene compounds to elute. Note that the pyrene reaction product, **5**, was not reliably eluted from the column, so reaction calculations were based on the conversion of **7** over time.

### 5.2.2 Michael Addition

P<sup>+</sup>OH<sup>-</sup>-\*BEA and P<sup>+</sup>OH<sup>-</sup>-CPG (20-40 mg) were again dehydrated at 200°C under vacuum for two hours prior to reaction. 2-cyclohexen-1-one, **6**, was purchased from Aldrich and nitromethane, **7**, was purchased from Aldrich. The reactants **6** and **7**

(approximately 15 mmol each) were measured into a glass vial with acetonitrile and sealed. The vial was purged with argon for 10 minutes. The solution was added to the reaction vessel containing the dehydrated catalyst under argon via cannula. Reactions (see Scheme 5.3) were run at 60°C and observed for several hours to several days, with sample preparation for GC/FID analysis as described above. The sample was analyzed by GC/FID with a temperature ramp from 40°C to 200°C at a rate of 10°/min. As control experiments, tert-butylphosphonium hydroxide, (TBPOH, purchased from Gelest, Inc. as a 40% solution in water, homogeneous reaction), hydroxide-containing ion-exchange resin (purchased from BioRad), extracted Si-\*BEA, and CPG were also tested.

The Michael Addition reaction of methylvinylketone, **9**, (purchased from Aldrich and stored in a freezer prior to use) and ethylcyanoacetate, **10**, (purchased from Aldrich) was also used as a base reaction for the materials (see Scheme 5.4). This reaction was more facile and could be done at room temperature. The catalysts (70 mg) were not dehydrated prior to reaction for this reaction series, and the reactions were done in air. The reactants, **9** and **10**, were added (approximately 2 mmol each) were added to 2 mL of acetonitrile (reagent grade, purchased from EM Scientific) in glass vials. The vials were capped and allowed to stir at room temperature for several hours to days. Sample preparation for GC/FID analysis was done as described above. The sample was analyzed by GC/FID with a temperature ramp from 40°C to 200°C at a rate of 10°/min.

### 5.3 Results and Discussion

The Knoevenagel Condensation of benzaldehyde and malononitrile (Scheme 5.1) was tested by several controls (see Table 5.1). A weak heterogeneous base, 3-aminopropyl-silica (AP-SiO<sub>2</sub>), had 90% yield at 7 hours. TMAOH, a strong

homogeneous base, has 99% yield of **3** after only 4 hours. Thus, the Knoevenagel reaction chosen reacts well with both weak and strong bases. A heated solution of the reactants, with no catalyst, has less than 2% yield of **3** after 71 hours. A material containing no base,  $P^+NO_3^-$ -CPG, showed no catalytic activity (<1% after 7 hours), as expected. Similarly, CPG alone showed no significant reaction at 7 hours.

The  $P^+OH^-$ -CPG had 77% yield of **3** after 72 hours. This suggested that there was indeed incorporation of a strong base within the CPG. A sample of CPG with no functionalization was exposed to the NaOH solution as in the ion-exchange of phosphonium-containing materials. This material also showed reactivity, 69% yield of **3** after 89 hours. Thus, most of the activity observed in the  $P^+OH^-$ -CPG was likely due to the presence of residual NaOH from the exchange solution, and not from  $OH^-$ -exchanged phosphonium moieties tethered to the pore walls. Because the  $P^+OH^-$ -CPG sample did have slightly higher activity than the NaOH-treated CPG, there may be some additional hydroxide, possibly as tethered phosphonium hydroxide moieties, within the  $P^+OH^-$ -CPG, but neither the ion-exchange tests discussed in Chapter 3 or the Knoevenagel condensation catalytic tests above can conclusively show this.

$P^+OH^-$ -\*BEA was also tested in the Knoevenagel condensation reaction, having 79% yield after 90 hours. A sample of extracted Si-\*BEA, exposed to NaOH solution, also showed activity of 56% in 72 hours. Si-\*BEA was calcined and then exposed to NaOH solution to determine if the catalytic activity was due to residual hydroxide as in the CPG samples above. There was no significant activity (2% yield) after 89 hours. Thus there appeared to be no significant physisorbed hydroxide remaining in the \*BEA samples after ion-exchange. The  $P^+NO_3^-$ -\*BEA also showed evidence of base activity,

73% in 91 hours. The catalytic activity observed in all of the uncalcined \*BEA samples must be due to some other base inherently present in the \*BEA materials. It was suspected that the SDA, TEAF, was contributing to the reaction. A homogeneous solution of TEAF did indeed show catalytic activity, having 83% yield of **3** after 24 hours. Although TGA indicated 96-99% of TEAF was generally removed in SDA extraction, there was sufficient TEAF remaining in the \*BEA samples to catalyze the Knoevenagel reaction. Thus, the catalytic results of  $P^+OH^-$ -\*BEA in the Knoevenagel condensation in the reaction can not prove the presence of a phosphonium hydroxide moiety within the zeolite.

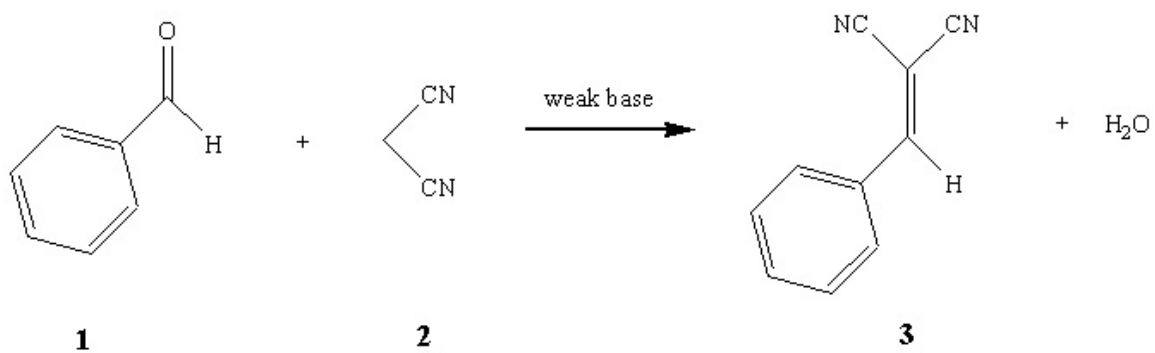
The Knoevenagel Condensation of 1-pyrenecarboxaldehyde and malononitrile was used to probe the location of the functional groups within the OFMS samples. TMAOH was an effective catalyst for the homogeneous reaction, having 91% conversion of **4** after only 1 hour (see Table 5.2). Because of the results above, TEAF was also tested as a homogeneous catalyst. TEAF had 44% conversion after 24 hours, so again catalytic results of the \*BEA samples were obscured by residual SDA.  $P^+OH^-$ -\*BEA,  $P^+NO_3^-$ -\*BEA, extracted Si-\*BEA, and calcined Si-\*BEA exposed to NaOH solution did not show any significant activity in the 1-pyrenecarboxaldehyde reaction. This suggested that the base sites in the \*BEA samples were indeed within the pores, because benzaldehyde was able to access the sites while the pyrene could not. However, as the homogeneous tests showed in both reactions, the residual TEAF in the pores of the zeolite was likely to be the source of the basic sites, not a phosphonium hydroxide moiety. Unlike the benzaldehyde case, CPG exposed to NaOH solution showed no change in conversion after 72 hours.  $P^+OH^-$ -CPG had 39% conversion of **4** in the same

amount of time. The pyrene catalytic test suggested that there was some other base site in the  $P^+OH^-$ -CPG that was not merely physisorbed hydroxide causing the activity. It is not clear why the 1-pyrenecarboxaldehyde did not appear to be affected by residual hydroxide and benzaldehyde did react. In the TEAF homogeneous reaction results, after 24 hours there was 83% yield of **3** and only 44% conversion of **4**. It may be that the pyrene is more difficult to react and required more base than what was physisorbed on the CPG.

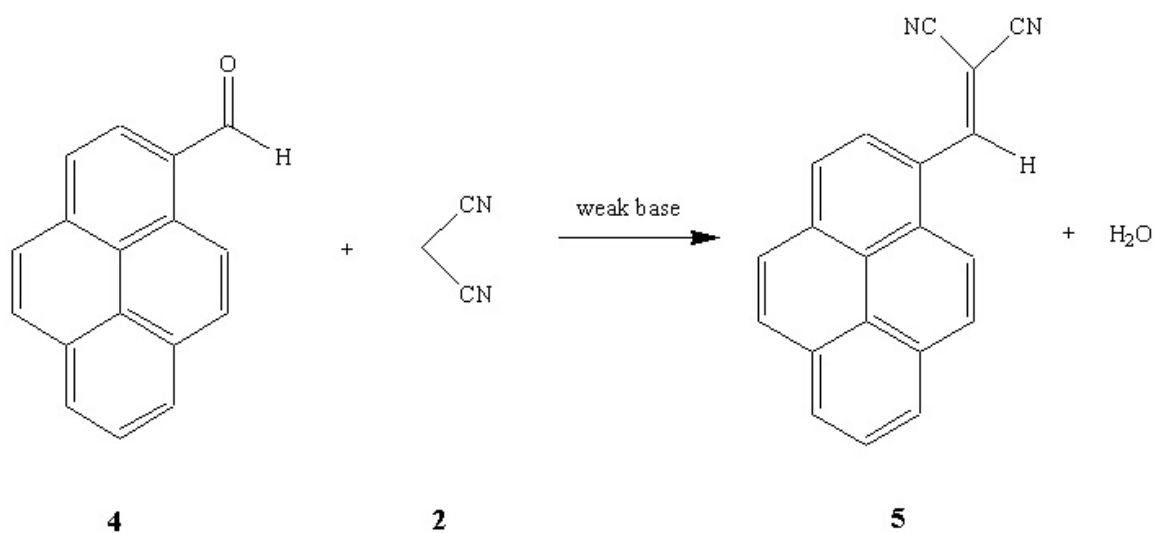
The OFMS samples were then examined in Michael addition reactions, requiring strong bases, to better probe the hydroxide group presence. The reaction of 2-cyclohexen-1-one and nitromethane (see Scheme 5.3) was first explored.  $P^+OH^-$ -CPG and  $P^+OH^-$ -\*BEA did not show any reactivity after 80 hours (see Table 5.3). Hydroxide ion-exchange resin and TBPOH did show activity. However, some of the  $P^+OH^-$ -CPG and  $P^+OH^-$ -\*BEA catalysts were discolored after reaction (yellow). It was suspected that the reaction temperature (60°C) could be degrading the functional groups in the presence of solvent.

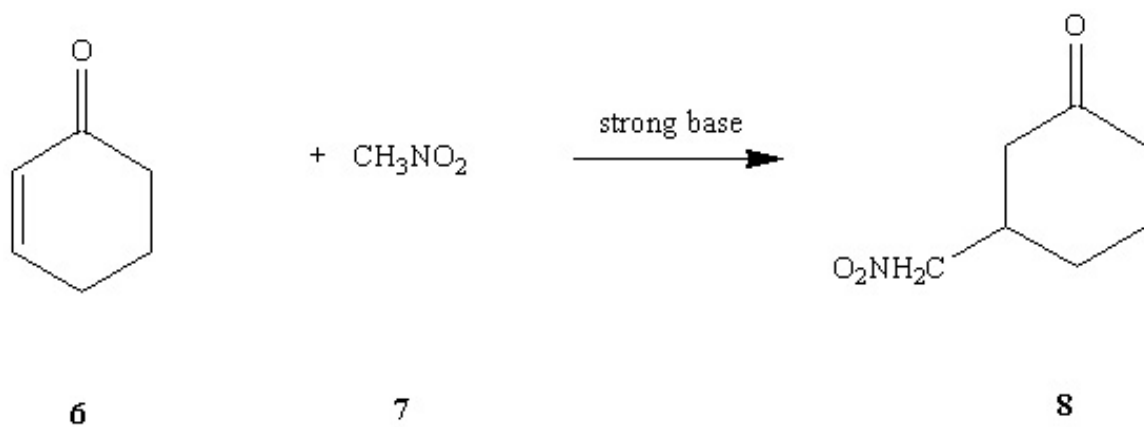
A more facile Michael addition reaction, of methylvinylketone and ethylcyanoacetate (see Scheme 5.4) can be performed even at room temperature. TBPOH, TEAF, and hydroxide ion-exchange resin all were reactive to **11** at room temperature (see Table 5.4). CPG exposed to the NaOH solution, did not show significant activity (2% yield of **11**). This added further evidence that although the physisorbed hydroxide in CPG can catalyze the benzaldehyde Knoevenagel condensation, it was not sufficient for more difficult reactions like the 1-pyrenecarboxaldehyde condensation and the Michael addition reactions.  $P^+OH^-$ -CPG

gave 55% yield of **11** after 47 hours, giving further evidence of a phosphonium hydroxide moiety tethered within the pores. The catalyst could be recovered by centrifugation and reused. The second use of the catalyst showed some decreased activity, 11% yield after 48 hours.  $P^+OH^-$ -\*BEA had 3% yield of **11** after 120 hours of reaction. An increase of the catalyst loading to 250 mg did not show any activity at 48 hours. Extracted Si-\*BEA had 5% yield after 48 hours, suggesting that TEAF or residual hydroxide was playing a role in the catalytic results. Even calcined Si-\*BEA exposed to NaOH exhibited a small amount of activity (0.5% after 22 hours). As in the Knoevenagel condensation, the presence of a strong base site within a phosphonium-containing OFMS could not be conclusively demonstrated.

**Scheme 5.1** Knoevenagel condensation of benzaldehyde (**1**) and malononitrile (**2**).

**Scheme 5.2** Knoevenagel condensation of 1-pyrenecarboxaldehyde (**4**) and malononitrile (**2**).



**Scheme 5.3** Michael addition of 2-cyclohexen-1-one (**6**) and nitromethane (**7**).

**Scheme 5.4** Michael addition of methylvinylketone (**9**) and ethylcyanoacetate (**10**).

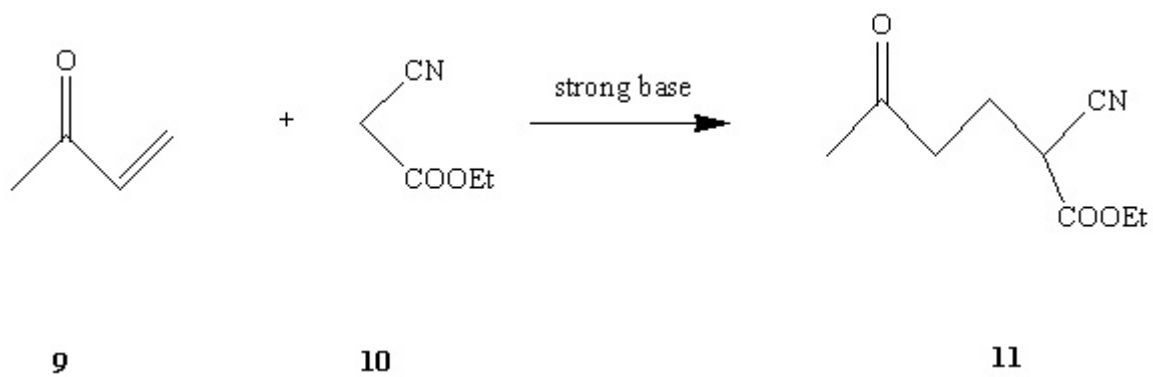


**Table 5.1** Knoevenagel condensation of **1** and **2** (see Scheme 5.1).

Catalyst	Reaction Time (hr)	Yield of <b>3</b> (%)
none	71	1.6
CPG-240	7	1
AP-SiO <sub>2</sub>	7	90
TMAOH	4	99
P <sup>+</sup> NO <sub>3</sub> <sup>-</sup> -CPG	7	0.8
P <sup>+</sup> OH <sup>-</sup> -CPG	72	77
CPG <sup>a</sup>	89	69
P <sup>+</sup> OH <sup>-</sup> -*BEA	90	79
P <sup>+</sup> NO <sub>3</sub> <sup>-</sup> -*BEA	91	73
Si-*BEA, extracted <sup>a</sup>	72	56
Si-*BEA, calcined <sup>a</sup>	89	2
TEAF	24	83

<sup>a</sup>Exposed to 0.001 N NaOH as in ion-exchange

**Table 5.2** Knoevenagel condensation of **4** and **2** (see Scheme 5.2).

Catalyst	Reaction Time (hr)	Conv. of <b>4</b> (%)
none	41	0
TMAOH	1	91
TEAF	24	44
P <sup>+</sup> OH <sup>-</sup> -CPG	72	39
CPG <sup>b</sup>	72	0
P <sup>+</sup> OH <sup>-</sup> -*BEA	90	0
P <sup>+</sup> NO <sub>3</sub> <sup>-</sup> -*BEA	91	2
Si-*BEA, extracted <sup>a</sup>	72	0
*BEA, calcined <sup>b</sup>	88	0

<sup>a</sup>Exposed to 1 N HNO<sub>3</sub>

<sup>b</sup>Exposed to 0.001 N NaOH as in ion-exchange

**Table 5.3** Michael addition of **4** and **5** (see Scheme 5.3).

Catalyst	Reaction Time (hr)	Yield of <b>6</b> (%)
none	80	0
TBPOH	2 <sup>a</sup>	55
OH-resin	93	55
P <sup>+</sup> OH <sup>-</sup> -CPG	80	0
P <sup>+</sup> OH <sup>-</sup> -*BEA	80	0

<sup>a</sup>Reaction run at room temperature

**Table 5.4** Michael addition of **9** and **10** (see Scheme 5.4).

Catalyst	Reaction Time (hr)	Yield of <b>11</b> (%)
none	120	0.3
TBPOH	2	12 <sup>a</sup>
TEAF	2	72
OH-resin	47	86
P <sup>+</sup> OH <sup>-</sup> -CPG	47	55
	48 <sup>b</sup>	11
CPG <sup>d</sup>	22	2
P <sup>+</sup> OH <sup>-</sup> -*BEA	120	3
	48 <sup>c</sup>	0
Si-*BEA, extracted <sup>d</sup>	48	5
*BEA, calcined <sup>d</sup>	22	0.5

<sup>a</sup>Many other products formed. Conversion of **10** was 92%

<sup>b</sup>Catalyst from above was recovered and reused

<sup>c</sup>Using 250 mg of catalyst

<sup>d</sup>Exposed to 0.001 N NaOH as in ion-exchange

CHAPTER SIX

SUMMARY AND CONCLUSIONS FOR  
PART ONE

The objective of this project was to incorporate a covalently attached moiety (e.g., an ammonium or phosphonium functionality) into the pore space of zeolite \*BEA for strong base catalysis. The presence of the positive charge center would allow the incorporation of a strong base, OH<sup>-</sup>, within a zeolite. The preparation of such a material was to be fully characterized by analytical techniques and used in shape-selective base catalysis.

An ammonium-containing organosilane was used in the synthesis of an OFMS. The \*BEA structure was formed from the synthesis gel and was stable to SDA extraction. Although the SDA could be extracted, use of the acidified pyridine solution for extraction left residual pyridine in the zeolite. This residual pyridine could be removed by two water washes for Si-\*BEA, but some pyridine remained in the Q-\*BEA samples, likely due to defect sites. In order to avoid pyridine affecting catalytic results, an acetic acid was used for subsequent \*BEA extractions. The Q-\*BEA samples showed evidence of a Si-C bond by <sup>29</sup>Si CP/MAS NMR, even after extraction of the SDA. However, N<sub>2</sub> adsorption results did not conclusively demonstrate the presence of a functional moiety within the pore space. Due to inconsistencies in the N<sub>2</sub> data, the ammonium functionality was tethered onto amorphous silica, CPG, in order to attain higher organic loadings to utilize <sup>13</sup>C CP/MAS NMR to study the stability of the ammonium functional group. The ammonium functional group exhibited degradation after heating to 100°C. It was not expected that the organic group in Q-\*BEA would survive either the zeolite synthesis (at 140°C) or the SDA extraction. Further work was done to attempt to incorporate a phosphonium functionality into an OFMS.

The phosphonium functionality was prepared by nucleophilic displacement of a halogen-containing alkyl group with trimethylphosphine. The reaction was examined with bromopropyl-functionalized CPG using  $^{13}\text{C}$  CP/MAS and  $^{31}\text{P}$  MAS NMR. The bromopropyl group had 86% reaction to phosphonium, resulting in an organic loading of approximately 0.36 mmol/g of phosphonium on CPG. Heat treatment of the phosphonium-containing CPG showed the bromide form was stable to 300°C under vacuum.

Similar reactions were done with bromopropyl-functionalized \*BEA. The \*BEA structure was stable to both extraction and nucleophilic displacement reactions. TGA analysis indicated the presence of organic groups within the zeolite, having an exotherm and weight loss around 300°C. Although  $^{31}\text{P}$  MAS NMR showed evidence of phosphonium groups, only 21% of the bromopropyl-functional groups were reacted, resulting in an organic loading of 0.0084 mmol/g of phosphonium. Lack of reaction of the Br-\*BEA material with triphenylphosphine (too large to enter pores) suggested that the functional groups in the OFMS sample were located within the zeolite pore space. Attempts were made to increase the phosphonium loading in OFMS materials by using the prepared phosphonium organosilane directly in the zeolite synthesis. The as-made sample did show a higher level of phosphonium in the zeolite, 0.42 mmol/g, but the phosphonium moiety was not stable to any extraction procedure attempted to remove the SDA.

The phosphonium halide-containing samples were ion-exchanged to nitrate using 1 N  $\text{HNO}_3$ . IR spectra indicated the presence of  $\text{NO}_3^-$  in the both the OFMS and CPG materials. Titration of the filtrate for removed halides determined that the exchange

efficiency of  $\text{Br}^-$  to  $\text{NO}_3^-$  was 56% for the  $\text{P}^+\text{Br}^-$ -CPG material. No removed halides could be detected in the  $\text{P}^+\text{Br}^-$ -\*BEA samples, however. Shape-selective ion-exchange with  $\text{NaBPh}_4$ , which was too large to enter the \*BEA pores, also suggested that the phosphonium moieties were located within the zeolite pores. Finally, ion-exchange to the hydroxide form of the materials had a 72% exchange efficiency from  $\text{NO}_3^-$  to  $\text{OH}^-$  for the  $\text{P}^+\text{NO}_3^-$ -CPG material, giving an overall exchange efficiency of 40% from bromide to hydroxide. Exchange results for the  $\text{P}^+\text{NO}_3^-$ -\*BEA did show removal of nitrate (0.008 mmol/g), but this was similar to the control Si-\*BEA sample and was not conclusive.

Catalytic experiments were done with the hydroxide-containing materials. Definite conclusions about the presence of a phosphonium hydroxide in the CPG could not be determined due to physisorbed hydroxide remaining on CPG. Michael addition reactions with methylvinylketone suggested the existence of a base site within CPG that was not due to physisorbed hydroxide. All of the uncalcined \*BEA samples were capable to catalyzing the Knoevenagel condensation reaction of benzaldehyde and malononitrile, even extracted Si-\*BEA. No significant reactivity was observed for the Michael addition in any of the \*BEA samples tested. This was due to the presence of residual TEAF, which could not be completely removed by extraction.

Neither the ion-exchange tests described in Chapter 3 nor the catalytic experiments in Chapter 4 were able to prove the presence of a phosphonium hydroxide moiety within an OFMS. Residual TEAF from extraction, physisorbed hydroxide from the ion-exchange, and the low number density of the phosphonium groups prevented clear conclusions of the nature of the functional group in the OFMS samples.  $^{31}\text{P}$  MAS

NMR does indeed show the success of the nucleophilic displacement reaction within Br-\*BEA and that the functional groups are located within the pore space of the zeolite.

Results from the functionalized CPG work show that the process of creating phosphonium-containing materials from a halogen-containing material is possible. The reactivity work suggests that subsequent ion-exchange of the halide form to hydroxide to create a heterogeneous material for strong base catalysis is feasible. However, the phosphonium group is susceptible to degradation in chemical environments, as seen in the SDA extraction procedure and in the Michael addition reaction at 60°C. This suggests that the incorporation of a quaternary moiety (ammonium or phosphonium) within a porous material is only appropriate where temperature and environment are mild. For example, the quaternary moieties could be grafted onto calcined mesoporous materials and subsequently ion-exchanged to a useful material.

## PART TWO

SELECTIVE OXIDATION OF ETHANE VIA  
HETEROPOLYANION-CONTAINING  
SOLID CATALYSTS

## CHAPTER SEVEN

SELECTIVE OXIDATION OF LIGHT  
ALKANES

## 7.1 Introduction

Oxidation steps are critical to the functionalization of chemicals and intermediates. Over 60% of chemicals and intermediates are prepared via a catalytic oxidation step at some stage of their production.<sup>1</sup> Many fine chemical processes use stoichiometric oxidants, e.g., permanganates and chromium salts that are harmful to the environment. Catalytic processes are attractive because they reduce the consumption of environmentally harmful oxidants and can improve the economics of the oxidation process. In the development of catalytic materials, often molecular oxygen (O<sub>2</sub>) or hydrogen peroxide (H<sub>2</sub>O<sub>2</sub>) can be used. This enables the process to be more environmentally friendly, because water is the co-product of reaction. Catalytic oxidations suffer from substrate-specificity, i.e., a particular catalyst is only effective for one reactant/product or set of reaction conditions. The versatility of many oxidation catalysts is limited, thereby restricting their industrial usefulness.

Some catalytic oxidation processes are listed in Table 7.1. The catalysts for these processes have been optimized for a particular reaction and set of conditions. The production of vinyl acetate results from a two-step oxidation. First the acetic acid is produced from carbonylation of methanol. The acetic acid is then reacted with ethylene in the presence of air to make vinyl acetate. Some of the reactants, e.g., methanol and propylene, are already partially oxidized. Typically, alkenes and aromatics are used as feedstocks because they are easy to functionalize. Alkenes are becoming particularly costly, as the demand for high purity alkenes as raw materials for many industrial processes (such as monomers or comonomers in polymerization) increases. It is desirable to remove the need for alkene feedstocks in the preparation of chemical

intermediates wherever feasible. The use of light alkanes as reactants for selective oxidation would allow one to take advantage of an under-utilized and relatively inexpensive feedstock and avoid competition with other processes for alkene raw materials. Currently, the selective oxidation of *n*-butane to maleic anhydride is the only catalytic commercial oxidation process that uses a light alkane as a reactant. Other light alkanes, i.e., methane, ethane and propane, are of interest as possible routes to methanol and formaldehyde (methane), acetic acid (ethane), and acrylic acid or acrylonitrile (propane).<sup>1</sup> The current production methods for these intermediates consist of multiple step processes through partially oxygenated raw materials which themselves must be produced (see Table 7.2).

The challenge of alkane use is that alkanes are more difficult to activate than alkenes. Alkane dehydrogenations to the corresponding alkene are typically performed at high temperatures (500-800°C) and are thermodynamically limited in the yield of alkenes.<sup>2</sup> Dehydrogenation catalysts also have a tendency to deactivate due to coking or thermal instability. Ethane dehydrogenation must be performed at particularly high temperatures in order to activate the C-H bond. Oxidative dehydrogenation is more thermodynamically favorable and allows the alkenes to be formed at lower temperatures (300-400°C), with less catalyst deactivation and coking. With the addition of oxygen into the reaction, however, alkane combustion becomes possible and allows over-oxidation products to form. Combustion products CO and CO<sub>2</sub> (referred to as total oxidation products, CO<sub>x</sub>) are favored thermodynamically. The use of propane and butane for selective oxidation is difficult because both the alkenes and the liquid oxygenates are particularly susceptible to additional oxidation to CO<sub>x</sub>. The high reaction temperatures

required to allow effective alkane activation increase the tendency of the oxygenated products to undergo total oxidation. Ethylene, rather than acetic acid, is usually the preferred product of ethane oxidation.<sup>3</sup> Selectivity control, forming the desired oxygenated product easily yet avoiding over-oxidation, becomes important for new catalyst development. A variety of catalyst systems have been studied for alkane activation: mixed metal oxides (bulk<sup>4-7</sup> or supported<sup>8,9</sup>), heteropolyacids,<sup>10-14</sup> and molecular sieves.<sup>15-19</sup> However, these catalyst systems are limited in versatility and robustness and are usually specific to a particular alkane substrate. An ideal selective oxidation catalyst would be able to activate light alkanes and be versatile for multiple substrates and products of reaction.

## 7.2 Ethane Selective Oxidation Catalysts

An effective catalyst for the selective oxidation of ethane was reported by Thorsteinson and co-workers.<sup>20</sup> The catalyst, a V/Nb/Mo oxide mixture optimized to composition of  $\text{Mo}_{0.73}\text{V}_{0.18}\text{Nb}_{0.09}\text{O}_x$ , was very active for the oxidative dehydrogenation to ethylene, even at temperatures as low as 200°C. Appreciable formation of ethylene was observed at atmospheric pressure and 350°C with 58% ethane conversion and 65% selectivity (see Table 7.3). No acetic acid was observed at atmospheric pressure. Ruth *et al.* reported the formation of acetic acid (2.5% selectivity) with the Thorsteinson catalyst at elevated pressures (290 psig).<sup>21</sup> At these conditions, a STY of 0.022 mmol/min/g catalyst of acetic acid could be produced. However, this catalyst was a complex mixture of different oxide phases that was difficult to prepare. Several studies found that differences in oxide preparation affected the catalyst performance.<sup>1</sup>

The use of promoters has been studied to modify the activity and selectivity of the V/Nb/Mo oxide Thorsteinson catalyst. The addition of a small amount of Pd to the mixed oxide ( $\text{Mo}_1\text{V}_{0.25}\text{Nb}_{0.12}\text{Pd}_{0.0005}\text{O}_x$ ) improved the selectivity to acetic acid (see Table 7.3).<sup>22</sup> Linke and co-workers also reported that the partial pressure of steam fed affected the catalyst performance. Other systems, such as vanadium oxides supported on titania, have been studied. Yet in the literature, acetic acid yields have generally remained low and often can only be obtained at elevated pressure.

### 7.3 Heteropolyanions

Heteropolyanions (HPAs) are polyoxometalates with one or more central organizing polyhedrons (the central atom being referred to as the “heteroatom,” e.g.,  $\text{Si}^{4+}$ ,  $\text{Ge}^{4+}$ ,  $\text{P}^{5+}$ , or  $\text{As}^{5+}$ ) about which “addenda” metal-oxygen polyhedrons (e.g.,  $\text{Mo}^{6+}$  or  $\text{W}^{6+}$ ) are arranged. The addenda metals can have other metal substitution (e.g., V or Nb). These metal oxide clusters have the general formula  $[\text{X}_x\text{M}_m\text{O}_y]^{q-}$ , where X is the heteroatom and M is the addenda atom. They are prepared by self-assembly in aqueous solutions and can be synthesized in a variety of structures and compositions (e.g., the Keggin unit, where  $x = 1$ ,  $m = 12$ , and  $y = 40$ ).<sup>23</sup> The overall anionic charge of the compound may be countered with protons or other cations (organic and inorganic) to make the corresponding salt.

These materials, unlike zeolites and other bulk metal oxides that have metal-oxygen lattices, consist of discrete anionic units of metal oxide that are the primary structure of the material. The primary structures are associated by the interstitial guest species (e.g., water) to arrange in a uniform fashion into crystals to form a secondary structure. Organic guest species (e.g., alcohols, ethers, amines) may also be incorporated

into the interstitial spaces between the metal oxide clusters. Aggregates of the secondary structures form a tertiary structure that describes the physical characteristics of the material (e.g., porosity, particle size, and surface area). Variations in the structure and composition affect the acidic and oxidative nature of these HPAs and thereby affect their activity and selectivity in oxidation reactions. Many reviews have documented the catalytic uses of HPAs, especially in homogeneous reactions at moderate temperatures (see Refs. 14 and 23 and citations therein.) Thermal decomposition of the *acid* form of HPAs has limited the application of these compounds as gas phase oxidation catalysts. The acid HPAs decompose from 200-400°C, depending on the composition, into a mixture of metal oxides.

Heteropolyanion salts, which are more stable, have been shown to be useful in gas phase oxidation reactions (see Table 7.4). HPAs have been used in the oxidation of a variety of substrates, including alkanes, alkenes, and alcohols. Sb and W-containing HPAs have been used for the oxidation of ethane to ethylene at elevated temperatures.<sup>10</sup> Showa Denko demonstrated that ethylene can be oxidized to acetic acid using Pd- $\text{H}_4[\text{SiW}_{12}\text{O}_{40}]^{24}$ . No formation of acetic acid was observed with either Pd(0) alone or HPA alone on silica. This method of acetic acid production is superior to the traditional methanol carbonylation because it eliminates the need for high purity CO as a feedstock and the use of expensive materials of construction. Mizuno and co-workers reported the use of Cs-containing HPAs, combined with another metal (depending on reaction), for the oxidation of alkanes (see Table 7.5).<sup>14,23</sup> Ethane and propane were both oxidized to their alkenes. Formic acid, acrylic acid, and methacrylic acid were formed from methane, propane, and isobutane, respectively.

Ueda and co-workers reported that a pyridine-exchanged heteropolyanion, pretreated to 420°C under flowing inert, was used as a precursor to a catalyst for the oxidation of light alkanes. The active phase formed from the HPA precursor was active for propane oxidation, having 12% conversion and 24% selectivity to acrylic acid.<sup>11,13</sup> This catalyst system was later shown to also convert ethane to acetic acid at 340°C with 10% selectivity at 1% ethane conversion.<sup>11</sup>

#### 7.4 Objectives

Previous work by Davis and co-workers<sup>25-28</sup> reported the development of a versatile selective oxidation catalyst system using HPA salts as catalyst precursors that was highly active and selective for both the oxidation of *n*-butane to maleic acid and the oxidation of propane to acrylic acid. The catalysts were formed from niobium- and pyridine-exchanged HPAs, specifically molybdophosphoric acid ( $\text{H}_3\text{PMo}_{12}\text{O}_{40}$ ) and molybdovanadophosphoric acid ( $\text{H}_4\text{PMo}_{11}\text{VO}_{40}$ ), by heat treatment to 420°C under helium. The catalysts are active over a range of reaction temperatures and with either hydrocarbon-rich or oxygen-rich flows. The focus of this project is to explore whether the new HPA catalyst system developed by Davis and co-workers could be used for the selective oxidation of ethane to acetic acid and ethylene.

## 7.5 References

- (1) Centi, G. *et al.*, *Selective Oxidation by Heterogeneous Catalysis*; Kluwer Academic/Plenum Publishers: New York, 2001.
- (2) Bhasin, M. M. *Top. Catal.* **2003**, *23*, 145.
- (3) Cavani, F.; Trifiro, F. *Catal. Today* **1999**, *51*, 561.
- (4) Novakova, E. K. *et al.*, *J. Catal.* **2002**, *211*, 226.
- (5) Solsona, B. *et al.*, *Appl. Catal., A* **2003**, *249*, 81.
- (6) Grasselli, R. K. *et al.*, *Top. Catal.* **2003**, *23*, 5.
- (7) Ledoux, M. J. *et al.*, *J. Catal.* **2001**, *203*, 495.
- (8) Solsona, B. *et al.*, *J. Catal.* **2001**, *203*, 443.
- (9) Kucherov, A. V. *et al.*, *Catal. Today* **2003**, *81*, 297.
- (10) Cavani, F. *et al.*, *Catal. Today* **1995**, *24*, 365.
- (11) Li, W.; Ueda, W. *Stud. Surf. Sci. Catal.* **1997**, *110*, 433.
- (12) Li, W. *et al.*, *Appl. Catal., A* **1999**, *182*, 357.
- (13) Ueda, W.; Suzuki, Y. *Chem. Lett.* **1995**, *7*, 541.
- (14) Mizuno, N.; Misono, M. *Chem. Rev.* **1998**, *98*, 199.
- (15) Luo, L. *et al.*, *J. Catal.* **2001**, *200*, 222.
- (16) Marchese, L. *et al.*, *J. Catal.* **2002**, *208*, 479.
- (17) Bulanek, R. *et al.*, *Appl. Catal., A* **2002**, *235*, 181.
- (18) Zhang, Q. *et al.*, *J. Catal.* **2001**, *202*, 308.
- (19) Concepcion, P. *et al.*, *Microporous Mesoporous Mater.* **2004**, *67*, 215.
- (20) Thorsteinson, E. M. *et al.*, *J. Catal.* **1978**, *52*, 116.
- (21) Ruth, K. *et al.*, *J. Catal.* **1998**, *175*, 27.

- (22) Linke, D. *et al.*, *J. Catal.* **2002**, *205*, 16.
- (23) Kozhevnikov, I. V. *Catalysis by Polyoxometalates*; John Wiley & Sons, 2002.
- (24) Suzuki, T. *et al.*, ; Showa Denko Kabushiki Kaisha: European, 1994.
- (25) Davis, M. E. *et al.*, *Angew. Chem., Int. Ed.* **2002**, *41*, 858.
- (26) Holles, J. H. *et al.*, *J. Catal.* **2003**, *218*, 42.
- (27) Dillon, C. J. *et al.*, *J. Catal.* **2003**, *218*, 54.
- (28) Dillon, C. J. *et al.*, *Catal. Today* **2003**, *81*, 189.
- (29) Tessier, L. *et al.*, *Catal. Today* **1995**, 335.

**Table 7.1** Current commercial production of chemical intermediates. Adapted from ref. 1.

Reactants	Products	Conversion (%)	Selectivity (%)
Methanol/ Air	Formaldehyde	99	94
Propylene/ Air/ Ammonia	Acrylonitrile	97-99	73-82
Methanol/ CO (30 bar)	Acetic Acid	-	99
Ethylene/ Acetic Acid/ Air	Vinyl Acetate	20-35	98-99
<i>n</i> -Butane/ Air	Maleic Anhydride	70-80	65-70

**Table 7.2** Alkane oxidations of development interest. Adapted from ref. 1.

Product	Possible Alkane Source	Current Technology
Methanol	Methane	Two-Step Methane Steam Reforming
Formaldehyde	Methane	Three-Step Methanol Oxidation
Acetic Acid	Ethane	Multi-Step Methanol Carbonylation
Acrylic Acid	Propane	Two-Step Process through Acrolein
Acrylonitrile	Propane	Propylene Ammoxidation

**Table 7.3** Selective ethane oxidation catalysts.

Catalyst	T	P	Flow	Conv.	Selectivity		STY <sup>b</sup>		Ref.
					C <sub>2</sub> <sup>=</sup>	Ac	C <sub>2</sub> <sup>=</sup>	Ac	
Mo <sub>0.73</sub> V <sub>0.18</sub> Nb <sub>0.09</sub> O <sub>x</sub>	350	0	13.3: 8.8: 125: 0	58	65	0	0.007	0	20
	350	290	6: 3.6: 14.4: 0	32	44	2.5	0.39	0.022	21
Mo <sub>1</sub> V <sub>0.25</sub> Nb <sub>0.12</sub> Pd <sub>0.0005</sub> O <sub>x</sub>	246	218	7.3: 1.5: 9.5: 0.1	4.7	1	59	0.004	0.012	22
VO <sub>x</sub> /TiO <sub>2</sub>	250	0	142: 8.3: 16.7: 0	1	18	36	0.004	0.007	29

<sup>a</sup>I = inert (He, N<sub>2</sub>)

<sup>b</sup>STY is in mmol/min/g catalyst

**Table 7.4** Gas-phase oxidations with heteropolyanion catalysts. Adapted from ref. 23.

Reaction	Catalyst	T (C)
Methacrolein + O <sub>2</sub> → Methacrylic Acid	CsH <sub>3</sub> [PMo <sub>11</sub> VO <sub>40</sub> ]	260
Isobutane + O <sub>2</sub> → Methacrylic Acid	H <sub>3</sub> [PMo <sub>12</sub> O <sub>40</sub> ]	350
<i>n</i> -Butane + O <sub>2</sub> → Maleic Anhydride	Bi[PMo <sub>12</sub> O <sub>x</sub> ] + VO <sup>2+</sup>	360
CH <sub>4</sub> + N <sub>2</sub> O → HCHO, CH <sub>3</sub> OH	H <sub>3</sub> [PMo <sub>12</sub> O <sub>40</sub> ]/SiO <sub>2</sub>	570
CH <sub>3</sub> OH + O <sub>2</sub> → HCHO, (CH <sub>3</sub> ) <sub>2</sub> O	H <sub>3</sub> [PMo <sub>12</sub> O <sub>40</sub> ]	200-290
C <sub>2</sub> H <sub>5</sub> OH + O <sub>2</sub> → CH <sub>3</sub> CHO, (C <sub>2</sub> H <sub>5</sub> ) <sub>2</sub> O	H <sub>3</sub> [PMo <sub>12</sub> O <sub>40</sub> ] + polysulfone	170
Isobutene + O <sub>2</sub> → Methacrolein	PbFeBi[PMo <sub>12</sub> O <sub>x</sub> ]	400

**Table 7.5** Selective oxidation of light alkanes with HPAs. Adapted from ref. 14.

Reaction	Catalyst	T (C)	Yield (%)
Methane → Formic Acid	$\text{Cs}_{2.5}\text{Pd}_{0.08}\text{H}_{1.34}[\text{PVMo}_{11}\text{O}_{40}]$	300	0.05
Ethane → Ethylene	$\text{Cs}_{2.5}\text{Mn}_{0.08}\text{H}_{1.34}[\text{PVMo}_{11}\text{O}_{40}]$	425	4.3
Propane → Acrylic Acid	$\text{Cs}_{2.5}\text{Fe}_{0.08}\text{H}_{1.26}[\text{PVMo}_{11}\text{O}_{40}]$	380	13
Propane → Propylene	$\text{Cs}_{2.5}\text{Cu}_{0.08}\text{H}_{3.34}[\text{PV}_3\text{Mo}_9\text{O}_{40}]$	380	10
Isobutane → Methacrylic Acid	$\text{Cs}_{2.5}\text{Ni}_{0.08}\text{H}_{1.26}[\text{PVMo}_{11}\text{O}_{40}]$	340	9.0

## CHAPTER EIGHT

REACTIVITY OF NIOBIUM- AND  
PYRIDINE-EXCHANGED  
HETEROPOLYANIONS FOR THE  
CONVERSION OF ETHANE

## 8.1 Introduction

Holles *et al.* described the preparation and alkane oxidation reactivity of niobium and pyridine-containing phosphomolybdates.<sup>1</sup> Specifically, molybdophosphoric acid ( $\text{H}_3\text{PMo}_{12}\text{O}_{40}$ , denoted  $\text{PMo}_{12}$ ) and molybdovanadophosphoric acid ( $\text{H}_4\text{PMo}_{11}\text{VO}_{40}$ , denoted  $\text{PMo}_{11}\text{V}$ ) were exchanged with niobium oxalate and pyridine to produce the exchanged HPAs (denoted  $\text{NbPMo}_{12}\text{pyr}$  and  $\text{NbPMo}_{11}\text{Vpyr}$ , respectively). The active catalyst was obtained by pretreatment of the exchanged HPAs in flowing helium to  $420^\circ\text{C}$ .

The catalysts were thoroughly characterized by TGA/DSC,  $^{31}\text{P}$  MAS NMR, and *in situ* XRD, XAS, and XPS, described by Dillon *et al.*<sup>2</sup> XRD and  $^{31}\text{P}$  MAS NMR showed that the Keggin unit remained intact during the niobium and pyridine exchange process. *In situ* XRD showed that without pyridine exchanged into the HPA, the Keggin unit decomposed to  $\text{MoO}_3$  at elevated temperatures ( $>500^\circ\text{C}$ ). In samples containing both niobium and pyridine, the Keggin unit decomposed to  $\text{MoO}_2$  at elevated temperatures ( $>500^\circ\text{C}$ ). Neither  $\text{MoO}_3$  nor  $\text{MoO}_2$  were active for selective oxidation. However, a mostly amorphous phase formed at  $420^\circ\text{C}$  in samples containing both niobium and pyridine. This phase was found to be active for selective oxidation of light alkanes. Thermogravimetric analysis and elemental analysis showed that by  $420^\circ\text{C}$ , all of the pyridine was removed from the material. During removal of pyridine by heat treatment to  $420^\circ\text{C}$ , the Keggin structure decomposed to lacunary structures, as seen by  $^{31}\text{P}$  MAS NMR. The catalyst was found to be in a reduced oxidation state after heat treatment, where  $\text{Nb}^{5+}$  was reduced to  $\text{Nb}^{4+}$  and some of the  $\text{Mo}^{6+}$  was reduced to  $\text{Mo}^{5+}$ .

These catalysts were shown to be active for *n*-butane oxidation (see Table 8.1).<sup>1</sup> Butane reactivity was tested at flow rates of 4: 2: 4: 5 mL/min of butane: oxygen: helium: steam and 380°C (using 0.2 g of NbPMo<sub>12</sub>pyr). The incorporation of pyridine was shown to be essential for active catalyst formation; PMo<sub>12</sub> and PMo<sub>11</sub>V had no significant conversion under the same conditions. The niobium-exchanged materials, without pyridine, (denoted NbPMo<sub>12</sub>, and NbPMo<sub>11</sub>V, respectively) also showed no activity. The pyridine-exchanged materials (denoted PMo<sub>12</sub>pyr and PMo<sub>11</sub>Vpyr, respectively) each had high activity, with butane conversions of 13.5%. Maleic acid selectivity (formed from maleic anhydride as liquid oxygenates were trapped in water for analysis) was also high (82 and 90% for PMo<sub>12</sub>pyr and PMo<sub>11</sub>Vpyr, respectively).

The incorporation of both niobium and pyridine resulted in active catalysts as well. NbPMo<sub>12</sub>pyr gave 15% conversion of butane, utilizing all of the oxygen available (15% was the maximum theoretical conversion at the butane: oxygen ratio of 2:1). Maleic acid was the major product, having 71% selectivity. 25% selectivity to total oxidation product (CO<sub>x</sub>) was observed, with small amounts of acetic acid and acrylic acid also being formed. NbPMo<sub>11</sub>Vpyr also had high butane conversion (15%) and selectivity to maleic acid (76%).

Although the addition of only pyridine to the HPA precursor resulted in active catalysts at lower flow rates, only 2.5% butane conversion was observed after an eight-fold increase in flow rates (32: 16: 32: 40 mL/min) with PMo<sub>12</sub>pyr. The addition of both niobium and pyridine was essential for catalyst activity at higher flow rates. NbPMo<sub>12</sub>pyr gave a butane conversion of 15% and maleic acid selectivity of 90% at the higher flow rates. This resulted in a space time yield (STY) of maleic acid of 0.84 mmol/min/g

catalyst. Similar results were obtained with NbPMo<sub>11</sub>Vpyr, having 14% butane conversion and 80% selectivity to maleic acid at 380°C and flow rates to 32: 16: 32: 40 mL/min of butane: oxygen: helium: steam, giving a STY of 0.76 mmol/min/g catalyst of maleic acid.

The same catalysts were also examined in the oxidation of propane to acrylic acid (see Table 8.2). As in the butane oxidation, neither of the acid forms of the HPAs (PMo<sub>12</sub> and PMo<sub>11</sub>V) had activity for propane oxidation (0.4% conversion for PMo<sub>11</sub>V, at 380°C and flow rates of 8: 4: 8: 10 mL/min of propane: oxygen: helium: steam). The addition of Nb did not significantly affect activity for propane with NbPMo<sub>11</sub>V (1.4% conversion). Unlike the butane studies, even the addition of pyridine to make PMo<sub>11</sub>Vpyr did not yield an active propane oxidation catalyst (3.4% conversion).

The addition of both niobium and pyridine was necessary for an active catalyst at these conditions (25% conversion for both NbPMo<sub>12</sub>pyr and NbPMo<sub>11</sub>Vpyr). However, NbPMo<sub>12</sub>pyr resulted in a significant amount of CO<sub>x</sub> (79% selectivity) with little acrylic acid (2%). Some maleic acid and acetic acid was also observed (14% and 2%, respectively). The substitution of vanadium into the HPA framework prevented over-oxidation to CO<sub>x</sub>. At the same conditions and conversion, NbPMo<sub>11</sub>Vpyr had only 15% selectivity to CO<sub>x</sub> and 21% to acrylic acid. Maleic acid and acetic acid selectivities were 43% and 19%, respectively. The product distribution between acrylic acid and maleic acid was affected by space velocity. Acrylic acid selectivity was increased to 49% (from 21%) and maleic acid decreased to 15% (from 43%) by the increase of flows of 32: 16: 32: 40 mL/min at 380°C (with 21% propane conversion). Acetic acid selectivity remained similar at 23%.

Preliminary work in these studies indicated that the exchanged HPAs would also be effective for the oxidation of ethane to acetic acid.<sup>1</sup> The catalytic study of the ethane oxidation was examined here to determine optimal process conditions, e.g., reaction temperature, pressure, flow composition, and HPA composition.

## 8.2 Experimental Section

### 8.2.1 *NbPMo<sub>12</sub>pyr Preparation*

Niobium pentachloride (NbCl<sub>5</sub>) was purchased from Aldrich and stored in a desiccator. The NbCl<sub>5</sub> (1.867 g) was dissolved in 15.0 mL of water. The water was added drop wise via pipet to the solid with vigorous stirring. The mixture was stirred at room temperature until a clear solution resulted. Ammonium hydroxide (3.0 mL) was added to basify the solution (pH = 12), and its addition produced a white precipitate, presumed to be niobium oxide. The precipitate was recovered by filtration and washing with ammonium hydroxide. The resulting white paste was allowed to dry exposed to ambient air overnight. Oxalic acid (1.560 g, purchased from Aldrich) was dissolved in 30 mL of water. The oxalic acid solution was then added drop wise via pipet to the dried niobium oxide with vigorous stirring. The slurry was stirred and heated to 80°C for 1-2 hours to allow the niobium oxide to completely dissolve. The resulting clear niobium oxalate solution was then allowed to cool to room temperature.

Molybdophosphoric acid, H<sub>3</sub>PMo<sub>12</sub>O<sub>40</sub> (hereafter denoted PMo<sub>12</sub>) was purchased from Aldrich. PMo<sub>12</sub> (yellow solid, 30.097 g) was dissolved in 46 mL of water to produce a clear, yellow solution. The niobium oxalate solution was added drop wise with stirring to the PMo<sub>12</sub> solution. The Nb-exchanged PMo<sub>12</sub> material, hereafter denoted NbPMo<sub>12</sub>, was allowed to heat to dryness, exposed to ambient air, overnight at 80°C to

produce green solids. The  $\text{NbPMo}_{12}$  (21.235 g) was crushed to a fine powder and dissolved in 127 mL of water. A solution of pyridine (6.650 g) and water (68 mL) was added slowly drop wise to the  $\text{NbPMo}_{12}$  solution. A light green precipitate began to form as pyridine was added. The pyridine-exchanged  $\text{NbPMo}_{12}$ , hereafter denoted  $\text{NbPMo}_{12}\text{pyr}$ , was heated to dryness exposed to ambient air overnight at  $80^\circ\text{C}$  to produce light green solids. Samples of  $\text{NbPMo}_{12}\text{pyr}$  were prepared having Nb/Keggin loadings of 0.04, 0.2, 0.4 (recipe shown), 0.6, 0.8, and 1.0 (see Figure 8.1). Samples were also prepared having only Nb-exchange (no pyridine) and pyridine alone (see Figure 8.2). It is important to note that unless otherwise stated, all  $\text{NbPMo}_{12}\text{pyr}$  results are given for a Nb/Keggin ratio of 0.4.

### 8.2.2 *NbPMo<sub>11</sub>Vpyr Preparation*

Molybdovanadophosphoric acid,  $\text{H}_4\text{PMo}_{11}\text{VO}_{40}$  (denoted  $\text{PMo}_{11}\text{V}$ ), was prepared according to known methods,<sup>3</sup> by Holles and co-workers.<sup>1</sup> The Nb- and pyridine-exchange was then performed as described above to prepare  $\text{NbPMo}_{11}\text{Vpyr}$  (see Figure 8.3). Samples of  $\text{NbPMo}_{11}\text{Vpyr}$  prepared by Holles and co-workers have a Nb/Keggin loading of 0.04, 0.12, 0.68, 0.87, and 0.98 (see Figure 8.4). It is important to note that unless otherwise stated, all  $\text{NbPMo}_{11}\text{Vpyr}$  results are given for a Nb/Keggin ratio of 0.68.

Alternatively,  $\text{PMo}_{11}\text{V}$  was purchased from Pred Materials, and ammonium niobium oxalate was obtained from HC Stark. Using these commercially available sources,  $\text{NbPMo}_{11}\text{Vpyr}$  was also prepared. Ammonium niobium oxalate (0.508 g) was dissolved in 4.5 mL of water. The slurry was heated to  $80^\circ\text{C}$  for 2 to 4 hours and allowed to stir covered at room temperature for 48 hours until only slightly cloudy.  $\text{PMo}_{11}\text{V}$  (orange solid, 3.862 g) was dissolved in 6 mL of water to produce a clear, orange

solution. The niobium oxalate solution was added drop wise to the  $\text{PMo}_{11}\text{V}$  solution. The Nb-exchanged  $\text{PMo}_{11}\text{V}$  material, denoted  $\text{NbPMo}_{11}\text{V}$ , was heated to dryness overnight at  $80^\circ\text{C}$  to produce dark green solids. The  $\text{NbPMo}_{11}\text{V}$  (2.835 g) was crushed to a fine powder and dissolved in 17 mL of water. A solution of pyridine (0.915 g) and water (9 mL) was added slowly drop wise to the  $\text{NbPMo}_{11}\text{V}$  solution. A light green precipitate began to form as pyridine was added. The pyridine-exchanged  $\text{NbPMo}_{11}\text{V}$ , hereafter denoted  $\text{NbPMo}_{11}\text{Vpyr}$ , was heated to dryness, exposed to ambient air, overnight at  $80^\circ\text{C}$  to produce orange-green solids. The sample of  $\text{NbPMo}_{11}\text{Vpyr}$  prepared with ammonium niobium oxalate has a Nb/Keggin loading of 0.68.

### 8.2.3 Reactivity Studies

Ethane reactions were performed in two BTRS Jr. Reactors (Autoclave Engineers, see Figure 8.5 for reactor schematics and Appendix A for reactor photos), each equipped with a 1/2-inch stainless steel reactor tube. One reactor was equipped with a back pressure regulator (purchased from Tescom Corp., special order model # 44-2300) and capable of reaction at high pressures (referred to hereafter as “high pressure reactor”). The second reactor was only equipped to run at atmospheric pressure (referred to hereafter as “low pressure reactor”). It is important to note that mixtures of alkanes and oxygen may be flammable at certain compositions. Caution was taken to ensure that the gas feed compositions used in the reactions were non-flammable. A detailed discussion of the flammability range calculations for ethane is presented in Appendix B. Feed gases consisted of ethane (99.99%, Matheson), oxygen (99.5%, Air Liquide), and 5% argon in helium (99.999%, Air Liquide). Ethylene (99.5%, Matheson) was also used to replace ethane to probe the mechanism of acetic acid formation. For pressurized reactions, the

feed rates were 8: 4: 27: 10 mL/min of ethane: oxygen: helium: steam. Atmospheric reactions had feed flow rates of 16: 8: 16: 20 mL/min of the same gases.

A standard catalyst volume of 0.6 mL was used, giving a gas hourly space velocity (GHSV) of 4500 hr<sup>-1</sup> for pressurized experiments and 6000 hr<sup>-1</sup> for atmospheric experiments. The catalyst (35-60 mesh) was dispersed in 1 mL of silicon carbide (16 mesh, purchased from Abrasives Unlimited), held in place by glass wool. The catalyst was pretreated *in situ* under flowing helium (200 mL/min) to 420°C, at a heating rate of 1.3°/min, and held for 10 hours. Gas streams were controlled by mass flow controller systems (purchased from Brooks Instruments). Liquid water was fed by syringe pump into the reactant gas mixing area, which was heated to allow complete vaporization (150-170°C for reaction at atmospheric pressure, 235°C for reaction at 230 psig).

The reactor effluent was fed directly to a multi-port valve for gas sampling. The product lines from the reactor and the sample valve were heated to approximately 150°C to prevent liquid condensation. The product analysis was done by GC/MS (HP 6890N), having a capillary column (HP Plot Q). Samples were run at a temperature program of 120°C for two minutes (to allow gas sampling) and then heating to 250°C at 10°/min. A known amount of argon in the helium feed stream to the reactor (see above) was used for an internal standard.

### **8.3 Results and Discussion**

#### *8.3.1 Study of Nb<sub>0.4</sub>PMo<sub>12</sub>pyr in High Pressure Ethane Reactions*

The behavior of the ethane oxidation for NbPMo<sub>12</sub>pyr was studied under pressure, at 230 psig, having flow rates of 8: 4: 27: *x* mL/min ethane: oxygen: helium: steam, where *x* was varied from 0 to 10. At a 2:1 ethane/oxygen ratio, the maximum theoretical

conversion of ethane, assuming total selectivity to ethylene (requiring the least amount of oxygen) is 33%. With no steam added to the feed stream, ethane conversion was 15.0% (see Figure 8.6). Selectivity was mostly to  $\text{CO}_x$  (83.4%). Some ethylene ( $\text{C}_2^=$ ) was formed (12.7%), and some acetic acid (Ac) was formed (3.9%). As steam was introduced to the feed, the conversion decreased. With decreasing conversion, selectivity to ethylene and acetic acid improved. At the highest steam feed observed (10 mL/min), the ethane conversion had dropped to 6.0%, but the ethylene and acetic acid selectivities had increased to 23.2% and 12.4%, respectively. The balance of the products formed was  $\text{CO}_x$  (64.5%).

As seen from the data given in Figure 8.7, however, the changes in conversion and selectivity do not affect the space time yield (STY) of acetic acid formed (0.003 mmol acetic acid/ min/ g catalyst for both  $x = 0$  and 10 mL/min). A plot of product selectivity vs. conversion (see Figure 8.8) showed the relationship between conversion and selectivity. As conversion increased, preference for selective oxidation products (ethylene and acetic acid) decreased and total oxidation products ( $\text{CO}_x$ ) increased. These results indicate that the variation of steam feed does not alter the reactivity of the system, and the changes observed in selectivity were simply a function of changes in the conversion. The amount of steam fed thus could not be used to significantly change the acetic acid production, and there was no optimal steam feed rate observed.

The effect of reaction temperature was examined at 230 psig and flows of 8: 4: 27: 10 mL/min of ethane: oxygen: helium: steam. As seen in the data given in Table 8.3, increasing temperature increased the ethane conversion, from 0.4% at 240°C to 8.1% at 330°C. Note that the homogeneous gas phase oxidation of ethane becomes dominant

upon further increase in temperature ( $T > 350^{\circ}\text{C}$  at 230 psig). As the conversion increased, the selectivity to  $\text{CO}_x$  also increased from 18.3% to 59.5% as the temperature was increased from 240 to  $330^{\circ}\text{C}$ , respectively. The selectivity to ethylene and acetic acid was high at  $240^{\circ}\text{C}$  (59.1 and 22.6%, respectively), but dropped to 35.7 and 4.8%, respectively, at  $330^{\circ}\text{C}$ . The highest STY of ethylene produced was 0.015 mmol/min/g catalyst at  $330^{\circ}\text{C}$ . The highest STY of acetic acid produced was 0.003 mmol/min/g catalyst at  $280^{\circ}\text{C}$ .

The GHSV was decreased, by increasing catalyst amount up to 2.4 mL in 2 grams of silicon carbide, over several runs for ethane reaction at  $280^{\circ}\text{C}$ , 230 psig, and flows of 8: 4: 27: 10 mL/min ethane: oxygen: helium: steam. In general, decreasing the space velocity increased the ethane conversion, but mostly  $\text{CO}_x$  was produced (see Figure 8.9). Acetic acid and ethylene selectivity decreased as GHSV decreased. Over-oxidation to  $\text{CO}_x$  occurred due to longer residence times in the catalyst bed at lower space velocities. Thus, decreasing the space velocity from 4500 to  $1200\text{ hr}^{-1}$  dropped the ethylene STY from 0.006 to 0.002 mmol/min/g catalyst (see Figure 8.10). A similar decrease in acetic acid production, from 0.003 to  $4.9 \times 10^{-4}$  mmol/min/g catalyst was observed. At similar GHSV, except with no steam fed, the competition between conversion and selectivity was again observed (see Table 8.4). By decreasing the space velocity, total oxygen consumption was observed, but primarily to  $\text{CO}_x$  (~90%). No significant changes in the production of acetic acid could be made by space velocity adjustments.

Holles *et al.* reported that Nb- and pyridine-exchange was critical for the HPA precursor to be an active catalyst for propane oxidation and for activity at high space velocities in the butane system.<sup>1</sup> In order to test the ethane system for similar results,

samples of  $\text{PMo}_{12}$ ,  $\text{NbPMo}_{12}$ , and  $\text{PMo}_{12}\text{pyr}$  were used as catalyst precursors for reaction at  $280^\circ\text{C}$ , 230 psig, and flows of 8: 4: 27: 10 mL/min ethane: oxygen: helium: steam (see Table 8.5). Without incorporating both Nb and pyridine into the HPA precursor, ethane conversions were only 0.1%. No acetic acid was observed, and the samples produced mostly  $\text{CO}_x$  (68-85%, with the balance ethylene). It was only in a Nb- and pyridine-exchanged HPA that ethane conversion and selectivity to acetic acid was observed at elevated pressure.

### 8.3.2 *Study of $\text{Nb}_{0.4}\text{PMo}_{12}\text{pyr}$ in Atmospheric Pressure Ethane Reactions*

The ethane oxidation reaction was then examined at atmospheric pressure for  $\text{NbPMo}_{12}\text{pyr}$ , having flow rates of 16: 8: 16:  $x$  mL/min ethane: oxygen: helium: steam, where  $x$  was varied from 0 to 20. Again, 0.6 mL of catalyst was used to have a GHSV of  $6000 \text{ hr}^{-1}$ , comparable to the pressurized reactions and retaining the ethane to oxygen ratio of 2:1. Without steam, ethane conversion was 30.5%, but 65.1% of the products formed were  $\text{CO}_x$  (see Figure 8.11). The selectivity to ethylene and acetic acid was 34.4% and 0.6%, respectively. Increasing amounts of steam flow in the feed improved the selectivity to ethylene and acetic acid, by decreasing the conversion to 18.1%. The gain in acetic acid was greater; acetic acid selectivity increased to 14.0% with 20 mL/min of steam fed. The STY of acetic acid increased from 0.002 to 0.021 mmol/min/g catalyst as the steam feed increased from 0 to 20 mL/min (see Figure 8.12). However, the improvement observed still was caused by the change in conversion, as seen in the plot of selectivity vs. conversion in Figure 8.13. No optimal steam feed rate was observed at atmospheric pressure.

The effect of reaction temperature was studied at atmospheric pressure at flow rates of 16: 8: 16: 20 mL/min of ethane: oxygen: helium: steam (see Table 8.6).

Decreasing the temperature from 380 to 300°C dropped the ethane conversion from 18.1 to 3.1%. For the same temperature change, the selectivity to CO<sub>x</sub> decreased from 38.1 to 10.6%. Ethylene and acetic acid selectivity improved from 47.8 and 14.0%, respectively, at 380°C, to 57.3 and 32.1% at 300°C. However, no gain in STY of either ethylene or acetic acid was observed because of the decrease in conversion (see Figure 8.14).

It is important to note that all of the data discussed so far was measured on the high pressure reactor, regardless of the reaction pressure studied. The effect of Nb and pyridine on catalyst performance at atmospheric pressure was studied on the low pressure reactor system. In order to properly compare results between the two different reactor systems, a duplicate reaction of NbPMo<sub>12</sub>pyr at 380°C, 0 psig and flows of 16: 8: 16: 20 mL/min ethane: oxygen: helium: steam was performed to compare with the results obtained using the high pressure reactor (see Table 8.7). The ethane conversion was only slightly lower between the two reactors (18.1 and 15.3% conversion on the high and low pressure system, respectively). Product selectivity, however, was not similar in the two systems. More CO<sub>x</sub> was observed in the low pressure reactor (57.1% vs. 38.1%) than on the high pressure reactor. As a result, less ethylene was observed (39.1% vs. 47.8%). The ethylene STY was only 0.050 mmol/min/g catalyst on the low pressure reactor, compared to 0.072 mmol/min/g catalyst.

The most striking difference between the reactor systems was the change in acetic acid observed. The production of acetic acid dropped an order of magnitude in the low pressure reactor. On the high pressure reactor, 14.0% selectivity to acetic acid was

observed; at the same conditions on the low pressure reactor, only 3.8% selectivity to acetic acid was found. This change was reflected in the drop in STY of acetic acid. The low pressure reactor measured only 0.005 mmol/min/g catalyst, instead of the 0.021 mmol/min/g catalyst found by the high pressure reactor.

Various possibilities were explored to explain these observations, such as GC/MS calibration, equipment contamination, hot spots in the reactor tube (see Figure A.5 in Appendix A) and catalyst source. No definitive explanation of the difference has yet been discovered, although efforts are continuing. Several differences between the two reactor configurations are being explored. On the high pressure reactor the gas feeds are mixed through a set of mixing coils contained within the heated reactor cabinet (see Figure 8.5A). Liquid water is also fed into one of these coils. A gas feed (helium) sweeps through the entrance of liquid water to the mixing assembly, to assist in the evaporation and dispersal of steam. All four streams are allowed to thoroughly heat and then mix at a tee prior to the entrance of the reactor.

Water is introduced differently in the low pressure reactor (see Figure 8.5B). The three gas streams are fed into the same mixing coils inside of the heated reactor cabinet. However, the combined gas stream then *exits* the reactor cabinet to sweep through the bottom of a 3/8-inch stainless steel tube filled with glass beads and heated to 170°C. Liquid water is fed to the bottom of the bead-filled tube. The gases should sweep the water into the tube for vaporization and mixing. From the top of the mixing tube, the reactant stream is fed into the reactor tube. Dissolved catalyst has occasionally been observed in the liquid product trap during reaction studies, even at steady state. It may be that some of the water is not completely vaporized and mixed with the gas stream in the

bead-filled tube. The presence of liquid water may affect the stability of the catalyst active phase and cause deactivation, increasing the selectivity to  $\text{CO}_x$  in the low pressure reactor.

The high pressure reactor also has a multi-port valve upstream of the reactor to allow the feed stream to bypass the reactor tube. This feature enables one to begin reactant flow while using the reactor bypass to allow time for the gas streams (especially the steam) to start up without entering the catalyst bed. The streams can then be sent into the reactor tube after coming to steady state. The low pressure reactor does not currently have this feature, and the reactant stream must go directly into the reactor tube during feed startup. Combined with the possible inefficiency of the bead-filled mixing tube for the water vaporization, it is likely that incomplete water vaporization, especially during reactor startup, causes catalyst deactivation. Because of the inconsistency in feed configuration between the two reactors, some of the reaction data presented can only be used for identifying trends in catalyst activity. The product selectivity distribution and STY of products will be discussed, but conclusions should be made with caution.

The oxidation reaction was performed at  $280^\circ\text{C}$  and 0 psig (on the low pressure reactor) at flow rates of 8: 4: 25: 10 mL/min in order to compare to the results at elevated pressure on the high pressure reactor (see Table 8.7). Changing the pressure from atmospheric to 230 psig at  $280^\circ\text{C}$  increased the ethane conversion from 2.0% to 6.0%. The selectivity to  $\text{CO}_x$  increased from 24.8 to 64.5%, while the ethylene selectivity decreased from 61.6% to 23.2%. Acetic acid selectivity remained about the same (compare 13.5% and 12.4%). Ethylene STY was the same at both pressures, 0.006 mmol/min/g catalyst. Acetic acid production was slightly improved under pressure at

0.003 mmol/min/g catalyst, instead of 0.001. It may be that the advantage of performing the ethane oxidation at atmospheric pressure is in part that higher reaction temperatures could be achieved without the homogeneous gas phase reaction becoming dominant. However, because the 280°C and 0 psig experiment was done on the low pressure reactor, which appeared to have artificially low selectivities to ethylene and acetic acid, the STYs of ethylene and acetic acid may be lower than what would have been obtained on the high pressure reactor configuration at atmospheric pressure and 280°C. This should be investigated to see if atmospheric pressure reactions are in fact more selective to acetic acid than at elevated pressure.

PMo<sub>12</sub>, NbPMo<sub>12</sub>, and PMo<sub>12</sub>pyr were used as catalyst precursors for reaction at 380°C, 0 psig, and flows of 16: 8: 16: 20 mL/min ethane: oxygen: helium: steam on the low pressure reactor (see Table 8.8). Little ethane conversion was noted in the PMo<sub>12</sub>, NbPMo<sub>12</sub>, and PMo<sub>12</sub>pyr samples (0.1 to 0.6%). No acetic acid was formed for PMo<sub>12</sub> and PMo<sub>12</sub>pyr at atmospheric pressure, as seen under pressurized conditions (see Table 8.5). This is different than the results reported by Ueda and co-workers, who found some acetic acid formed with PMo<sub>12</sub>pyr at atmospheric pressure (10% selectivity at 1% ethane conversion).<sup>5</sup> This discrepancy could be due to differences in catalyst performance on the low pressure reactor, which has consistently reported lower acetic acid production than expected. PMo<sub>12</sub> produced only CO<sub>x</sub> as products. NbPMo<sub>12</sub> did have 8.2% selectivity to acetic acid and 52.8% to ethylene (the balance was CO<sub>x</sub>), which was not observed in the pressurized runs. The formation of an active catalyst for ethane oxidation at atmospheric pressure required the combination of both Nb and pyridine in the exchanged HPA precursor.

Because the presence of Nb was found to be critical in the precursor HPA, the effect of Nb loading per Keggin unit was examined at 380°C, 0 psig, and flows of 16: 8: 16: 20 mL/min. The study of Nb loading in NbPMo<sub>12</sub>pyr samples was performed entirely on the low pressure reactor. As seen in Table 8.8, ethane conversion was only 0.6% for PMo<sub>12</sub>pyr (Nb/Keggin ratio = 0). No acetic acid was formed, and selectivity to CO<sub>x</sub> was 69.5%. The addition of a small amount of Nb (0.04 Nb/Keggin) did not affect the ethane conversion significantly (0.9%). The product selectivity was altered (see Figure 8.15). The selectivity to CO<sub>x</sub> dropped to 37.5% as ethylene selectivity increased to 55.5%. Acetic acid was also observed, at 7.1% selectivity. For Nb/Keggin of 0.2, CO<sub>x</sub> selectivity continued to drop (34.2%) and ethylene increased (61.1%), but selectivity to acetic acid decreased (4.6%). The ethane conversion continued to improve as a function of Nb/Keggin loading, until a maximum at Nb/Keggin = 0.4 (15.3%). The conversion gradually then decreased with increased Nb/Keggin ratio. Ethylene selectivity, after dropping at Nb/Keggin of 0.4, continued to increase up to Nb/Keggin of 1.0. The STY of ethylene increased as a function of Nb loading, up to a maximum of 0.092 mmol/min/g catalyst at a loading of 0.8 (see Figure 8.16). Acetic acid STY was greater for the higher Nb loadings, having a maximum of 0.007 mmol/min/g catalyst at Nb/Keggin of 0.8 and 1.0. Selectivity vs. conversion, in Figure 8.17, exhibited competition between conversion and selectivity to ethylene and acetic acid. The effect of conversion on acetic acid was less for the Nb loading series than for variations in other reaction parameters (e.g., steam feeds) on the high pressure reactor. The issues with the low pressure reactor performance may be dampening out effects of Nb content on product selectivity. It would be beneficial to further examine the effect of Nb loading on NbPMo<sub>12</sub>pyr.

### 8.3.3 Study of $Nb_{0.68}PMo_{11}Vpyr$ in Ethane Reactions

Holles *et al.* found that the incorporation of vanadium into the Keggin HPA precursor was essential for selectivity in propane oxidation to acrylic acid.<sup>1</sup>  $NbPMo_{11}Vpyr$  was prepared (by Holles and co-workers, as described previously) and used in ethane reactions, both at atmospheric pressure and at elevated pressure. Experiments were first conducted on the high pressure reactor system.  $NbPMo_{11}Vpyr$  was studied at 280°C and 230 psig, with flows of 8: 4: 27: 10 mL/min of ethane: oxygen: helium: steam (see line 4 of Table 8.9). Under pressure 2.2% of ethane was converted by  $NbPMo_{11}Vpyr$ . The conversion for  $NbPMo_{11}Vpyr$  was less than that obtained under the same conditions (on the same reactor) for  $NbPMo_{12}pyr$ , at 6.0% (see line 4 of Table 8.7). The vanadium-substituted catalyst had lower selectivity to  $CO_x$  (40.3% instead of 64.5% for  $NbPMo_{12}pyr$ ). This resulted in a higher selectivity to ethylene for  $NbPMo_{11}Vpyr$  (46.8% instead of 23.2% for  $NbPMo_{12}pyr$ ). No change was observed in acetic acid selectivity (13.0% for  $NbPMo_{11}Vpyr$  and 12.4% for  $NbPMo_{12}pyr$ ). STY of ethylene was higher for the vanadium-substituted catalyst at 0.008 mmol/min/g catalyst, instead of 0.006, due to improved selectivity. STY of acetic acid was slightly lower for  $NbPMo_{11}Vpyr$  at 0.002 mmol/min/g catalyst, instead of 0.003, because of lower conversion. At elevated pressure the addition of vanadium into the Keggin precursor primarily improved selectivity to ethylene over  $CO_x$ , but did not affect the formation of acetic acid.

$NbPMo_{11}Vpyr$  was also run at atmospheric pressure (on the high pressure reactor system) and 380°C, with flows of 16: 8: 16: 20 mL/min ethane: oxygen: helium: steam and a GHSV of 6000 hr<sup>-1</sup>. An ethane conversion of 15.5% was observed (see Table 8.9,

line 1) and 31.0% selectivity to acetic acid. Note that the NbPMo<sub>12</sub>pyr, under the same conditions on the high pressure reactor, had only 14.0% selectivity to acetic acid at 18.1% ethane conversion (compare line 1 of Table 8.9 with line 1 of Table 8.7). The STY of acetic acid was increased from 0.021 (for NbPMo<sub>12</sub>pyr) to 0.062 mmol/min/g catalyst for NbPMo<sub>11</sub>Vpyr. The addition of vanadium into the Keggin precursor had a favorable affect on the acetic acid formation at atmospheric pressure, although not as significant as that observed in propane (only CO<sub>x</sub> was formed from propane in the absence of vanadium). NbPMo<sub>12</sub>pyr had higher selectivity to both CO<sub>x</sub> (38.1%) and ethylene (47.8%). NbPMo<sub>11</sub>Vpyr had selectivity to CO<sub>x</sub> of 32.7% and to ethylene of 36.2%, because of the increased formation of acetic acid.

When measurement inconsistencies were found using NbPMo<sub>12</sub>pyr at atmospheric pressure on the low pressure reactor compared to the high pressure reactor (comparing lines 1 and 2 on Table 8.7, as discussed previously), repeat studies of the NbPMo<sub>11</sub>Vpyr reactivity at atmospheric pressure on the low pressure reactor was done. Comparing lines 1 and 2 on Table 8.9, a decrease in the conversion was observed on the low pressure reactor (9.4%) from the high pressure reactor (15.5%). Note that line 2 of Table 8.9 was done with only 0.3 mL of catalyst. Flows were adjusted accordingly to maintain the same GHSV. A greater selectivity to CO<sub>x</sub> was observed on the low pressure reactor, as seen with NbPMo<sub>12</sub>pyr, (46.0 instead of 32.7%). More ethylene was observed for NbPMo<sub>11</sub>Vpyr on the low pressure reactor (49.0% instead of 36.2%), reflected in the significantly decreased formation of acetic acid (5.0% instead of 31.0%). The decrease in acetic acid was observed for NbPMo<sub>12</sub>pyr also when comparing the low pressure reactor with the high pressure reactor, although the conversion difference was less (18.1% on the

high pressure reactor vs. 15.3% on the low pressure reactor for NbPMo<sub>12</sub>pyr). The decrease in acetic acid selectivity was reflected in an order of magnitude lower STY of acetic acid on the low pressure reactor, 0.006 mmol/min/g catalyst, instead of 0.062.

The two catalysts, NbPMo<sub>12</sub>pyr and NbPMo<sub>11</sub>Vpyr, should also be compared at atmospheric pressure using the data from the low pressure reactor (compare line 2 from Table 8.7 with line 2 from Table 8.9). On the low pressure reactor, NbPMo<sub>11</sub>Vpyr still had reduced ethane conversion than NbPMo<sub>12</sub>pyr (9.4% compared to 15.3%). The selectivity to CO<sub>x</sub> was also reduced in the vanadium-substituted sample (46.0% vs. 57.1%). More ethylene was observed for NbPMo<sub>11</sub>Vpyr (49.0%) than in NbPMo<sub>12</sub>pyr (39.1%), unlike the high pressure reactor, where the ethylene selectivity dropped from 47.8% to 36.2% with the addition of vanadium. The selectivity to acetic acid still increased in NbPMo<sub>11</sub>Vpyr tested on the low pressure reactor (5.0% compared to 3.4% for NbPMo<sub>12</sub>pyr), but not as significantly. Thus, the acetic acid STY increased slightly for NbPMo<sub>11</sub>Vpyr to 0.006 mmol/min/g catalyst from 0.004 with NbPMo<sub>12</sub>pyr. It is speculated that some factor inherently different in the design of the two reactors is responsible for the inconsistency in performance for the same catalyst at the same conditions. This difference resulted in decreased catalyst activity (conversion) and increased CO<sub>x</sub> formation by over-oxidation of the acetic acid (and some ethylene) formed. Feeding an acetic acid solution into the reactor tube containing silicon carbide, at reaction conditions (380°C, 16: 8: 16: 20 mL/min ethane: oxygen: helium: steam, where the steam is from a dilute aqueous acetic acid solution of known concentration) showed that no contamination or hot-spot in the reactor tube was causing the acetic acid to over-oxidize to CO<sub>x</sub> in the absence of a catalyst.

To compare the difference between atmospheric pressure and elevated pressure for NbPMo<sub>11</sub>Vpyr, ethane reaction was done on the low pressure reactor at 280°C and atmospheric pressure (compare lines 3 and 4 on Table 8.9). Note that the 230 psig experiment was performed on the high pressure reactor. The ethane conversion increased slightly, from 1.1 to 2.2% as the pressure was increased from 0 to 230 psig at 280°C. Selectivity to CO<sub>x</sub> increased from 29.9 to 40.3% with increased pressure. Ethylene and acetic acid selectivity both decreased with increased pressure, from 51.3 and 18.7%, respectively, to 46.8 and 13.0%, respectively. The STY of ethylene and acetic acid were slightly higher under pressure, at 0.008 and 0.002 mmol/min/g catalyst, respectively, because of higher conversion.

The effect of Nb loading in vanadium-containing catalysts was examined on the low pressure reactor, at 380°C and atmospheric pressure (see Figure 8.18). The catalyst loading was 0.3 mL, so reduced flow rates of 8: 4: 8: 10 mL/min of ethane: oxygen: helium: steam were used to maintain the same GHSV. Note that the catalyst samples used were exchanged by Holles and co-workers using PMo<sub>11</sub>V prepared by Holles and NbCl<sub>5</sub>. No PMo<sub>11</sub>Vpyr sample, Nb/Keggin = 0, was available from those preparations for comparison. Results from PMo<sub>12</sub>pyr and extrapolation from Figure 8.18 suggest that a PMo<sub>11</sub>Vpyr sample would have little activity. At a Nb/Keggin loading of 0.04, only 1.0% ethane was converted. The conversion increased with increasing Nb loading, to 9.4% at Nb/Keggin = 0.68. (Note that this was the same sample loading that produced 15.5% conversion at these conditions in the high pressure reactor.) Further increases of Nb past 0.68 resulted in a decrease in conversion. In the range of Nb/Keggin of 0.12 to 0.87, product distribution remained constant, regardless of conversion, at approximately

45% CO<sub>x</sub>, 49% ethylene, and 6% acetic acid. The 0.04 and 0.97 samples both showed increased selectivity to ethylene and decreased amounts of CO<sub>x</sub> and acetic acid. In spite of the similar selectivities, changes in conversion due to Nb loadings greatly affected the STY of ethylene and slightly increased the STY to acetic acid (see Figure 8.19). The maximum in both was observed at a Nb/Keggin of 0.87, with STYs of 0.086 and 0.009 mmol/min/g catalyst of ethylene and acetic acid, respectively. This was the highest STY of acetic acid measured on the low pressure reactor. This suggests that out of all the various parameters and catalyst compositions studied, Nb<sub>0.87</sub>PMo<sub>11</sub>Vpyr should have the highest production of acetic acid. The changes in selectivity as a function of conversion (Figure 8.20) were less dominant in the NbPMo<sub>11</sub>Vpyr series than in the NbPMo<sub>12</sub>pyr series (Figure 8.17).

One may obtain PMo<sub>11</sub>V and ammonium niobium oxalate from commercial sources instead of preparing the Keggin synthetically and using NbCl<sub>5</sub> as a precursor to niobium oxalate. Reactivity differences between the sample prepared by Holles and one prepared from commercial sources (both at Nb/Keggin = 0.68), were examined at atmospheric pressure on the low pressure reactor (see Table 8.10). The product selectivity of the two samples was similar, at 46% CO<sub>x</sub>, 50% ethylene, and 4% acetic acid. The conversion was higher for the catalyst prepared from commercial sources than the Holles material (15.7% vs. 9.4%) on the low pressure reactor. Because of the higher conversion, STYs of ethylene and acetic acid were higher with the sample from commercial sources, 0.101 and 0.008 mmol/min/g catalyst, respectively. Because the Holles material performed better when measured on the high pressure reactor (15.5% conversion), it would be desirable to measure the performance of the sample prepared

from commercial sources under the same reactor configuration, preferably at a Nb/Keggin loading of about 0.87. Efforts are underway to change the configuration in the low pressure reactor to be the same as the design of the high pressure reactor.

#### 8.3.4 *Study of Nb<sub>0.4</sub>PMo<sub>12</sub>pyr Reactivity at Other Flow Compositions*

Because not all of the oxygen was being utilized in the ethane oxidation, the ethane/oxygen ratio was increased from 2:1 (see Table 8.11). At a ratio of 3:1, the ethane and oxygen conversions over NbPMo<sub>12</sub>pyr decreased, from 15.3 to 6.4% and 47.7 to 36.8%, respectively (compare lines 1 and 2). The selectivity to acetic acid did increase to 7.3% from 3.8%, but this could simply be a conversion effect. No change in the STY of acetic acid was observed. At a ratio of 4:1, however the ethane conversion was 12.9%, having 77.2% oxygen conversion. Selectivity to acetic acid was 5.6%. The acetic acid STY was 0.008 mmol/min/g catalyst (compared to 0.005 for 2:1 ethane/oxygen ratio), suggesting that it may be possible to continue to increase acetic acid production by increasing the ethane/oxygen ratio even further. Similar work should be done with the Nb<sub>0.87</sub>PMo<sub>11</sub>Vpyr, preferably made with commercial materials.

#### 8.3.5 *Ethane Reactivity with Metals Other Than Nb*

Holles and co-workers exchanged other metal cations with pyridine into the PMo<sub>12</sub> Keggin to determine if other metals had similar activity and selectivities in butane oxidation.<sup>1</sup> Although some metals (e.g., Ti and Mo) possessed activity in the butane oxidation to maleic acid, none performed as well as Nb. HPAs exchanged with other metals known to be active for ethane oxidation (Ta, Sb, and Zr) were also used as catalyst precursors in ethane oxidation. Catalyst precursors prepared by Holles and co-workers were measured for activity in the low pressure reactor, at 380°C and 0 psig, for flow rates

of 16: 8: 16: 20 mL/min ethane: oxygen: helium: steam. As seen in Table 8.12, some acetic acid was observed with each of the catalysts, but none of the other metals attempted (Ta, Sb, Zr, and Ti) had significant conversions of ethane (<2%). The butane system examined by Holles *et al.* exhibited more versatility with metal exchange than ethane. Nb has a special role in the formation of an active catalyst during pretreatment that cannot be duplicated for ethane oxidation.

### 8.3.6 Study of Ethylene Reactions with $Nb_{0.4}PMo_{12}pyr$

In order to probe the mechanism of formation of acetic acid from ethane, ethylene was used as a reactant feed.  $NbPMo_{12}pyr$  was studied at 0 psig, at a range of temperatures, using 16: 8: 16: 20 mL/min of ethylene: oxygen: helium: steam as the feed mixture (see Table 8.13). At 380°C all of the oxygen was consumed, with an ethylene conversion of 28.0%.  $CO_x$  was the major product, at 76.7% selectivity, but acetic acid was also formed at 17.0% selectivity. Other products observed included acetaldehyde (AcAld, 0.58%), ethanol (EtOH, 0.04%), methyl acetate (MeAc, 0.02%), ethyl acetate (EtAc, 0.03%), acetone (0.17%), propanoic acid (0.05%), acrylic acid (3.7%), and maleic acid (1.7%).

Decreasing the temperature decreased the conversion and  $CO_x$  formation. At 240°C (note:  $D_2O$  was fed as the source of steam) ethane conversion was 1.8%.  $CO_x$  selectivity decreased to 64.5%. Acetic acid selectivity increased to 30.4%. The selectivity of acetaldehyde, ethanol, methyl acetate, and ethyl acetate all increased as the temperature decreased (to 1.1, 2.5, 0.31, and 1.1%, respectively, at 240°C). No acetone, propanoic acid, acrylic acid or maleic acid was observed at 240°C. This suggests that an ethoxy or acetate species might be involved in the formation of acetic acid from ethylene.

Tessier and Merzouki found acetic acid production to be dominant at low temperatures (250-300°C) and ethylene production dominant at higher temperatures, suggesting two different reaction pathways.<sup>6,7</sup> Addition of steam improves the transformation of the adsorbed ethoxy species to acetic acid and then assists in the desorption.<sup>8</sup> Acetic acid formation is a balance between the selectivity at low conversion (low temperatures) and the desorption of the products from the surface (high temperatures). The selectivity to what may be primary products of ethane oxidation may be artificially low because the ethylene studies were done on the low pressure reactor. Further examination should be done on the mechanism of acetic acid formation from ethylene.

D<sub>2</sub>O was used as the source of steam for the 240°C reaction in order to probe the effect of water on acetic acid formation from ethylene. Mass spectroscopy was used to quantify the amount of deuterium substitution of the acetic acid observed. A distribution of d<sub>0</sub>, d<sub>1</sub>, d<sub>2</sub>, and d<sub>3</sub> substitution was calculated by extraction of m/z = 60, 61, 62, and 63. The peak areas were integrated, giving substitution of 0.9% (d<sub>0</sub>), 7.3% (d<sub>1</sub>), 32.1% (d<sub>2</sub>), and 59.6% (d<sub>3</sub>), respectively. Clearly, the D<sub>2</sub>O in the gas feed was involved in the formation of acetic acid. The low amount of d<sub>0</sub>-acetic acid was likely due to the formation of H<sub>2</sub>O as a result of ethane oxidation.

D<sub>2</sub>O was eliminated from the feed to see if the removal of steam resulted in the increase of total oxidation products, CO<sub>x</sub>. CO<sub>x</sub> did increase, but less than expected. Ethylene conversion was similar to that with steam (1.7%), but there was a slight increase in CO<sub>x</sub> production (71.9%). Deuterated acetic acid and liquid water were still observed even during the second hour after D<sub>2</sub>O removal. Selectivities of the liquid oxygenates all decreased with the removal of steam, but they were still present. It may be that some

adsorbed surface species were still being desorbed from the catalyst, but it was surprising that any desorption would be still occurring during the second hour without steam. It is possible that some D<sub>2</sub>O remained in the feed (due to poor mixing as previously discussed) even after the syringe pump was stopped that prolonged the exposure of the catalyst to D<sub>2</sub>O.

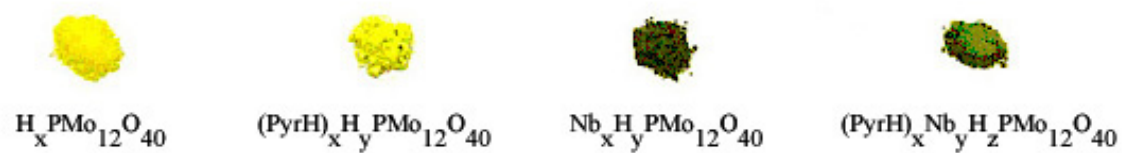
#### 8.4 References

- (1) Holles, J. H. *et al.*, *J. Catal.* **2003**, *218*, 42.
- (2) Dillon, C. J. *et al.*, *J. Catal.* **2003**, *218*, 54.
- (3) Tsigdinos, G. A.; Hallada, C. J. *Inorg. Chem.* **1968**, *7*, 437.
- (4) Davis, M. E. *et al.*, *Angew. Chem., Int. Ed.* **2002**, *41*, 858.
- (5) Li, W.; Ueda, W. *Stud. Surf. Sci. Catal.* **1997**, *110*, 433.
- (6) Tessier, L. *et al.*, *Catal. Today* **1995**, 335.
- (7) Merzouki, M. *et al.*, In *New Frontiers in Catalysis*; Guzzi, L., al., e., Eds.; Elsevier Science, 1993.
- (8) Centi, G. *et al.*, *Selective Oxidation by Heterogeneous Catalysis*; Kluwer Academic/Plenum Publishers: New York, 2001.

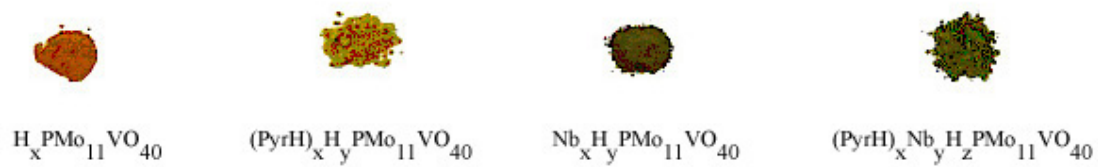
**Figure 8.1**  $\text{Nb}_x\text{PMo}_{12}\text{pyr}$ , with varying Nb/Keggin ratios.



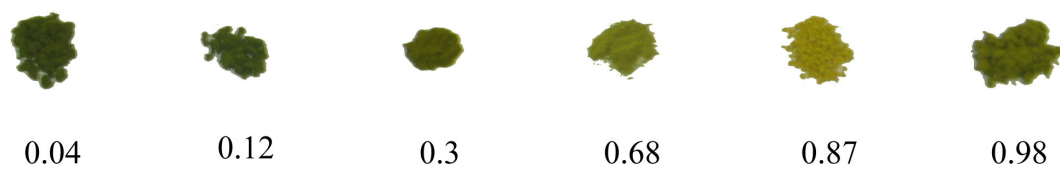
**Figure 8.2** Phosphomolybdic acid and its niobium- and pyridine-exchanged forms.



**Figure 8.3** Phosphovanadomolybdic acid and its niobium- and pyridine-exchanged forms.

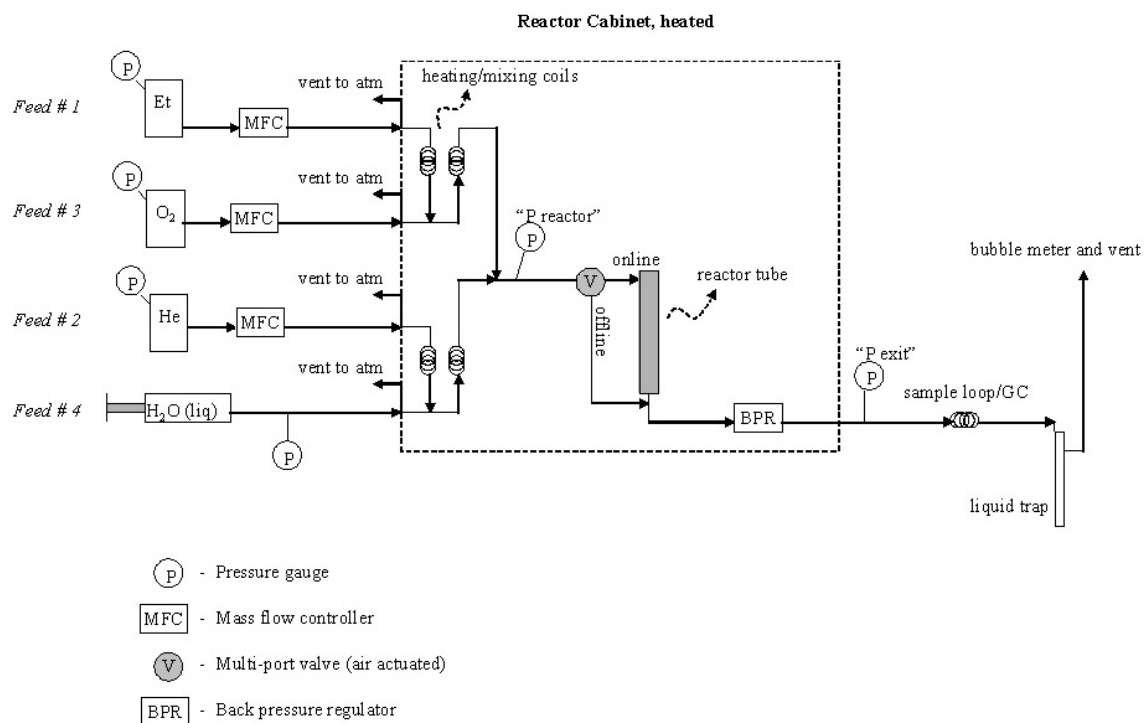


**Figure 8.4**  $\text{Nb}_x\text{PMo}_{11}\text{Vpyr}$ , with varying Nb/Keggin ratios.



**Figure 8.5** Autoclave Engineers BTRS, Jr. reactor schematics: (A) high pressure reactor system and (B) low pressure reactor system.

(A)



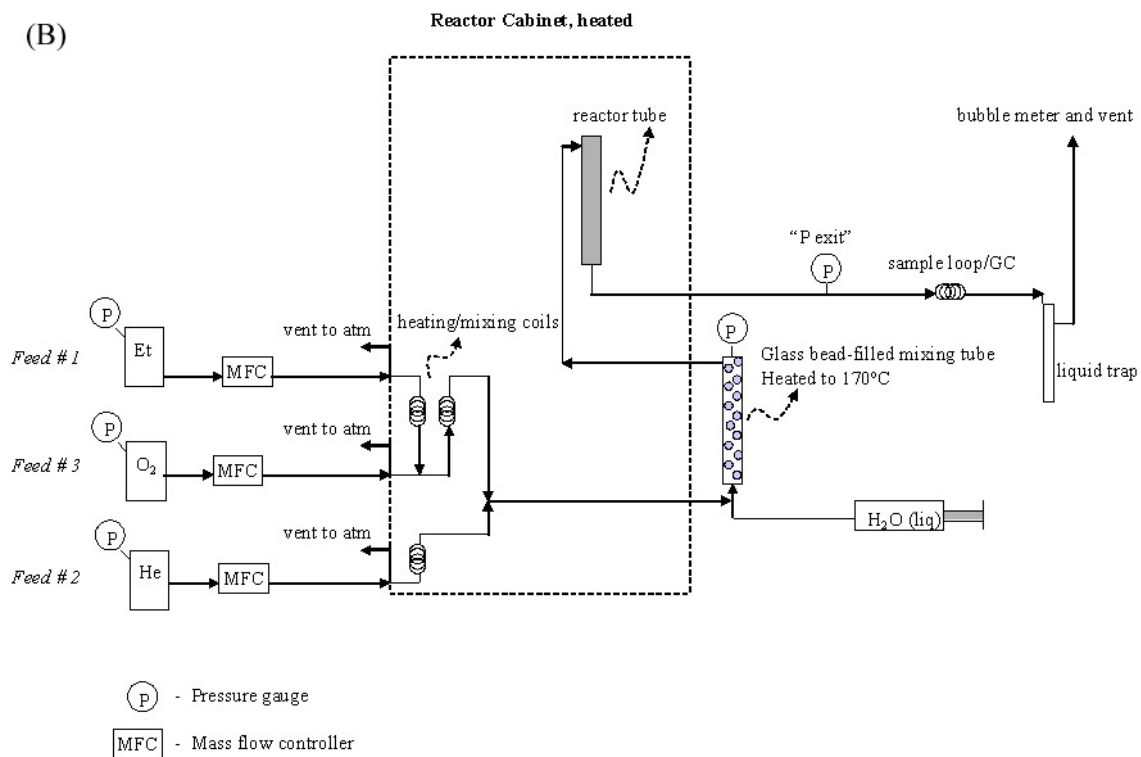


**Figure 8.6** Ethane reactivity of NbPMo<sub>12</sub>pyr at 280°C, 230 psig, 8: 4: 27: x mL/hr (ethane: oxygen: helium: steam) on high pressure reactor.

Data listed in Table C.1

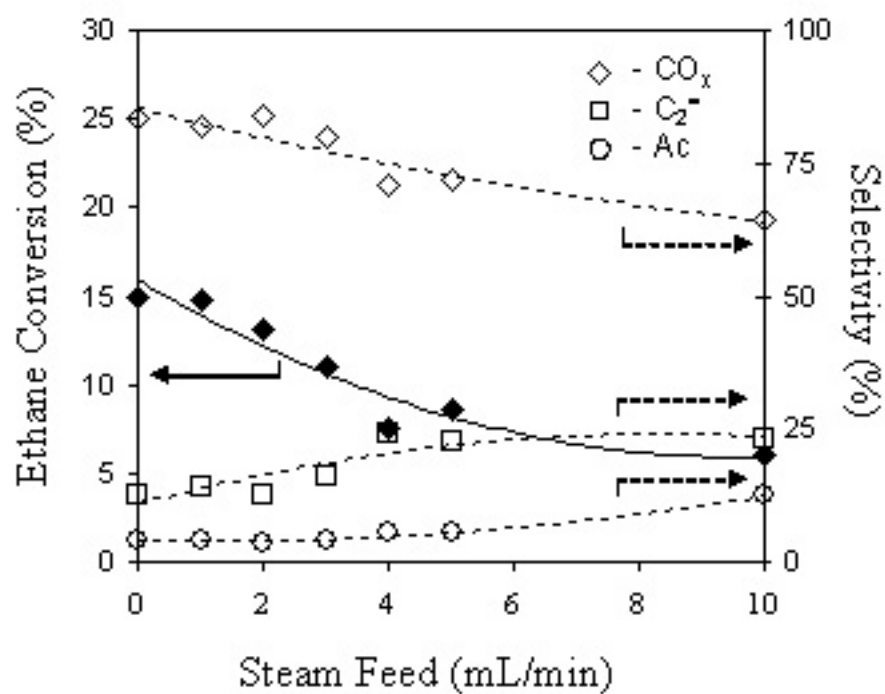


**Figure 8.7** Space time yield of products for NbPMo<sub>12</sub>pyr at 280°C, 230 psig, 8: 4: 27: x mL/hr (ethane: oxygen: helium: steam) on high pressure reactor.

Data listed in Table C.1

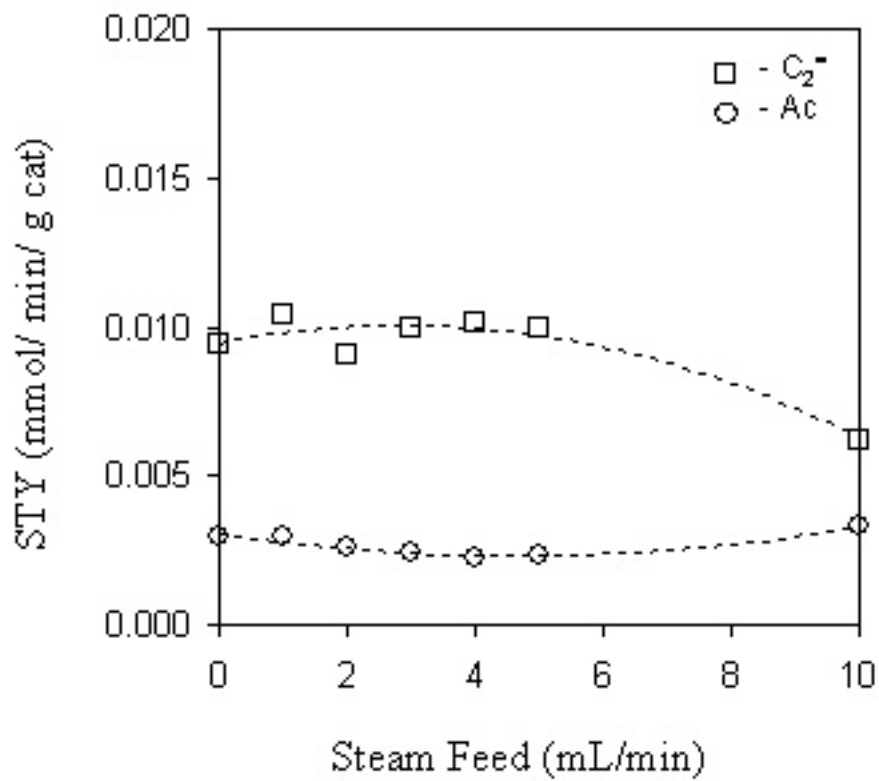


**Figure 8.8** Selectivity vs. conversion for NbPMo<sub>12</sub>pyr at 280°C, 230 psig, 8: 4: 27: x mL/hr (ethane: oxygen: helium: steam) on high pressure reactor.

Data listed in Table C.1

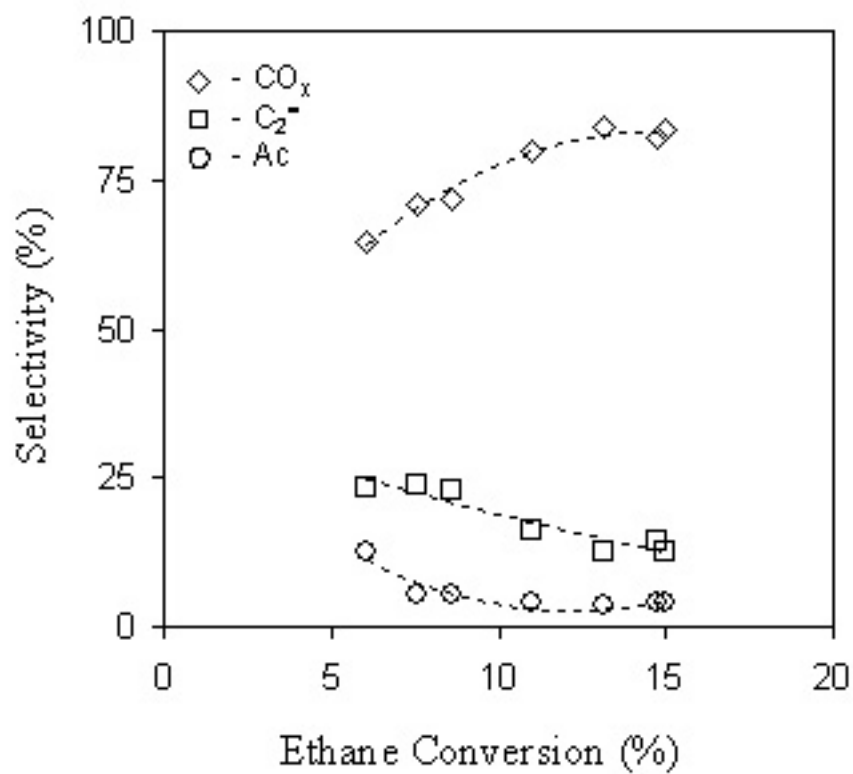


**Figure 8.9** Ethane reactivity of NbPMo<sub>12</sub>pyr at 280°C, 230 psig, 8: 4: 27: 10 mL/hr (ethane: oxygen: helium: steam) on high pressure reactor. Catalyst volume was varied.

Data listed in Table C.2

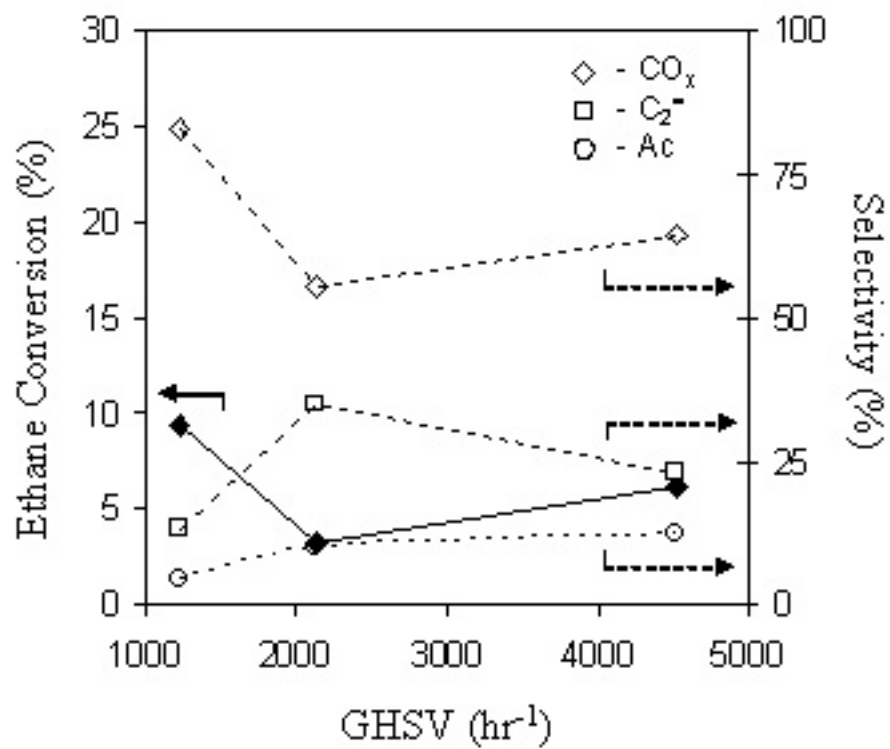


**Figure 8.10** Space time yield of products for NbPMo<sub>12</sub>pyr at 280°C, 230 psig, 8: 4: 27: 10 mL/hr (ethane: oxygen: helium: steam) on high pressure reactor. Catalyst volume was varied.

*Data listed in Table C.2*

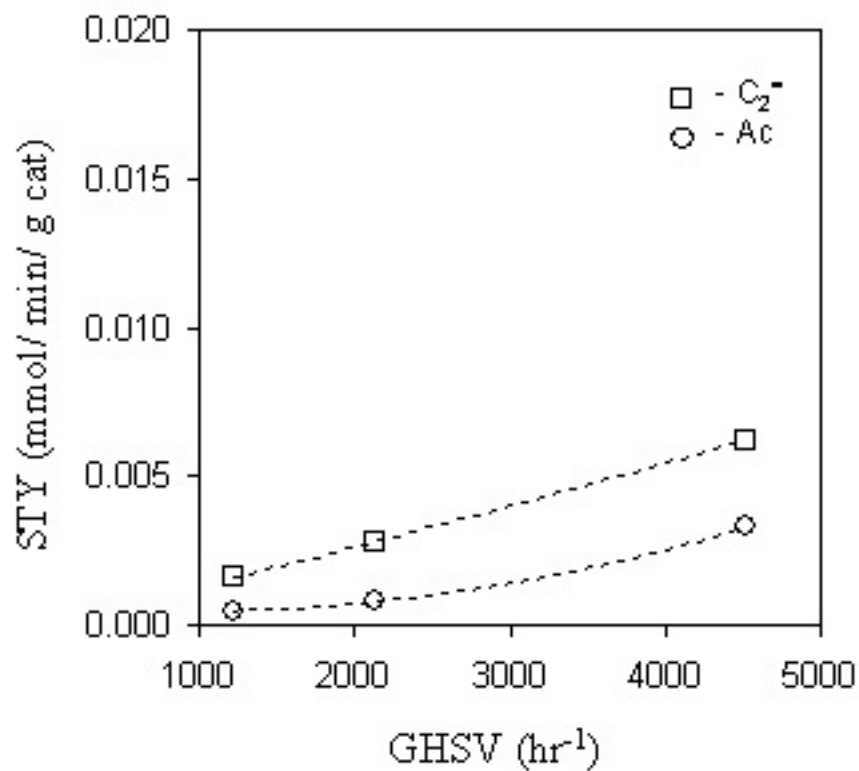


**Figure 8.11** Ethane reactivity of NbPMo<sub>12</sub>pyr at 380°C, 0 psig, 16: 8: 16: x mL/hr (ethane: oxygen: helium: steam) on high pressure reactor.

Data listed in Table C.3

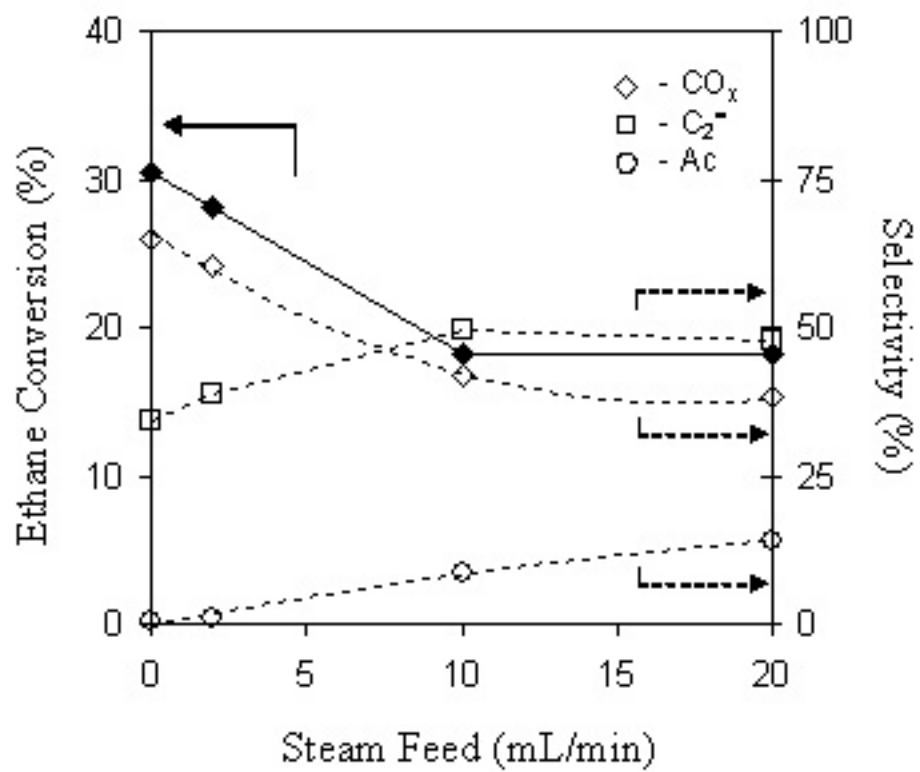


**Figure 8.12** Space time yield of products for NbPMo<sub>12</sub>pyr at 380°C, 0 psig, 16: 8: 16: x mL/hr (ethane: oxygen: helium: steam) on high pressure reactor.

*Data listed in Table C.3*

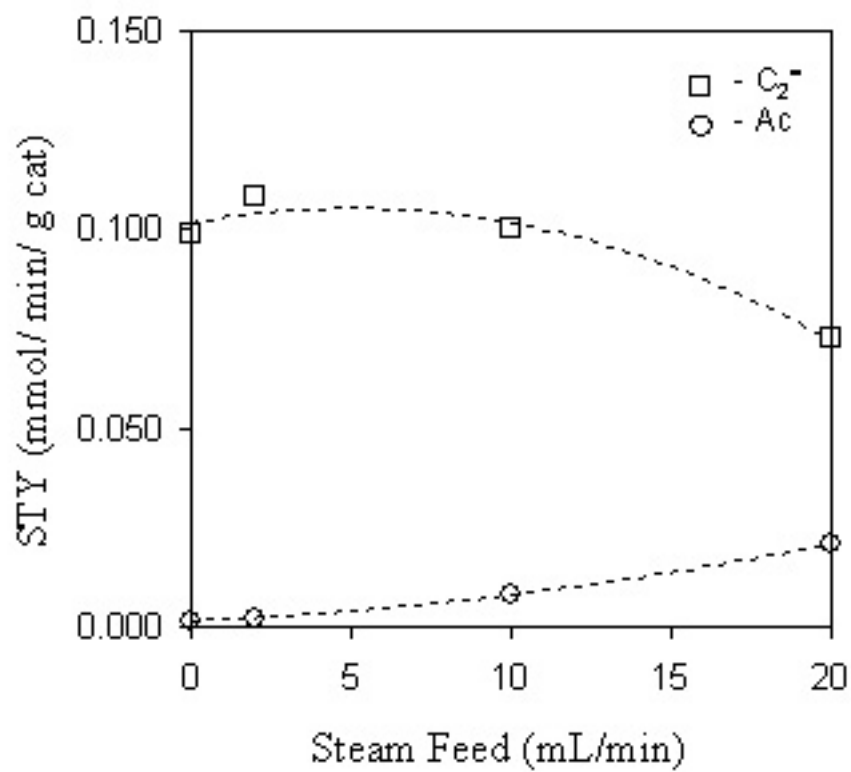


**Figure 8.13** Selectivity vs. conversion for NbPMo<sub>12</sub>pyr at 380°C, 0 psig, 16: 8: 16: x mL/hr (ethane: oxygen: helium: steam) on high pressure reactor.

Data listed in Table C.3

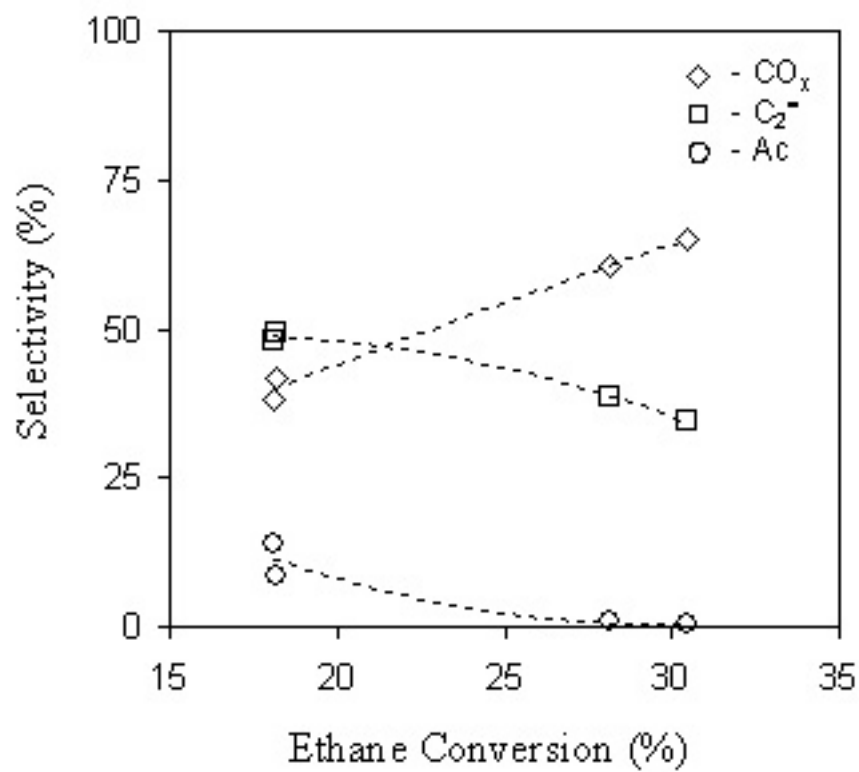


**Figure 8.14** Ethane reactivity with temperature of NbPMo<sub>12</sub>pyr at 0 psig, 16: 8: 16: 20 mL/hr (ethane: oxygen: helium: steam) on high pressure reactor, except 280°C run on low pressure reactor.

*Data listed in Table 8.6 and C.4*

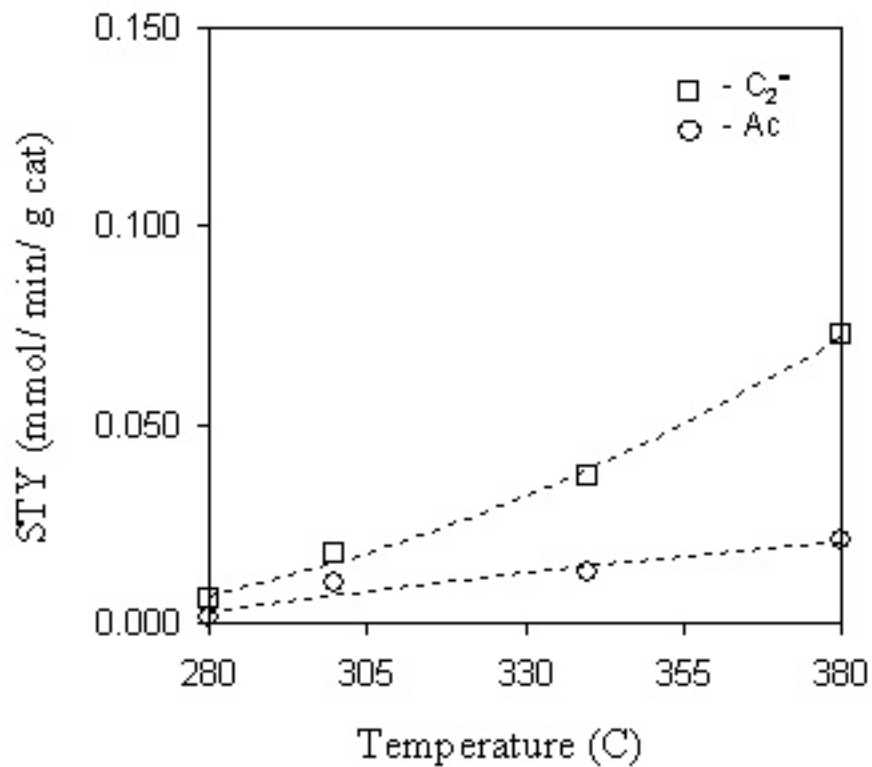


**Figure 8.15** Ethane reactivity with Nb loading of NbPMo<sub>12</sub>pyr at 380°C, 0 psig, 16: 8: 16: 20 mL/hr (ethane: oxygen: helium: steam) on low pressure reactor.

Data listed in Table C.5

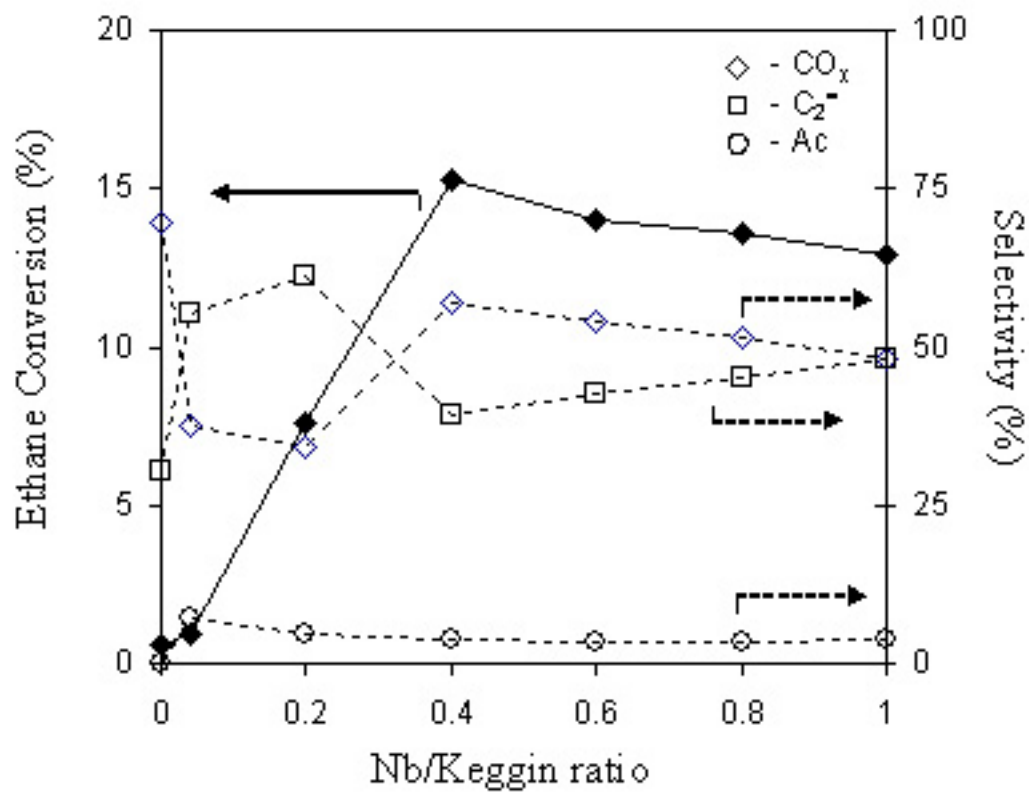


**Figure 8.16** Space time yield of products for Nb loading of NbPMo<sub>12</sub>pyr at 380°C, 0 psig, 16: 8: 16: 20 mL/hr (ethane: oxygen: helium: steam) on low pressure reactor.

Data listed in Table C.5

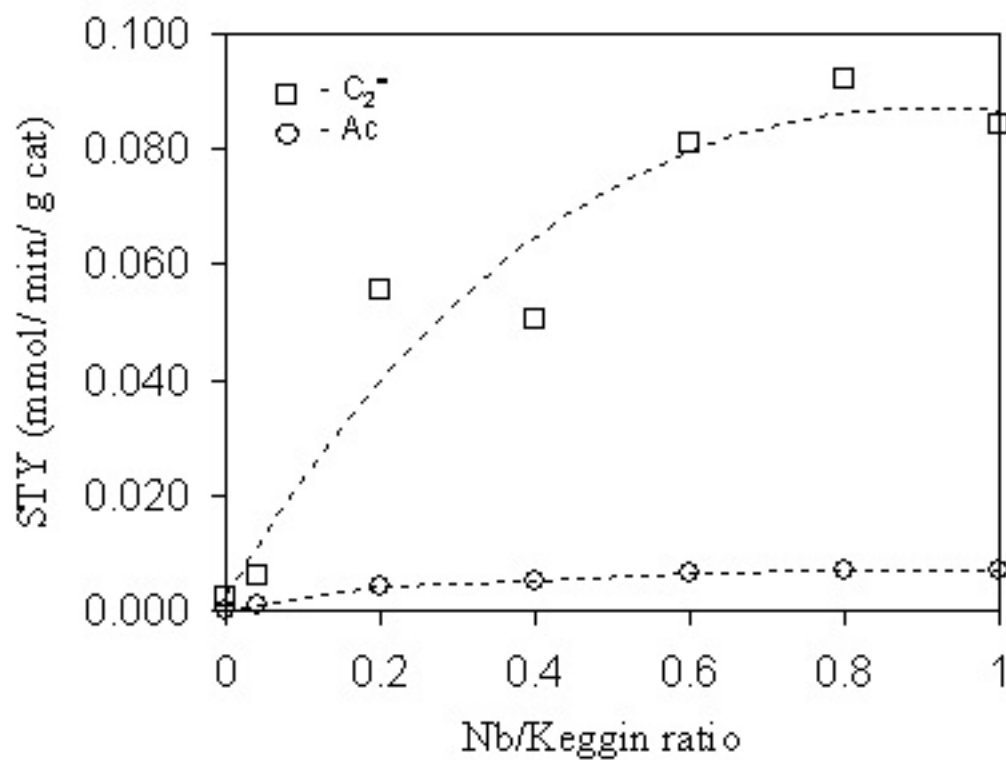


**Figure 8.17** Selectivity vs. conversion for Nb loading of NbPMo<sub>12</sub>pyr at 380°C, 0 psig, 16: 8: 16: 20 mL/hr (ethane: oxygen: helium: steam) on low pressure reactor.

Data listed in Table C.5

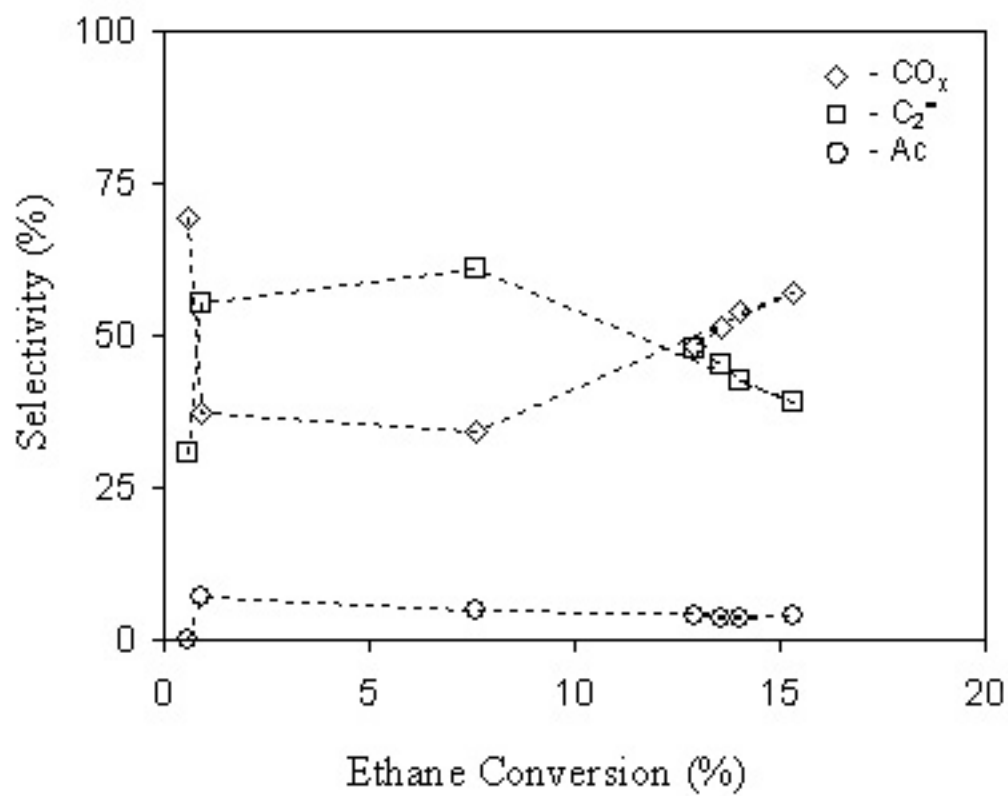


**Figure 8.18** Ethane reactivity with Nb loading of NbPMo<sub>11</sub>Vpyr at 380°C, 0 psig, 8: 4: 8: 10 mL/hr (ethane: oxygen: helium: steam) on low pressure reactor, V<sub>catalyst</sub> = 0.3 mL.

Data listed in Table C.6

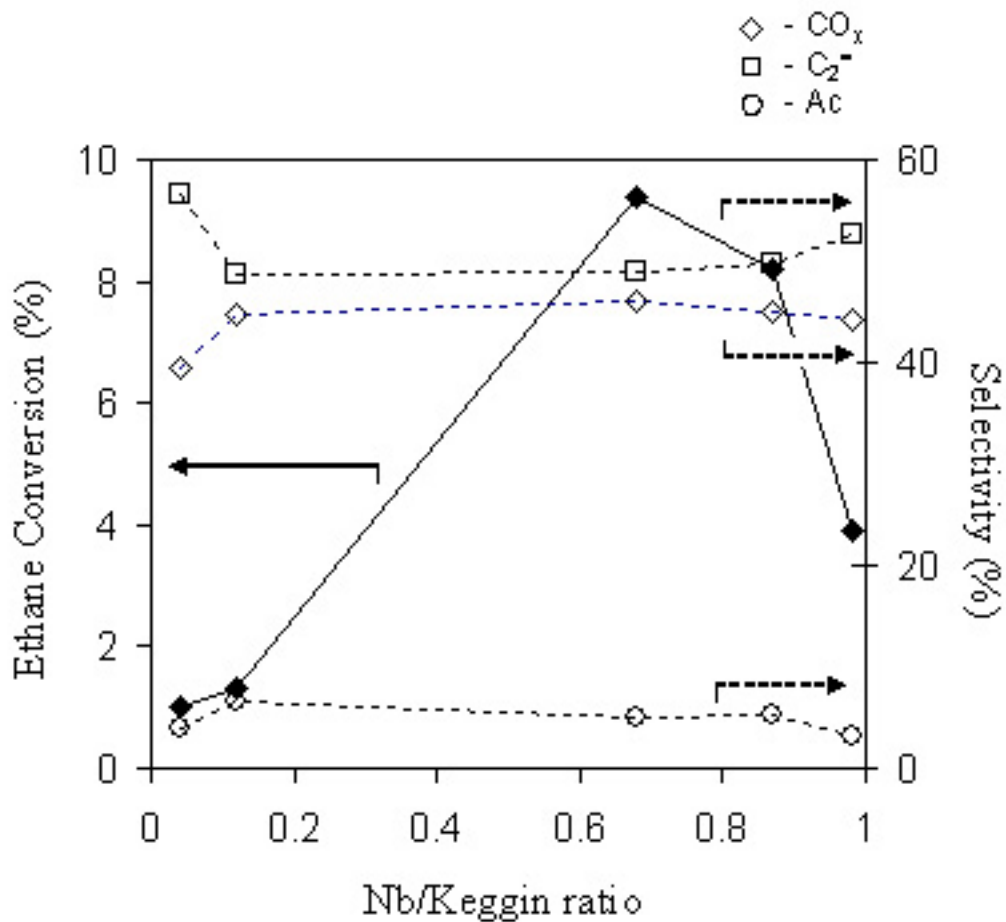


**Figure 8.19** Space time yield of products for Nb loading of NbPMo<sub>11</sub>Vpyr at 380°C, 0 psig, 8: 4: 8: 10 mL/hr (ethane: oxygen: helium: steam) on low pressure reactor, V<sub>catalyst</sub> = 0.3 mL.

Data listed in Table C.6

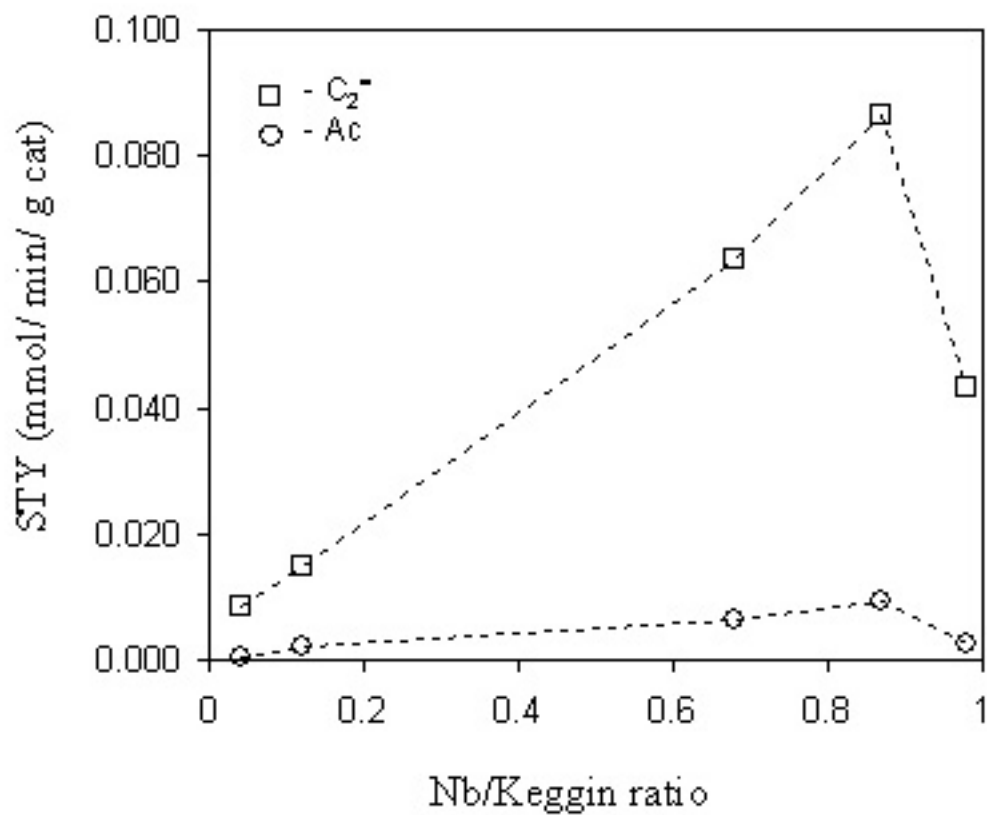


**Figure 8.20** Selectivity vs. conversion for Nb loading of NbPMo<sub>11</sub>Vpyr at 380°C, 0 psig, 8: 4: 8: 10 mL/hr (ethane: oxygen: helium: steam) on low pressure reactor, V<sub>catalyst</sub> = 0.3 mL.

Data listed in Table C.6

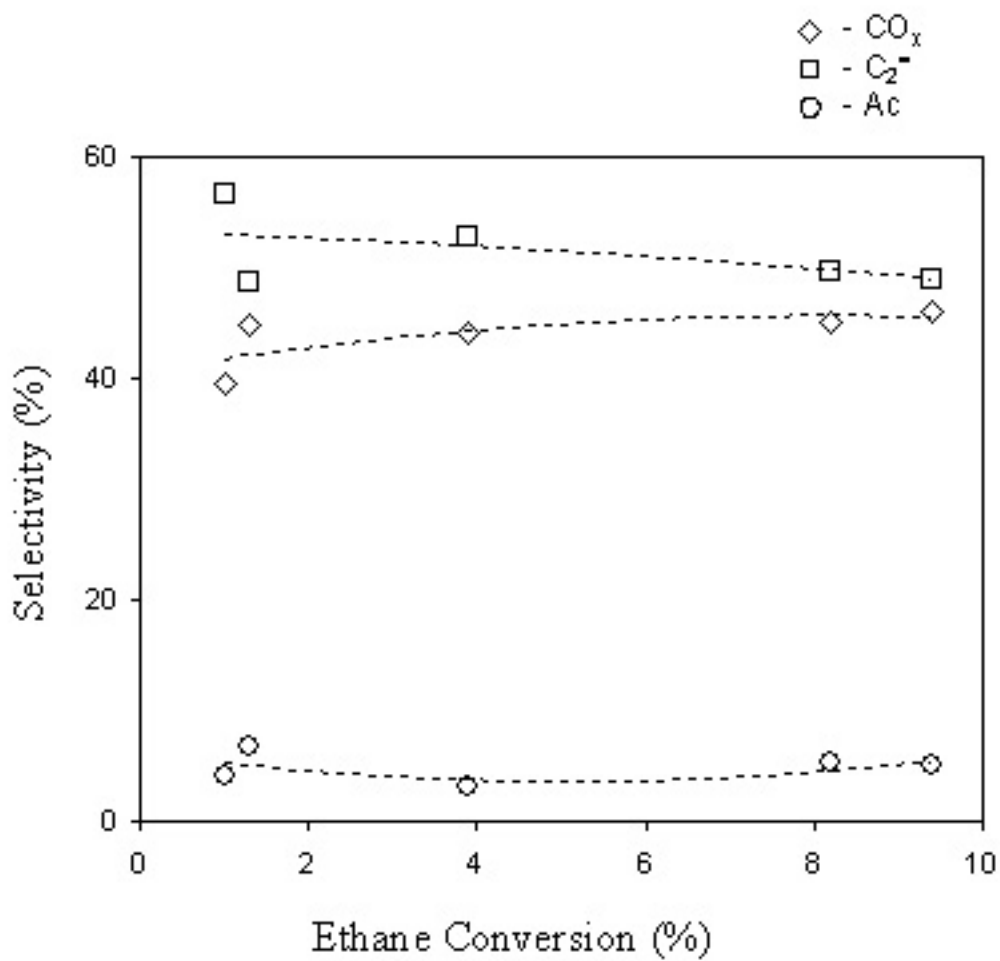


**Table 8.1** *n*-Butane reactivity at 380°C. Adapted from ref. 1.

Catalyst	Flow C <sub>4</sub> : O <sub>2</sub> : He: H <sub>2</sub> O	Conv. (%)	Selectivity <sup>a</sup>				STY <sup>b</sup>
			CO <sub>x</sub>	Ac	AA	MA	MA
PMo <sub>12</sub>	4: 2: 4: 5	0.2	64	34	2	0	0
NbPMo <sub>12</sub>	4: 2: 4: 5	3	13	7	2	70	0.017
PMo <sub>12</sub> pyr	4: 2: 4: 5	13.5	14	3	1	82	0.097
	32: 16: 32: 40	2.5	9	6	6	71	0.11
NbPMo <sub>12</sub> pyr	4: 2: 4: 5	15	25	3	1	71	0.084
	32: 16: 32: 40	15	5	3	1	90	0.84
PMo <sub>11</sub> V	4: 2: 4: 5	0.5	31	17	0	50	1.6x10 <sup>-3</sup>
NbPMo <sub>11</sub> V	4: 2: 4: 5	0.4	42	19	4	25	6.3x10 <sup>-4</sup>
PMo <sub>11</sub> Vpyr	4: 2: 4: 5	13.5	5	3	1	90	0.11
NbPMo <sub>11</sub> Vpyr	4: 2: 4: 5	15	16	5	2	76	0.090
	32: 16: 32: 40	14	9	5	3	80	0.76

<sup>a</sup>Ac = acetic acid; AA = acrylic acid; MA = maleic acid

<sup>b</sup>STY is in mmol/min/g catalyst

**Table 8.2** Propane reactivity at 380°C. Adapted from ref. 1.

Catalyst	Flow C <sub>3</sub> : O <sub>2</sub> : He: H <sub>2</sub> O	Conv. (%)	Selectivity <sup>a</sup>					STY <sup>b</sup>
			CO <sub>x</sub>	C <sub>3</sub> <sup>=</sup>	Ac	AA	MA	AA
PMo <sub>11</sub> V	8: 4: 8: 10	0.4	30	54	4	0	0	0
NbPMo <sub>11</sub> V	8: 4: 8: 10	1.4	22	44	16	10	0	1.4x10 <sup>-3</sup>
PMo <sub>11</sub> Vpyr	8: 4: 8: 10	3.4	10	37	30	17	0	5.5x10 <sup>-3</sup>
NbPMo <sub>12</sub> pyr	8: 4: 8: 10	25	79	1	2	2	14	0.008
NbPMo <sub>11</sub> Vpyr	8: 4: 8: 10	25	15	-	19	21	43	0.18
	32: 16: 32: 40	21	11	0	23	49	15	0.62

<sup>a</sup>C<sub>3</sub><sup>=</sup> = propylene; Ac = acetic acid; AA = acrylic acid; MA = maleic acid

<sup>b</sup>STY is in mmol/min/g catalyst

**Table 8.3** Temperature effects for NbPMo<sub>12</sub>pyr at 230 psig, 8: 4: 27: 10 mL/hr  
(ethane: oxygen: helium: steam) on high pressure reactor.

Temperature (C)	Conversion			Selectivity		STY <sup>a</sup>	
	C <sub>2</sub>	O <sub>2</sub>	CO <sub>x</sub>	C <sub>2</sub> <sup>=</sup>	Acetic	C <sub>2</sub> <sup>=</sup>	Acetic
330	8.1	36.7	59.5	35.7	4.8	0.015	0.002
280	6.0	28.4	64.5	23.2	12.4	0.006	0.003
240	0.4	1.1	18.3	59.1	22.6	0.001	4.0x10 <sup>-4</sup>

<sup>a</sup>STY is in mmol/min/g catalyst

**Table 8.4** Ethane reactivity of NbPMo<sub>12</sub>pyr at 280°C, 230 psig, (8: 4: 27: 0) mL/hr (ethane: oxygen: helium: steam) on high pressure reactor. Catalyst volume was varied.

GHSV (hr <sup>-1</sup> )	Conversion		Selectivity			STY <sup>a</sup>	
	C <sub>2</sub>	O <sub>2</sub>	CO <sub>x</sub>	C <sub>2</sub> <sup>=</sup>	Acetic	C <sub>2</sub> <sup>=</sup>	Acetic
975	15.1	100	87.7	7.8	4.5	0.002	0.001
1638	20.4	100	90.3	6.3	3.4	0.003	0.002
3900	15.0	87.4	83.4	12.7	3.9	0.009	0.003

<sup>a</sup>STY is in mmol/min/g catalyst

**Table 8.5** Ethane reactivity of  $\text{PMo}_{12}$ ,  $\text{NbPMo}_{12}$ ,  $\text{PMo}_{12}\text{pyr}$ , and  $\text{NbPMo}_{12}\text{pyr}$  at  $280^\circ\text{C}$ , 230 psig, 8: 4: 27: 10 mL/hr (ethane: oxygen: helium: steam) on high pressure reactor.

Catalyst	Conversion		Selectivity			STY <sup>a</sup>	
	$\text{C}_2$	$\text{O}_2$	$\text{CO}_x$	$\text{C}_2^=$	Acetic	$\text{C}_2^=$	Acetic
$\text{PMo}_{12}$	0.1	0.4	81.1	18.9	0	$6.5 \times 10^{-5}$	0
$\text{NbPMo}_{12}$	0.1	0.4	67.9	32.1	0	$1.1 \times 10^{-4}$	0
$\text{PMo}_{12}\text{pyr}$	0.1	0.7	84.6	13.4	0	$8.6 \times 10^{-5}$	0
$\text{NbPMo}_{12}\text{pyr}$	6.0	28.4	64.5	23.2	12.4	0.006	0.003

<sup>a</sup>STY is in mmol/min/g catalyst

**Table 8.6** Ethane reactivity with temperature of NbPMo<sub>12</sub>pyr at 0 psig, 16: 8: 16: 20 mL/hr (ethane: oxygen: helium: steam) on high pressure reactor.

Temperature (C)	Conversion			Selectivity		STY <sup>a</sup>	
	C <sub>2</sub>	O <sub>2</sub>	CO <sub>x</sub>	C <sub>2</sub> <sup>=</sup>	Acetic	C <sub>2</sub> <sup>=</sup>	Acetic
380	18.1	46.1	38.1	47.8	14.0	0.072	0.021
340	6.5	14.0	21.7	59.1	19.2	0.037	0.012
300	3.1	6.5	10.6	57.3	32.1	0.017	0.010

<sup>a</sup>STY is in mmol/min/g catalyst

**Table 8.7** Comparison of ethane reactivity of NbPMo<sub>12</sub>pyr between reactors and pressures. Reactor and flows used noted in table.

Temperature (C)	Conversion			Selectivity		STY <sup>a</sup>		
	C <sub>2</sub>	O <sub>2</sub>	CO <sub>x</sub>	C <sub>2</sub> <sup>=</sup>	Acetic	C <sub>2</sub> <sup>=</sup>	Acetic	
0 psig	Flow = 16: 8: 16: 20 mL/min (ethane: oxygen: helium: steam)							
380	high <sup>b</sup>	18.1	46.1	38.1	47.8	14.0	0.072	0.021
380	low <sup>b</sup>	15.3	47.7	57.1	39.1	3.8	0.050	0.005
0 psig	Flow = 8: 4: 25: 10 mL/min (ethane: oxygen: helium: steam)							
280	low <sup>b</sup>	2.0	6.3	24.8	61.6	13.5	0.006	0.001
230 psig	Flow = 8: 4: 27: 10 mL/min (ethane: oxygen: helium: steam)							
280	high <sup>b</sup>	6.0	28.4	64.5	23.2	12.4	0.006	0.003

<sup>a</sup>STY is in mmol/min/g catalyst

<sup>b</sup>Refers to the reactor used

**Table 8.8** Ethane reactivity of  $\text{PMo}_{12}$ ,  $\text{NbPMo}_{12}$ ,  $\text{PMo}_{12}\text{pyr}$ , and  $\text{NbPMo}_{12}\text{pyr}$  at  $380^\circ\text{C}$ , 0 psig, 16: 8: 16: 20 mL/hr (ethane: oxygen: helium: steam) on low pressure reactor.

Catalyst	Conversion		Selectivity			STY <sup>a</sup>	
	$\text{C}_2$	$\text{O}_2$	$\text{CO}_x$	$\text{C}_2^=$	Acetic	$\text{C}_2^=$	Acetic
$\text{PMo}_{12}$	0.1	0.9	100	0	0	0	0
$\text{NbPMo}_{12}$	0.3	0.9	39.0	52.8	8.2	0.002	$3.0 \times 10^{-4}$
$\text{PMo}_{12}\text{pyr}$	0.6	2.8	69.5	30.5	0	0.002	0
$\text{NbPMo}_{12}\text{pyr}$	15.3	47.7	57.1	39.1	3.8	0.050	0.005

<sup>a</sup>STY is in mmol/min/g catalyst

**Table 8.9** Comparison of ethane reactivity of NbPMo<sub>11</sub>Vpyr between reactors and pressures. Reactor and flows used noted in table.

Temperature		Conversion			Selectivity		STY <sup>a</sup>	
(C)		C <sub>2</sub>	O <sub>2</sub>	CO <sub>x</sub>	C <sub>2</sub> <sup>=</sup>	Acetic	C <sub>2</sub> <sup>=</sup>	Acetic
0 psig		Flow = 16: 8: 16: 20 mL/min (ethane: oxygen: helium: steam)						
380	high <sup>b</sup>	15.5	40.8	32.7	36.2	31.0	0.075	0.062
		Flow = 8: 4: 8: 10 mL/min (ethane: oxygen: helium: steam), V <sub>cat</sub> = 0.3 mL						
380	low <sup>b</sup>	9.4	32.6	46.0	49.0	5.0	0.064	0.006
0 psig		Flow = 4: 2: 12.5: 5 mL/min (ethane: oxygen: helium: steam), V <sub>cat</sub> = 0.3 mL						
280	low <sup>b</sup>	1.1	4.4	29.9	51.3	18.7	0.003	0.001
230 psig		Flow = 8: 4: 27: 10 mL/min (ethane: oxygen: helium: steam)						
280	high <sup>b</sup>	2.2	8.0	40.3	46.8	13.0	0.008	0.002

<sup>a</sup>STY is in mmol/min/g catalyst

<sup>b</sup>Refers to the reactor used

**Table 8.10** Comparison of ethane reactivity of (A) NbPMo<sub>11</sub>Vpyr prepared with NbCl<sub>5</sub> and synthetic Keggin and (B) NbPMo<sub>11</sub>Vpyr prepared with purchased Keggin and ammonium niobium oxalate, all on the low pressure reactor at a Nb/Keggin ratio of 0.68.

Temperature	Conversion		Selectivity			STY <sup>a</sup>	
	C <sub>2</sub>	O <sub>2</sub>	CO <sub>x</sub>	C <sub>2</sub> <sup>=</sup>	Acetic	C <sub>2</sub> <sup>=</sup>	Acetic
(A)	Flow = 16: 8: 16: 20 mL/min (ethane: oxygen: helium: steam)						
380	9.4	32.6	46.0	49.0	5.0	0.064	0.006
(B)	Flow = 8: 4: 8: 10 mL/min (ethane: oxygen: helium: steam), V <sub>cat</sub> = 0.3 mL						
380	15.7	45.7	45.6	50.2	4.2	0.101	0.008

<sup>a</sup>STY is in mmol/min/g catalyst

**Table 8.11** Comparison of ethane reactivity of NbPMo<sub>12</sub>pyr for different flow compositions at 380°C, 0 psig, on low pressure reactor, using 0.6 mL of catalyst.

Flowrates (mL/min)	Conversion			Selectivity		STY <sup>a</sup>	
	C <sub>2</sub>	O <sub>2</sub>	CO <sub>x</sub>	C <sub>2</sub> <sup>=</sup>	Acetic	C <sub>2</sub> <sup>=</sup>	Acetic
16: 8: 16: 20	15.3	47.7	57.1	39.1	3.8	0.050	0.005
15: 5: 15: 20	6.4	36.8	39.1	53.6	7.3	0.037	0.005
16: 4: 16: 20	12.9	77.2	50.1	44.3	5.6	0.062	0.008

<sup>a</sup>STY is in mmol/min/g catalyst

**Table 8.12** Comparison of ethane reactivity of various metal-exchanged  $M\text{PMo}_{12}\text{pyr}$  at 380°C, 0 psig, 16: 8: 16: 20 mL/hr (ethane: oxygen: helium: steam) on low pressure reactor.

Catalyst	Conversion		Selectivity			STY <sup>a</sup>	
	C <sub>2</sub>	O <sub>2</sub>	CO <sub>x</sub>	C <sub>2</sub> <sup>=</sup>	Acetic	C <sub>2</sub> <sup>=</sup>	Acetic
TaPMo <sub>12</sub> pyr	0.1	0.4	87.6	8.8	3.6	1.1x10 <sup>-4</sup>	1.6x10 <sup>-5</sup>
SbPMo <sub>11</sub> Vpyr	0.6	1.0	10.7	86.1	3.2	0.012	4.5x10 <sup>-4</sup>
ZrPMo <sub>12</sub> pyr	0.2	0.6	34.8	63.3	1.9	0.001	3.8x10 <sup>-5</sup>
TiPMo <sub>12</sub> pyr	1.3	6.0	81.4	18.0	0.6	0.006	1.9x10 <sup>-4</sup>
NbPMo <sub>12</sub> pyr	15.3	47.7	57.1	39.1	3.8	0.050	0.005

<sup>a</sup>STY is in mmol/min/g catalyst

**Table 8.13** Ethylene reactivity of NbPMo<sub>12</sub>pyr at 0 psig, 16: 8: 16: 20 mL/hr  
(ethylene: oxygen: helium: steam) on low pressure reactor.

T (C)	Conversion				Selectivity <sup>a</sup>				STY <sup>b</sup>
	C <sub>2</sub> <sup>=</sup>	O <sub>2</sub>	CO <sub>x</sub>	Acetic	AcAld	EtOH	MeAc	EtAc	Acetic
380	28.0	100	76.7	17.0	0.58	0.04	0.02	0.03	0.042
340	27.3	98.2	68.9	23.1	0.60	0.09	0.13	0.20	0.054
280	13.8	48.7	65.4	24.7	0.54	0.46	0.74	0.75	0.030
240 <sup>c</sup>	1.8	8.6	64.5	30.4	1.1	2.5	0.31	1.1	0.006
240 <sup>d</sup>	1.7	8.8	71.9	25.9	0.36	1.4	0.03	0.36	0.005

<sup>a</sup>AcAld = acetaldehyde, EtOH = ethanol, MeAc = methyl acetate, EtAc = ethyl acetate

<sup>b</sup>STY is in mmol/min/g catalyst

<sup>c</sup>Using D<sub>2</sub>O was source of steam

<sup>d</sup>One hour after removal of D<sub>2</sub>O from gas stream. Data is from the average of the second hour.

CHAPTER NINE

SUMMARY AND CONCLUSIONS FOR  
PART TWO

Previous work<sup>1,2</sup> showed that the niobium- and pyridine-exchanged HPA materials were active and selective in the oxidation of light alkanes, specifically *n*-butane and propane, to liquid oxygenates, maleic acid and acrylic acid, respectively. Production of maleic acid from *n*-butane was as high as 0.84 mmol/min/g catalyst at 380°C and flow rates of 32: 16: 32: 40 mL/min of *n*-butane: oxygen: helium: steam, using NbPMo<sub>12</sub>pyr. The incorporation of vanadium into the HPA precursor was important to have an active catalyst for the conversion of propane to acrylic acid (as high as 0.62 mmol/min/g catalyst at 380°C and 32: 16: 32: 40 mL/min of propane: oxygen: helium: steam). In this work, the application of these catalysts to ethane oxidation to acetic acid and ethylene was explored, studying a variety of reaction parameters, e.g., reaction temperature and pressure, reactant feed composition, and catalysts composition.

Increased amounts of steam (0 to 10 mL/min) at elevated pressure (230 psig) increased the selectivity of NbPMo<sub>12</sub>pyr to both ethylene and acetic acid, but lowered conversion. At 230 psig and 280°C, ethane conversion decreased from 15.0% without steam to 6.0% with 10 mL/min of steam. At these conditions, CO<sub>x</sub> selectivity decreased from 83.4 to 64.5% as steam was increased. Acetic acid selectivities increased from 3.9% without steam to 12.4% with 10 mL/min of steam. No improvement in acetic acid STY could be obtained simply by varying steam flow rates (STY was 0.002 to 0.003 mmol/min/g catalyst over the steam range of 0 to 10 mL/min). At this pressure, increasing temperatures (from 240 to 300°C) increased ethane conversion from 0.4 to 8.1%, but also increased selectivity to CO<sub>x</sub> (from 18.3% to 59.5%). The temperature increase decreased acetic acid selectivity from 22.6% to 4.8%. Lower GHSV at elevated

pressure (230 psig, 280°C) caused the ethylene and acetic acid to over-oxidize to CO<sub>x</sub> (up to 83% selectivity). A decrease in acetic acid production, from 0.003 to 4.9x10<sup>-4</sup> mmol/min/g catalyst was observed as space velocity decreased from 4500 to 1200 hr<sup>-1</sup>.

Increased amounts of steam (0 to 20 mL/min) also increased the selectivity of NbPMo<sub>12</sub>pyr to both ethylene and acetic acid at atmospheric pressure while lowering conversion. Ethane conversion was 30.5% without steam and decreased to 18.1% with 20 mL/min of steam. CO<sub>x</sub> selectivity decreased from 65.1 to 38.1% while acetic acid increased from 0.6 to 14.0% for the same conditions, respectively. The maximum STY of acetic acid obtained with NbPMo<sub>12</sub>pyr obtained was 0.021 mmol/min/g catalyst at 380°C, 0 psig, and flows of 16: 8: 16: 20 mL/min of ethane: oxygen: helium: steam (on the high pressure reactor). The selectivity to ethylene and acetic acid improved at lower temperatures (as low as 300°C), but ethane conversion decreased. The overall STY of the products (ethylene and acetic acid) was best at 380°C.

The incorporation of vanadium into the Keggin unit on acetic acid production was examined at 230 psig and 280°C on the high pressure reactor. The conversion for NbPMo<sub>11</sub>Vpyr (2.2%) was less than that obtained under the same conditions (on the same reactor) for NbPMo<sub>12</sub>pyr (6.0%). No change was observed in acetic acid selectivity (13.0% for NbPMo<sub>11</sub>Vpyr and 12.4% for NbPMo<sub>12</sub>pyr). STY of ethylene was higher for NbPMo<sub>11</sub>Vpyr at 0.008 mmol/min/g catalyst (0.006 mmol/min/g catalyst for NbPMo<sub>12</sub>pyr). STY of acetic acid was slightly lower for NbPMo<sub>11</sub>Vpyr at 0.002 mmol/min/g catalyst (0.003 mmol/min/g catalyst for NbPMo<sub>12</sub>pyr). At elevated pressure (230 psig) the addition of vanadium into the Keggin precursor primarily improved selectivity to ethylene, but did not affect the formation of acetic acid.

The effect of vanadium was also examined at atmospheric pressure and 380°C on the *high* pressure reactor. The conversion for NbPMo<sub>11</sub>Vpyr (15.5%) was again less than that obtained under the same conditions (on the same reactor) for NbPMo<sub>12</sub>pyr (18.1%). NbPMo<sub>12</sub>pyr, however, had only 14.0% selectivity to acetic acid. NbPMo<sub>11</sub>Vpyr had 31.0% selectivity to acetic acid at atmospheric pressure, resulting in an increased STY of 0.062 mmol/min/g catalyst (NbPMo<sub>12</sub>pyr had 0.021 mmol/min/g catalyst of acetic acid). The addition of vanadium into the Keggin precursor had a favorable affect on the acetic acid formation at atmospheric pressure.

Proper analysis of some of the data could not be done due to inconsistencies between the two different reactors used. Although ethane conversions were only slightly lower for NbPMo<sub>12</sub>pyr between the two reactors (18.1 and 15.3% conversion on the high and low pressure system, respectively), more CO<sub>x</sub> was observed in the low pressure reactor (57.1% vs. 38.1% for NbPMo<sub>12</sub>pyr at 380°C, 0 psig, and 16: 8: 16: 20 mL/min ethane: oxygen: helium: steam) than on the high pressure reactor. This resulted in lower ethylene selectivity and an order of magnitude lower acetic acid selectivity on the low pressure reactor. The low pressure reactor measured only 0.005 mmol/min/g catalyst, instead of the 0.021 mmol/min/g catalyst found by the high pressure reactor for NbPMo<sub>12</sub>pyr at 380°C, 0 psig, and 16: 8: 16: 20 mL/min ethane: oxygen: helium: steam.

Similar discrepancies between the two reactors were observed for NbPMo<sub>11</sub>Vpyr, although the conversion difference was greater (9.4% on the low pressure reactor vs. 15.5% on the high pressure reactor). More CO<sub>x</sub> was observed on the low pressure reactor (46.0% vs. 32.7% for NbPMo<sub>11</sub>Vpyr at 380°C, 0 psig, and 16: 8: 16: 20 mL/min ethane: oxygen: helium: steam) than on the high pressure reactor. Acetic acid selectivity (5.0%)

was significantly lower on the low pressure reactor than on the high pressure reactor (31.0%). The decrease in acetic acid selectivity was reflected in the lower STY of acetic acid on the low pressure reactor, 0.006 mmol/min/g catalyst, instead of 0.062 mmol/min/g catalyst. The deactivation effect due to reactor configurational differences appeared to be more pronounced for NbPMo<sub>11</sub>Vpyr than NbPMo<sub>12</sub>pyr.

The addition of both Nb and pyridine with the HPA was crucial for active catalyst formation, for reactions both at atmospheric pressure and 230 psig. The acid forms, PMo<sub>12</sub> and PMo<sub>11</sub>V, had no activity for ethane oxidation, either at atmospheric pressure or 230 psig. The exchange of Nb alone to make NbPMo<sub>12</sub> and NbPMo<sub>11</sub>V did not improve the activity. Only the incorporation of both Nb and pyridine resulted in an active catalyst for both the PMo<sub>12</sub> and PMo<sub>11</sub>V systems. Substitution of other metals for Nb (Ta, Sb, Ti, and Zr) did not achieve significant ethane conversion.

Variations in the Nb/Keggin loading for NbPMo<sub>12</sub>pyr and NbPMo<sub>11</sub>Vpyr were studied on the low pressure reactor system. NbPMo<sub>12</sub>pyr had a maximum acetic acid production (on the low pressure reactor) of 0.007 mmol/min/g catalyst for a Nb/Keggin loading of 0.8 and 1.0, at atmospheric pressure. The STY of ethylene also increased as a function of Nb loading, up to a maximum of 0.092 mmol/min/g catalyst at a loading of 0.8. NbPMo<sub>11</sub>Vpyr had maximum acetic acid production at atmospheric pressure (on the low pressure reactor) with the Nb/Keggin loading of 0.87, at 0.009 mmol/min/g catalyst. Ethylene STY at this loading was also at maximum (0.086 mmol/min/g catalyst). The NbPMo<sub>11</sub>Vpyr catalyst at Nb/Keggin of 0.68 (Holles material) gave significantly more acetic acid STY on the high pressure reactor vs. the low pressure reactor (0.061 vs. 0.006 mmol/min/g catalyst). This appeared to not be the optimal Nb loading, and it would be

beneficial to repeat the reaction at atmospheric pressure on a properly configured reactor for 0.87 Nb/Keggin to determine whether the maximum STY of acetic acid is greater than 0.061 mmol/min/g catalyst.

Sources of raw material for catalyst preparation affected the activity of the catalyst. NbPMo<sub>11</sub>Vpyr prepared by Holles from synthetic Keggin (PMo<sub>11</sub>V) and NbCl<sub>5</sub> at a Nb/Keggin loading of 0.68 had only 9.4% conversion (on the low pressure reactor, at 380°C, 0 psig, and 16: 8: 16: 20 mL/min ethane: oxygen: helium: steam). This same catalyst showed 15.5% conversion at the same reaction conditions on the high pressure reactor. NbPMo<sub>11</sub>Vpyr prepared at the same Nb/Keggin loading (0.68) using PMo<sub>11</sub>V obtained from Pred Materials and ammonium niobium oxalate had 15.7% conversion (compared to 9.4% for the Holles material on the same reactor under the same conditions) on the low pressure reactor. Selectivities were similar for both materials (46% CO<sub>x</sub>, 50% ethylene, and 4% acetic acid). Because the Holles material had higher conversion and acetic acid STY (0.061 mmol/min/g catalyst) on the high pressure reactor, it is likely that the NbPMo<sub>11</sub>Vpyr made from commercial Keggin and ammonium niobium oxalate will perform even better on the high pressure reactor configuration and have even higher yield of acetic acid.

The results of this work suggest areas of further study, after proper feed configuration is achieved on the low pressure reactor system. Specifically, comparisons for both NbPMo<sub>12</sub>pyr and NbPMo<sub>11</sub>Vpyr activity at 280°C should be made between new runs at atmospheric pressure and the previous work at 230 psig to determine whether the atmospheric reactions have improved selectivity to acetic acid. NbPMo<sub>12</sub>pyr showed higher ethane conversion at higher pressures (from 2.0% to 6.0%) but similar acetic acid

selectivity (13.5% and 12.4%) on the low and high pressure reactor, respectively, for atmospheric and 230 psig reactions, respectively. Because the low pressure reactor appeared to have lower acetic acid production even for identical conditions and catalysts, atmospheric pressure reactions could in fact have even higher acetic acid selectivity on a properly configured reactor.

The difference between NbPMo<sub>12</sub>pyr and NbPMo<sub>11</sub>Vpyr at atmospheric pressure at 380°C was not significant for data measured under the same conditions on the low pressure reactor. The low pressure reactor measured 0.004 vs. 0.006 mmol/min/g catalyst of acetic acid for NbPMo<sub>12</sub>pyr and NbPMo<sub>11</sub>pyr, respectively, while the high pressure reactor reported 0.021 and 0.062 mmol/min/g catalyst of acetic acid for NbPMo<sub>12</sub>pyr and NbPMo<sub>11</sub>pyr, respectively, for the same conditions. This could again be due to reactor configurational issues and needs to be addressed further.

Configurational differences between the low and high pressure reactor may also have reduced some of the effect on acetic acid formation due to Nb/ Keggin loading in NbPMo<sub>12</sub>pyr and NbPMo<sub>11</sub>Vpyr. Maximum STY of ethylene and acetic acid was observed at Nb/Keggin of 0.8 for NbPMo<sub>12</sub>pyr at atmospheric pressure and 380°C (0.092 and 0.007 mmol/min/g catalyst, respectively). Maximum STY of ethylene and acetic acid was observed at Nb/Keggin of 0.87 for NbPMo<sub>11</sub>Vpyr at atmospheric pressure and 380°C (0.086 and 0.009 mmol/min/g catalyst, respectively). Variations in Nb/Keggin loadings were done using NbPMo<sub>11</sub>Vpyr prepared by Holles and co-workers on the low pressure reactor. NbPMo<sub>11</sub>Vpyr prepared using PMo<sub>11</sub>V obtained from Pred Materials and ammonium niobium oxalate had higher ethane conversion (15.7% compared to 9.4% for the Holles material) on the same reactor under the same conditions. Further study of

the effect of Nb loadings in both NbPMo<sub>12</sub>pyr and NbPMo<sub>11</sub>Vpyr (using the PMo<sub>11</sub>V from Pred Materials and ammonium niobium oxalate) on a properly configured reactor system would be of interest.

Higher ethane/oxygen ratios appeared to increase the selectivity to acetic acid. At a ratio of 4:1, the ethane conversion was 12.9% for NbPMo<sub>12</sub>pyr at atmospheric pressure, compared to 15.3% at a ratio of 2:1, while selectivity to acetic acid increased to 5.6% from 3.8%. The acetic acid STY increased to 0.008 mmol/min/g catalyst for a ratio of 4:1 (compared to 0.005 for 2:1 ethane/oxygen ratio), suggesting that it may be possible to continue to increase acetic acid production by increasing the ethane/oxygen ratio even further (10:1 and greater). Similar variations in ethane/oxygen ratios should also be done with the NbPMo<sub>11</sub>Vpyr.

Feeding ethylene in the place of ethane resulted in the formation of acetic acid. At low conversions, selectivity to methyl acetate, ethyl acetate, and ethanol increased, suggesting that the acetic acid may be formed from an adsorbed ethoxy group on the catalyst surface. Steam from the feed is involved in the formation of acetic acid. Deuterated acetic acid was observed in the product when D<sub>2</sub>O was used to provide steam to the reaction. It would be interesting to continue mechanistic studies after low pressure reactor modification to determine the true primary products of reaction. The formation of other deuterated products using D<sub>2</sub>O to provide steam, such as methyl acetate, ethyl acetate and ethanol should be closely monitored at low ethylene conversions to determine which species are important in ethylene conversion to acetic acid. Ethylene reactions should also be performed using a <sup>13</sup>C-labelled solution of each of these compounds as the

water feed to determine whether the  $^{13}\text{C}$  label appears in acetic acid. This would provide evidence for what surface species are involved in acetic acid formation.

- (1) Davis, M. E. *et al.*, *Angew. Chem., Int. Ed.* **2002**, *41*, 858.
- (2) Holles, J. H. *et al.*, *J. Catal.* **2003**, *218*, 42.

CHAPTER TEN

CONCLUSIONS

This thesis was composed of two separate and unrelated projects. The first project examined the preparation of base-containing molecular sieves for strong base catalysis, e.g., the Michael addition reaction. The objective of this project was to incorporate a covalently attached moiety (e.g., an ammonium or phosphonium functionality) into the pore space of zeolite \*BEA to allow the incorporation of a strong base, OH<sup>-</sup>, within a molecular sieve. An ammonium functional group could not be used in OFMS preparation because it exhibited degradation after heating to 100°C. It was not expected that the organic group in Q-\*BEA would survive either the zeolite synthesis (at 140°C) or the SDA extraction. Further work was done to attempt to incorporate a phosphonium functionality into an OFMS.

The phosphonium functionality was prepared by nucleophilic displacement of a halogen-containing alkyl group with trimethylphosphine. Bromopropyl-functionalized mesoporous silica, Br-CPG, was reacted to create the phosphonium functionality at a yield of 86%. This resulted in an organic loading of approximately 0.36 mmol/g of phosphonium on CPG. Heat treatment of the phosphonium-containing CPG showed the bromide form was stable to 300°C under vacuum. Similar reactions were done with bromopropyl-functionalized \*BEA. The \*BEA structure was stable to both extraction and nucleophilic displacement reactions. Only 21% of the bromopropyl-functional groups were reacted, resulting in an organic loading of 0.0084 mmol/g of phosphonium. Lack of reaction of the Br-\*BEA material with triphenylphosphine (too large to enter the pores) suggested that the functional groups in the OFMS sample were located within the zeolite pore space. Attempts were made to increase the phosphonium loading in OFMS

materials by using the prepared phosphonium organosilane directly in the zeolite synthesis, but the phosphonium moiety was not stable to any extraction procedure attempted to remove the SDA.

The phosphonium halide-containing samples were ion-exchanged to nitrate using 1 N HNO<sub>3</sub>. Titration of the filtrate for removed halides determined that the exchange efficiency of Br<sup>-</sup> to NO<sub>3</sub><sup>-</sup> was 56% for the P<sup>+</sup>Br<sup>-</sup>-CPG material. No removed halides could be detected in the P<sup>+</sup>Br<sup>-</sup>-\*BEA samples, however. Shape-selective ion-exchange with NaBPh<sub>4</sub>, which was too large to enter the \*BEA pores, also suggested that the phosphonium moieties were located within the zeolite pores. Finally, ion-exchange to the hydroxide form of the materials had a 72% exchange efficiency from NO<sub>3</sub><sup>-</sup> to OH<sup>-</sup> for the P<sup>+</sup>NO<sub>3</sub><sup>-</sup>-CPG material, giving an overall exchange efficiency of 40% from bromide to hydroxide. Exchange results for the P<sup>+</sup>NO<sub>3</sub><sup>-</sup>-\*BEA did show removal of nitrate (0.008 mmol/g), but this was similar to the control Si-\*BEA sample and was not conclusive.

Neither the ion-exchange tests described nor the catalytic experiments were able to prove the presence of a phosphonium hydroxide moiety within an OFMS. All of the uncalcined \*BEA samples were capable to catalyzing the Knoevenagel condensation reaction of benzaldehyde and malononitrile, even extracted Si-\*BEA. Michael addition reactions with methylvinylketone did suggest the existence of a base site within P<sup>+</sup>OH<sup>-</sup>-CPG that was not due to physisorbed hydroxide. No significant reactivity was observed for the Michael addition in any of the \*BEA samples tested. Residual TEAF from extraction, physisorbed hydroxide from the ion-exchange, and the low number density of the phosphonium groups prevented clear conclusions of the nature of the functional group in the OFMS samples.

Results from the functionalized CPG work show that the process of creating phosphonium-containing materials from a halogen-containing material and subsequent ion-exchange of the halide form to hydroxide to create a heterogeneous material for strong base catalysis is feasible. However, the phosphonium group is susceptible to degradation in chemical environments, suggesting that the incorporation of a quaternary moiety (ammonium or phosphonium) within a porous material is only appropriate where temperature and environment are mild.

The second part of this thesis examines the use of niobium- and pyridine-exchanged heteropolyanions as catalyst precursors for the selective oxidation of light alkanes with dioxygen. NbPMo<sub>12</sub>pyr showed higher ethane conversion at higher pressures (from 2.0% to 6.0%) but similar acetic acid selectivity (13.5% and 12.4%) at 280°C for atmospheric and 230 psig reactions, respectively. No improvement in acetic acid STY could be obtained simply by varying steam flow rates or changing reaction temperatures while keeping all other parameters constant. Lower GHSV caused the ethylene and acetic acid to over-oxidize to CO<sub>x</sub>. The maximum STY of acetic acid obtained with NbPMo<sub>12</sub>pyr obtained was 0.021 mmol/min/g catalyst at 380°C, 0 psig, and flows of 16: 8: 16: 20 mL/min of ethane: oxygen: helium: steam (on the high pressure reactor).

At elevated pressure (230 psig) the addition of vanadium into the Keggin precursor primarily improved selectivity to ethylene, but did not affect the formation of acetic acid. At atmospheric pressure the addition of vanadium into the Keggin precursor had a favorable affect on the acetic acid formation. The ethane conversion increased slightly, from 1.1 to 2.2% as the pressure was increased from 0 to 230 psig at 280°C.

Ethylene and acetic acid selectivity both decreased with increased pressure. The STY of ethylene and acetic acid were slightly higher under pressure, at 0.008 and 0.002 mmol/min/g catalyst, respectively, because of higher conversion. NbPMo<sub>11</sub>Vpyr had maximum production of acetic acid at 380°C, 0 psig, and flows of 16: 8: 16: 20 mL/min of ethane: oxygen: helium: steam (on the high pressure reactor), resulting in an increased STY of acetic acid at 0.062 mmol/min/g catalyst. This was the highest STY of acetic acid observed during all of the ethane oxidation experiments.

Proper analysis of some of the data could not be done due to inconsistencies between the two different reactors used. Ethane conversions were only slightly lower for NbPMo<sub>12</sub>pyr between the two reactors, and more CO<sub>x</sub> was observed in the low pressure reactor. This resulted in lower ethylene selectivity and an order of magnitude lower acetic acid selectivity on the low pressure reactor. The conversion difference between the two reactors was greater for NbPMo<sub>11</sub>Vpyr. The deactivation effect due to reactor configurational differences appeared to be more pronounced for NbPMo<sub>11</sub>Vpyr than NbPMo<sub>12</sub>pyr. Sources of raw material (i.e., PMo<sub>11</sub>V and niobium source) for catalyst preparation affected the activity of the catalyst. NbPMo<sub>11</sub>Vpyr prepared using PMo<sub>11</sub>V obtained from Pred Materials and ammonium niobium oxalate had higher ethane conversion than NbPMo<sub>11</sub>Vpyr prepared by Holles from synthetic Keggin (PMo<sub>11</sub>V) and NbCl<sub>5</sub>.

The addition of both Nb and pyridine with the HPA was crucial for active catalyst formation, for reactions both at atmospheric pressure and 230 psig. Substitution of other metals for Nb (Ta, Sb, Ti, and Zr) did not achieve significant ethane conversion. NbPMo<sub>12</sub>pyr had a maximum ethylene and acetic acid production (on the low pressure

reactor) of 0.092 and 0.007 mmol/min/g catalyst, respectively, for a Nb/Keggin loading of 0.8, at atmospheric pressure. NbPMo<sub>11</sub>Vpyr had maximum ethylene and acetic acid production (also on the low pressure reactor) of 0.086 and 0.009 mmol/min/g catalyst, respectively, for a Nb/Keggin loading of 0.87, at atmospheric pressure. Since the high pressure reactor configuration gave better acetic acid production at atmospheric pressure with Nb<sub>0.4</sub>PMo<sub>12</sub>pyr and Nb<sub>0.68</sub>PMo<sub>11</sub>Vpyr, the optimal Nb/Keggin loadings of Nb<sub>0.8</sub>PMo<sub>12</sub>pyr and Nb<sub>0.87</sub>PMo<sub>11</sub>Vpyr should be re-examined.

Higher ethane/oxygen ratios appeared to increase the selectivity to acetic acid for NbPMo<sub>12</sub>pyr at atmospheric pressure. Similar variations in ethane/oxygen ratios should also be done with the NbPMo<sub>11</sub>Vpyr. Feeding ethylene in the place of ethane resulted in the increased production of acetic acid. Steam from the feed is involved in the formation of acetic acid. Deuterated acetic acid was observed in the product when D<sub>2</sub>O was used to provide steam to the reaction. Further mechanistic studies after low pressure reactor modification should be done to determine the true primary products of reaction.

APPENDICES

## Appendix A: BTRS, Jr. Reactors

**Figure A.1** Autoclave Engineers BTRS, Jr. reactor (high pressure reactor).

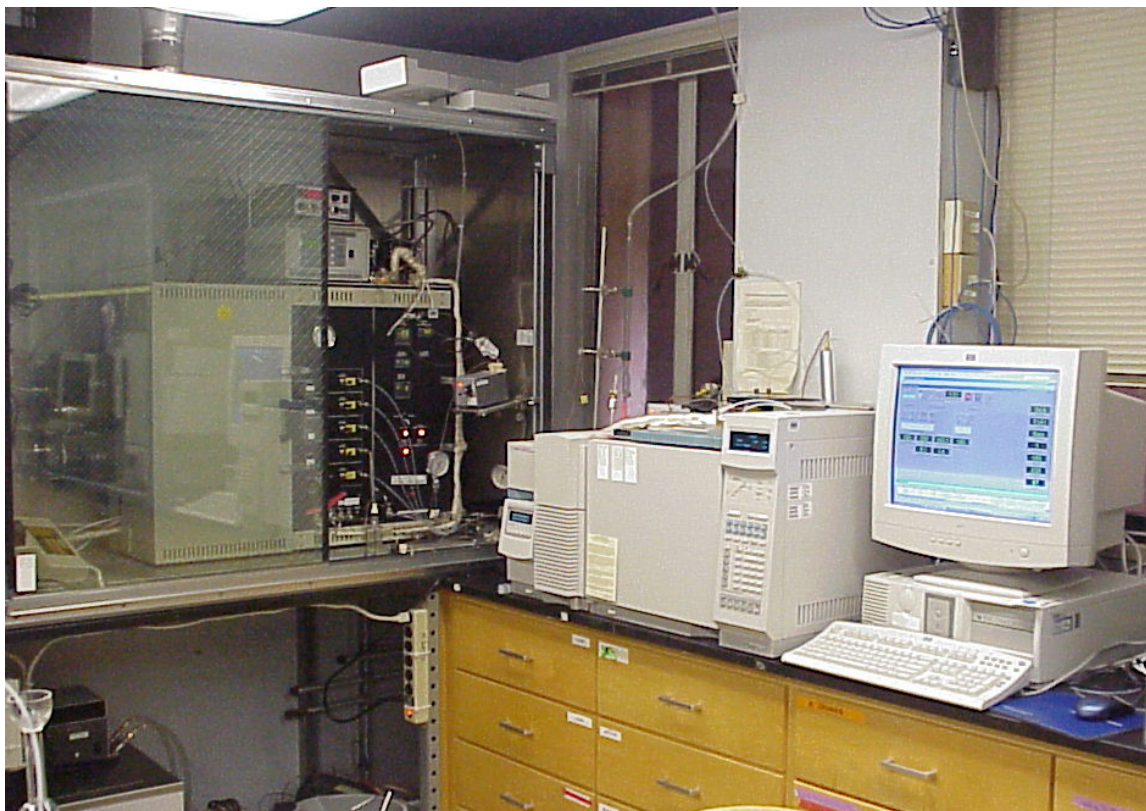


**Figure A.2** Autoclave Engineers BTRS, Jr. reactor (low pressure reactor).

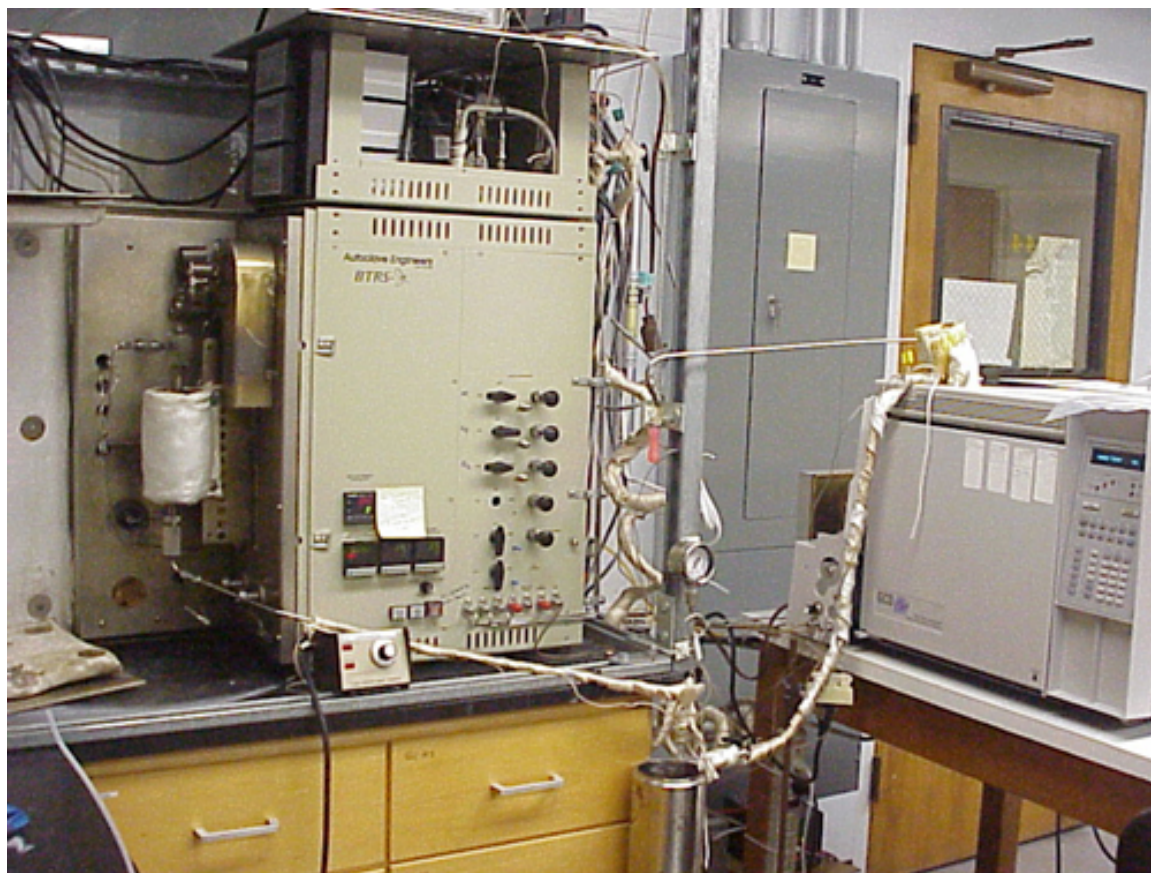


**Figure A.3** Configuration of reactor tube in the reactor furnace on high pressure reactor.

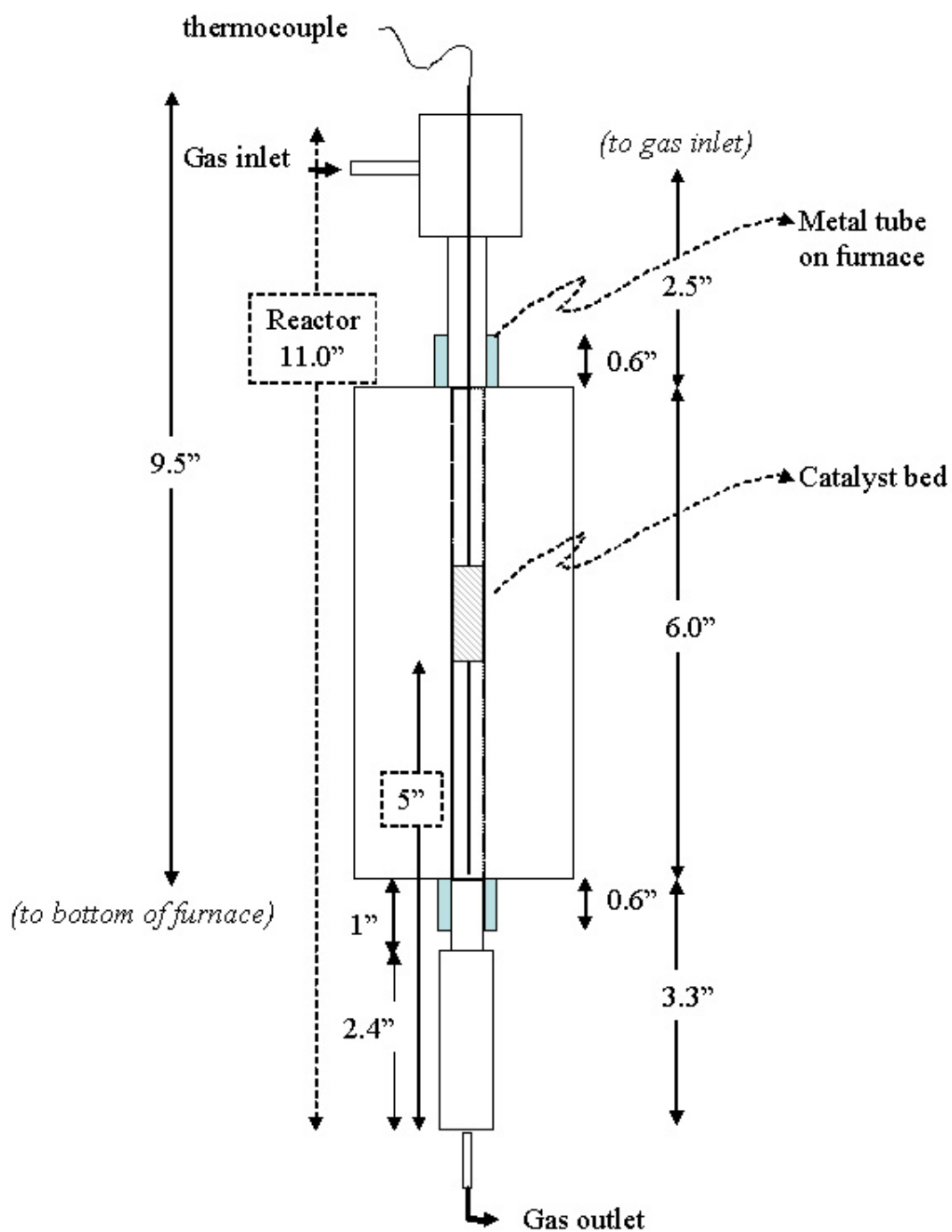


**Figure A.4** Configuration of reactor tube in the reactor furnace on low pressure reactor.

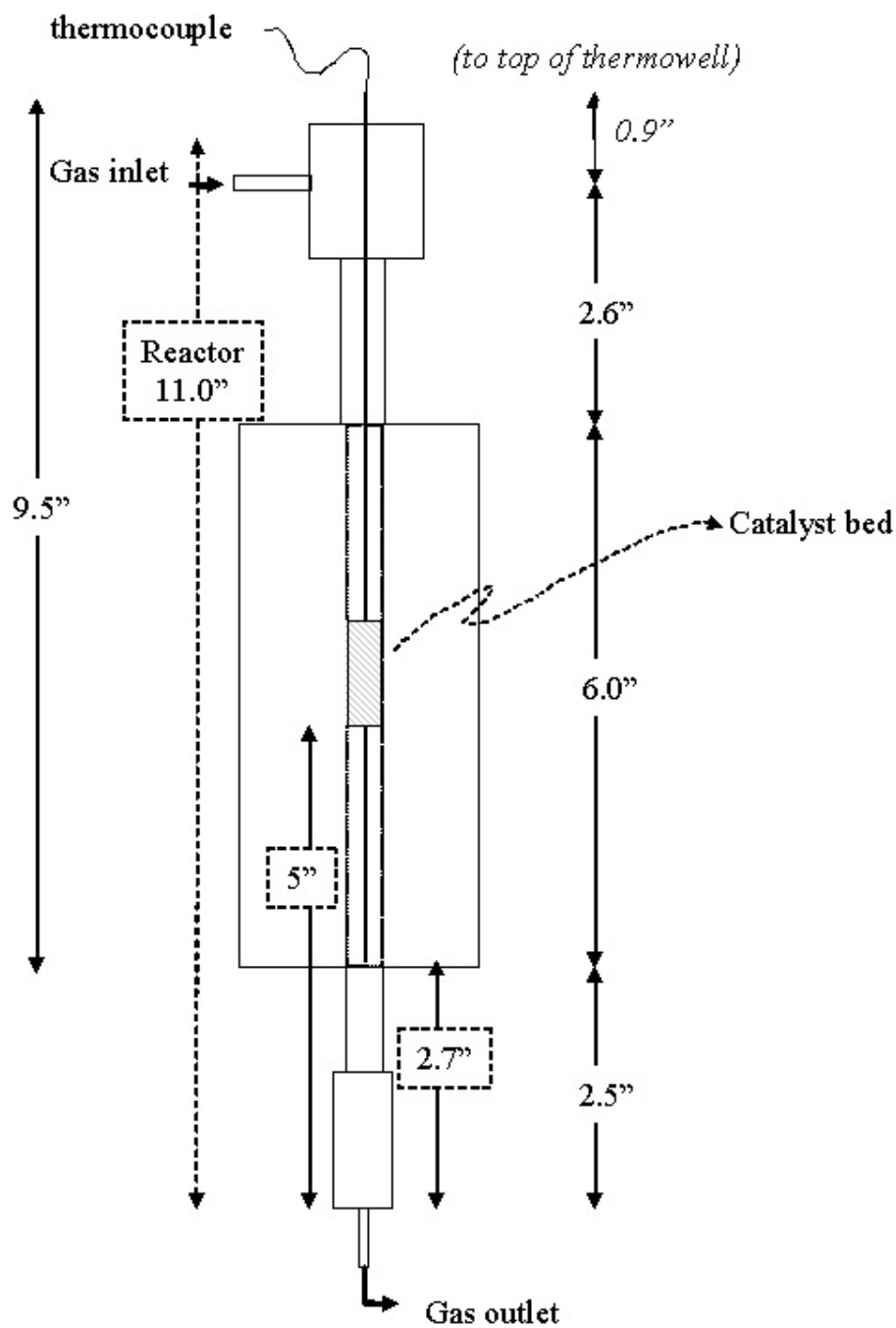
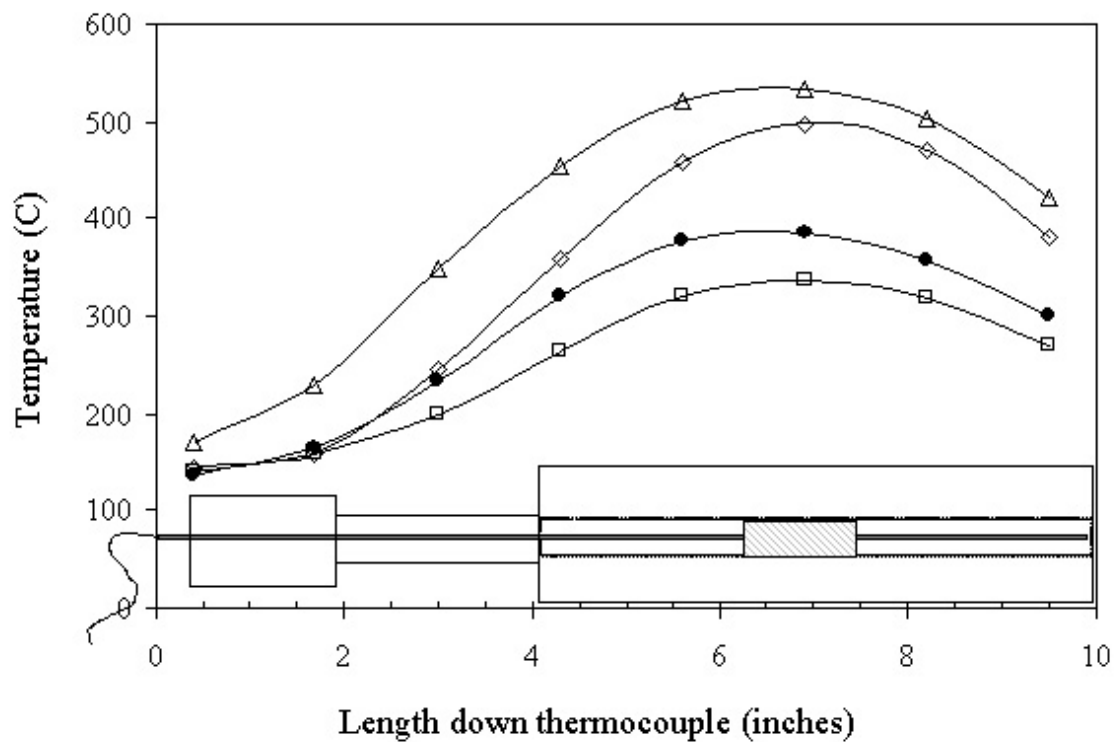


**Figure A.5** Temperature profile in reactor tube filled with glass wool on low pressure reactor. (● - temperature profile when temperature controller is set to 380°C).



## Appendix B: Flammability Calculations

Flammability calculations were performed to ensure that the ethane/oxygen mixtures used as feed for the reaction studies were non-flammable. The author would like to acknowledge Marcia Cooper and Professor Joseph Shepherd for their assistance in providing the data and methods for the calculations.

### B.1 Flammability Limit Data

Data for the flammability range for a variety of gases may be found in Bulletin 627 from the Bureau of Mines.<sup>1</sup> The data are presented in the form of charts and graphs, at particular temperatures and pressures (usually room temperature and atmospheric pressure) and levels of inert (data gathered in air, oxygen, or with additional inert). The flammability range consists of a lower flammability limit (LFL) and upper flammability limit (UFL). The limits are *usually* expressed in terms of volume percent of the hydrocarbon in the gas mixture. Below the LFL, the gas stream cannot sustain a flame. Likewise, above the UFL, no flame may be maintained. It is between the two limits that the mixture is flammable, either by encountering an ignition source or by self-igniting if above the auto-ignition temperature (AIT). Other relevant information, such as the AIT, heat of combustion ( $\Delta H_c$ ), and quenching distances for a traveling flame front, may also be found in the Bulletin.

### B.2 Temperature Corrections

Because the flammability ranges usually presented in the data are at room temperature, a correction must be applied to adjust the range for elevated temperatures, such as the reaction temperatures in this study. The LFL and UFL are affected by temperature, where the LFL is decreased and the UFL is increased, thereby *widening* the

flammability range with elevated temperature. The limits change linearly with temperature for a particular hydrocarbon:<sup>1</sup>

$$\text{LFL}_{T(C)} = \text{LFL}_{25\text{ C}} - (0.75 / \Delta H_c) \cdot (T - 25)$$

$$\text{UFL}_{T(C)} = \text{UFL}_{25\text{ C}} + (0.75 / \Delta H_c) \cdot (T - 25)$$

where

$\text{LFL}_{T(C)}$  is the lower flammability limit at temperature T (in °C)

$\text{LFL}_{25\text{ C}}$  is the lower flammability limit at room temperature (25°C)

$\Delta H_c$  is the heat of combustion of the hydrocarbon in kcal/mol at 25°C

$\text{UFL}_{T(C)}$  is the upper flammability limit at temperature T (in °C)

$\text{UFL}_{25\text{ C}}$  is the upper flammability limit at room temperature (25 °C)

Charts developed from experimental data are also available in Bulletin 627 that provide this empirical correlation for hydrocarbons. (Note the  $\Delta H_c$  of ethane is 341.3 kcal/mol, taken from Table 2 of the Bulletin, page 21.)

### B.3 Pressure Corrections

Increase in pressure above atmospheric pressure also affects the LFL and UFL. The effect is more significant in the UFL. No empirical equations for flammability limits as a function of pressure were found in the author's search for flammability data (although such correlations may exist). Charts developed from experimental data at a variety of pressures for some gases are presented in the Bulletin, although the information available is limited. In particular, Figure 38 from Bulletin 627 was used for the ethane flammability calculations as a function of pressure (in air, at 25°C) for the reactivity experiments conducted in this study. The chart presents the flammability limits as a

function of added inert (nitrogen) beyond what would be found in air at several pressures (see Figure B.1). The amount of oxygen in the reaction stream was used to calculate what would be an equivalent amount of “air,” using the amount of helium *and* steam fed to substitute as nitrogen. (Note that different inert gases suppress flammability differently, and it is an approximation to the calculations by assuming that the helium and steam behave the same as nitrogen. This was necessary because no information was available for the behavior of ethane under pressure with oxygen and added helium.) The percentage of excess inert added was then calculated and used to read the LFL and UFL at 0 psig for atmospheric reactions and 250 psig for the pressure reactions (an approximation for 230 psig, which was the actual reaction pressure) from Figure B.1. The LFL and UFL at reaction pressure were then adjusted for temperature as described above and used to determine if the proposed reactant gas stream was flammable.

#### **B.4 Quenching Distance**

Although the ethane reactions were run using non-flammable reactant mixtures, the quenching distance of ethane was researched to give further confidence in the safety of the experimental setup. A traveling flame front will be extinguished in any diameter smaller than its quenching distance. In typical applications a flame arrestor, which restricts the diameter of flow, is used to prevent the flame front from traveling through a system. Note that the catalyst bed itself will act as a flame arrestor. The quenching distance of ethane is 1.8 mm.<sup>2</sup> The addition of flame arrestors into the BTRS, Jr., reactor assemblies was not necessary, however, because the 1/8-inch diameter tubing used for gas flow has an inner diameter of 1.57 mm, smaller than ethane’s quenching distance. The tubing on either side of the reactor tube would not allow any flames to propagate

through the system. Additionally, any sharp increase of pressure in the system would cause the pressure relief disk on the high pressure reactor (set at approximately 1600 psig) to rupture and safely vent the contents of the reactor.

**B.5 References**

- (1) Zabetakis, M. G.; Bureau of Mines, 1965; Vol. Bulletin 627.
- (2) Turns, S. R. *An Introduction to Combustion: Concepts and Applications*; McGraw-Hill: New York, 1996.

**Figure B.1** Ethane flammability data for various pressures.<sup>1</sup>

Reprinted with permission from US Bureau of Mines.

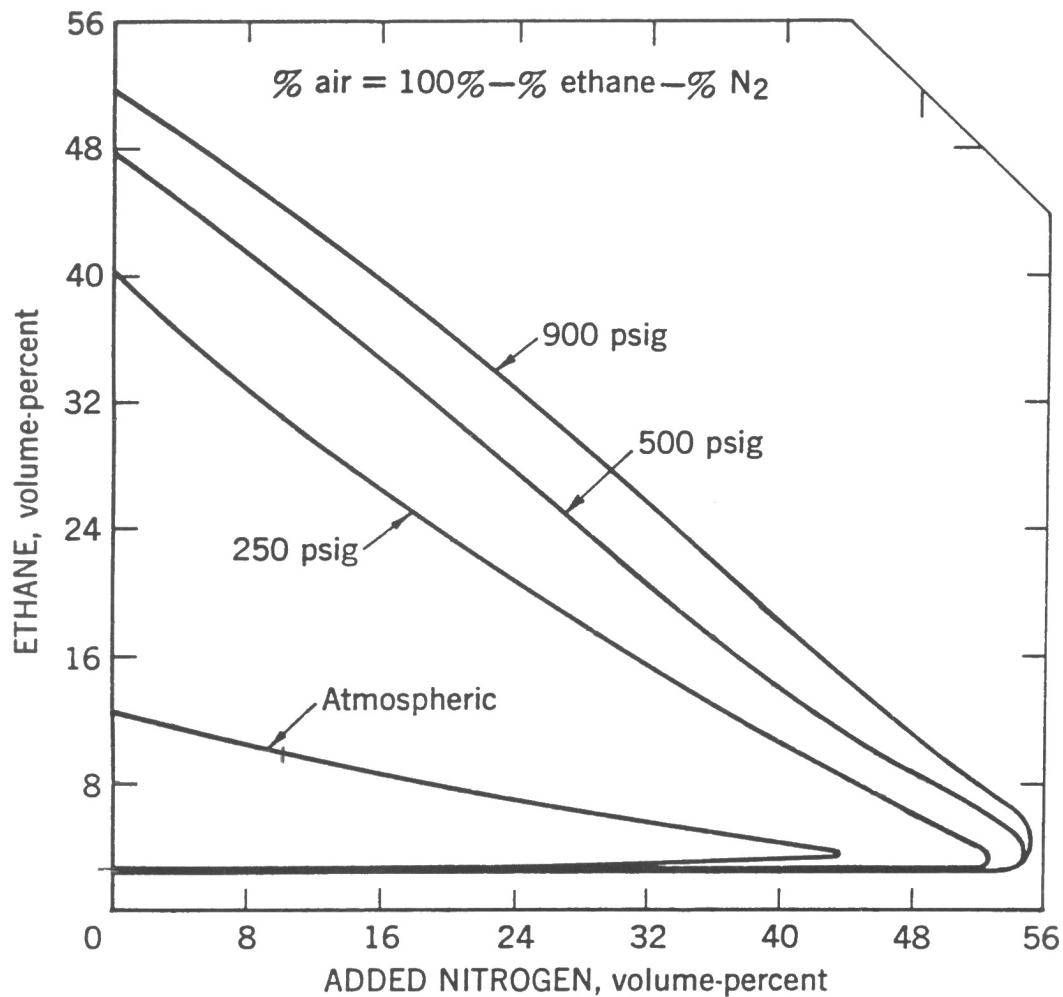


FIGURE 38.—Effect of Pressure on Limits of Flammability of Ethane-Nitrogen-Air Mixtures at 26° C.

### Appendix C: Reactivity Data Tables

The following are tables of data used to create the figures of Chapter 8, as indicated in the table captions.

**Table C.1** Ethane reactivity of NbPMo<sub>12</sub>pyr at 280°C, 230 psig, 8: 4: 27: *x* mL/hr (ethane: oxygen: helium: steam) on high pressure reactor.

*Data for Figures 8.6, 8.7, and 8.8*

Steam Feed (mL/min)	Conversion			Selectivity		STY <sup>a</sup>	
	C <sub>2</sub>	O <sub>2</sub>	CO <sub>x</sub>	C <sub>2</sub> <sup>=</sup>	Acetic	C <sub>2</sub> <sup>=</sup>	Acetic
0	15.0	87.4	83.4	12.7	3.9	0.009	0.003
1	14.8	86.2	81.8	14.2	4.0	0.010	0.003
2	13.1	86.8	83.9	12.6	3.6	0.009	0.003
3	11.0	61.6	79.9	16.2	3.9	0.010	0.002
4	7.5	40.4	70.8	23.9	5.3	0.010	0.002
5	8.6	40.9	71.9	22.8	5.3	0.010	0.002
10	6.0	28.4	64.5	23.2	12.4	0.006	0.003

<sup>a</sup>STY is in mmol/min/g catalyst

**Table C.2** Ethane reactivity of NbPMo<sub>12</sub>pyr at 280°C, 230 psig, (8: 4: 27: 10) mL/hr (ethane: oxygen: helium: steam) on high pressure reactor. Volume of catalyst varied.

*Data for Figures 8.9 and 8.10*

GHSV (hr <sup>-1</sup> )	Conversion		Selectivity			STY <sup>a</sup>	
	C <sub>2</sub>	O <sub>2</sub>	CO <sub>x</sub>	C <sub>2</sub> <sup>=</sup>	Acetic	C <sub>2</sub> <sup>=</sup>	Acetic
1225	9.3	52.8	83.0	13.0	4.0	0.002	4.9x10 <sup>-4</sup>
2138	3.3	12.1	55.6	34.7	9.7	0.003	0.001
4523	6.0	28.4	64.5	23.2	12.4	0.006	0.003

<sup>a</sup>STY is in mmol/min/g catalyst

**Table C.3** Ethane reactivity of NbPMo<sub>12</sub>pyr at 380°C, 0 psig, 16: 8: 16: *x* mL/hr  
(ethane: oxygen: helium: steam) on high pressure reactor.

*Data for Figures 8.11, 8.12, and 8.13*

Steam Feed (mL/min)	Conversion			Selectivity		STY <sup>a</sup>	
	C <sub>2</sub>	O <sub>2</sub>	CO <sub>x</sub>	C <sub>2</sub> <sup>=</sup>	Acetic	C <sub>2</sub> <sup>=</sup>	Acetic
0	30.5	99.1	65.1	34.4	0.6	0.099	0.002
2	28.2	88.2	60.6	38.7	0.7	0.108	0.002
10	18.2	50.2	41.8	49.5	8.7	0.100	0.008
20	18.1	46.1	38.1	47.8	14.0	0.072	0.021

<sup>a</sup>STY is in mmol/min/g catalyst

**Table C.4** Ethane reactivity with temperature of NbPMo<sub>12</sub>pyr at 0 psig, 16: 8: 16: 20 mL/hr (ethane: oxygen: helium: steam) on high pressure reactor, except 280°C run on low pressure reactor.

*Data for Figure 8.14*

Temperature (C)	Conversion			Selectivity		STY <sup>a</sup>	
	C <sub>2</sub>	O <sub>2</sub>	CO <sub>x</sub>	C <sub>2</sub> <sup>=</sup>	Acetic	C <sub>2</sub> <sup>=</sup>	Acetic
380	18.1	46.1	38.1	47.8	14.0	0.072	0.021
340	6.5	14.0	21.7	59.1	19.2	0.037	0.012
300	3.1	6.5	10.6	57.3	32.1	0.017	0.010
280 <sup>b</sup>	2.0	6.3	24.8	61.6	13.5	0.006	0.001

<sup>a</sup>STY is in mmol/min/g catalyst

<sup>b</sup>Flows are 8: 4: 25: 10 mL/min, GHSV = 4700 hr<sup>-1</sup>, run on low pressure reactor.

**Table C.5** Ethane reactivity with Nb loading of NbPMo<sub>12</sub>pyr at 380°C, 0 psig, 16: 8: 16: 20 mL/hr (ethane: oxygen: helium: steam) on low pressure reactor.

*Data for Figures 8.15, 8.16, and 8.17*

Nb/Keggin loading	Conversion			Selectivity		STY <sup>a</sup>	
	C <sub>2</sub>	O <sub>2</sub>	CO <sub>x</sub>	C <sub>2</sub> <sup>=</sup>	Acetic	C <sub>2</sub> <sup>=</sup>	Acetic
0	0.6	2.8	69.5	30.5	0	0.002	0
0.04	0.9	3.0	37.5	55.5	7.1	0.006	0.001
0.2	7.6	22.4	34.2	61.1	4.6	0.055	0.004
0.4	15.3	47.7	57.1	39.1	3.8	0.050	0.005
0.6	14.0	51.5	54.0	42.6	3.4	0.081	0.006
0.8	13.6	48.2	51.4	45.2	3.4	0.092	0.007
1.0	12.9	44.2	48.2	47.9	3.9	0.084	0.007

<sup>a</sup>STY is in mmol/min/g catalyst

**Table C.6** Ethane reactivity with Nb loading of NbPMo<sub>11</sub>Vpyr at 380°C, 0 psig, 8: 4: 8: 10 mL/hr (ethane: oxygen: helium: steam) on low pressure reactor, V<sub>catalyst</sub> = 0.3 mL.

*Data for Figures 8.18, 8.19, and 8.20*

Nb/Keggin loading	Conversion		Selectivity			STY <sup>a</sup>	
	C <sub>2</sub>	O <sub>2</sub>	CO <sub>x</sub>	C <sub>2</sub> <sup>=</sup>	Acetic	C <sub>2</sub> <sup>=</sup>	Acetic
0.04	1.0	3.2	39.4	56.6	4.0	0.009	0.001
0.12	1.3	3.7	44.7	48.6	6.7	0.015	0.002
0.68	9.4	32.6	46.0	49.0	5.0	0.064	0.006
0.87	8.2	26.8	45.1	49.7	5.3	0.086	0.009
0.98	3.9	13.5	44.2	52.7	3.1	0.043	0.003

<sup>a</sup>STY is in mmol/min/g catalyst